Dipl.-Ing. Susanne Schutting, BSc.

Optical CO₂ Sensors for the Investigation of the Global Carbon Dioxide Cycle

DISSERTATION

Zur Erlangung des akademischen Grades

„Doktorin der technischen Wissenschaften"

eingereicht an der

Technischen Universität Graz

Betreuer

Univ.-Prof. Dipl.-Chem. Dr. rer.nat., Ingo Klimant

Institut für analytische Chemie und Lebensmittelchemie

Graz, Juli 2015

EIDESSTATTLICHE ERKLÄRUNG

Ich erkläre an Eides statt, dass ich die vorliegende Arbeit selbstständig verfasst, andere als die angegebenen Quellen/Hilfsmittel nicht benutzt, und die den benutzten Quellen wörtlich und inhaltlich entnommenen Stellen als solche kenntlich gemacht habe. Das in TUGRAZonline hochgeladene Textdokument ist mit der vorliegenden Dissertation identisch.

STATUTORY DECLARATION

I declare that I have authored this thesis independently, that I have not used other than the declared sources/resources and that I have explicitly marked all material which has been quoted either literally or by content from the used sources.

Datum/Date   Unterschrift/Signature

Der genießt wahre Muße, der Zeit hat, den Zustand seiner Seele zu fördern.

&

Es ist nicht wichtig, was Du betrachtest, sondern was Du siehst.

Henry David Thoreau

Zusammenfassung

CO_2 ist neben dem pH-Wert und Sauerstoff einer der wichtigsten Parameter für Umwelt und Industrie. Der Fokus dieses Projektes lag auf der Detektion von Kohlenstoffdioxid mittels optischen *Plastik-Typ* Sensoren, basierend auf pH-sensitiven Indikator-Farbstoffen. Derzeit hauptsächlich als Indikator verwendet wird 8-hydroxypyrene-1,3,6-trisulfonat (HPTS), jedoch besteht große Nachfrage an alternativen pH-sensitiven Farbstoffen mit verbesserten optischen Eigenschaften.

In Kapitel 1 wird eine neue Farbstoffklasse, basierend auf Diketo-Pyrrolo-Pyrrolen (DPPs), vorgestellt. Diese DPP-Farbstoffe weisen hohe Quantenausbeuten, hohe pK_s-Werte und gute Photostabilität auf. Diese Farbstoffe sind selbst-referenzierend und daher ideal für ratiometrische Messungen. Sensoren, die auf diesen DPPs basieren, können mittels Absorptions- oder Fluoreszenzmessungen ausgelesen werden. Durch unterschiedliche Startpigmente bzw. Substituenten können die dynamischen Bereiche der Sensoren angepasst werden. Kapitel 2 präsentiert einen hoch sensitiven CO_2 Sensor, dessen Fluoreszenzeigenschaften mittels kommerziell erhältlicher RGB Kamera ausgelesen werden können.

Eine zweite Klasse von pH-sensitiven Indikator-Farbstoffen wird in Kapitel 3 präsentiert. Die Verwendung dieser di-OH-aza-BODIPYs in optischen CO_2 Sensoren ermöglicht die Messung im nahen Infrarot-Bereich (NIR). Diese ebenfalls selbst-referenzierenden Farbstoffe zeigen außergewöhnliche Photostabilität und hohe pK_s-Werte, welche durch das Substitutionsmuster variiert werden können. Sensoren, welche darauf basieren, können mittels Absorption oder absorptionsmoduliertem *Inner-Filter-Effekt* ausgelesen werden.

Kapitel 4 präsentiert den Prototypen eines Multifaser-Sensors (MuFO) mit 100 frei positionierbaren optischen Fasern für die CO_2 Messung mit nur einer Anregungsquelle und Auslesung mit einer kommerziell erhältlichen Digitalkamera.

Abstract

Carbon dioxide is one of the most important parameters, besides pH and oxygen, for environmental and industrial monitoring. This project focused on optical *plastic type* sensors based on pH-sensitive indicator dyes for its detection. Up to now, state-of-the-art CO_2 sensors are almost exclusively based on the pH-indicator 8-hydroxypyrene-1,3,6-trisulfonate (HPTS), but alternative self-referencing (dual-emitting) indicator dyes are highly desired.

Chapter 1 presents a new class of indicator dyes based on diketo-pyrrolo-pyrroles (DPPs). Those dyes feature high fluorescence quantum yields, high pK_a values and good photostability. Both the protonated and the deprotonated form are excitable in the blue part of the spectrum. Hence, those self-referenced dyes are excellently suitable for ratiometric measurements. Sensors based on those dyes can be read out via absorption or via fluorescence intensity. By diversifying the starting pigments and using different substituents the optical CO_2 sensors were tuned to cover different dynamic ranges. A highly sensitive CO_2 sensor was prepared and presented in chapter 2. Its fluorescence properties perfectly match the color channels of commercially available RGB cameras.

Chapter 3 presents a second class of new indicator dyes based on BF_2-chelated tetraarylazadipyrromethenes (aza-BODIPYs). The use of di-OH-aza-BODIPY dyes in carbon dioxide sensors enables measurements in the near infrared (NIR) region. These dyes show very high pK_a values and excellent photostability. Carbon dioxide sensors based on those self-referenced aza-BODIPYs can be read out via absorption modulated inner filter effect. The dynamic ranges of the carbon dioxide sensors can be individually tuned by using di-OH-aza-BODIPY dyes with different substituents.

Chapter 4 presents a prototype of a multiple fiber optics (MuFO) device with not one, but 100 freely positionable fibers excitable with one collective excitation source and read-out via imaging with a commercially available digital camera.

Acknowledgement

THANK YOU, Ingo and Sergey. You were the most inspiring supervisors I could get. Your ideology, enthusiasm and passion for your work carried me along every single day and motivated me for new steps.

To the "old crew"- Klaus, Birgit, Lisi, Daniel, Babsi N., Tobi A. and B., Tijana, Torsten, Lego-Philipp, Gerda and Michela: Thank you for making me feel a member of this working group from the first day on. I enjoyed every discussion (serious or not), every lunch, every minute with you at this institute. Klaus, winning the first ACFC badminton cup with you as my partner was an honor. Birgit, your "Bloody Mary" was and will be the best of all! Lisi, not a single day is going by where I am not getting hungry at 11:30, thanks to you. Daniiiel, you are the perfect example of the loveliest confused professor in the world. Michela, with pleasure I learned the correct pronunciation of the word "comment" from you, especially because it took you at least 20 tries. Tobi A., thank you for drinking at least half of my drinks at the "Glühweinstand". Tobi B., I love your cheese fondue, but eating it with friends like you makes it really special. Babsi N., your lab journals were the most accurate ones I have ever seen. Torsten, thank you for eating my raisin bread… without you I would have gained just too much weight. Tijana, your dry humor is unique and Philipp, I have never seen anybody before sitting on a table while having his diploma exam. And Gerda, your vocal and rhythmic arts were and always will be outstanding.

To the "new crew"- Mokka-Berni, blonde Berni, Ulli, Willy, David, Martin, Peter, Philipp (small), Heidi, Josef, Shiwen, Christoph, Eva, Rahel, Pia, Silvia, Anna and Larissa: Thank you all for accompanying me during my last years/months at the institute. Ulli, you were one of the most pleasant office mates I´ve ever had. Heidi, you are such a nice person… please, stay as you are. Special thanks to my beer-buddy David and my soccer-match-ticket-dealer Phips! Martin, the jungle camp would not have been so funny without you. Peter, my "favorite librarian" and social-activity-organizing-partner, thank you. Mokka-Berni, you are an excellent whisky-buddy, although you are mixing it sometimes with energy drinks. Josef, you are one of the most helpful and social people I know, thank you. Shiwen, do not forget your passport. Eva, I am sure you will make the best sticking-together CO_2 sensor layers ever known. Blonde Berni, thanks for introducing me to the park house and for the delicious toast sessions. Willy, I have only two words for you: "mustard-colored jeans"… made my day. Christoph, I have never messed up so many "Quiz duell"-matches as I did while I was playing against you. Silvia, your sunny nature lightens up every single day. Rahel, I will miss your chocolate cake. Pia, thank you for your tireless dedication. Anna, I will miss the chats in the tram. ;) Larissa, you are one of the most adorable persons I´ve ever met.

To the "everlasting crew"- Eveline, Manuela, Iris, Erika, Marion: You are the heart of the institute. Please, never stop to be so helpful and dedicated. I have no words to describe how badly I will miss you.

Special thanks to Jan and Günter! From the MPI to the TU, I appreciated and enjoyed every discussion during work and chat during the breaks.

Last but not least, the "round-about crew"- Herbert, Helmar, Paul, Nina, Iris, Andrea, Sigi, Claudia, Erich, Barbara S. and Barbara P.-Z.: Herbert, I would have not been able to print anything without you. Helmar, Sigi, Iris and Nina, thank you for the puzzle evenings… although I think I will never go to Venice. Andrea, thank you for helping me during the lab course. Erich and Barbara S., I enjoyed your lectures. Your passion for food chemistry was absolutely infectious. Babsi P.-Z., thank you for organizing the dancing lessons. Paul and Claudia, you are so lovely people. Please, stay as you are.

<div align="center">Thank you all. You became friends, not only colleagues.</div>

To the four most important persons in my life: *Mum, Dad, Chri* and *Julia*. I can not and don´t want to imagine how life would be without you. Thank you for the talks, the patience, the hours filled with love and happiness, for being as you are and for taking me as I am.

Table of Contents

Theoretical Background

Scope of the Thesis

Carbon dioxide is one of the most important parameters concerning different processes in nature, science and industry. Whereas by oxygen monitoring only aerobic activities can be observed, also anaerobic activities are observeable by monitoring carbon dioxide. 98% of the worlds carbon dioxide deposits are stored in the deeper oceans. The increasing carbon dioxide level causes problems like *global warming (greenhouse effect)* or the *acidification of the oceans*. The latter causes not only a lowered pH, but also several consequences on the oceans flora and fauna.

For marine science the demands on detection methods can range from the atmospheric pCO_2 level (0.04 kPa ≈ 400 µatm in the gas phase ≈ 11.6 µmol/l in seawater at 298.15 K) to very high pCO_2 values, e.g. in the vicinity of volcanic seeps. Especially for field experiments where time, equipment and staff are limited, it is important that the method is easily adaptable to the respective conditions of the experiment and that it gives as much simultaneous information as possible concerning spatial and temporal distribution of the analyte concentration.

Routine detection techniques of CO_2 like infrared (IR) spectroscopy, gas chromatography (GC) or the Severinghaus electrode are well established, but suffer from different drawbacks. Although several new concepts of chemosensors for the detection of CO_2 were published in recent years, optical *plastic type* sensors are the most common ones. These sensors consist of a pH-sensitive indicator dye and a base (acting as lipophilic buffer), embedded in a polymer matrix and represent a promising alternative to the known routine techniques. The dynamic range of the CO_2 sensors can be tuned by varying the pK_a value of the indicator dye, by using different bases or matrix materials. Up to now, state-of-the-art CO_2 sensors are almost exclusively based on the fluorescent pH-indicator 8-hydroxypyrene-1,3,6-trisulfonate (HPTS), the base tetraoctyl ammonium hydroxide (TOAOH) and ethyl cellulose as matrix material. Alternative materials, especially self-referencing (dual-emitting) indicators with spectral properties in the visible range, as well as in the NIR region are presented in this thesis.

Carbon Dioxide and the Marine Ecosystem

The Global Carbon Cycle

The global carbon cycle describes the exchange of carbon (as CO_2, CO, CH_4, organic matter, fossil fuels, etc.) between the *reservoirs*, which are acting either as source (release of carbon) or sink (uptake of carbon). The major reservoirs of carbon on earth are: the atmosphere, the oceans and the terrestrial system (also: the lithosphere, the aquatic biosphere and fossil fuels),[1,2] where the largest and dominating reservoir – the oceans – and the terrestrial system are linked via the atmosphere.[3]

Figure I shows an overview of the carbon reservoirs, their capacities and the fluxes and rates inbetween. Especially the anthropogenic impact has left a big footprint on the global carbon cycle during the last two to three centuries. The development of new machines and technologies during the industrial revolution brought a strong increase in carbon fluxes, in particular concerning carbon dioxide and methane.
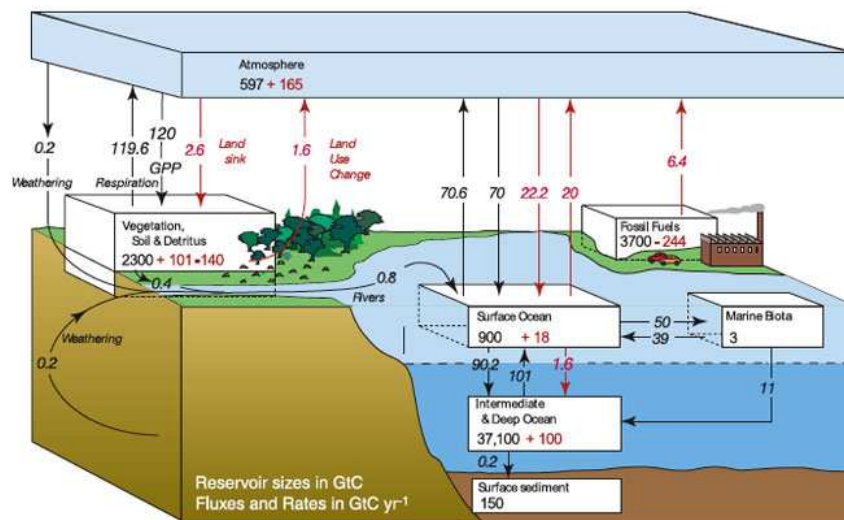
Figure I. *Global carbon cycle.*[4] ***Red****: anthropogenic fluxes;* ***Black****: natural fluxes (before industrial revolution).*

Atmospheric Carbon Dioxide

One of the strongest leverage effects to the global carbon cycle is the atmospheric CO_2 level and its interactions with the cycle. Its changing rate is highly affected by anthropogenic influences, biogeochemical and climatological processes.[1] Here, the main focus will be the balance between atmospheric carbon dioxide and the ocean, which is the major sink for CO_2.[3]

Sources of Carbon Dioxide

As mentioned before, the carbon reservoirs (either sink or source) are linked to each other and exchange carbon and/or carbon dioxide. However, there are several big sources – natural or anthropogenic - of carbon dioxide. Especially during the last two centuries the anthropogenic sources had a high impact on earth´s atmosphere pCO_2 level:

- *Natural sources*: The biggest (short-term) natural sources for carbon dioxide are volcanic carbon dioxide seeps,[5] total global emission of CO_2 from soils,[6] decay of organic matter, heterotrophic respiration and natural fires.[7] Ice core analysis showed that the atmospheric CO_2 level altered several times between 180 and 280 µatm before the industrial revolution in the 19th century.[8] Therefore, even for short-term exposures with high levels of carbon dioxide, such as during volcanic activities, no significant long-term effects were recordable.

- *Anthropogenic sources*: The level of atmospheric CO_2 is strongly affected by human activities. In the 18th/19th century, when industry started to introduce more efficient manufacturing machines and processes, the anthropogenic impact on the atmospheric carbon dioxide level increased rapidly and led to a sharp increase of atmospheric CO_2 up to more than 360 µatm.[8,9] Today, the major sources for anthropogenic CO_2 are: anthropogenic deforestation,[4,10,11] iron and steel production,[12] agricultural economy,[2] burning fossil-fuels[2,4,11] and cement-manufacturing emissions.[4,13] All these sources transport carbon from the terrestrial reservoir to the atmosphere as carbon dioxide and therefore affect the carbon dioxide level of the ocean.

Carbon Dioxide in the Ocean

CO_2 is exchanged across the ocean-atmosphere interface, even forced by strong and continuous winds over the ocean surface.[2] Thus, the atmospheric carbon dioxide level is in a dynamic equilibrium with the surface layer of the oceans, which is influenced by different processes, such as upwelling (nutrient-rich upward current from the deep sea), downwelling (nutrient-rich downward current to the deep sea), vertical diffusion, advection and gravitational drift of biogenic materials.[2] The major driving forces are:

- *Chemical processes:*

Dissolution in water (figure II): After CO_2 is dissolved in water, it forms carbonic acid H_2CO_3. This formation is the slowest step in these equilibria series compared to the ionization of the carbonic acid, which is much faster and yields bicarbonate ions and protons.[14] Bicarbonate is the dominant species. Firstly, bicarbonate can dissociate to carbonate ions and protons, but carbonate ions can also be reprotonated by the protons build during the dissociation of carbonic acid. In this case the concentration of carbonate is lowered again.

The equilibria between the three species – bicarbonate ions ~90%, carbonate ions ~10% and unionized dissolved carbon dioxide <1% at a pH of ~8.2[9,14] – are in balance with other acid-base equilibria (e.g. boric acid) and the pH value of the ocean. Although it seems sometimes, as the pH is influencing the equilibria of the carbonate cycle, the opposite is the truth – the carbonate system acts as buffer of the ocean. The carbonate equilibria, the pK_a values for carbonic acid, the relation to pH and to the boric acid equilibrium can also be seen in the Bjerrum plot in figure II (right).[15]

The sum of the concentrations of unionized dissolved carbon dioxide, HCO_3^- and CO_3^{2-} is also known as the (total) *dissolved inorganic carbon C_T* and is only ~2 mmol/kg (surface layer, North Atlantic).[14,16]

Carbon dioxide shows increased solubility in cold seawater with higher density and salinity. When the water is sinking down, the carbon dioxide is transported to deeper depths.
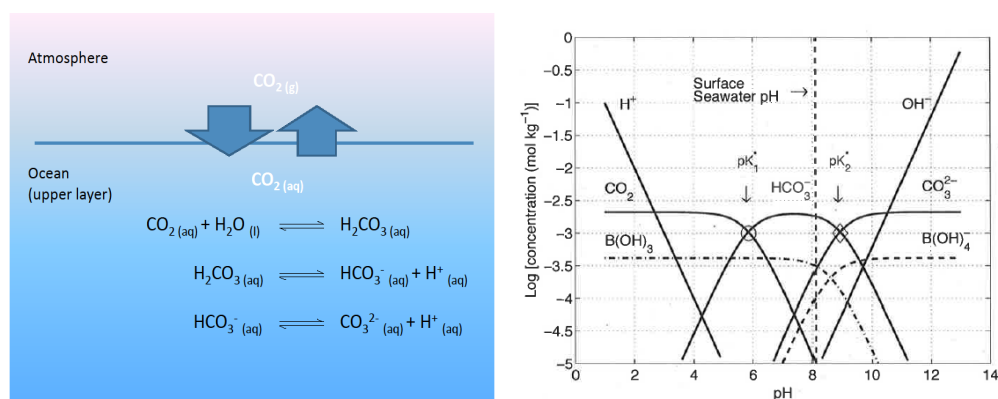
Figure II. Left: *Reactions of carbon dioxide in water.*[14,16] ***Right:*** *the Bjerrum plot*[15] *(DIC = 2.1 mmol/kg, S = 35, T = 25°C). Here, pK_{a1} and pK_{a2} of carbonic acid are 5.86 and 8.92, respectively.*

- *Biological processes (figure III)*:

  The *organic biological pump:*[2] CO_2 uptake is also forced by biological processes, such as the carbon dioxide consumption during phytoplankton photosynthesis in depths of the ocean where light can still penetrate. Inorganic compounds and organic matter are produced. This is also called *primary production.*[2] The products are then transported (via sinking, advection or mixing) to the deep sea, where they re-mineralize or are decomposed by bacteria. The transfer rate from the surface layer to the deep sea is called *new production.*[2] Via upwelling CO_2 is partially transferred back to the surface layer of the ocean.

  The *carbonate pump*[1,17,18] is a special case of the organic biological pump. $CaCO_3$ shells can be built by different planktonic species. Afterwards they sink to the seafloor (gravitational drift of biogenic materials)[2] and can re-dissolve, because $CaCO_3$ shows increased solubility in colder water and under higher pressure.[9] Again, via upwelling CO_2 is only partially transferred back to the surface layer of the ocean. Thus, CO_3^{2-} is "pumped" to deeper layers of the ocean. The three main producers for $CaCO_3$ are coccolithophores, foraminifera and euthecosomatous pteropods,[9] whereas 23-56% of the total open marine $CaCO_3$ flux are covered by planktonic foraminifera.[18]
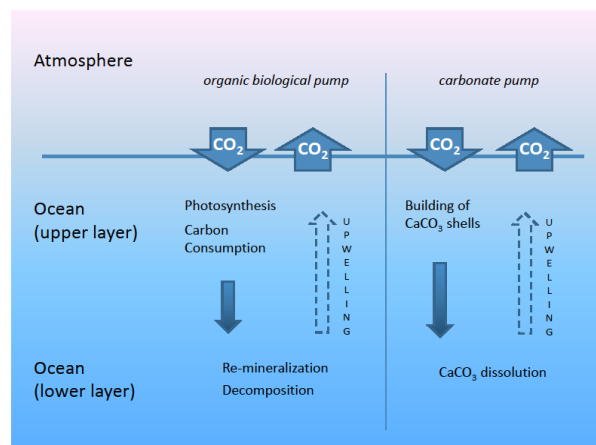
Figure III. Scheme of the responsible biological processes for the uptake/storage of carbon dioxide in the ocean.

The upper layer of the ocean is defined as an almost homogeneous layer of seawater, which shows only small changes in temperature and density in dependence to the depth. The depth of this layer is often called *isothermal layer depth (ILD)* in case of limitation

by temperature changes or *mixed layer depth (MLD)* in case of limitation by density changes.[19]

The above described processes are displaying the major paths of storing carbon/ carbon dioxide in the deeper ocean. Thus, the lower part of the oceans is enriched with CO_2 and is overlaid with the upper layer containing less carbon dioxide. Therefore, the upper layer is acting as a barrier between the atmosphere and the lower ocean layer[3] and CO_2 from the lower layer can not re-equilibrate with the atmosphere. Nowadays, there are ~720 Gt of carbon dioxide in the atmosphere, but more than the fiftyfold in the lower ocean layer.[1]

More or less one third of the anthropogenic produced atmospheric carbon dioxide is absorbed by the oceans[13] and can there be stored in different ways:[2]

- As *dissolved inorganic carbon (DIC or C_T)*: the sum of dissolved CO_2, carbonic acid, bicarbonate ions and carbonate ions
- As *dissolved organic carbon (DOC)*: small and large molecules (simply hydrocarbons to polysaccharides)[20]
- As *particulate organic carbon (POC)*: the sum of living organisms and fragments of dead plants and animals

Consequences of the CO_2 Increase

The level of atmospheric CO_2 is expected to be 730 µatm to over 1000 µatm by the end of 2100, which would lead to a drop of the oceans pH of 0.3 to 0.4 units.[21,22] Influences of the elevated pCO_2 will thus be definitely amplified and are discussed in this section.

As carbon dioxide is the most important greenhouse gas besides methane, tropospheric ozone, nitrous oxid and chlorofluorocarbons (CFCs), it is a decisive parameter concerning global warming, also known as *greenhouse effect*.[11,23,24]

Here, solar infrared radiation is needed for many natural processes and is absorbed by the earth's atmosphere and surface. To keep the energy and/or heat balance at equilibrium thermal radiation is re-emitted by the earth's surface. Molecules, such as carbon dioxide, absorb the thermal radiation and are therefore responsible for the warm up of the first layer of the atmosphere – the troposphere (10-15 km), where the

greenhouse effect mainly happens.[11]

Global warming can cause various effects, e.g. melting of ice caps, that causes a noise increase in the oceans and a rise of the sea level.[3,25] Tropical forests for example tend to increase the respiration rate, decrease the growth and show increased natural fire risk.[7] This again leads to higher levels of atmospheric carbon dioxide, which is only partially compensated by the ocean reservoir.

The likelihood of extreme events like floodings or extended droughts is enhanced by global climate change.[26] In consequence, natural or man-made water reservoirs are increasingly stressed. They show higher temperature, increased evaporation, decreased precipitation and up-concentration related eutrophication.[26,27] Additionally, the magnitude of high and low water level is influenced by agricultural economy, as more water is needed during dry periods.[28] These affects can lead to a dramatic decline of the reservoirs or even to their disappearance.

CO_2 enhanced uptake by the oceans leads to an increase of the T_C and a correlated increase in proton concentration.[9] This carbon dioxide increase leading to a lowered pH value is also called *ocean acidification* or *seawater acidification*.[9] A widely known factor to express the CO_2-buffering via pH lowering is the *Revelle factor (also buffer factor) R_f*.[15] It describes the uptake capacity of carbon dioxide in the oceans when the level of atmospheric CO_2 rises and was well explained by Zeebe and Wolf-Gladrow.[15]

$$R_f = \left(\frac{\frac{d[CO_2]}{[CO_2]}}{\frac{dDIC}{DIC}} \right)_{TA=constant}$$

Concerning the flora and fauna, on the one hand, the acidification causes a decrease of the saturation of $CaCO_3$ and therefore has an impact on the calcification rates.[9] This means, that – as mentioned before – the uptake of CO_2 lowers the concentration of carbonate ions. Calcifying species like corals, molluscs, echinoderms and crustaceans[9] build their skeletons and shells using Ca^{2+} and CO_3^{2-} ions. As the Ca^{2+} concentration in seawater is almost constant (although depending on the salinity), the limiting factor for these species is the concentration of carbonate ions.[9] Hence, calcifying species are increasingly restricted in building their $CaCO_3$ shells. Additionally, if there are less

shells built, less CO_3^{2-} is transported to the deeper oceans and therefore, stays in the upper ocean layer and in the atmosphere.

The acidification affects the acid-base physiology of the extracellular body fluids of the animals, e.g. blood, haemolymph or coelomic fluid,[29] and lowers the pH value of the blood. An increase of pCO_2 in the blood is also called *hypercapnia*.[9] As a consequence the oxygen binding of some species is influenced negatively. This relation is described by the *Bohr coefficient C_B* (P_{50} = pO_2 required to achieve 50% oxygen saturation of the respiratory protein).[9,30]

$$C_B = \frac{\Delta log P_{50}}{\Delta pH}$$

Some species are able to suppress their metabolism to counteract low pH or high pCO_2 values by reducing their protein synthesis.[9] Although reversible at short-term exposure, this affects the growth and reproductive potential in a negative way and is even worse at long-term exposure. Hence, the reproducibility is restricted and leads sooner or later to a decrease of the diversity of species.

Fishes are affected concerning their olfactory senses. For example, several coral reef fishes get susceptible for predation, as well as predator fishes change their hunting behavior.[21,31] Even fish species, e.g. cod, which show CO_2 independent behavior to the smell of predatory or non-predatory fishes, may e.g. change their movements.[32]

According to de Baar and Stoll[3] the uptake of CO_2 in the oceans will be affected, as the chemical dissolution processes will decrease with rising carbon dioxide level and the biological processes (carbonate pump, etc.) will probably stay constant or show a slight increase.

Although there are more disadvantages, also the advantages of the increasing CO_2 level should be mentioned, e.g. a CO_2 related decrease of ammonia[33] or seagrass that shows increased photosynthetic rates and net productivity and thus, features great affinity to areas with elevated pCO_2 values.[34,35]

However, one should be aware of the fact that a dramatic decrease of the human caused global CO_2 emissions will not automatically end in an immediate drop of the atmospheric carbon dioxide level. The capacity of the oceans might be as high to take up a big part of the anthropogenic carbon dioxide, but this might take a long time. De Baar and Stoll already discussed this problem in 1992: *"Only after several thousands to*

millions of years most, but not all, of the fossil fuel CO_2 will be taken up by the oceans."[3]

So called *carbon (dioxide) capture and storage (CCS)* strategies are under development, but not yet fully investigated concerning their long-term consequences. A definition of CCS was provided by a special report – *IPCC Special Report on Carbon Dioxide Capture and Storage* – on this topic of the *Intergovernmental Panel on Climate Change (IPCC): "Carbon dioxide (CO_2) capture and storage (CCS) is a process consisting of the separation of CO_2 from industrial and energy-related sources, transport to a storage location and long-term isolation from the atmosphere."*

One of these strategies would be the sub-seabed geological storage of carbon dioxide. Here, carbon dioxide is collected and pumped into sub-seabed geological formations, e.g. the porous formations remaining from oil drilling rigs. Deep sea injection strategies were already discussed in 1992 from de Baar and Stoll.[3] Here, CO_2 is collected and pumped into deeper ocean layers. However, scientists are still investigating the consequences, if carbon dioxide erupts quickly due to geological formation fractures or if it is transported back to the upper ocean layer and the atmosphere.

Calculations

It was already mentioned, that although the upper layer of the ocean is in a dynamic equilibrium with the atmosphere, the biggest part of the carbon dioxide is stored in the deeper layers of the ocean. Numerical, almost 98% of the carbon dioxide are stored in the ocean, due to its further reactions in water.[15] The carbonate system is influenced by various factors, such as temperature, salinity or other species in the seawater that show acid-base equilibria, e.g. boric acid (table I). The focus of this thesis is the detection of carbon dioxide in seawater, but not only the concentration of dissolved carbon dioxide is of great interest, but also the concentrations of HCO_3^- and CO_3^{2-} ions are. The equations to describe and calculate the carbonate system are well collected and explained by Zeebe and Wolf-Gladrow in *CO₂ in Seawater: Equilibrium, Kinetics, Isotopes.*[15] The following section is an extraction of this book and should give an overview of how to calculate the ratios between the species of the carbonate system – dissolved CO_2, HCO_3^- and CO_3^{2-}.

***Table I**. Averaged standard chemical composition of seawater at a salinity of 35.[15,16]*

Ion	g/kg	mol/kg
Cl^-	19.3524	0.54586
Na^+	10.7837	0.46906
Mg^{2+}	1.2837	0.05282
SO_4^{2-}	2.7123	0.02824
Ca^{2+}	0.4121	0.01028
K^+	0.3991	0.01021
CO_2	0.0004	0.00001
HCO_3^-	0.1080	0.00177
CO_3^{2-}	0.0156	0.00026
$B(OH)_3$	0.0198	0.00032
$B(OH)_4^-$	0.0079	0.00010
Br^-	0.0673	0.00084
Sr^{2+}	0.0079	0.00009
F^-	0.0013	0.00007
OH^-	0.0002	0.00001
$\sum$	**35.1717**	**1.11994**
Ionic Strength		**0.69734**

Initially, a few definitions have to be mentioned:

The sum of the species of the carbonate system (dissolved CO_2 incl. H_2CO_3, HCO_3^- and CO_3^{2-}) is called *dissolved inorganic carbon*, shortly *DIC*. Other abbreviations are $\sum CO_2$, TCO_2 or C_T. This terms focus on the carbon.

$$DIC = [CO_2] + [HCO_3^-] + [CO_3^{2-}]$$

The *carbonate alkalinity (CA)* focuses on the charges, is part of the total alkalinity and is defined as:

$$CA = [HCO_3^-] + 2*[CO_3^{2-}]$$

The *total alkalinity (TA or A_T)* also focuses on the charges and includes also boron compounds and others:

$$TA = [HCO_3^-] + 2*[CO_3^{2-}] + [B(OH)_4^-] + [OH^-] - [H^+] + \text{minor components}$$

In total, the carbonate system can be calculated via six variables: DIC, CA, $[H^+]$, $[CO_2]$, $[HCO_3^-]$ and $[CO_3^{2-}]$, where two have to be known to enable the calculation of the remaining four.

Conversion of ppm to µmol/l

To express the concentration of carbon dioxide several units are used. Companies are mostly using the unit ppm, where one has to define which ppm is meant: mg CO_2/l or volume percent*10000 at 1 atmosphere (sometimes ppmv). Scientists usually prefer molarity units, e.g. mol/l, mmol/l or µmol/l.

The conversion of ppm (volume percent*10000 at 1 atmosphere) to molarity can be carried out by using *Henrys law*, where the molarity of a dissolved gas is calculated from its partial pressure in the gas phase above the solution.

$$c_{aq} = k_H \cdot f$$

Where f Fugacity of the substance [atm]

     c_{aq} Concentration of the substance in solution [mol/kg]

     k_H Henry constant [mol/kg*atm]

The Henry constant shows significant temperature dependence. Zeebe and Wolf-Gladrow recommend the calculation of Weiss (1974):[15]

$$\ln k_H = \frac{9345.17}{T} - 60.2409 + 23.3585 \cdot \ln\left(\frac{T}{100}\right) + S$$
$$\cdot \left[0.023517 - 0.00023656 \cdot T + 0.0047036 \cdot \left(\frac{T}{100}\right)^2\right]$$

Where k_H Henry constant dependent on the temperature [mol/kg*atm]

$\quad\quad T$ Temperature [K]

$\quad\quad S$ Salinity; ~35 g salt/kg seawater (see table I) [g/kg]

The molarity of carbon dioxide at different temperatures will be calculated as an example. The results are shown in table II. The atmospheric level of carbon dioxide is ~400 ppm, which is equal to ~400 µatm (400 ppm = 400 µatm = 0.0004 atm). As the result of the Henrys law calculation gives mol/kg, this unit is converted to mol/l considering the density of seawater, being higher than that of freshwater.

Table II. *Temperatures from 20-30°C, the respective Henry constants, the carbon dioxide concentration in µmol/kg and µg/kg, the seawater density and the CO_2 concentrations in µmol/l and µg/l, calculated from the atmospheric level of CO_2 (0.0004 atm) at a salinity of 35.1717.*

Temperature		$ln\ k_H$	k_H	Seawater Density	$c(CO_2)_{aq}$	$c(CO_2)_{aq}$
[°C]	[K]		[mol/kg*atm]	[g/l]	[µmol/l]	[µg/l]
20.00	293.15	-3.430	0.03238	1024.8	13.27	584.1
25.00	298.15	-3.563	0.02837	1023.3	11.61	511.0
30.00	303.15	-3.683	0.02515	1021.7	10.28	452.3

Calculation of [CO$_2$], [HCO$_3^-$] and [CO$_3^{2-}$]

The equilibria between the species [CO$_2$], [HCO$_3^-$] and [CO$_3^{2-}$] show two equilibrium constants K_1 and K_2, also called first and second dissociation constants of carbonic acid.

$$K_1 = \frac{[HCO_3^-] \cdot [H^+]}{[CO_2]}$$

$$K_2 = \frac{[CO_3^{2-}] \cdot [H^+]}{[HCO_3^-]}$$

There are several equations for the calculation of K_1 and K_2. Zeebe and Wolf-Gladrow recommend the equations from Roy et al.:[16]

$$\ln K_1 = 2.83655 - \frac{2307.1266}{T} - 1.5529413 \cdot ln(T) - \left(0.207608410 + \frac{4.0484}{T}\right)$$
$$\cdot \sqrt{S} + 0.0846834 \cdot S - 0.00654208 \cdot \sqrt{S^3} + ln(1 - 0.001005 \cdot S)$$

$$\ln K_2 = -9.226508 - \frac{3351.6106}{T} - 0.2005743 \cdot \ln(T)$$
$$- \left(0.106901773 + \frac{23.9722}{T}\right) \cdot \sqrt{S} + 0.1130822 \cdot S - 0.00846934$$
$$\cdot \sqrt{S^3} + ln(1 - 0.001005 \cdot S)$$

Where $K_{1,2}$ Equilibrium constants (1st and 2nd dissociation constants of carbonic acid)

T   Temperature [K]

S   Salinity; ~35 g salt/kg seawater (see table I) [g/kg]

For a salinity of ~35 and a temperature of 25°C (298.15 K) $\ln K_1$ should give -13.4847 and $\ln K_2$ should give -20.5504.

As mentioned, by knowing two variables of the carbonate system, the remaining four can be calculated. Here, the calculation of the carbonate system is shown based on known pH and CO_2 concentration (from direct measurement).

$$pH = -log[H^+]$$

$$DIC = [CO_2] \cdot \left(1 + \frac{K_1}{[H^+]} + \frac{K_1 \cdot K_2}{[H^+]^2}\right)$$

Where DIC   dissolved inorganic carbon [mol/l]

[H$^+$]   proton concentration calculated from the measured pH [mol/l]

[CO$_2$] concentration of dissolved CO_2, incl. [H$_2$CO$_3$] [mol/l]

Using the DIC, the proton concentration and the equilibrium constants, the concentrations of HCO$_3^-$ and CO$_3^{2-}$ and the carbonate alkalinity can be calculated.

$$[HCO_3^-] = \frac{DIC}{\left(1 + \frac{[H^+]}{K_1} + \frac{K_2}{[H^+]}\right)}$$

$$[CO_3^{2-}] = \frac{DIC}{\left(1 + \frac{[H^+]}{K_2} + \frac{[H^+]^2}{K_1 \cdot K_2}\right)}$$

$$CA = [HCO_3^-] + 2 \cdot [CO_3^{2-}]$$

As already mentioned, the equilibria of the carbonate system, as well as the total alkalinity, are affected by various processes, such as $CaCO_3$ formation and dissolution, photosynthesis, respiration and others.[15] Figure IV gives an overview in which way the system is influenced by these processes. For example: If one mole $CaCO_3$ is built, one mole Ca^{2+} and one mole CO_3^{2-} are used. In this case, the DIC is one unit lower, because one mole carbon is used, but the TA is lowered by two units, because the used carbonate ion is doubly charged.
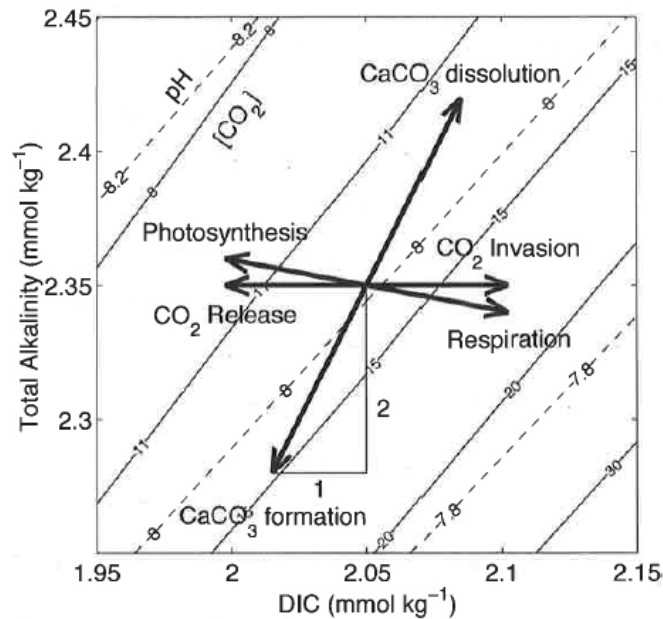
Figure IV. *Influencing processes on DIC and total alkalinity, constant pH values (dashed lines) and CO_2 concentrations (solid lines).*[15]

Basics

Absorption

If a molecule absorbs photons, an electron can undergo a transition from the ground state to an excited state, this means a transition from the highest occupied molecule orbital to the lowest unoccupied orbital (HOMO → LUMO). There are several electronic transitions, which can be lined up according to their energy:[36]

$$n \rightarrow \pi^* < \pi \rightarrow \pi^* < n \rightarrow \sigma^* < \sigma \rightarrow \pi^* < \sigma \rightarrow \sigma^*$$
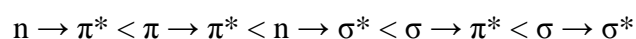
If the excited electron keeps the same spin, both, the ground and the excited state are singlet states, because the multiplicities of both states are equal to one. Transitions between the singlet ground state S_0 and the singlet excited state S_1, S_2, S_3, … are called singlet-singlet transition (figure V).

If the excited electron undergoes intersystem crossing (described below) to an energetically lower state and changes its spin, the multiplicity is 3. Hence, this excited state is called an excited triplet state T_1 (singlet-triplet transition).
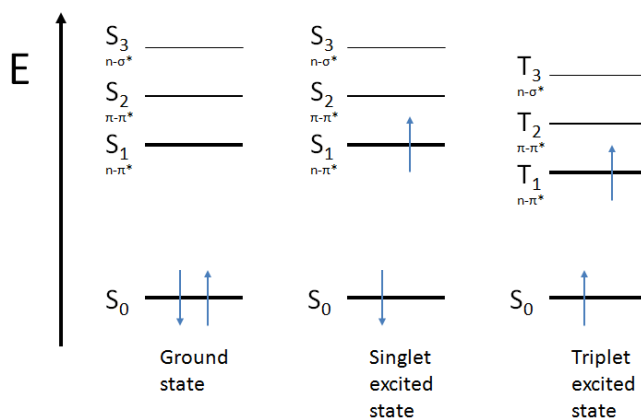
Figure V. *Scheme of ground state, singlet excited state and triplet-excited state.*

Luminescence

After absorption of photons and transition of an electron to an excited state, luminescence can occur. Luminescence is the emission of photons from an electronically excited state.[36] In case of organic compounds luminescence is mostly the transition from the 1st or 2nd excited state to the ground state and features rather broad spectra caused by electronic excitation, as well as vibrational and rotational excitation.

There are different types of luminescence, which can be categorized by the type of excitation, e.g. chemiluminescence (excitation via chemical processes) or bioluminescence (excitation via biochemical processes). Here, the focus will be on *photoluminescence*, where the excitation process is initiated by the absorption of photons (figure VI). Photoluminescence can be divided into *fluorescence*, *phosphorescence* and *delayed fluorescence*.

When an electron is in the excited state, there are several ways to get back to the ground state.[36] The possibly occurring de-excitation process are described below:

- *Internal conversion (IC)*. This process occurs between vibrational levels, where the spin does not change, e.g. $S_x...S_3$, $S_2 \rightarrow S_1$. It is non-radiative and can also occur from S_1 to S_0, although in this case fluorescence or intersystem crossing are more likely.

- *Fluorescence*. Fluorescence is a direct photon-emitting de-excitation process from the excited singlet state. The excited electron undergoes the $S_1 \rightarrow S_0$ transition back to the ground state with lower energy (vibrational relaxation in the excited state S_1). Therefore, the emission spectrum is mostly shifted to higher wavelengths. The difference between the absorption maximum and the emission maximum is called *Stokes shift*.

- *Intersystem crossing (ISC)*. ISC is a non-radiative process. Here, the electron changes its spin while undergoing the transition from S_1 to an energetically similar excited triplet state, followed by relaxation to the lowest excited triplet state T_1. ISC occurs despite the transition $S_1 \rightarrow T_1$ is forbidden, because of spin-orbit coupling.

- *Phosphorescence*. Phosphorescence is a photon-emitting de-excitation process from the excited triplet state T_1 to the ground state S_0. Although also forbidden, this transition occurs in cases where the spin-orbit coupling is sufficiently large. Phosphorescence is more likely at lower temperatures and in rigid media. The energy loss until it comes to phosphorescence is even higher than that for fluorescence. Hence, the maximum of the phosphorescence is shifted to even higher wavelengths.

- *Delayed fluorescence*. If the lifetime of the excited triplet state T_1 is long enough and the energetic difference to S_1 is small, the excited electron can undergo a transition from T_1 back to S_1. During the de-excitation from S_1 to S_0 photons are emitted. There are two types of delayed fluorescence: *thermally activated* and

triplet-triplet annihilation (TTA) initiated. Thermally activated means the occurrence of the process is enhanced at higher temperatures. This process is also called *E*-type delayed fluorescence (first observed with eosin).[36] TTA means a collision between two molecules in the excited triplet state (occurs in highly concentrated samples). One of the molecules is then directly and non-radiative de-excited to the ground state S_0, whereas the other molecule undergoes a transition back to the excited singlet state S_1. This process is also called *P*-type delayed fluorescence (first observed with pyrene).[36] Spectrally delayed fluorescence displays the same characteristics as "normal fluorescence".
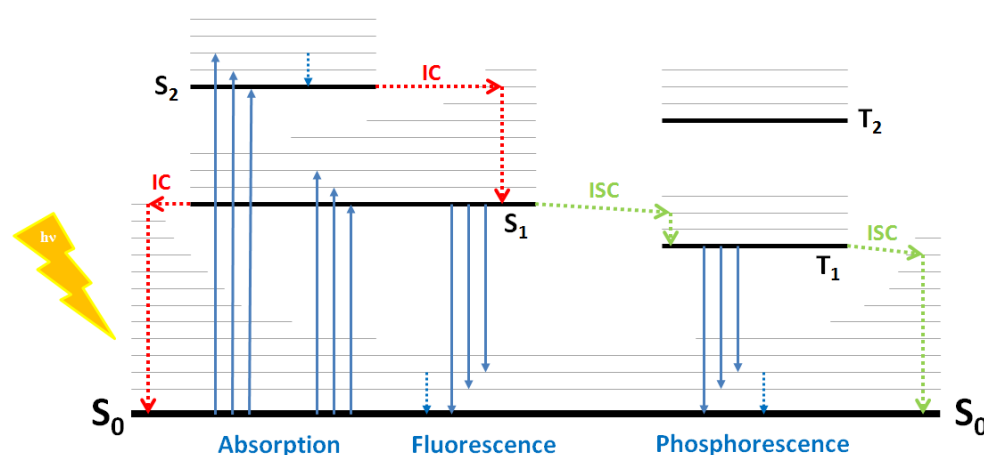
Figure VI. *Perrin-Jablonski diagram.*

Besides these de-excitation possibilities, there are several competitive ways of de-excitation:[36] intramolecular charge transfer, conformational change, electron transfer, proton transfer, energy transfer, excimer formation, exciplex formation or photochemical transformation.

Table III shows the characteristic times for the transitions between the vibrational levels. One should notice that absorption is the fastest, followed by vibrational relaxation. In general, photon absorption is as fast as photon emission. In case of fluorescence the enhanced time is caused by a short remain in the excited state. More processes, like intersystem crossing and again short remains in the excited states, lead to even longer times in case of phosphorescence and delayed fluorescence, although delayed fluorescence shows the same spectral characteristics as fluorescence.

Table III. *Characteristic times for different transitions between the vibrational levels.*[36]

Transition	Time [sec]	
Absorption	10^{-15}	
Vibrational relaxation	$10^{-12} – 10^{-10}$	
Lifetime of the excited state S_1	$10^{-10} – 10^{-7}$	→ Fluorescence
Intersystem crossing	$10^{-10} – 10^{-8}$	
Internal conversion	$10^{-11} – 10^{-9}$	
Lifetime of the excited state T_1	$10^{-6} - 1$	→ Phosphorescence

Sensors

In general, *sensing* means a continuous and reversible measurement of an analyte concentration, whereas a *sensor* is described as a sensing element that registers (molecular recognition) the analyte information and transduces it into an electrical signal.

A widely used definition for chemical sensors is the *Cambridge Definition:*[37,38]

"Chemical sensors are miniaturized devices that can deliver real-time and on-line information on the presence of specific compounds or ions in even complex samples."

Sensors in principle can be described with 3 main parts: The analyte or the receptor for the analyte in case of reagent-mediated based principles, the transduction platform, where the analyte is registered and the generation of a measureable signal occurs, and a signal processing step.[38] In case of optical sensors the transduction step is most widely based on absorption, luminescence or refractive index.

Sensors have to meet different requirements that vary with the demands of the user and the expected measurement conditions, but generally the most important parameters for a sensor are:[38]

- *Sensitivity*. In general sensors should be tunable to a very high sensitivity. This means, the degree of response of the sensor by an increasing analyte concentration change. However, the required sensitivity of a sensor can vary, from very sensitive to less sensitive, and often depends on the measurement conditions. Ideally, the response of the sensor shows a linear correlation with the analyte concentration. In

case of optical sensors the linear range is sometimes only a small section of the allover dynamic range.

- *Selectivity (Cross-sensitivity).* The sensor should selectively and accurate respond to the analyte that is in demand and should not be interfered by other species with sometimes analyte-similar properties.

- *Stability.* The long-term stability during measurements or during long-term storage is a very important parameter in different fields, e.g. storage of glucose sensor stripes for diabetes patients or long-term measurements of the ocean acidification.

- *Robustness.* Sensors are sometimes applied under harsh conditions, such as high temperatures, high pressure or extreme mechanical stress, and should ideally withstand them.

Besides these parameters, a sensor system should be easy to miniaturize and free of drifts, this means an appropriate protection against interferences should be applied, too. A sensor should feature fast response and recovery times and easy-to-use-facilities. Ideally, materials, production, maintenance and use should be cheap.

Optical Chemical Sensors

In case of optical chemical sensors the transduction mechanism is based on optical properties of the analyte itself or an analyte-sensitive intermediate (here called *indicators* or *indicator dyes*). Although there are challenges to meet, optical chemical sensors show several advantages in comparison to routine techniques (e.g. electrochemical sensors).

Challenges:
-   In general, the indicator dyes (in case of reagent-mediated sensors) should feature good photostability (bleaching prevention), high molar absorption coefficients and quantum yields (high brightness), the possibility to tune their sensitivity and they should be compatible with commercially available (low-cost) light sources, e.g. LEDs. Ideally, they feature self-referencing spectral properties and the structural conditions for a covalent coupling to the matrix.
-   Matrix materials should show a low pH-dependent swelling and the possibility of covalent coupling of the indicator to prevent leaching. The water uptake should be high for pH sensors, but low for CO_2 sensors. In case of multi-layer systems the adhesion between the single layers and the support (fiber or planar support) should be robust against mechanical and chemical stress.
-   Optical pH sensors show dependency on the ionic strength and a narrow dynamic rang (pK_a ±1.5 pH unit).[39]

Advantages:
-   In general, optical chemical sensors are easy to miniaturize and inexpensive.
-   Via fiber optics measurements can be carried out in certain distances to the sample site.
-   The read-out can be carried out in a non-contact mode via an optical window, e.g. in food packaging applications.
-   There is no need for a separated reference element (as e.g. in precision electrochemical sensors). Analyte-insensitive reference materials can be combined with the analyte-sensitive chemistry in one sensing layer or one makes use of self-referencing indicators. Self-referencing indicators are more robust and counteract signal changes caused by leaching, photodegradation or aggregation.

- Optical sensors do not suffer from interferences of magnetic fields.
- *Plastic type* CO_2 sensors are less affected by the ionic strength, than e.g. the Severinghaus electrode.
- Optical sensors are easily tunable concerning their dynamic range and sensitivity. In case of optical carbon dioxide sensors, the sensitivity of the sensors can be tuned via the indicator (pK_a value), the matrix and the base.

Optical chemical sensors can be influenced by various parameters, such as the sample composition, temperature, sample polarity, viscosity or electrochemical properties. On one hand, this enables optical sensors to measure these parameters, but on the other hand, measurements are also influenced by them. Hence, experiments/measurements should be carried out thoughtfully with respect to possible cross-talks.

Sensor Geometries

Optical chemical sensors can be manufactured in different geometries. The most popular category is the fiber optic chemical sensor (FOCS) platform,[38] using optical fibers to guide the optical signal back and forward to the sample. FOCS can be divided into active and passive formats. Active describes a direct modification of the fiber itself, whereas for passive formats the fiber is only used for the transport of the optical signal. Passive FOCS are often combined with a planar optode system at the end of the fiber. Planar waveguide chemical sensor (PWCS) platforms represent the second biggest category. Here, the actual sensing element is placed on a support (glass or plastic), which can act as wave guiding element or only as support.

Both types, FOCS and PWCS are using mostly the transduction mechanisms of absorption and luminescence. Colorimetric measurements (absorption) show lower sensitivity, but are highly robust. Especially when the color change is preferred to be also visible with the naked eye, absorption based sensors are widely used. Fluorescence measurements are highly sensitive, cheap, easy to miniaturize and easy to carry out e.g. excitation and emission light can be guided through the same fiber and can be separated via an optical filter system. Besides, also the utilization of reflection or refractometric principles is common.

Measurement Principles

One can distinguish between direct and reagent-mediated sensing.[38] Direct sensing uses the intrinsic optical properties of the analyte itself, such as absorption or luminescence. In case of reagent-mediated sensors the optical properties of an analyte-sensitive intermediate agent are utilized (*indicator dye* or *indicator*), especially when the analyte does not show any useful optical properties. One third category, that should be noted, are *ionophore-based sensors*. These sensors are not only based on an analyte-sensitive intermediate. The analyte is registered by a receptor (ionophore), which does not show any photophysical changes itself, but initiates another secondary process with respective spectral changes.[40,41]

However, there are several sensing principles that can be made use of, especially for reagent-mediated sensing. This thesis focuses on absorptive and fluorescence based principles using pH-sensitive indicator dyes.

The following list shows an overview of the most popular principles:

- *Absorption*. Here, an analyte-dependent change (increase, decrease or ratiometric) of the absorption maximum (UV-Vis range or near infrared) is observed. Colorimetric measurements are generally very robust, but less sensitive than fluorescence based principles. Absorption based optical sensors are used especially when the color change should be visible with the naked eye.

- *Luminescence*. Luminescence in general represents a versatile and promising tool for detection (directly or reagent-mediated). Not only its intensity can be used, but also the spectral properties, its polarization or its temporal behavior. Thus, luminescence enables a wide field of applications, e.g. monitoring at high sample throughput or imaging.

  In case of fluorescence, the analyte-dependent changes of different parameters, e.g. decay time, energy transfer, quenching efficiency, intensity, polarization can be used. Fluorescence based methods feature high sensitivity and are relatively easy to realize.

  Phosphorescent emitters are often used as references or as secondary emitters for colorimetric indicators (Inner-filter effect).[42]

- *Refractive index (Reflection).* For measuring the refractive index (RI), the optical fiber is partially decladded, light is sent through and detected on the opposite fiber end. Thus, the refractive index of the investigated sample is measured.[43,44] A special

case of these kind of sensors is the *surface plasmon resonance (SPR) technique.* SPR is also based on the measurements of the refractive index of a thin layer of the sample of interest, which is adsorbed on a metal layer.[45] Via the thickness and composition of the metal layer the sensitivity of the sensor can be tuned.[46,47]

- *Reflectometry (Backscattering).* This technique is based on the reflected (backscattered) light response of the investigated sample after an initial light impulse. It is also called *optical time domain reflectometry.*[48]

Materials

Optical chemical sensors can be tuned and enhanced for the requirements of the measurement via "twisting screws" like the matrix or the indicator. In general, the adhesion of the sensing chemistry to the wave guiding elements (fiber or planar support) should be good and the support materials should not absorb light or show background fluorescence.

Demands like high photostability, chemical stability, high molar absorption coefficients, high quantum yields, compatibility with low-cost excitation sources and a tunable sensitivity occur in case of the indicator dyes, which are the core components of reagent-mediated optical sensors. Indicators with absorption/ luminescence intensity maxima in the near infrared (NIR) region are highly desirable for several reasons, e.g. dramatically reduced autofluorescence, low light scattering and the availability of low-cost excitation sources and photodetectors.

Quantitatively, the matrix is the main component of an optical sensor. The indicator dye (and possible other additives) is immobilized in the matrix. The easiest way of immobilization is to simply embed the indicator. However, to prevent e.g. leaching, it is preferred to immobilize the indicator dye via covalent coupling. Thus, leaching is prevented, signal stability is enhanced, signal drifts diminished and long-term applications are promoted. Hence, matrix materials should feature the structural possibility for covalent coupling, as well as the indicators. Additionally, matrices should be mechanically and chemically stable and they should take up adequate water (high uptake for pH sensors; low uptake for CO_2 sensors), but should display a low pH-dependency of the swelling (in case of pH sensors) and the required permeability or analyte-dissolving properties.

In this thesis optical carbon dioxide sensors based on pH-sensitive indicator dyes are used. In the following sections state-of-the-art materials for optical pCO_2 sensors will be described. Additionally, caused by the relation to optical pH-sensors, materials for these sensors will be briefly described, too.

Matrices

pH-sensors. For an optical pH sensor the matrix should be able to take up water and therefore should be proton-permeable. Hence, the major part of optical pH sensors uses hydrophilic matrix materials,[39] such as cellulose and its acetates, polyurethane hydrogels or polyacrylamides, but there are also less hydrophilic or even hydrophobic alternatives, like sol-gels (less hydrophilic) or poly(vinyl chloride) (hydrophobic). The latter category requires proton carriers, such as tetraphenylborate or similar.[39]

Carbon dioxide sensors. In earlier days, so called *wet sensors* based on buffer systems were used, separated from the sample via a gas-permeable and ion-impermeable membrane. When the water vapor pressure or the osmotic pressure of the sample was extremely different to the sensor system, hydration/dehydration occurred and recalibration was necessary.[49] Additionally these systems suffered from intensity loss at high pCO_2 values and very slow response times at low pCO_2 levels.

To overcome the drawbacks of the wet sensors, so called *dry sensors*, where *plastic type sensors* developed by Mills et al.[50,51] are the most common ones, were developed. Here, the indicator dye is embedded in the polymer matrix together with a base (lipophilic buffer), mainly a quaternary ammonium hydroxide. For optical carbon dioxide sensors the water uptake of the matrix should be low. Hence, the polymer matrix should be rather hydrophobic, permeable for carbon dioxide and impermeable for charged species like protons, to prevent interferences by the pH of the (aqueous) sample. If the sensor matrix itself can not fully meet these demands, a protection layer, e.g. silicone, is necessary and acts as proton barrier. State-of-the-art polymer for optical carbon dioxide sensors is ethyl cellulose with varying ethoxyl contents, although it shows a quite strong temperature dependency and sensors show rather moderate long-term stability. Hence, alternatives like amorphous perfluorinated polymers (PTFE derivatives) are under investigation.

Indicators

Indicator dyes show ideally different spectral or photophysical properties with changing analyte concentration. For both, optical pH and carbon dioxide sensors, the pK_a value of the indicator dye can give information about the dynamic range of the sensor. In case of pH sensors, the optical sensors show the highest sensitivity in the equivalence point of the titration/ calibration curve (pH = pK_a; see also Henderson-Hasselbalch equation). Hence, the rule of thumb means the dynamic range is ~pK_a ± 1.5 pH unit, with respect to the fact that the pK_a value can be influenced by the environment, e.g. by the matrix. For carbon dioxide sensors the rule of thumb says the higher the pK_a value of the indicator, the higher the sensitivity. The higher the pK_a values the less carbon dioxide is necessary to protonate the indicator, although this rule is rather applicable if one compares indicators with similar structures.

Generally, one can classify pH-sensitive indicators as *PPT (photoinduced proton transfer)* indicators, *PET (photoinduced electron transfer)* indicators or no PPT/ no PET indicators.

- *Indicators that show PPT (figure VII)*, e.g. 1-hydroxypyrene-3,6,8-trisulfonate (HPTS; proton donor; $pK_a^* < pK_a$), have a different electron density in the excited state than in the ground state. Therefore, they show different pK_a values in the excited state than in the ground state (lower pK_a for proton donor molecules; higher pK_a for proton acceptors). This leads to a rather fast deprotonation (donors) or protonation (acceptors) of the molecule. According to this acid-base behavior, both, the absorption and luminescence spectra feature pH-dependency.
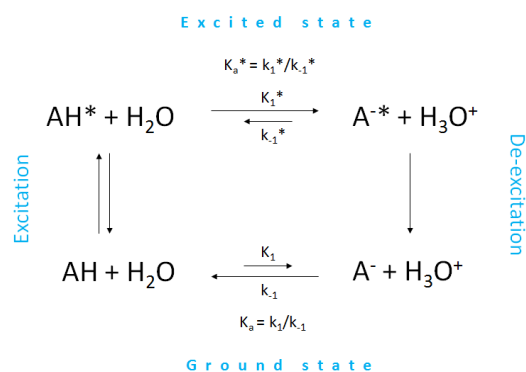

Figure VII. *Scheme of photoinduced proton transfer (PPT)*[36] *of an acidic dye (donor molecule; $pK_a^* < pK_a$). K_a and K_a^*: protolysis equilibrium values in the ground/excited state.*

- *PET indicators* are chromophores (fluorophores) that become pH-sensitive by attaching phenols or amines to their structure, also called PET-groups.[52–55] These PET-groups are acting as electron donors and hence, reduce the excited fluorophore (photoinduced reduction). Hence, fluorescence is enhanced with increasing protonation of the PET-group (figure VIII).
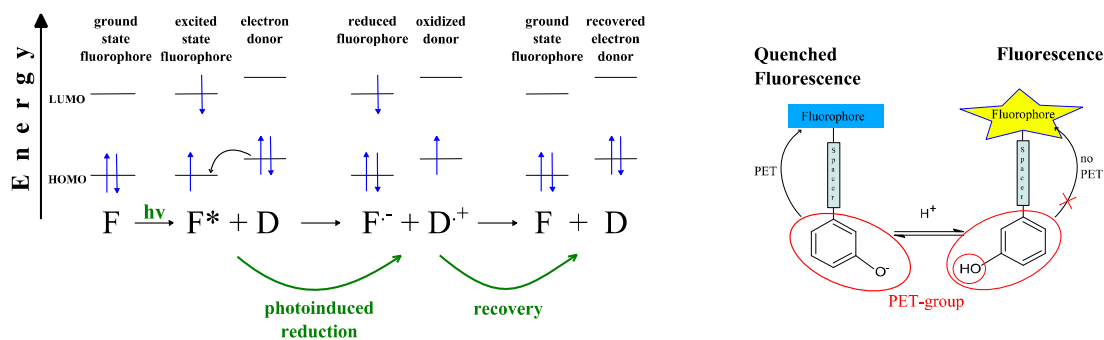

Figure VIII. *Scheme of photoinduced electron transfer (PET).*

- *Indicators that show no PPT or PET* feature still changes in absorption and luminescence spectra related to a pH change. Although, this is not based on an acid-base behavior, but on several processes, e.g. protolysis and lactonization equilibria in case of fluorescein and its derivatives.

Common colorimetric pH-sensitive indicators for the UV-Vis range are triphenylmethane dyes like thymol-blue[56,57] or *m*-cresol-purple[57,58] or phenol-red.[59–61]

Widely used fluorescent pH-sensitive indicators for the UV-Vis range are fluorescein and its derivatives,[62] coumarin and its derivatives[63] or 1-hydroxypyrene-3,6,8-trisulfonate (HPTS; excitable in the blue range of the spectrum) and its derivatives.[50,57,64–67]

Common pH-sensitive indicators for the near infrared (NIR) region would be SNARF (seminaphthorhodafluors) dyes,[68] cyanine dyes[69,70] or aza-BODIPY indicators.[71]

Carbon dioxide sensors. For optical carbon dioxide sensors based on the acid-base chemistry of pH-sensitive indicator dyes (described above) state-of-the-art indicators are thymol-blue, *m*-cresol-purple and especially HPTS (table IV) for fluorescence based sensors.

Thymol-blue and *m*-cresol-purple are displaying two protonation steps, that means two pK_a values, where the first one is too low to show up in optical carbon dioxide sensors. Here, only the pK_{a2} values are relevant for the dynamics of the optical sensors. Both dyes show a rather low photostability and are only colorimetric indicators. To enable luminescence read-out systems based on these dyes, one could make use of the so called *inner-filter effect*, where the light of one or more secondary emitters is filtered according to the pH-dependent colorimetric change of the indicator (figure IX).
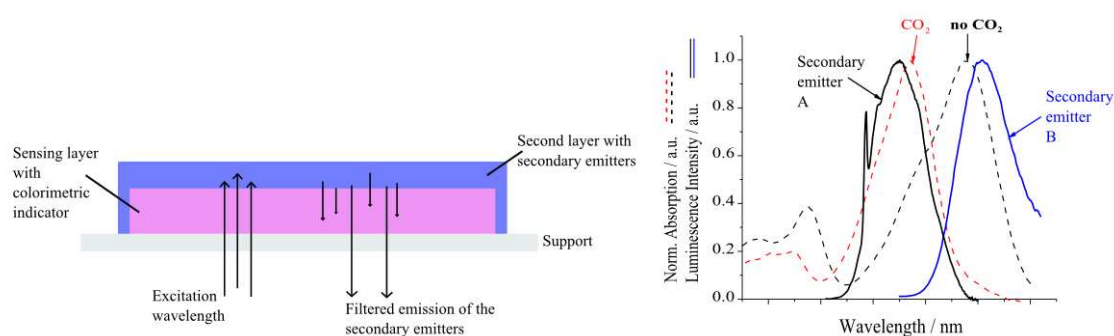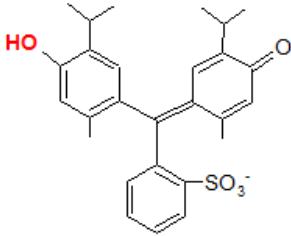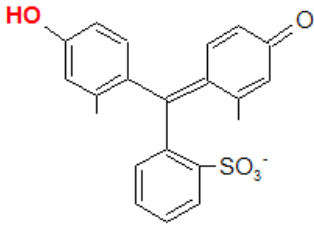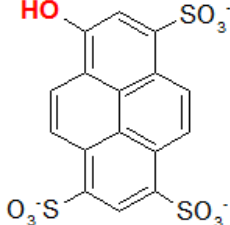
Figure IX. *Scheme of the inner-filter-effect*. ***Left***: *layer system of the sensor*. ***Right***: *Spectral theory*.

HPTS was for a long time the indicator of choice for optical carbon dioxide sensors, because of an ideal pK_a value, high stability and a large stokes shift (~60 nm for the ionic form in solution; see table IV).[49] However, HPTS suffers from maxima at rather short wavelengths for both forms, where only the ionic form is excitable in the blue part of the spectrum. Addition of reference materials is often necessary to achieve reliable measurements, but photobleaching (indicator, reference dye or both) can cause a dramatic ratio change in this scheme.

Hence, alternative self-referencing (dual-emitting) indicators which overcome these drawbacks, preferably in the NIR region, are highly desired.

Table IV. *State-of-the-art indicators for optical carbon dioxide sensors: structures with respective pK$_a$ values; absorption and emission maxima for both, protonated and the ionic (deprotonated) form. Deprotonatable sites are marked in red; Properties of thymol-blue,[57] m-cresol-purple[57] and HPTS[50,57] measured in aqueous solution.*

Thymol-blue	m-cresol-purple	HPTS
pK$_{a2}$ 8.86 Absorption: $\lambda_{max,prot}$ 432 nm $\lambda_{max,ionic}$ 590 nm	pK$_{a2}$ 8.28 Absorption: $\lambda_{max,prot}$ 428 nm $\lambda_{max,ionic}$ 571 nm	pK$_a$ 7.3-8.0 Absorption: $\lambda_{max,prot}$ 403 nm $\lambda_{max,ionic}$ 455 nm Fluorescence: $\lambda_{max,prot}$ 435 nm $\lambda_{max,ionic}$ 512 nm

- *Bases (lipophilic buffer).* As mentioned before, optical plastic type sensors need a base, also called lipophilic buffer. It keeps the deprotonated (anionic) form of the indicator dissolved in organic solvents/polymers. Here, quaternary ammonium hydroxide bases,[57,72] e.g. tetraoctylammonium hydroxide (TOAOH), tetrabutylammonium hydroxide (TBAOH) or hexadecyltrimethylammonium hydroxide (CTA; also cetyltrimethylammonium hydroxide) are the most common ones. The alkyl chains should be long enough (hydrophobicity) to keep the base in the polymer. However, by varying their length one can slightly tune the sensitivity of an optical carbon dioxide sensor, e.g. TOAOH is the most sensitive one of the presented three.

Carbon Dioxide Sensor Preparation

First, a so called *cocktail* containing the matrix material and the indicator dye dissolved in an organic solvent is prepared and flushed with carbon dioxide gas. Afterwards the base is added to achieve the final cocktail.

In case of PWCS the final cocktail is knife coated with a certain film thickness to obtain extensive sensor foils, suitable for example for imaging. Sensor spots can be achieved via pipetting small volumes on a planar support or cutting the knife-coated planar optode. In general, the sensor layer should be rather hydrophobic, which is negligible in case of gaseous samples at room temperature. If temperatures are extremely high or low humidity can condensate. In this case and for aqueous samples a protection layer, e.g. silicone, is necessary (figure X), because the sensor matrix itself can not fully meet the demand of proton exclusion,
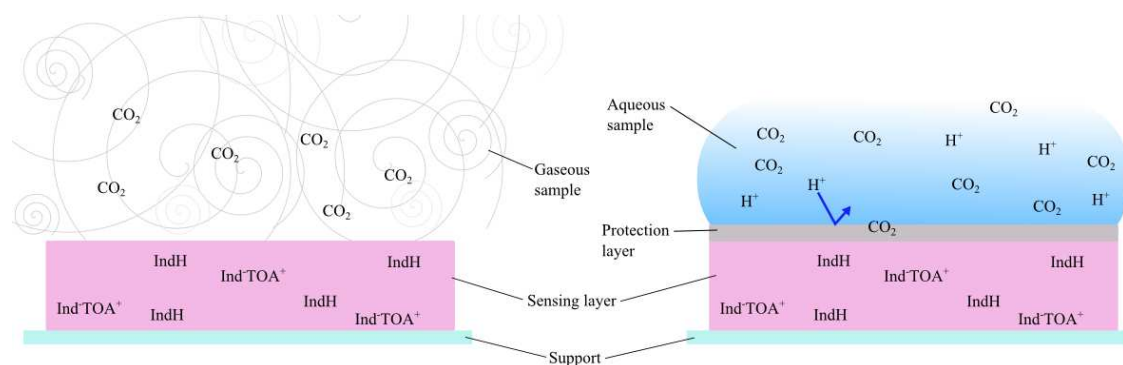
Figure X. *Scheme of sensor with/without protection layer.*

For fluorescence based sensors light scatterer, e.g. titanium dioxide, can be added to the sensor layer or the protection layer to enhance the signal intensity. It has to be ensured, that the scatterer is well dispersed and the particle size is small enough. Otherwise so called *pinholes* can be built and the sensor might show cross-talk to the samples pH value.

In case of FOCS the fibers can be dipped into the cocktail (mainly for micro sensors) or one can cut the knife-coated planar optode and fix it to the fiber end.

Fields of Application - Optical Carbon Dioxide Sensors

Optical carbon dioxide sensors represent a promising tool for a variety of applications, such as:

- Biotechnology (bioprocess monitoring)
- Medicine (capnography; blood gas analysis)
- Environmental science (monitoring of atmospheric carbon dioxide levels and environmental processes)
- Meterological science
- Marine science (observation and investigation of ocean acidification and its effects on the marine ecosystem)
- Chemical industry (process monitoring and controlling)
- Food and beverage science/industry (controlled atmosphere packaging; gas diffusion into packages)

Fields like capnography or food packaging are dealing with rather high pCO_2 values and require less sensitive sensors, e.g. the pCO_2 value of the exhaled air of the human body contains around 3 to 6 kPa. Modern food packaging methods, also called MAP (modified atmosphere packaging),[73–75] use defined gas atmospheres, where oxygen is excluded. The artificial atmosphere can be pure carbon dioxide, e.g. for bakeries,[75] or a mixture of nitrogen and carbon dioxide. In the case of vegetables and fruits the pCO_2 value should be kept around ~5 kPa.[73]

In marine science the sensors have to meet different requirements. The atmospheric level of pCO_2 (0.04 kPa ≈ 400 µatm in the gas phase ≈ 11.6 µmol/l in seawater at 298.15 K), which is in equilibrium with the upper layer of the ocean requires very sensitive sensors. On the other hand, there are volcanically active sites, e.g. the Aeolian Islands (Sicily, Italy) in the Tyrrhenian Sea, where carbon dioxide is outgasing from the seafloor, either continuous (bubbling) or discontinuous (CO_2 enriched pore water affected by tides). Around these seeps the pCO_2 value in the seawater can reach increased levels (up to several thousand µatm).

Comparison: Carbon Dioxide Detection Methods for Marine Applications

Introduction

So far only optical chemical sensors from the so called *plastic type* were discussed, as the focus of this thesis was on these sensors. This section will give an overview on routine techniques for measuring carbon dioxide in marine environments based on a technical report written by S. Schutting and D. de Beer (2013; deliverable number D3.2 of the EU-project ECO2 (project number 265847); *Technical report on chemical sensor performance*; DOI 10.3289/ECO2_D3.2.).

Technical data sheets were obtained from the homepages of CONTROS GmbH (www.contros.eu) and Microelectrodes Inc. (www.microelectrodes.com). Additionally, written requests via email were sent to CONTROS GmbH to Melanie Herrmann. Data and information about the GasPro – dissolved CO_2 probes were received from S. Graziani (Sapienza University of Rome – CERI).

After a brief description of the most widely used sensing techniques for carbon dioxide, commercially available sensing techniques will be compared in detail with alternative prototype devices – the GasPro – dissolved CO_2 probes and the multi-branched optical carbon dioxide sensor system (MuFO; see also chapter 4) – concerning operational parameters of the sensors and sensing systems.

The technical information will be complemented with experiences from users. In 2012 the HydroC device from CONTROS, the MuFO, the GasPro – dissolved CO_2 probe and a profiler with different electrodes were tested on a field trip at Panarea Island (Sicily, Italy). Here, the feedback of the diving team is summarized. In 2013 the MuFO device was used for a lab experiment at SAMS (Scottish Association for Marine Science) Institute in Oban (Scotland) and the feedback of the users is also summarized.

Carbon dioxide can be measured optically or electrochemically. The most relevant detection method based on electrochemistry is the Severinghaus electrode. Optical techniques are infrared spectroscopy, spectrophotometry or optical chemical sensors.

Severinghaus electrode. The Severinghaus electrode was developed in the late 1950´s and was long time the method of choice for measuring pCO_2 in solutions, especially in blood.[76–78] It consists of a pH glass electrode, which is placed in a buffer chamber

(mostly sodium bicarbonate solution). The buffer is separated from the sample via a hydrophobic gas-permeable and ion-impermeable membrane, where CO_2 can enter the chamber, but ions can not. CO_2 then reacts with the buffer solution in the following way:

$$CO_2 + H_2O \leftrightarrow H_2CO_3 \leftrightarrow HCO_3^- + H^+$$

The protons change the pH value within the buffer chamber. Thus, the CO_2 caused pH change is measured by the pH electrode.

The Severinghaus electrode shows excellent selectivity.[79] However, compared to optical chemical sensors based on the same reaction principle, the electrode suffers from electromagnetic interferences and has a slower response.

Infrared (IR) spectroscopy. IR spectroscopy is a direct measurement method. An infrared spectrum is like a fingerprint of a molecule, as in case of carbon dioxide. Organic molecules absorb infrared radiation and convert it into energy of molecular vibration. Carbon dioxide shows characteristic vibrations at 2349 cm^{-1} (asymmetrical stretch) and at 546 cm^{-1} (bending vibration), which are observable in the IR spectrum, because of a dipole change.[80] The symmetrical stretch at 1735 cm^{-1} is inactive in the IR, because it does not change the dipole of the molecule.

IR spectroscopy is used in several fields as detection method of choice,[81] for example medicine (capnography),[82,83] investigation of the carbon cycle (soil respiration)[84] and others. It is a fast[61] and non destructive method, but is mostly suitable for measurements in gaseous phase[85,86] since water causes a significant interference. The instruments are usually rather bulky and expensive.

Sepctrophotometry. This detection technique is an indirect measurement making use of the pH affecting property of carbon dioxide by applying spectrophotometry within an equilibrated pH-sensitive dye solution of known characteristics.[87,88]

The compared *optical carbon dioxide sensors* are based on the following principle:

$$CO_2 + H_2O + Ind^-TOA^+ \leftrightarrow TOA^+HCO_3^- + IndH$$
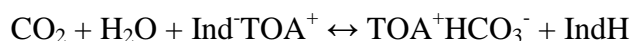
In these so called *plastic type sensors*[50,51,57,89] the indicator dye (Ind^-; IndH) is embedded in the polymer matrix together with a base (TOA^+; lipophilic buffer). When CO_2 and water form bicarbonate ions and protons, the protons are changing the

33

protonation state of the indicator dye. The indicator ideally features different spectral properties for both, the protonated and ionic (deprotonated) form, which can be used for analysis. Materials (matrices, indicators and bases), measurement principles, as well as sensor geometries have been already discussed in previous chapters of this thesis. These optical carbon dioxide sensors feature low affection by ionic strength, are easy to miniaturize and are therefore, a promising alternative to the presented up-to-now-routine techniques.

Besides these techniques, carbon dioxide can also be analyzed via *Gas chromatography (GC)*. Gas chromatography is a very popular detection method for carbon dioxide and other greenhouse gases.[90] State-of-the-art equipment would be e.g. PORAPLOT Q or PORAPLOT Q UltiMetal from Agilent Technologies (www.agilent.com) and a thermal conductivity detector (TCD) or a barrier ionization discharge (BID) detector.

It shows high sensitivity and high sample trough-put,[90] but in case of non-gaseous samples, for example seawater, a respective sample preparation or accurate sampling is necessary. Therefore, a direct on-line measurement, e.g. in marine science, is hardly realizable and the sample preparation is mostly cost- and time consuming.

Technical Comparison

Here, a comparison concerning operational parameters of the carbon dioxide sensors and sensing systems listed below will be shown and summarized in table V in the end of this section. Companies and developing scientists often provide the measuring range of their devices in ppm without specifying which ppm is meant: either mg CO_2/l or volume percent* 10000 at 1 atm. In the following section the units given from the manufacturer will be listed, as well as a respective concentration in µmol/l or similar. The carbon dioxide concentration can be calculated from partial pressure, temperature and salinity. Hence, the accuracy of the CO_2 measurements is not only dependent on the sensors behavior, but also on the accuracy of these parameters. Compared systems will be:

- HydroC from CONTROS GmbH
- GasPro (dissolved CO_2 probes) from Sapienza University of Rome
- Optical chemical sensors (MuFO) from Graz University of Technology
- Severinghaus CO_2 sensors (microelectrode MI 720) from Microelectrodes Inc.

HydroC (CONTROS GmbH)

Figure XI. *HydroC device from Contros (Picture © CONTROS).*

Principle. The HydroC from CONTROS GmbH is an underwater carbon dioxide sensor for in-situ and online measurements of dissolved carbon dioxide, which is already commercially available. Dissolved gas molecules diffuse through a thin-film composite membrane into the detector chamber, until equilibration is reached between the gas chamber and the water phase. Inside the chamber the CO_2 concentration-dependent IR light transmission is recorded. To shorten the response time, water is continuously pumped across the membrane with a rate of 100 ml/sec. The logger is designed to measure in the water column.

Stability/drift. The system is very stable, adaptive for long-term measurements and so called *zeroing*s (regular zero gas measurements during the employment) can be carried out. An annual recalibration carried out by the manufacturer is recommended. Explicit information about the life time of the sensor was not available. However, during the annual calibration wearing parts may be renewed. Hence, in theory there may be no limitation of lifetime.

Temperature range. CONTROS offers two versions of the HydroC: A normal version with a temperature range from +3 to +30°C and an arctic version with a temperature range from -2 to +15°C.

Response time. The t_{63} response of the sensor is <1 min and the t_{90} response is around 2.5 min. The exact response time can be obtained anytime during the deployment by analyzing the signal recovery after a zeroing procedure. The actual temporal resolution can be higher than the response time if a time-lag-correction algorithm is applied on the data.[91]

Measuring range. The standard measuring range is from 200 to 1000 ppm or, if required, the calibration can be extended up to 6000 ppm. As calculation in mg/l would result in an impossible range for dissolved CO_2 (200-6000 mg CO_2/l), it is assumed, that this values correlate to $6.8*10^{-3}$ to $3.4*10^{-2}$ mmol/l and $2.0*10^{-1}$ mmol/l, respectively.

Maintenance. The HydroC device has a power consumption of 300 mA and additionally 600 mA for the water pump. The power consumption can be customized by using the integrated sleep mode and a smaller (less consumable) water pump, as well as by adapting the temperature control settings of the sensor. The device can be powered either via cable, by non-rechargeable batteries or by rechargeable batteries. The latter can be charged via cable while they are inside of the housing. The membrane should be changed (by the user) every 3 months in case of continuous use or when strong fouling occurs. An annual recalibration of the HydroC device is recommended.

Deployment. CONTROS offers the HydroC device as a "Plug and Play" system including the software, a sensor manual and an USB adapter, as well as a connection cable for configuration or lab purposes. The HydroC can be easily handled under water by only one person. Besides stationary measurements on moorings, it can be used for transect measurements by trawling, scuba divers, an AUV (autonomous underwater vehicle) or a ROV (remotely operated underwater vehicle). Measurements in the sediment are not possible. Due to different types and sizes of power sources, the deployment time depends on the frequency of measurements and the power consumption of the device. The turnover time can be only one hour, including data download, data check and battery exchange.

Userfriendliness. The system shows high accuracy (1%), it has an internal datalogger and can be connected to other devices, e.g. a CTD (conductivity, temperature and depth measuring device). The software is understandable and easy to use. Data can be processed fast. Additionally, CONTROS offers assistence for an optimal configuration of the device to meet the requirements of the user.

Depth. The device can be used up to 6000 m water depth.

Size. ø 90 x 376 mm, 4.7 kg in air (2.2 kg in water)

Costs. The HydroC device is commercially available for around 24000 € (Generation II with Sea-Bird pump SBE-5T, 2000 m depth rating, 200-1000 ppm, RS 232, +3 to +30°C, SubConn connector, internal datalogger) including an accessories kit (software detect 2.0 incl. manual, 3 spare membranes, USB 2.0 to RS 232 adapter, sensor manual

and certification), cable equipment and offshore case. 5 membranes are available for 500 €. An annual recalibration costs 1750 €

GasPro - Dissolved CO₂ Probes (Sapienza University of Rome)

Figure XII. *The GasPro - Dissolved CO₂ probe.*

Principle. The GasPro device is a small, light-weight, accurate and low-cost prototype for long-term monitoring applications and is in continuous development. Different configurations are in use to meet the requirements of different environments, site conditions and experimental demands. The device measures dissolved CO_2 in water, in the gas phase or in the soil. In case of measurements in the water phase the partial pressure of the surrounding dissolved gas is measured. Here, the dissolved gas molecules diffuse through a TeflonAF membrane into the small-volume detector chamber. The detector is a 20 mm ø CO_2-NDIR cell. In the following, the model "GasPro-pCO_2" for deployment in marine environments up to a depth of 50 to 60 m is presented. The device is designed for long-term applications and therefore, developed with low power consumption. Thus, pumps are usually not integrated in the system, although they can be adapted for a faster response e.g. during short-term measurements. *Stability/drift.* Although, there is usually no artificial hydrodynamics (no pumps) that can enhance the prevention of biofilm growth, the membrane material is rather resistant against biofouling. In case of highly eutrophic environments an occasional cleaning of the membrane is recommended to prevent drifts. No zeroing can be performed with this

system. The sensors and logger are highly robust. So far no failure was observed during deployment. No data on the total life time of the system is available.

Temperature range. The probe operates at temperatures from 0 to 40°C.

Response time. The sensor shows a t_{90} response time of 40 sec. However, the unit response time depends on gas diffusion rates across the membrane and equilibration between the gas volume of the sensor chamber and the surrounding water. Without pumps the systems response depends on currents and concentration gradients, with a minimum of ~2 min being required.

Measuring range. The measuring range (zero resolution 1 ppm) is 0 to 5000 ppm (0 to $1.7*10^{-1}$ mmol/l) with a full scale resolution of 15 ppm ($5.1*10^{-4}$ mmol/l). If required, the device can be calibrated to higher ranges.

Maintenance. The device can be powered either by non-rechargeable batteries for long-term applications (must be replaced after approx. 4000 measurements) or by rechargeable batteries (chargeable via a cable). The loggers require 2 batteries. The integrated data logger and low power consumption (6-12 VDC; warm-up 2-30 min/40 mA) of the sensor make it suitable for long-term monitoring with sample frequencies of either 1/min, 1/10min, 1/hour, 1/day, 1/week or 1/month. The data format is ASCII with real time clock information (date, hour, minute, second; resolution: 1 sec).

Deployment. Besides batteries no exchange of parts is needed between deployments. If the batteries need to be exchanged, the turnover time is about 1 hour, including removal of biofouling. The GasPro device can be used as stand-alone (SD-card as removable memory) or connected to control units for data transmission in real time. Downloading of 4000 data points takes approximately 10 minutes. The operation time depends on the measurement interval. When measuring every 10 minutes, the batteries will have sufficient power for at least 4 weeks. When the interval is longer, the deployment time can be proportionally longer.

Userfriendliness. As it is a prototype the software is simple, the interface may be improved and manuals are not available. The servicing, calibration and redeployment can be done by only one person. Without a pump the battery life was very long and the device could be shifted from location to location without need of battery change.

Depth. Under water it can be used at operation depths of 60 m (standard), 100 m or 200 m.

Size. ø 78 x 283 mm, 0.7 kg in air (slightly positively buoyant in seawater).

Costs. The material costs for the dissolved CO_2 probe up to now are appr. 2500 € (hours of work not included). 2 batteries for loggers cost 27 € each. Depending on both the housing materials and the machining for the different prototypes the costs can vary widely.

Optical Chemical Sensors/ MuFO (Graz University of Technology)

Figure XIII. Optical chemical sensors combined with the multi-branched optical carbon dioxide sensor system (see also chapter 4). 100 optodes positioned on a stick in bundles of 20 fibers each.

Principle. This sensor system features 100 freely positionable CO_2 optodes with collective excitation source and read-out. The optodes can be positioned anywhere in the habitat, within the range of the optode length. It can thus provide the CO_2 dynamics in many sites within that habitat, including e.g. sediments, watercolumn, musselbeds, corals, etc. The measurement principle is based on optical chemosensing. The principle of the multi-branched optical carbon dioxide sensor system is described in more detail in chapter 4 of this thesis.

Stability/drift. The photostability of the used dye and the protection ability against poisoning of the sensor are the limiting factors during long-term measurements. The sensing foils on the fiber tips should be exchanged periodically (time interval depends

on the dye and the illumination intervals). Information about the life time is not yet available as the development of the MuFO system is still ongoing.

Temperature range. So far the optical sensors of the prototype were tested in a temperature range from +5 to +35°C. Their temperature-dependence is quite high. Therefore it is necessary to either calibrate at the same temperature as the measurement (if the measurement temperature is expected to be rather constant) or to develop a mathematical description of the temperature-dependence. In the latter case the temperature has to be monitored next to the sensors to include it later on in the data analysis.

Response time. Generally, the optical CO_2 sensors measure continuously. In case of alternating pCO_2 values in the laboratory the t_{90} response time was about 20 sec. At lower pCO_2 values the response times can be even longer.

Measuring range. The measuring range of the optodes can be adjusted to the requirement of the user starting from ~200 ppm ($6.8*10^{-3}$ mmol/l) up to a few thousand ppm (e.g. 5000 ppm = $1.7*10^{-1}$ mmol/l) by choosing the suitable dye for the desired concentration range.

Maintenance. The accumulators of the MuFO have to be charged via cable after appr. 24 h of permanent use (duration of charging: ~10 h). The accumulators of the camera have to be recharged or exchanged every 9 h (duration of charging: ~2 h) and are the limiting factor for the deployment length. Data are saved to the SD card of the camera. For both, charging the camera batteries and downloading the data, the camera has to be removed from the MuFO housing, after which the camera has to be refocused. Thus the turnover time between deployments is approximately 10 hours.

Deployment. The MuFO prototype has an operating software and manuals for the sensor preparation, the calibration, the general handling and the software. Connected to a computer it can be controlled manually, e.g. for lab-applications, or programmed for an auto-start for a later measurement, e.g. for the diving team. The sensor tips are flexible, robust and well protected by metal sleeves. The contact surface is very small (ø ~1.5 mm). Thus, the optodes can be used for profiling too, either in a fixed array of sensors or by using a single optode that penetrates the sediments step wise. Measurements in the gas phase are possible, too.

Userfriendliness. After long-term measurements the amount of produced data is huge. Therefore, the analysis can take quite a long time. The positioning of the sensors is complicated.

Depth. Up to now the optical sensors were tested in water depths down to 20 m.

Size. ø 280 x 400 mm; fiber length 5-6 m

Costs. Optodes are inexpensive (selfmade sensing foils cost up to a few € per sensor). Price-calculation depends strongly on the material costs of the read-out device. The material costs for the MuFO up to now are around 3000 € (hours of work not included).

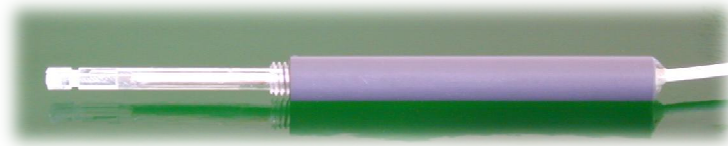**Severinghaus CO$_2$ Sensors – Microelectrode MI 720 (Microelectrodes Inc.)**

Figure XIV. *The Severinghaus CO$_2$ sensor microelectrode MI 720 (Picture © Microelectrodes Inc.)*

Principle. The Severinghaus electrode is an electrochemical sensor for CO$_2$ measurements. It is a pH electrode in a chamber with buffer solution (usually a 1 mM NaHCO$_3$ solution with a pH of 8.2). Through a membrane the CO$_2$ concentration in this chamber can equilibrate with the sample. The pH in the chamber shifts proportionally to the samples CO$_2$ level and this pH is measured.

Stability/drift. The sensors have a tendency to drift of appr. 1 mV/day (when measuring in the concentration range below 200 µM, the electrode shows a drift of about 1-3 µM per day). Therefore, they must be calibrated regularly. This limits their application for long term monitoring, although they are well applicable to monitor dynamics. As the sensing surface is small, the sensitivity to biofouling is very limited. The sensors can be used for several weeks to months, after which the membrane should be exchanged. The pH transducer has a life time of appr. 1 year. During measurements weak volatile acids can cause interferences.

Temperature range. This information was not available.

Response time. According to the specifications, the pCO$_2$ microelectrode has a response time of less than 1 min. However, stabilization times of several minutes are more typical. Therefore, measurements that are made frequently are best binned over 3 min.

Measuring range. The sensors behave log-linear from ca 3 μmol/l to 30 mmol/l, this means from below air saturation to CO_2 saturated water. The data sheet from the company indicates a range of 0.1-100 mmol/l and 4.4-440 ppm, both may be a mistake. Upon request, the company elucidated that the sensors are tested at 0.1 and 30% carbon dioxide in a gas mixture.

Maintenance. The maintenance depends on the electronic loggers on which they are mounted. The company provides an amplifier (MV-ADPT Millivolt Adapter) with a battery life of 5 years. The loggers will need further battery power for data acquisition and storage. This will depend on the brand of logger. When the amplifier MV-ADPT Millivolt Adapter is used for the primary amplification, the battery charging or exchange depends further entirely on the logger system in which it is embedded. Also the downloading of the data depends on the logger system. The time needed for maintenance of the sensor between deployments is approximately 30 minutes. The chamber with membrane has to be regularly exchanged, which is a very simple operation. After this exchange the sensor must be recalibrated.

Deployment. The servicing, calibration and redeployment can be done by only one person. When mounted on basic loggers, deployment can be done by scuba diving or snorkeling. The sensors can measure in the water column and inside sediments.

Userfriendliness. Electrodes are easy to handle. They are small and do not need complicated software solutions.

Depth. The electrode can be pressure compensated and can be used in water depths from at least 2000 m. High pressure will affect the sensor offset, thus an in situ calibration is needed. For this a water sample from the deployment depth must be taken and analyzed for pH, DIC and alkalinity. From the appropriate equilibrium values the total carbonate system can be calculated, including the pCO_2.[15]

Size. ø 6 x 86 mm

Costs. A pCO_2 microelectrode from Microelectrodes Inc. is commercially available for 490 USD (≈ 366 €). Additionally, the costs for a logger house plus electronics need to be included. The preamplifier costs 199 USD (≈ 149 €).

Table V. *Overview of technical data of different CO_2 sensors (i.n.a. = information not available). Descriptions of the principles of the respective devices are mentioned above.*

	HydroC	Optical chemical sensors	Microelectrode MI 720	GasPro dissolved CO_2 probe
Commercial availability	yes	No (prototype)	yes	No (prototype)
Response time	T_{63} <1 min T_{90} ~2.5 min	20 to 120 sec (depends on the layer thickness and the pCO_2 level change)	< 60 sec	40 sec (depends strongly on the water movement; normally 5-7 min)
Depth range	down to 6000 m	20 m (at least)	2000 m	60 m (standard), 100 m or 200 m
Costs	24000 € (standard version)	3000 € material costs (hours of work not included)	366 € (490 USD)	2500 € material costs (hours of work not included)
Costs for maintenance/ equipment	5 membranes for 500 €; Annual maintenance for 1750 €	i.n.a.	Preamplifier for ~149 € (199 USD)	2 batteries for loggers for 27 € each
T-range	3 to 30°C (standard) -2 to +15°C (arctic version)	5 to 35°C	i.n.a.	0 to 40°C
Sediment measurement	No	Yes (5 to 10 cm depth)	Yes (~1 mm depth)	Yes
Robustness	very robust	robust	i.n.a.	robust
Stability	very stable, but an annual recalibration is recommended	limiting factors: photostability of indicator dye and poisoning	i.n.a.	very stable, but daily cleaning because of biofouling can be needed
Dimensions	ø 90 x 376 mm 4.7 kg in air (2.2 kg in water)	ø 280 x 400 mm fibers 5-6 m (slightly positively buoyant in seawater)	ø 6 x 86 mm	ø 78 x 283 mm 0.7 kg in air (slightly positively buoyant in seawater)
Measuring range	200 to 1000 ppm (standard) or 200 to 6000 ppm*	6-200 µmol/l (depends on sensing chemistry)	4.4 to 440 ppm**	0 to 5000 ppm (0 - 1.7*10^{-1} mmol/l; others available)

* This is not a possible range for dissolved CO_2, as it would mean 0.2-6 g CO_2/l. Possibly meant is a measuring range of $6.8*10^{-3}$ - $2.0*10^{-1}$ mmol/l.
** Possibly incorrect. Experienced range: 3 µmol/l to 30 mmol/l

Experiences from Users

In 2012 the compared devices CONTROS HydroC, Optodes (MuFO), the GasPro – dissolved CO_2 probe and a profiler equipped with different glass electrodes were tested all together off Panarea Island (Sicily, Italy). In the submarine exhalative field located east of Panarea Island, the devices were tested at different sites with different geochemical characteristics. Sites with and without CO_2 seeping were studied. The diving teams operating with the devices were from the HYDRA Institute (Elba, Italy) and GEOMAR/CONTROS (Kiel, Germany). The GasPro device was also used during a field trip to CO_2 seeps in a coral reef in New Guinea.

In 2013 the multi-branched optical carbon dioxide sensor system (MuFO) was applied again off Panarea Island. Additionally, it was tested at the SAMS (Scottish Association for Marine Science; Oban, Scotland) from Anna Lichtschlag and Peter Taylor in a lab experiment.

The divers and scientists gave the following feedback:

HydroC. The HydroC device from CONTROS was small and very well manageable under water for the divers. On one occasion the battery was incorrectly connected and consequently the device did not log data. In the meantime measures have been taken to avoid this problem. The very short response time enabled measurements of the dynamics better than the GasPro device.

GasPro. A pump can be attached to the GasPro device, resulting in similar response times than the HydroC. The GasPro was easy to handle, because of its small dimensions. Because of its low weight it was slightly positively buoyant in seawater and the divers had to attach additional weight on the device. Near seeps with strongly reducing fluid chemistry biofouling occurred on the membrane, that had to be removed every 3 days *(it should be noted, that all sensors suffered from biofouling near these seeps)*. Use of an external pump would have reduced biofouling of the membrane. Biofouling is most easily removed with freshwater. On one occasion a logger had stopped after 10 measurements. A file with settings appeared empty, probably because of mishandling of the software. The file was replaced with one from another logger, after which the problem was solved and did not reoccur.

Comparison HydroC and GasPro. The HydroC and the GasPro are compareable devices. The HydroC is more expensive, but this version with pump has a shorter

response time, is supported by the services of the company, can be auto-zeroed to compensate for drift and can be used at much larger depths. The tested version of the GasPro device was a low-cost solution with basic (and reliable) performance. Therefore, it can be used in larger numbers, e.g. to monitor carbon dioxide dynamics in a heterogeneous habitat surrounding a seep. Also the GasPro can be equipped with a pump to reduce response times. Obviously, the use of pumps will compromise the battery life and thereby user-friendliness. Both systems are versatile with respect to power solutions; different batteries or external power supplies can be used.

MuFO. On land the MuFO system was difficult to handle, because of the 5-6 m long optical fibers and the weight – because of slightly positively buoyant behavior in seawater, additional weights were necessary (~8 kg). These weights made it extra heavy on land. Later the optical fibers were fixed to a frame, which made handling and deployment easier. During the lab experiment the system was good to handle in principle. The battery change was complicated, because the camera had to be removed from the device every time. After changing the batteries of the camera it had to be focused again. The software was easy to understand and to handle, but the amount of data was huge and therefore, analysis took a long time.

Microelectrode. The microsensor profiler with the Severinghaus pCO_2 sensor was big and heavy on land. The divers found it difficult to transport. Special care had to be taken to prevent breaking of the electrodes on the bottom. Under water it was easy to handle except in case of high currents. The profiler was designed for deployments by winch from research vessels and can be mounted with ten different sensors. However, it is not the most elegant solution for divers. It would be possible to mount the electrodes to small loggers that can easily be handled by divers. The CO_2 electrode from Microelectrodes Inc. suffered from a higher drift than the CONTROS and GasPro devices. Advantageous was that it can be used for profiling and thus, can obtain data from inside the sediments or can be coupled to benthic (micro)biology. Another advantage was its price and ease of maintenance. Also, it could be easily mounted on a multisensor logger, thus the CO_2 signals can be compared with other parameters.
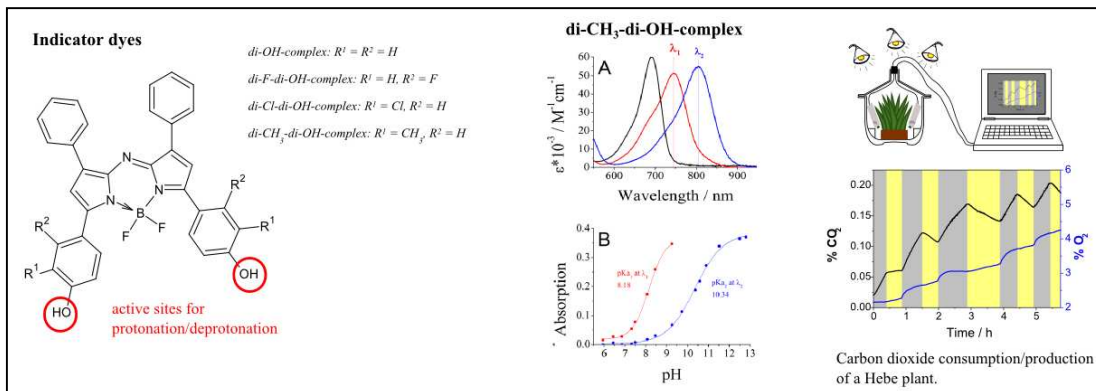
Results - Overview

Chapter 1 - Diketo-Pyrrolo-Pyrrole Dyes as New Colorimetric and Fluorescent pH Indicators for Optical Carbon Dioxide Sensors
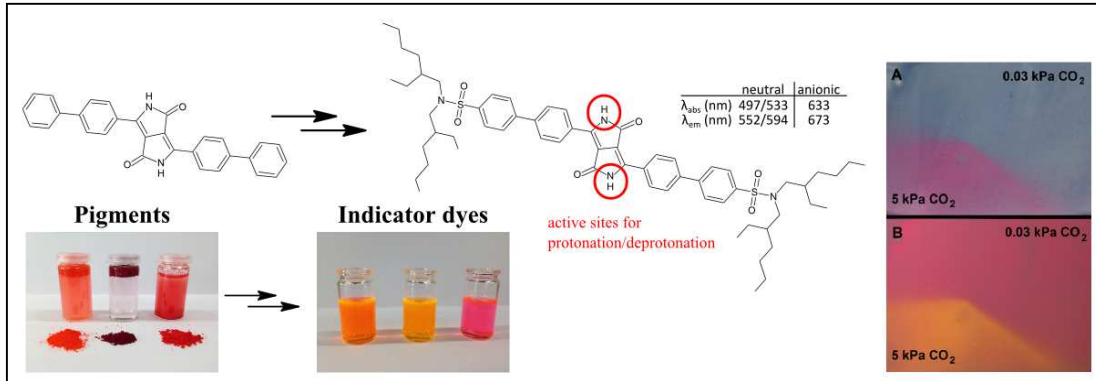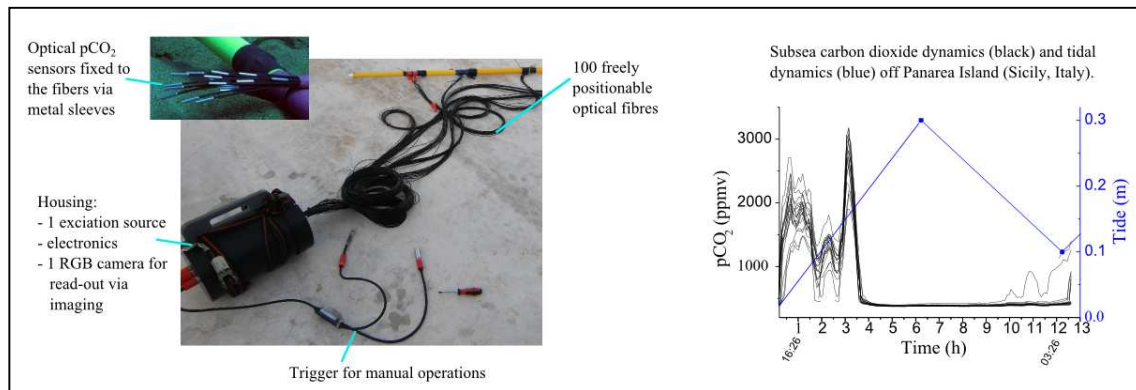

Chapter 2 - New Highly Fluorescent pH Indicator for Ratiometric RGB Imaging of pCO_2
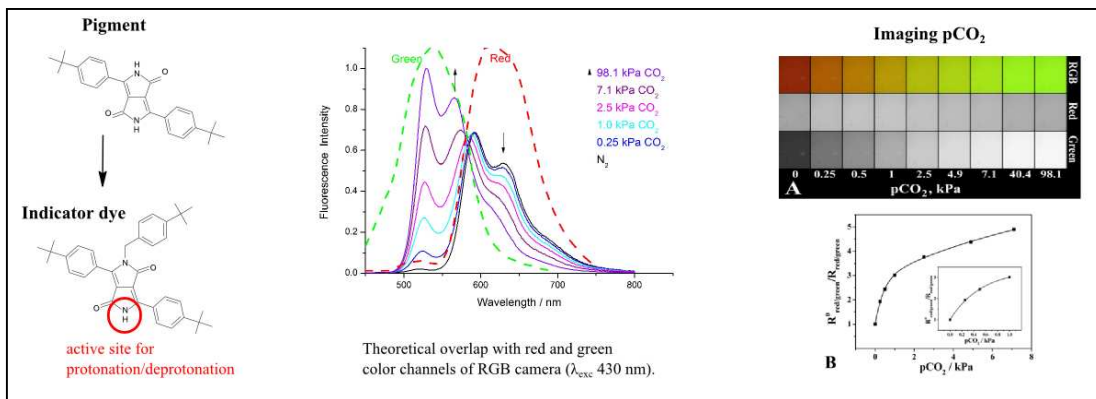
Chapter 3 - NIR Optical Carbon Dioxide Sensors Based on Highly Photostable Dihydroxy-aza-BODIPY Dyes

Chapter 4 - Multi-Branched Optical Carbon Dioxide Sensors for Marine Applications

Chapter 1

Scope of this chapter

Optical *plastic type* sensors consist of a pH-sensitive indicator dye and a base, embedded in a polymer matrix and represent a promising alternative to the known routine detection techniques of carbon dioxide. Up to now, state-of-the-art CO_2 sensors are almost exclusively based on the fluorescent pH-indicator 8-hydroxypyrene-1,3,6-trisulfonate (HPTS).

Although HPTS features high fluorescence quantum yields (~1), good photostability, a pK_a value meeting the demands for physiological measurements and a large Stokes shift (~60 nm in solution and ~50 nm embedded in ethyl cellulose), it suffers from different drawbacks, such as only moderate absorption coefficients (24000 $M^{-1}cm^{-1}$) or absorption and emission maxima at rather short wavelengths. Thus, ratiometric read-out is only enabled, if the exciation wavelength is chosen in the UV region of the spectrum. If this is not the case, addition of reference materials is required for reliable measurements, but here, photobleaching of the indicator dye, the reference or both can cause significant changes in the signals and the respective ratio.

In the following chapter a new indicator class based on diketo-pyrrolo-pyrroles is presented. These dyes meet the requirements of high molar absorption coefficients, high quantum yields for the protonated (neutral) forms, larger Stokes shifts than HPTS, good photostability and absorption and emission spectra at higher wavelengths. Additionally, they feature tuneable pK_a values according to their substitution pattern. Hence, they represent a promising alternative pH-sensitive indicator class to HPTS.

Despite these advantages, DPP indicators can be improved. Their sensitivity can be further tuned to meet the users demands, their photostability could be improved, as well as the quantum yields of the deprotonated (ionic) forms.

Diketo-Pyrrolo-Pyrrole Dyes as New Colorimetric and Fluorescent pH Indicators for Optical Carbon Dioxide Sensors

Authors: Susanne Schutting, Sergey M. Borisov and Ingo Klimant

New indicators for optical CO_2 sensors are synthesized in two steps from the commercially available diketo-pyrrolo-pyrrole (DPP) pigments Irgazin Ruby and Irgazin Scarlet. After introduction of bis(2-ethylhexyl) sulfonamide groups via a simple two-step synthesis the pigments are rendered highly soluble in organic solvents and in polymers and show pH-dependent absorption and emission spectra. The new indicators have molar absorption coefficients in a 20000-50000 $M^{-1}cm^{-1}$ range, possess quantum yields close to unity and feature good photostability. The indicators along with a quaternary ammonium base are embedded into ethyl cellulose to give optical carbon dioxide sensors. The absorption and emission spectra of the deprotonated form are bathochromically shifted by more than 100 nm compared to the protonated form (λ_{max} absorption 496-550 nm; λ_{max} emission 564-587 nm). This enables colorimetric read-out and self-referenced ratiometric fluorescence intensity measurements. Importantly, the dynamic range of the sensors based on the new indicators is significantly different (0-10 kPa and 1-100 kPa CO_2) which enables a broad variety of applications.

Introduction

Carbon dioxide is one of the most important analytes on earth. Therefore its detection is an important task in many fields, e.g. in biotechnology for controlling the fermentation processes in bioreactors,[92,93] in medicine for monitoring the CO_2 content in patients breath,[61,94] in marine research for investigating long-term consequences of ocean acidification for underwater flora and fauna[9,95–98] and in food packaging for controlling the gas content in modified atmosphere packaging.[99] The Severinghaus electrode shows

linearity in a range between 1 kPa and 11 kPa,[77] but it is not well applicable to measure low pCO_2 (e.g. the usual marine levels of about 0.04 kPa or 400 ppm), it suffers from the electromagnetic interferences and can only be applied in aqueous solutions. IR analyzers are robust and fast,[61] but are mostly suitable for CO_2 detection in gases[85,86] since interference from water is very significant. On the other hand, optical CO_2 chemosensors represent promising analytical tools which can be realized in the form of fiber-optic sensors or planar optodes suitable for imaging applications.[51] Most colorimetric sensors rely on triphenylmethane dyes.[57,89,100] The inner filter effect[101–104] and Förster Resonance Energy Transfer (FRET)[105,106] have been used to convert the colorimetric sensors into the luminescence intensity-based ones. The read-out via fluorescence intensity and high cross-sensitivity to oxygen are severe limitations of the first and the second scheme, respectively. The latter also refers to a phosphorescent carbon dioxide probe.[107] One of the most popular fluorescent pH indicators for CO_2 sensors is 8-hydroxypyrene-1,3,6-trisulfonate (HPTS).[50] It is known for its high fluorescence quantum yield of ~1,[108,109] good photostability,[64] and large Stokes´ shift.[64,110] Thus, HPTS was used in numerous pCO_2 sensors in a variety of applications. So called *plastic type* sensors on HPTS basis (which typically make use of the indicator and a quaternary ammonium base in a hydrophobic polymer or a sol-gel) are popular due to the flexibility of formats, fast dynamic response and simplicity in preparation,[51,65,66,89,111–113] but those of Severinghaus type were also reported.[114] The disadvantages of HPTS include moderate molar absorption coefficients (24000 $M^{-1}cm^{-1}$)[115] and the fact that ratiometric measurement is only possible if the UV light is used for the excitation. Several alternative sensing concepts have been proposed recently. They explore the changes in the microenvironment during the carbamate formation monitored with help of a microviscosity probe[116] or aggregation-induced emission.[117] In a similar concept the change in microenvironment due to the protonation of an amidine is detected via a solvatochromic probe.[118] Notably, all these new probes operate at rather high pCO_2 and mostly rely on the measurements of fluorescence intensity, only the probe reported by Wolfbeis and co-workers is suitable for ratiometric read-out.[118]

Diketo-pyrrolo-pyrrole (DPP) pigments were discovered in the 1980s and since that time mainly used as low cost pigments for applications with high-quality demands.[119,120] DPPs are applied in biophotonics and optoelectronics[121] for preparation of low bandgap conjugated polymers[122–125] or copolymers used in semiconductors.[126] Only a few fluorescent probes based on DPP chromophores have been reported so far.[127,128]

Particularly Qu et al. proposed a fluoride probe based on deprotonation of the lactam in the DPP chromophore which resulted in a bathochromic shift of the absorption and emission spectra. We perceived that DPP chromophores could be suitable for designing optical carbon dioxide sensors since they rely on an acid base equilibrium. In this study we present a new alternative class of pH sensitive indicators for CO_2 sensors, which are based on diketo-pyrrolo-pyrrole dyes that are rendered highly soluble in organic solvents and in polymers by introducing dialkyl sulfonamide groups. The indicators show significantly different absorption and emission spectra for the neutral and deprotonated form which enables colorimetric read-out and self-referenced ratiometric fluorescence intensity measurements. The sensors also feature tunable sensitivity, large relative signal change at low pCO_2 and good photostability.

Experimental

Materials.

3,6-bis(1,1´-biphenyl)-2,5-dihydropyrrolo[3,4-c]pyrrole-1,4-dione (Irgazin Ruby), 3,6-bis-phenyl-2,5-dihydropyrrolo[3,4-c]pyrrole-1,4-dione (Irgazin Scarlet), 1,6,7,12-tetraphenoxy-N,N´-bis(2,6-diisopropylphenyl)-perylene-3,4:9,10-tertracarboxylic bisimide (Lumogen-Red) and N,N´-bis(2,6-diisopropylphenyl)-perylene-3,4:9,10-tertracarboxylic bisimide (Lumogen-Orange) were purchased from Kremer Pigments (Germany, www.kremer-pigmente.com). The purity of these materials is confirmed by the elementary analysis (Table S1 of the supporting information). Chlorosulfonic acid has been received from Fluka (Sigma-Aldrich, www.sigmaaldrich.com). Ethyl cellulose (EC49, ethoxyl content 49%), dimethylformamide (anhydrous), sodium sulfate (anhydrous), triethylamine, sodium 8-hydroxy-pyrene-1,3,6-trifulfonate (HPTS), tetrakis(decyl)ammonium hydroxide (TDA, 10% in methanol) and tetraoctylammonium hydroxide solution (TOAOH, 20% in methanol) were obtained from Sigma-Aldrich. The silicone components vinyl terminated polydimethylsiloxane (viscosity 1000 cSt.), (25-35% methylhydrosiloxane)-dimethylsiloxane copolymer (viscosity 25-35 cSt.), 1,3,5,7-tetravinyl-1,3,5,7-tetramethylcyclotetrasiloxane, the platinum-divinyltetramethyldisiloxane complex, anhydrous diethyl ether and bis(2-ethylhexyl)amine were received from ABCR (Germany, www.abcr.de). Ultrafine titanium dioxide P170 was purchased from Kemira (www.kemira.com). Nitrogen, 5%

carbon dioxide in nitrogen, 0.2% carbon dioxide in nitrogen and carbon dioxide (all of 99.999% purity) were obtained from Air Liquide (Austria, www.airliquide.at). HPTS(TOA)$_3$ was prepared as reported previously.[112] Toluene, tetrahydrofuran (THF), ethanol and hexane were purchased from VWR (Austria, www.vwr.com). Poly(ethylene terephthalate) (PET) support Melinex 505 was obtained from Pütz (Germany, www.puetz-folien.com). Silica-gel, as well as the buffer salts 2-(cyclohexylamino)-ethansulfonic acid (CHES) and cyclohexylaminopropansulfonic acid (CAPS) were received from Roth (www.carlroth.com). For HPLC experiments methanol picograde was purchased from LGC Standards (www.lgcstandards.com) and de-ionized water was filtered via a Barnstead NANOpure ultrapure water system for HPLC experiments.

Synthesis of 3,6-bis[4´(3´)-disulfo-1,1´-biphenyl-4-yl]-2,5-dihydropyrrolo[3,4-c]pyrrole-1,4-dione dipotassium salt (1).

Irgazin Ruby (1 g, 2.3 mmol) was stirred in chlorosulfonic acid (10 ml, 150 mmol) for 4 h at 60 °C. The mixture was cooled to ambient temperature, pipetted on ice and washed with cold deionized water until reaching a neutral pH. The centrifuged sediment was then hydrolyzed in 250 ml of a mixture of deionized water (180 ml), acetone (30 ml) and dimethylformamide (40 ml) and potassium carbonate was added until reaching a slightly basic pH. After the solvent mixture was evaporated under reduced pressure, the crude product was dissolved in a mixture of water:methanol (HPLC grade, 1:1) and purified via semi-preparative high performance liquid chromatography eluting isocratic with a H_2O:MeOH (55:45) to obtain a dark violet powder of **1**. Matrix assisted laser desorption/ionization – time of flight (MALDI-TOF) for 1: m/z of [MH]$^+$ found 676.99, calculated 676.99; m/z of [MK]$^+$ found 714.94, calculated 714.94. ^{1}H NMR spectra indicate formation of a mixture of isomers containing sulfo-groups in position 5 and 6 of the biphenyl.

Synthesis of 3,6-bis[4´-bis(2-ethylhexyl)sulfonylamide-1,1´-biphenyl-4-yl]-2,5-dihydropyrrolo[3,4-c]pyrrole-1,4-dione (2).

Irgazin Ruby (1 g, 2.3 mmol) was stirred in chlorosulfonic acid (7 ml, 105 mmol) for 3 h at 60 °C. The mixture was cooled to ambient temperature, pipetted on ice and washed with cold de-ionized water until reaching a neutral pH. The sediment was collected via

centrifugation and was washed three times with diethyl ether:tetrahydrafurane (10:1). The sediment was dissolved in anhydrous dimethylformamide (50 ml) and bis(2-ethylhexyl)amine (4 ml, 13 mmol) and triethylamine (3 ml, 22 mmol) were added. The mixture was stirred overnight at ambient temperature, diluted with deionized water and neutralized with acetic acid. The dye was extracted with dichloromethane, hydrochloric acid, ethanol and sodium chloride where added to facilitate the phase separation. The organic phase was collected, dried over anhydrous sodium sulfate and evaporated to dryness under reduced pressure. The crude product was purified via column chromatography on silica gel using toluene/tetrahydrofuran (95:5). The product was dissolved in dichloromethane and precipitated with hexane to give a dark red powder (0.69 g, 29% of theoretical yield of **2**). MALDI-TOF: m/z of [MH]$^+$ found 1047.6, calculated 1047.6. ^{1}H NMR (300MHz, CDCl$_3$) δ 8.46 (s, 4H), 7.81 (m, 4H), 7.69 (m, 8H), 3.06-2.88 (m, 8H), 1.61 (s, 4H), 1.26-1.21 (m, 32H), 0.85-0.80 (m, 24H). Analysis for C$_{62}$H$_{86}$S$_2$N$_4$O$_6$ found: C68.96, H7.28, N7.11, calculated: C69.00, H7.66, N7.10.

Synthesis of 3-(phenyl)-6-(4-bis(2-ethylhexyl)sulfonylamide-phenyl)-2,5-dihydropyrrolo[3,4-c]pyrrole-1,4-dione (3) and 3,6-bis[4-bis(2-ethylhexyl)sulfonylamide-phenyl]-2,5-dihydropyrrolo[3,4-c]pyrrole-1,4-dione (4).

Irgazin Scarlet (2 g, 6.9 mmol) was dispersed in the mixture of sulfuryl chloride (2 ml, 24 mmol) and chlorosulfonic acid (6 ml, 90 mmol) and was stirred for 12 h at 65 °C. The protocol used for the preparation of **2** was followed, but 10 ml (33 mmol) of bis(2-ethylhexyl)amine and 4 ml (29 mmol) triethylamine were used instead. The crude products were purified via column chromatography on silica gel eluting with a gradient of toluene:acetone (75:25) to obtain **3** and 97:3 to obtain **4**. The products were recrystallized from n-butanol to give **3** as dark red crystals (0.54 g, 13% of theoretical yield of **3**) and **4** as an orange powder (0.4 g, 6% of theoretical yield of **4**). MALDI-TOF for **3**: m/z of [MH]$^+$ found 592.3214, calculated 592.3209. ^{1}H NMR (300MHz, DMSO-d6) δ 8.52 (s, 1H), 8.46 (t, 2H), 8.34 (dd, 2H), 7.87 (d, 2H), 7.84-7.69 (m, 2H), 2.95 (m, 4H), 1.57 (m, 2H), 1.44-1.08 (m, 16H), 0.85 (m, 12H). Analysis for C$_{34}$H$_{45}$SN$_3$O$_4$ (**3**) found: C 70.66, H 8.09, N 5.29, calculated: C 71.09, H 8.28, N 5.35. MALDI-TOF for **4**: m/z of [MH]$^+$ found 895.5469, calculated 895.5441. ^{1}H NMR (300MHz, CDCl$_3$) δ 8.43 (d, 4H), 7.82 (m, 4H), 2.98-2.89 (m, 8H), 1.55 (m, 4H), 1.44-

1.01 (m, 32H), 0.84 (m, 24H). Analysis for $C_{50}H_{78}S_2N_4O_6$ **(4)** found: C 67.24, H 8.65, N 6.12, calculated: C 67.08, H 8.78, N 6.26.

Preparation of the Sensing Foils.

"Cocktail 1" containing X mg dye and 100 µl tetraoctylammonium hydroxide solution (20% TOAOH in MeOH) was purged with carbon dioxide gas. "Cocktail 2" containing 200 mg ethyl cellulose dissolved in 3800 mg of a toluene:ethanol mixture (6:4) was added to the "cocktail 1". For the absorption measurements X was 2.4 mg (1.2%w/w in respect to the polymer) in case of **2** and 3.0 mg (1.5%w/w) for **3** and **4**. For the emission measurements X was 0.8 mg (0.4%w/w) for **2** and 0.5 mg (0.25%w/w) for **3** and **4**. The resulting mixture was knife-coated on a dust-free PET support. A sensing film of ~7.5 µm thickness was obtained after evaporation of the solvent. The sensing film was covered with a gas-permeable ~22 µm thick silicone layer by knife-coating "cocktail 3" consisting of 800 mg vinyl terminated polydimethylsiloxane, 32 µl (25-35% methylhydrosiloxane)-dimethylsiloxane copolymer, 2 µl 1,3,5,7-tetravinyl-1,3,5,7-tetramethylcyclotetrasiloxane and 4 µl platinum-divinyltetramethyldisiloxane complex dissolved in 1600 mg hexane. For emission measurements a similar layer was prepared but 200 mg of titanium dioxide were dispersed in "cocktail 3". The silicon layers were kept in an oven (60 °C) for 10-15 min to complete polymerization.

Methods.

^{1}H NMR spectra were recorded on a 300 MHz instrument (Bruker) in $CDCl_3$ and DMSO-d6 with TMS as standard. Absorption spectra were recorded on a Cary 50 UV-Vis Spectrophotometer (www.varianinc.com). The determination of the molar absorption coefficients was carried out as an average of 3 independent measurements. Fluorescence spectra were recorded on a Hitachi F-7000 fluorescence spectrometer (www.hitachi.com) equipped with a red-sensitive photomultiplier R928 from Hamamatsu (www.hamamatsu.com). The relative fluorescence quantum yields were determined according to Demas and Crosby.[129] The solutions of Lumogen-Orange ($\Phi \approx$ 1) and Lumogen-Red ($\Phi \approx 0.96$)[130,131] in chloroform were used as standards for the protonated and the deprotonated form, respectively. The absolute fluorescence quantum yields were determined on a Fluorolog3 fluorescence spectrometer (www.horiba.com) equipped with a NIR-sensitive photomultipier R2658 from Hamamatsu (300-1050 nm)

and an integrating sphere (Horiba). Three independent measurements were performed for determination of the relative and the absolute quantum yields and the average value obtained in the two methods was used. In case of the sensing materials only the absolute quantum yields were determined. Photobleaching experiments were performed by irradiating the samples (2.5 ml) with the light of a high-power 10 W LED array (λ_{max} 458 nm, 3 LEDs, www.led-tech.de) operated at 6 W input power. A lens (Edmund optics, www.edmundoptics.de) was used to focus the light of the LED array on the glass cuvette (photon flux: ~4600 µmol·s^{-1}·m^2 as determined with a Li-250A light meter from Li-COR, www.licor.com). The photodegradation profiles were obtained by monitoring the absorption spectra of the respective dye dissolved in tetrahydrofuran. For experiments with ratiometric read-out a two-phase lock-in amplifier (SR830, www.thinksrs.com) and a home-made device consisting of two separate detection channels, which was described previously in detail,[132] were used. Each detection channel was equipped with a photomultiplier module H9306-02 from Hamamatsu. A 450 nm LED (www.roithner-laser.com) combined with a short-pass BG-12 filter served as an excitation source. The emission of the neutral form was filtered through HC 562/40 band-pass filter (www.ahf.de) and an RG-630 long-pass filter from Schott was used for the deprotonated form. A four-armed optical filter bundle (www.leoni-fiber-optics.com) was used to guide the excitation light to the sensing foil and to guide back the emission to the two detection channels. Gas calibration mixtures were obtained using a gas mixing device from MKS (www.mksinst.com). The gas mixture was humified to about 100% relative humidity prior entering the calibration chamber. Temperature was controlled by a cryostat ThermoHaake DC50. Semi-preparative HPLC was performed on a Knauer Smartline Instrument with Autosampler 3800 (Manager 5000, Pump 1000, UV Diode Array Detector 2600 and Fraction Collector Teledyne Isco Foxy Jr. FC100 modules) equipped with a Machery-Nagel VP 125/21 Nucleodur 100-5 C18 ec column (internal diameter: 21.0mm) with a VP 20/16 Nucleodur C18 ec pre-column at a flow rate of 13ml/min. The pH of the buffer solutions (CHES and CAPS) was controlled by a digital pH meter (InoLab pH/ion, www.wtw.com) calibrated at 25 °C with standard buffers of pH 7.0 and pH 4.0 (www.wtw.com). The buffers were adjusted to constant ionic strength (IS = 0.05 M) using sodium chloride as the background electrolyte.

Results and Discussion

Synthesis.

We expected the diketo-pyrrolo-pyrrole chromophore to be pH-sensitive due to the deprotonation of the lactam ring. Preliminary experiments with suspensions of DPP pigments confirmed this hypothesis. However, DPP pigments are known to have planar structure and possess very poor solubility in the organic solvents.[133] In fact the DPP dyes are mostly applied as non-soluble pigments in paints. The low solubility prevents the dyes from application as indicators in optical sensors. Typically, the DPP pigments are rendered soluble by an alkylation of the lactam nitrogen atoms[134] but this modification is of course not suitable for preparation of pH indicators. A water-soluble disulfonate **1** (Scheme 1.1) was prepared via chlorosulfonation of the commercially available pigment Irgazin Ruby (Pigment Red 264) and subsequent hydrolysis of the product in aqueous medium. This dye was found to be pH sensitive and was used for the estimation of the pK_a (see below). A simple 2-step strategy was established to convert the DPP pigments into lipophilic pH indicators highly soluble in organic solvents and polymers (Scheme 1.1) and thus to make the dyes suitable for application in plastic carbon dioxide sensors. Two different pigments containing phenyl or biphenyl substituents in the 3,6 position of the DPP were used. The chloro-sulfonation (first step) was carried out with large excess of chlorosulfuric acid to prevent possible hydrolysis during sulfonation. The chlorosulfonation of Irgazin Scarlet (Pigment Red 255, **DPP**) proved to be more difficult than for Irgazin Ruby and required addition of sulfuryl chloride to achieve acceptable yields. To minimize the formation of side products due to hydrolysis the second step (reaction with a branched secondary amine) was performed without thorough purification of the chlorosulfonated intermediate.
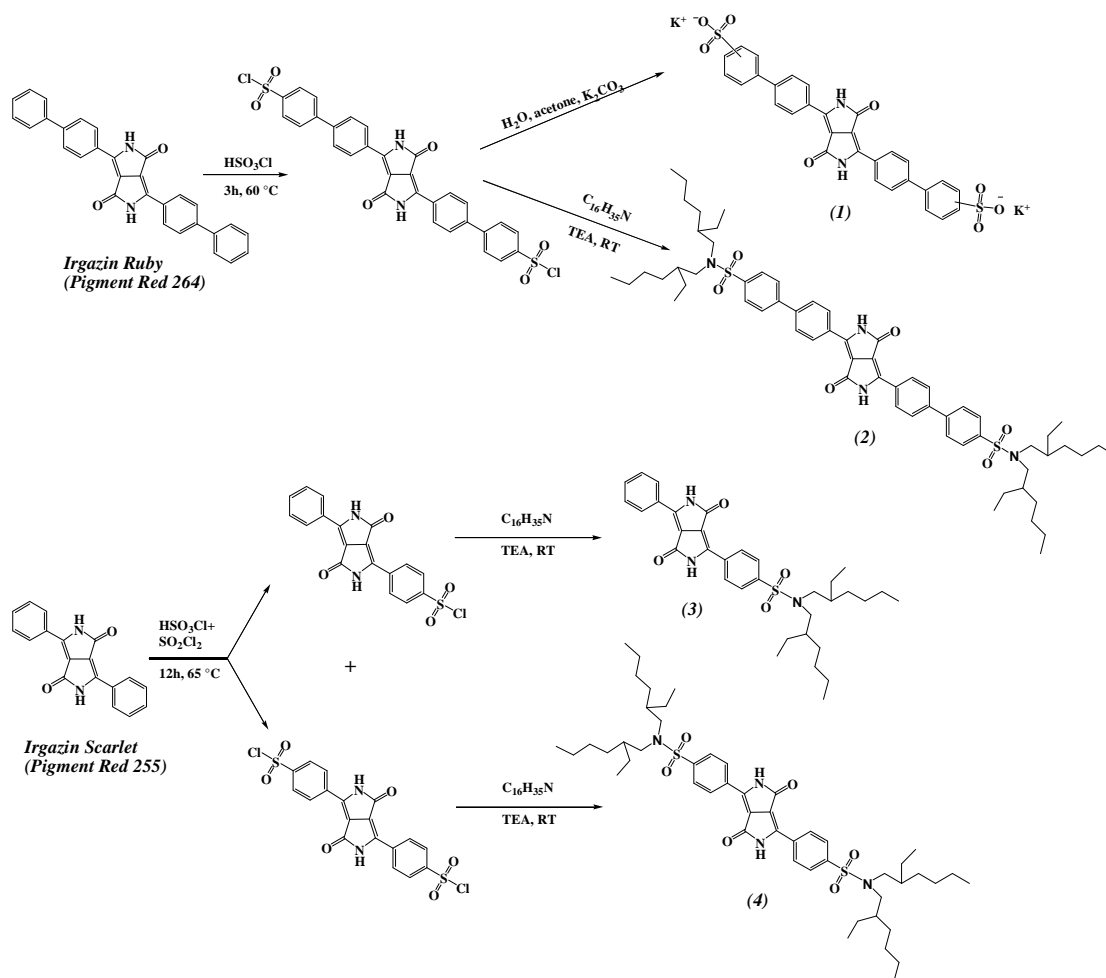
Scheme 1.1. *Synthesis of dye **1** and **2** and dye **3** and **4**, respectively.*

Properties of the Disulfonate 1.

The disulfonate **1** was used for the estimation of the pH-sensing properties of the DPP dyes in aqueous solution. The dye shows a bathochromic shift of the absorption and emission spectra upon deprotonation (Fig. 1.1). The response of the dye is described by a typical sigmoidal dependence and the pK_a value is estimated to be 11.8. This value is rather high and indicates potential suitability of DPPs for design of highly sensitive carbon dioxide sensors. Since the electron-withdrawing effect of the sulfonamide groups is stronger than that of the sulfonate (the Hammett substituent constants are 0.65 (*p*) and 0.51 (*m*) for SO_2NMe_2 and 0.35 for SO_3^-)[56] the pK_a value for **2** is expected to be lower compared to **1**. For **4** bearing two sulfonamide groups in the proximity of the DPP core even lower pK_a values can be expected. The dye **3** containing a single sulfonamide group is likely to occupy intermediate position.
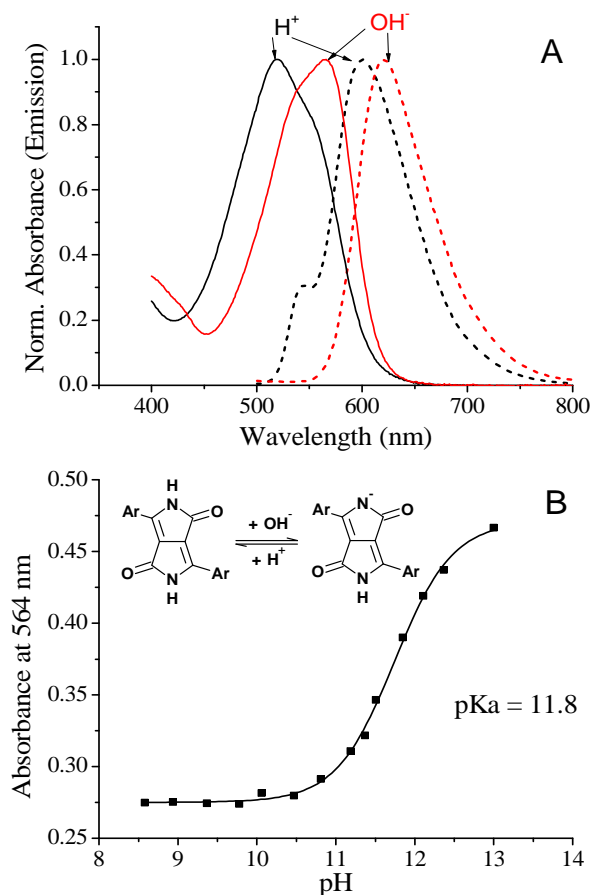
Figure 1.1. A: Absorption (solid lines) and emission (dashed lines) spectra for the neutral (black lines) and deprotonated (red lines) forms of 1 in aqueous buffer. B: titration curve for dye 1 and the scheme illustrating the protonation/deprotonation equilibrium.

Photophysical Properties of the Sulfonamides.

As expected the synthetic modification renders all the dyes soluble in organic solvents. The dyes bearing two sulfonamide groups (**2** and **4**) are excellently soluble in common organic solvents such as toluene, chloroform, tetrahydrofuran etc. The solubility of **3** (which bears only one sulfonamide group) in toluene is worse than for **2** and **4** but is good in more polar solvents such as tetrahydrofuran (THF) or ethanol. The highly lipophilic alkyl chains render all the dyes insoluble in water. The absorption and emission spectra of the indicator **2** in THF are shown in Fig. 1.2 and for the other indicators as well as for the unmodified pigment **DPP** – in Fig.S1.1 of the supporting information. Note that due to low solubility of the latter in THF the dye was dissolved in dimethylsulfoxide (DMSO) and the values obtained match those reported by Lunak et al[136]. The photophysical properties of the new dyes are summarized in Table 1.1. As

can be seen, the neutral form of the indicators absorbs in the blue-green part of the spectrum.

Table 1.1. *Photophysical properties of all the DPP dyes in tetrahydrofuran: absorption maxima (λ_{abs}), molar absorption coefficients (ε), emission maxima (λ_{em}) and fluorescence quantum yields (Φ) for neutral and deprotonated forms. For comparison the respective data are shown also for Irgazin Scarlet (DPP) dissolved in dimethylsulfoxide.*

Dye	Neutral form			Deprotonated form		
	λ_{abs} ($\varepsilon \cdot 10^{-3}$) [nm ($M^{-1}cm^{-1}$)]	λ_{em} [nm]	Φ^{*}	λ_{abs} ($\varepsilon \cdot 10^{-3}$) [nm ($M^{-1}cm^{-1}$)]	λ_{em} [nm]	Φ^{*}
2	497(42.8); 533(50.1)	552; 594	1	633(25.6)	673	0.09
3	495(20.8); 532(22.0)	577; 612	0.68	633(19.2)	660	0.07
4	491(29.8); 528(36.9)	543; 583	1	655(23.0)	708	0.11
DPP	472(26.3); 506(35.0)	519; 556	0.72	587(16.8)	634	0.34

* The displayed fluorescence quantum yields (Φ) represent an average of three independent measurements and are determined with the uncertainty of 10%.

The absorption of the deprotonated form is bathochromically shifted by about 100 nm and is located in the red part of the spectrum. Interestingly, the neutral form of the mono-substituted sulfonamide **3** absorbs at longer wavelengths than the double-substituted **4**, but the absorption of both dyes is bathochromically shifted compared to the parent pigment Irgazin Scarlet despite higher polarity of DMSO compared to THF. On the other hand, the deprotonated form of **3** absorbs at shorter wavelengths than **4** in its basic form. Molar absorption coefficients are rather different for all the DPP dyes and vary from about 20000 to 50000 $M^{-1}cm^{-1}$. Interestingly, the ε values are significantly lower for the mono-substituted sulfonamide **3** compared to the symmetrical double-substituted derivative **4** and the non-modified pigment **DPP**. As can be observed, **2** absorbs more efficiently than **3** and **4**. For all the dyes, the ε values for the deprotonated form are lower than those for the neutral form. This correlates well with significantly broader absorption of this form (FWHM: ~120 nm for **2** and **3** and ~100 nm for **4**) compared to the absorption of the neutral form (FWHM: ~70 nm for **2** and **3** and ~60 nm for **4**). Both the neutral and the deprotonated forms of the new indicator are fluorescent (Fig. 1.2). The emission of the neutral form is located in the

yellow-orange part of the spectrum and is very strong. In fact, the fluorescence quantum yields Φ for the symmetrical double-substituted sulfonamides **2** and **4** are close to unity. The fluorescence of the neutral form of **3** is less efficient (Φ = 0.68). The Stokes´ shifts are rather small for symmetrical **2** and **4** (19 nm and 15 nm, respectively) and are slightly larger for **3** (35 nm). However, this is of less relevance for the sensing applications since very efficient excitation in the second band (located about 30 nm shorter than the most intense absorption band) is possible for all the indicators. In solutions the fluorescence of the deprotonated form is much weaker than that of the neutral form (Φ = 0.07-0.11, Table 1.1).
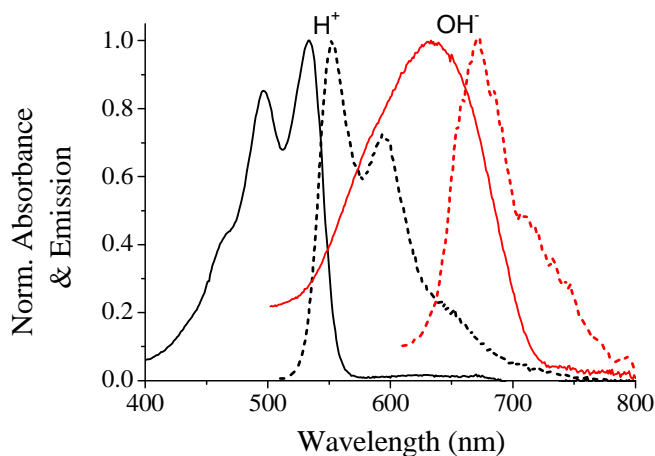
Figure 1.2. *Absorption (solid lines) and emission (dashed lines) spectra for the neutral (black lines) and deprotonated (red lines) forms of **2** in tetrahydrofuran.*

Photostability.

Photobleaching experiments were carried out for the THF solutions of the dyes. A high power blue LED array (λ_{max} 458 nm) was used for the excitation of the neutral form. 8-hydroxy-pyrene-1,3,6-trisulfonate in its lipophilic tetraoctylammonium ion pair (HPTS(TOA)$_3$) which is the most common state-of-the-art indicator for plastic carbon dioxide sensors was used for comparison. The photodegradation profiles are displayed in fig. S1.2. All DPP dyes showed significantly better photostability than HPTS(TOA)$_3$. The photostability of the doubly-substituted sulfonamides **2** and **4** was much higher than for the mono-substituted **3** which correlates well both to the amount of electron-withdrawing sulfonamide groups and the fluorescence quantum yields. Therefore, it can

not be concluded whether lower photostability of **3** compared to that for **2** and **4** is due to higher probability of photooxidation processes (due to higher electron density on the DPP core) or the photodegradation pathways involving the formation of the triplet states.

Carbon Dioxide Sensors.

The indicators along with tetraoctylammonium hydroxide were embedded in ethyl cellulose to obtain plastic carbon dioxide sensors. Clearly, the sensors respond to carbon dioxide in altering their color (blue in the absence of CO_2 and pink in the presence of CO_2) which enables colorimetric detection of carbon dioxide (Fig. 1.3).
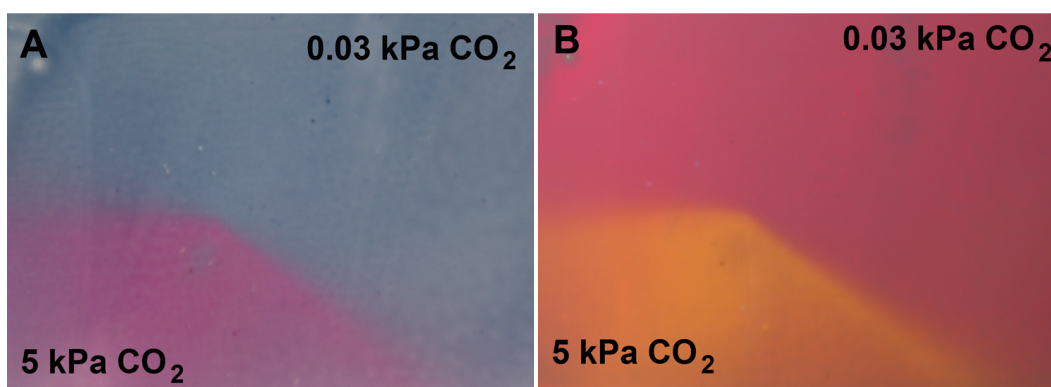
*Figure 1.3. Photographic images of the planar optode based on **2** in EC49 under ambient air and a flux of 5 kPa carbon dioxide: (A) under ambient light; (B) in the darkness under UV light (365 nm).*

Distinct changes in the fluorescence color (from deep red to orange) are also evident. Fig. 1.4 and Fig. S1.3 show the absorption and the emission spectra of the sensing materials based on **2**-**4**. Although the major trends established for THF solutions are preserved also in the solid state sensors it is evident that the absorption of the deprotonated form becomes narrower compared to the solutions. A shoulder in the absorption spectrum at about 560 nm is also clearly visible. The presence of several isosbestic points indicates that only two forms of an indicator are present in the acid-base equilibrium.

Importantly, the fluorescence quantum yields of the deprotonated form nearly double in ethyl cellulose (Table 1.2) and reach ~0.2 which enables sufficient signal for the ratiometric measurements. For all the sensors the fluorescence emission intensities for

both the neutral and the deprotonated form were increasing with CO_2 concentration (Fig. 1.4, Fig S1.3). The increase in the intensity of the deprotonated form is explained by more efficient absorption of the neutral form at the excitation wavelength (e.g. λ_{exc} 505 nm for **2)** and rather efficient Förster Resonance Energy Transfer (FRET) at this dye concentration (0.4% w/w for **2**). This is due to very good overlap between the emission of the neutral form and the absorption of the deprotonated form. FRET may also be the reason for lower quantum yields determined in ethyl cellulose for the neutral form of the dyes compared to the solution measurements (Tables 1.1 and 1.2).

Table 1.2. Photophysical properties of all the DPP dyes in ethyl cellulose film (EC49): absorption maxima (λ_{abs}), molar absorption coefficients (ε), emission maxima (λ_{em}) and fluorescence quantum yields (Φ) for the neutral and deprotonated forms.

Dye	Neutral form			Deprotonated form		
	λ_{abs} [nm]	λ_{em} [nm]	Φ	λ_{abs} [nm]	λ_{em} [nm]	Φ
2	505; 541	565	0.64	606	653	0.19
3	516; 550	587	0.64	597	641	0.18
4	496; 534	564	1	615	682	0.17

As can be seen (Fig. S1.4) dye concentration barely affects the colorimetric read-out but is crucial for the emission measurements due to FRET. In fact, in case of high dye concentration (1.2% w/w) the emission spectrum is dominated by the deprotonated form at pCO_2 below 5 kPa. On the other hand, in case of low dye concentration the neutral form clearly dominates the emission at this pCO_2 (Fig. S1.4). Thus, the dynamic range of the sensing materials using emission read-out can be tuned by adjusting the concentration of the indicators. Fig. 1.4 also shows the respective calibration plots for the sensors based on **2-4**. Despite rather different structure of **2** and **3** the sensors show comparable sensitivity. Both sensors operate in the dynamic range from 0 to 10 kPa CO_2 and retain dynamics at atmospheric pCO_2 of 0.04 kPa. At lower carbon dioxide levels it is very difficult to ensure that the system (flow through cell, gas mixing device, connectors etc.) is completely decarbonated and thus some contamination with CO_2 can be observed. In fact, the experimental values at very low pCO_2 deviate from the expected linear dependence (Fig. S1.5). Therefore, determination of the Limit of

Detection (LOD) was not possible. On the other hand, the effect of contamination is negligible in case of much less sensitive sensor based on….(dynamic range 1-100 kPa CO_2, LOD = 0.07 kPa, Fig. S1.6)

Since the electron-withdrawing sulfonamide groups are expected to lower the pK_a value of the indicator (and consequently the sensitivity of the sensor) it is likely that the effect of two distant groups (in **2**) is roughly equal to that of one group located in close proximity to the DPP core (in **3**). Importantly, **4** bearing two sulfonamide groups close to the diketo-pyrrolo-pyrrole shows much lower sensitivity. Thus, the highly sensitive sensors based on **2** and **3** can be promising for application in marine research and the one based on **4** is adequate for the food packaging applications where pCO_2 is typically rather high. On the other hand, all three materials can be suitable for monitoring physiologically relevant pCO_2 in breath-by-breath measurements. It should be mentioned here that the sensitivity of the sensors can also be fine-tuned by substituting the polymer matrix and/or the quaternary ammonium base.[137] In fact, by employing ethyl cellulose with lower content of the ethoxyl groups (46% instead of 49%) the sensitivity can be reduced by roughly 2-fold. As even ethyl cellulose was used as a model matrix one should also give consideration to the possibility of using other matrix systems. The less bulky tetrabutyl ammonium base has a similar effect on the sensitivity. As in the case of all optical carbon dioxide sensors the sensitivity significantly reduces at higher temperature and improves at lower (Fig. S1.7). This is due to better solubility of carbon dioxide in polymers at lower temperature. Substitution of ethyl cellulose for other matrices (polymer or sol-gel) may help to minimize the temperature cross-talk.
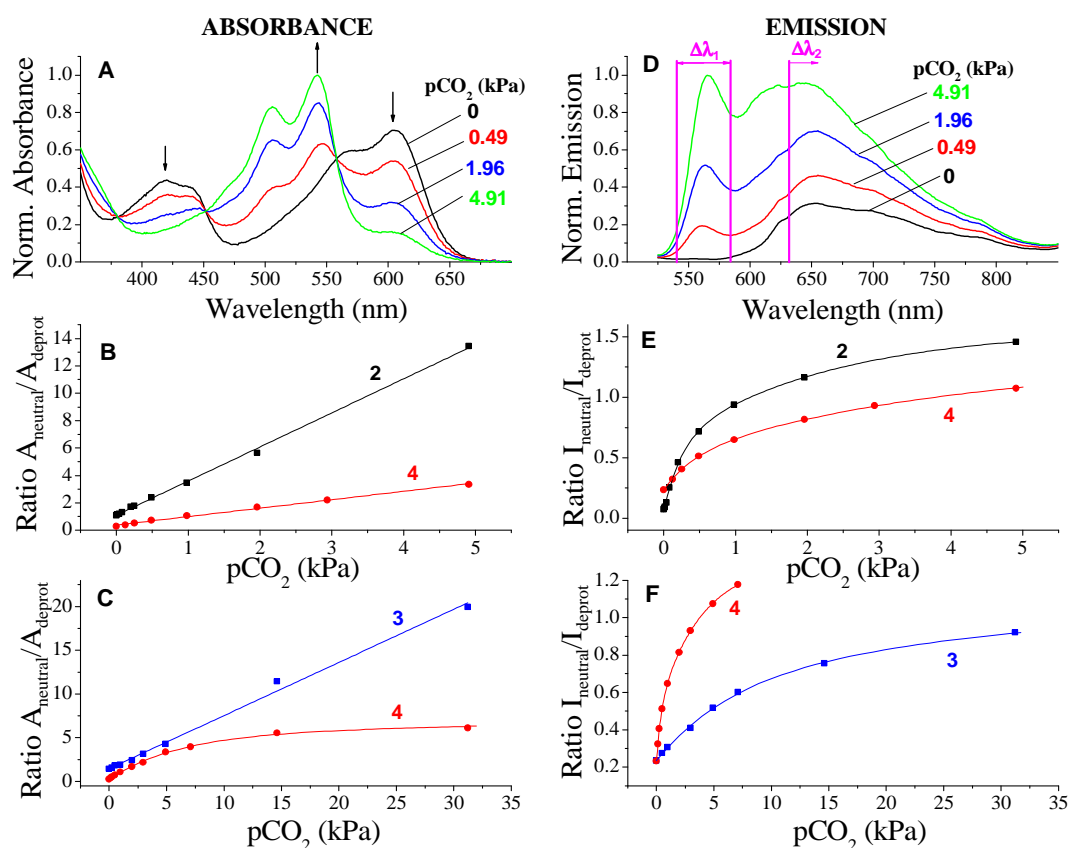
Figure 1.4. *Absorption (**A**) and emission (**D**) spectra for the carbon dioxide sensor based on **2** (25 °C). Calibration curves for the sensors based on **2-4**: the ratio of absorption (**B and C**) and fluorescence intensity (**E and F**) in the λ_{max} of the absorption and emission spectra (λ_{exc} 505 nm for **2**, 510 nm for **3** and 495 nm for **4**), respectively, of the neutral and deprotonated forms of the indicators (25 °C).*

Comparison of the Optical and Sensing Properties with State-of-the-art Sensors.

Since HPTS is one of the most frequently used fluorescent pH indicators for CO_2 sensors a comparison between the sensors based on this indicator and the new DPP indicators is interesting. Generally, the new indicators and HPTS show comparable molar absorption coefficients. The fluorescence quantum yields of the neutral form of the DPP indicators are comparable to the Φ for HPTS but the deprotonated forms of the former possess lower brightness. The 2-wavelength absorption/reflectance measurements are possible for both indicator classes, but for DPPs the wavelength is significantly longer. In fact, the absorption maximum of the protonated form of HPTS is located in the UV region (395 nm). The DPPs are excellently suitable for ratiometric emission measurements under blue excitation, whereas only unreferenced measurements of fluorescence intensity are possible for HPTS under the same

conditions (Fig. S1.8). Therefore, the addition of a reference dye is required in case of HPTS. Although HPTS and DPP-based sensors show generally similar spectral response to carbon dioxide (bathochromically shifted absorption and emission from the deprotonated form) the neutral form of DPPs is much more analytically useful than for HPTS. Thus, the fluorescence from the neutral form of the new indicators increases in the presence of carbon dioxide (Fig. 1.4). Importantly, the relative signal changes at lower pCO_2 are very high (Fig. 1.5) since virtually no fluorescence from the neutral form is observed in the absence of CO_2. On the contrary, the HPTS-based sensors show maximum fluorescence for the deprotonated form and relative signal changes at low pCO_2 are about 2 orders of magnitude lower. Thus, the new dyes (**2** and **3**) are particularly promising for monitoring low pCO_2 with high resolution. On the other hand, at high pCO_2 the resolution of HPTS sensors is better than those based on **2** and **3**, but as was shown above **4** is excellently suitable for measurements in this dynamic range.
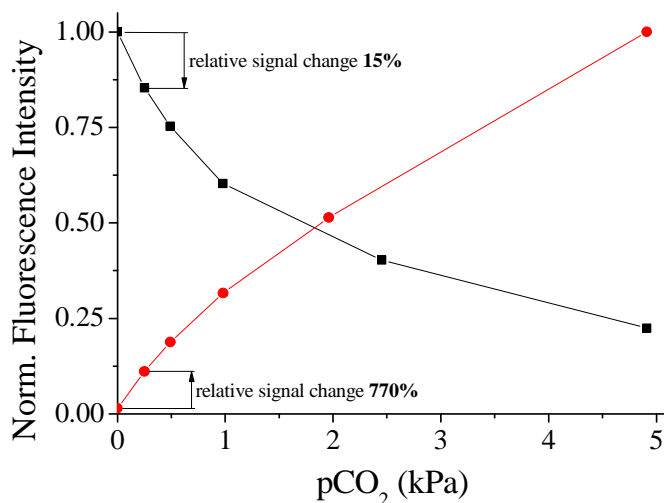
Figure 1.5. Comparison of CO_2 sensors containing HPTS and *2*, respectively. Decreasing emission intensities for HPTS (at 505 nm, black squares) and increasing emission intensities for *2* (at 565 nm, red circles) with increasing pCO_2.

Sensor Response Times and Reproducibility.

The dynamic response was estimated by abruptly changing the pCO_2 from 0.25 kPa to 4.91 kPa and back for **2** and **3** and from 4.91 kPa to 98.13 kPa and back for **4**. The t_{90} time (time needed for 90% of the signal change to occur) was estimated to be about 90 s and about 40 s for the response and recovery, respectively. Evidently, the response and recovery times are influenced by the thickness of the sensing layer and the thickness of the silicon layer. The thicknesses of both can be reduced to enable faster response, however higher concentration of the indicator will be necessary to ensure sufficient S/N ratio. The dynamic range of the material is expected to shift due to more efficient FRET at higher dye concentration albeit only for the fluorescence measurements. Evidently, increasing the dye concentration will not significantly influence the dynamic range upon colorimetric measurement. To demonstrate the reproducibility of the sensors we performed prolong measurements with alternating pCO_2 using 450 nm LED for the excitation and detecting fluorescence in 2 channels: 542-582 nm for isolating the emission of the neutral form and >630 nm for the basic form, respectively. The ratio of the intensities in the two channels served as an analytical parameter. All the sensors show highly reproducible response without a noticeable drift (Fig. 1.6, Fig. S1.9 and S1.10). Importantly, the sensors based on **2** and **3** show excellent photostability (no degradation of fluorescence intensity for the neutral and deprotonated forms) even within several hours of continuous excitation. In case of **4** a very minor drift due to photobleaching is observed after 5 h of continuous read-out. Importantly, photobleaching of the indicator reduces its concentration and therefore FRET efficiency which can result in the drift of calibration plots. However it should be mentioned here that we used continuous irradiation in order to access the photostability. Typically, a short pulse of 100 ms is more than sufficient to access the fluorescence intensity in both channels and the acquisition will be performed once in several seconds. Thus, the operating lifetime of the sensors can be extended by several orders of magnitude. Comparison with the sensors based on $HPTS(TOA)_3$ reveal rather strong drift due to significantly faster photobleaching of the dye in identical conditions (Fig. S1.11).
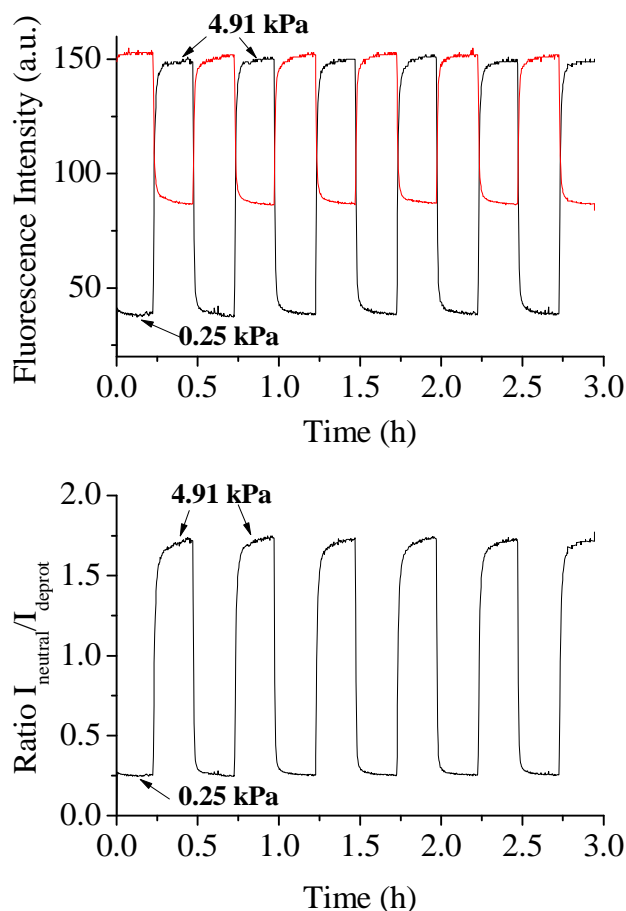
Figure 1.6. Above: *Fluorescence intensity for the neutral (black line) and deprotonated (red line) forms of **2** (up) and **Below:** calculated ratio I$_{neutral}$/I$_{deprot}$ (down) for pCO$_2$ alternating between 0.25 kPa and 4.91 kPa under continuous excitation with 450 nm LED (25 °C). The optical windows correspond to those in Fig. 1.4D. Note that the curves do not reflect the dynamic response times since a set-up ensuring 100% humidity was used which significantly slows complete gas exchange in the measurement chamber.*

Conclusions

In conclusion, we synthesized and characterized a new class of pH sensitive indicator dyes for optical CO$_2$ sensors. A simple two-step-synthesis was presented starting from low-cost diketo-pyrrolo-pyrrole pigments. Chemical modification led to the lipophilic dyes highly soluble in organic solvents and in polymers. The prepared sensors show characteristic absorption and emission bands for the neutral and the deprotonated forms and are suitable for absorption/reflectance measurements and for ratiometric 2-wavelength emission measurements under blue excitation. The sensors can also be used

for colorimetric semi-quantitative measurements and for imaging of carbon dioxide distribution on surfaces. The sensors feature excellent photostability and large relative signal change at low pCO_2. The sensitivity could be tuned over a wide range by using sulfonamide substituents differing in position and quantity. The new dyes represent a promising alternative to the state-of-the-art indicators such as absorption-based triphenylmethane dyes and fluorescent 8-hydroxy-1,3,6-trisulfonate.

Acknowledgements

Supporting Information

to *Diketo-Pyrrolo-Pyrrole Dyes as New Colorimetric and Fluorescent pH Indicators for Optical Carbon Dioxide Sensors*
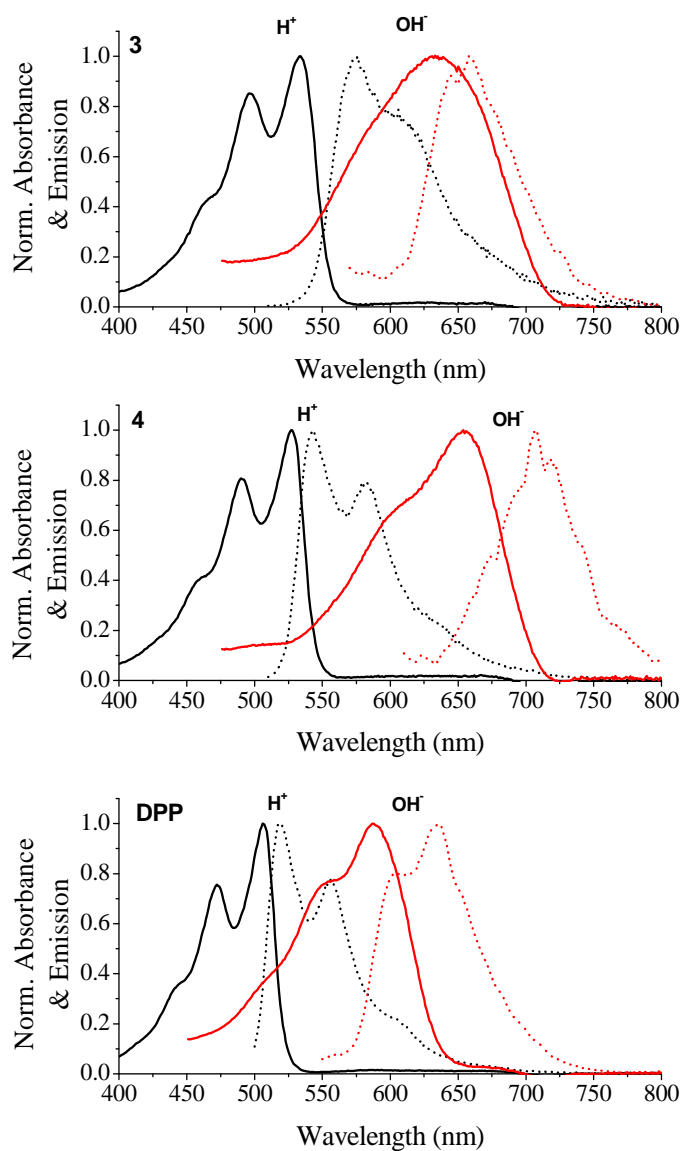
Figure S1.1. Absorption (solid lines) and emission (dashed lines) spectra for the neutral (black lines) and deprotonated (red lines) forms of 3 and 4 in tetrahydrofuran and DPP in dimethylsulfoxide.
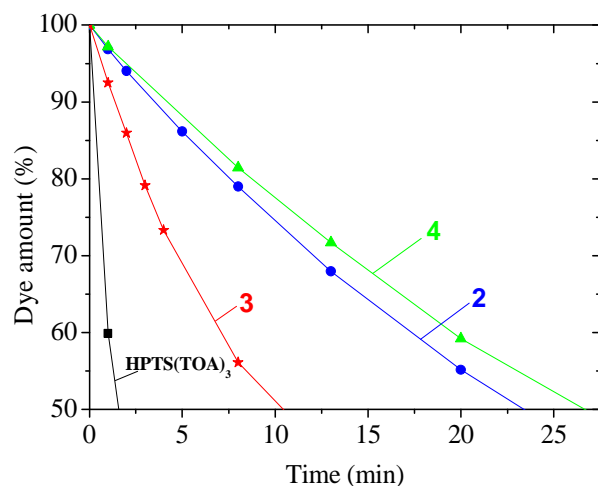
Figure S1.2. *Photodegradation profiles for the DPP dyes and HPTS dissolved in air-saturated tetrahydrofuran obtained from the absorption spectra of the neutral form of **2-4** and the deprotonated form of HPTS(TOA)₃ used for comparison.*
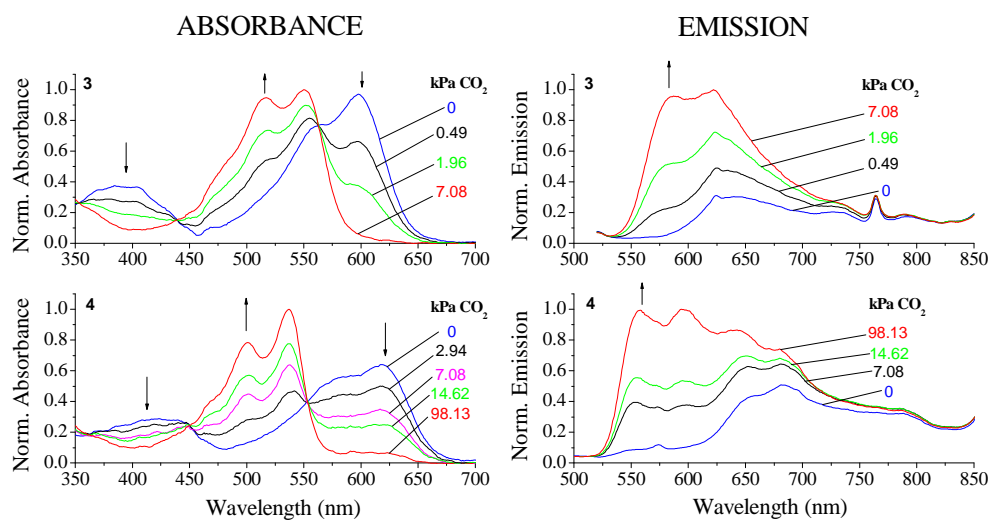
Figure S1.3. *Absorption (left) and emission spectra (right) for the carbon dioxide sensors based on **3** and **4** (25°C).*

ABSORBANCE   EMISSION
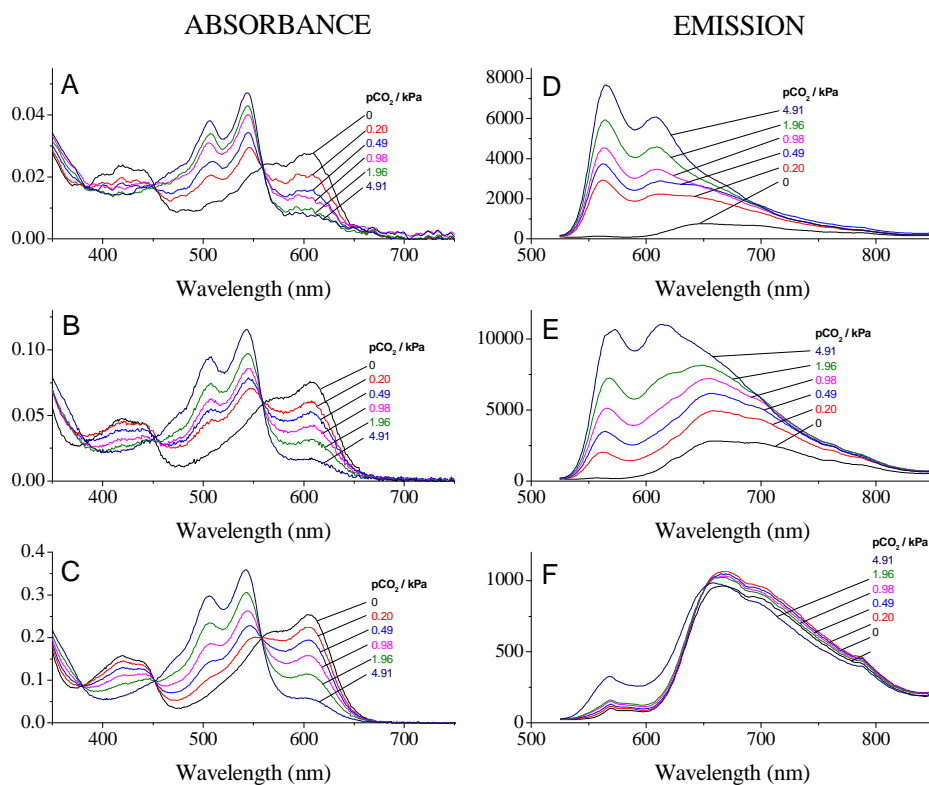
*Figure S1.4. Absorption and emission (λ_{exc} = 505 nm) spectra for 0.125% w/w (A, D), 0.4% w/w (B, E) and 1.2% w/w (C, F) of **2** in ethyl cellulose (EC 49) at 25 °C.*
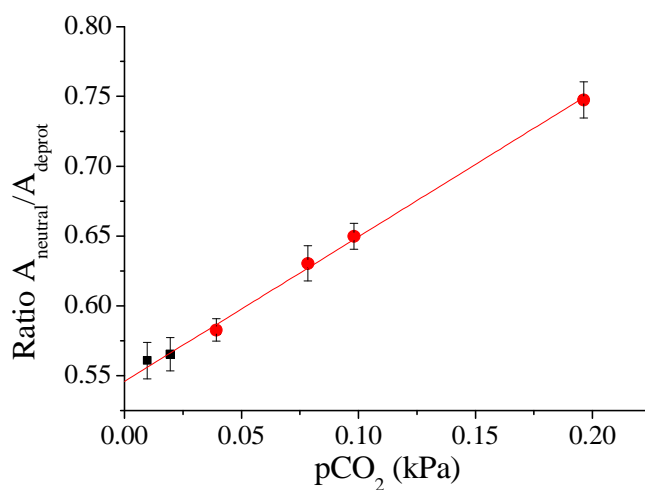
*Figure S1.5. Calibration curve (absorption) of a sensor based on **2** at 25°C.*
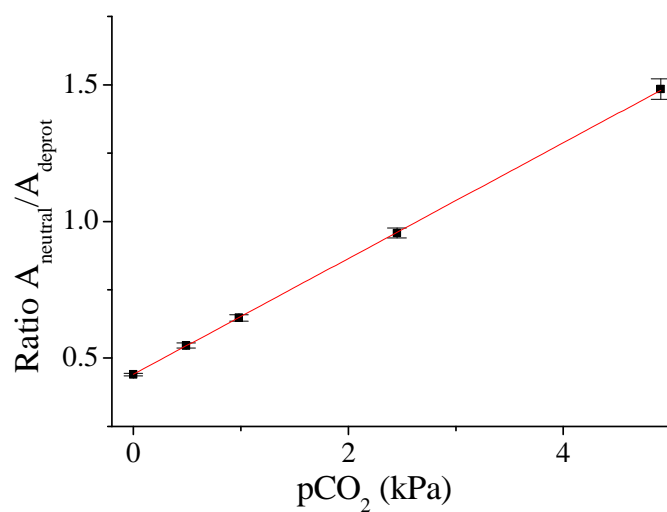
Figure S1.6. *Calibration curve (absorption) of a sensor based on* *4* *at 25°C. Calculated LOD 0.07 kPa.*
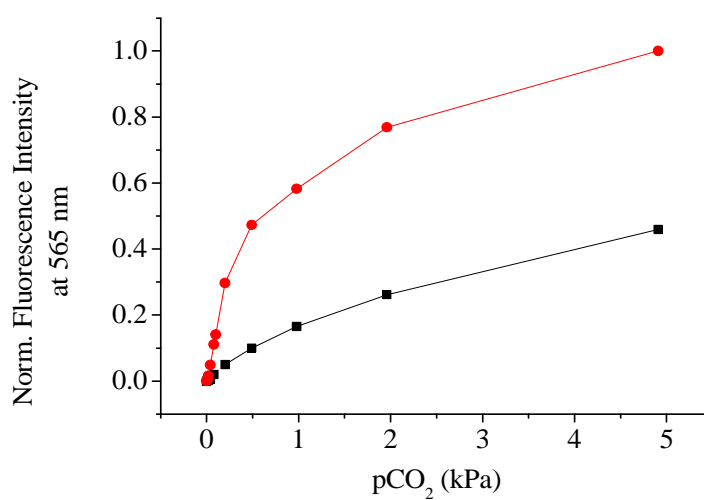
Figure S1.7. *Temperature dependence for the CO_2 sensor containing dye* *2* *in EC49 with TOAOH as base calibrated at 25 °C (red circles) and at 5°C (black squares).*

74
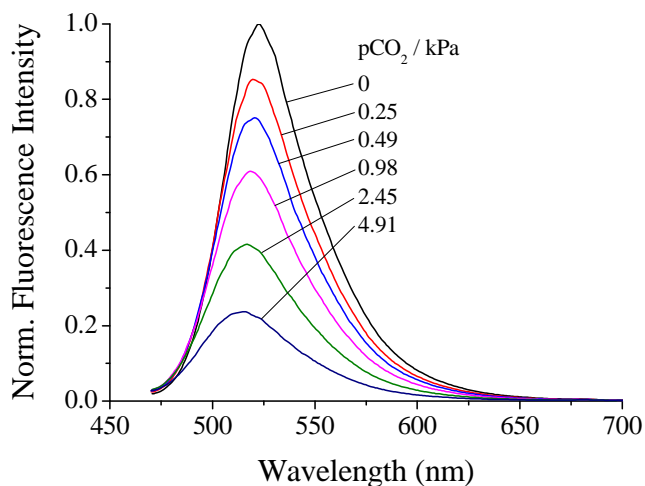
Figure S1.8. *Emission spectrum of a CO$_2$ sensor based on HPTS(TOA)$_3$ in EC 49 (λ_{exc} = 450 nm).*
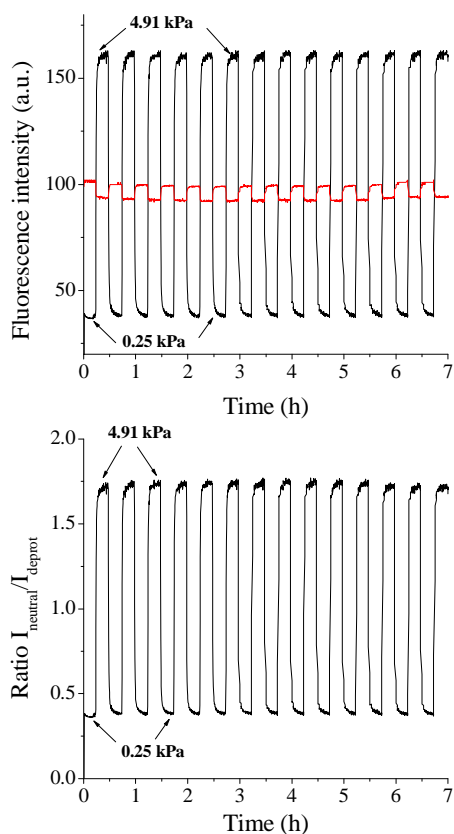
Figure S1.9. *Fluorescence intensity for the neutral (black line) and deprotonated (red line) forms of **3 (up)** and calculated ratio I$_{neutral}$/I$_{deprot}$ **(down)** for pCO$_2$ alternating between 0.25 kPa and 4.91 kPa under continuous excitation with 450 nm LED (25 °C).*

75
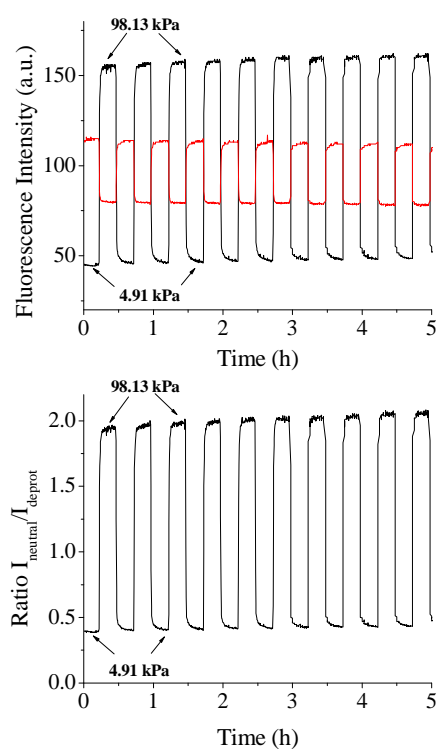
Figure S1.10. *Fluorescence intensity for the neutral (black line) and deprotonated (red line) forms of **4 (up)** and calculated ratio $I_{neutral}/I_{deprot}$ **(down)** for pCO_2 alternating between 4.91 kPa and 98.13 kPa under continuous excitation with 450 nm LED (25 °C).*

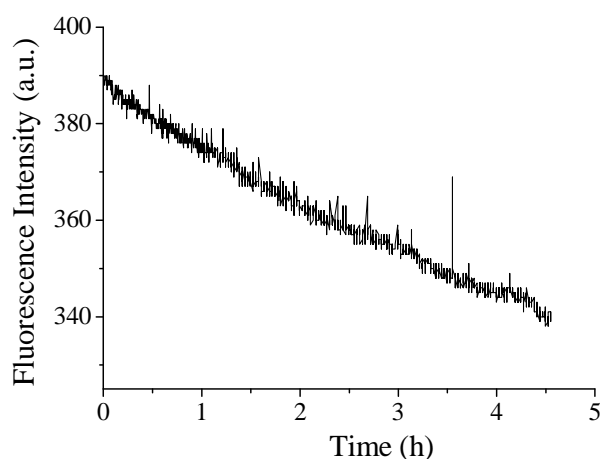***Figure S1.11.*** *Fluorescence intensity of the deprotonated form of HPTS(TOA)$_3$ (542-582 nm window) in EC 49 under continuous excitation with 450 nm LED (0 kPa CO_2, 25 °C).*
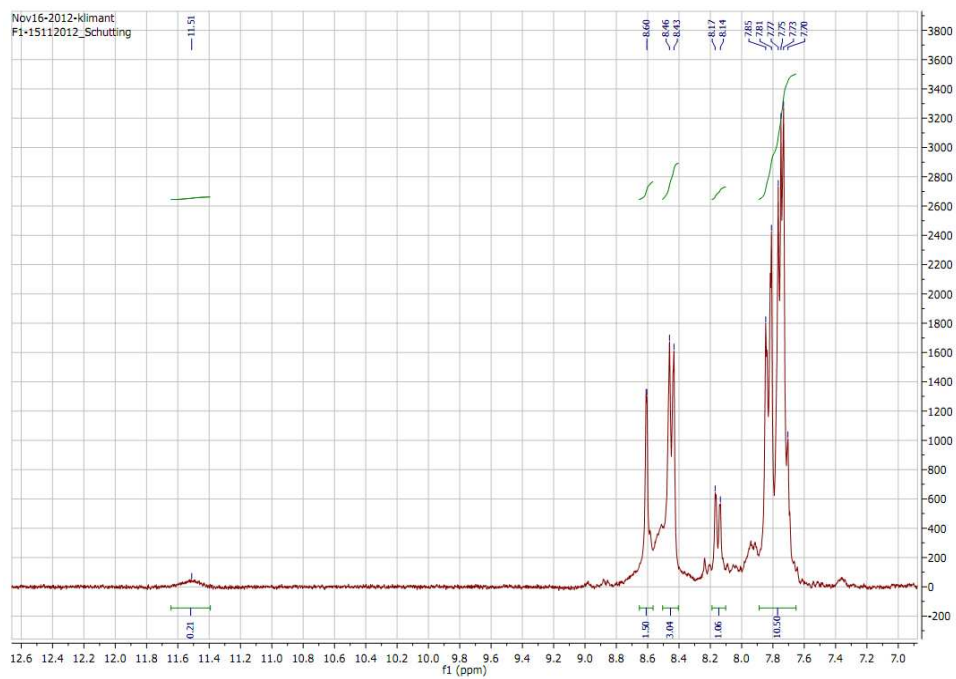
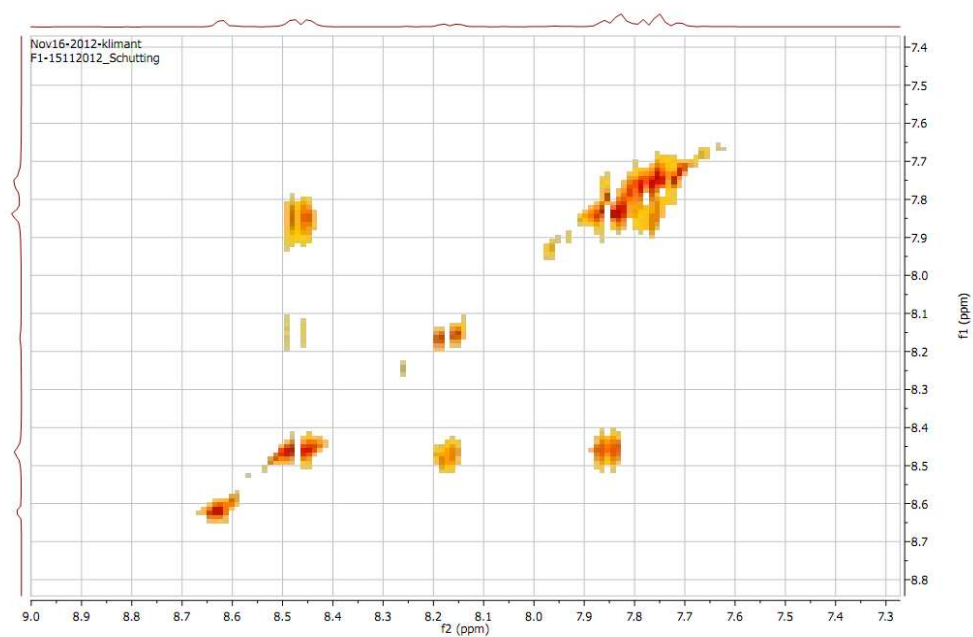***Figure S1.12***. *^{1}H NMR spectrum of **1** (300 MHz, DMSO-d6).*

Figure S1.13. *^{1}H ^{1}H COSY NMR spectrum of **1** (DMSO-d_6).*
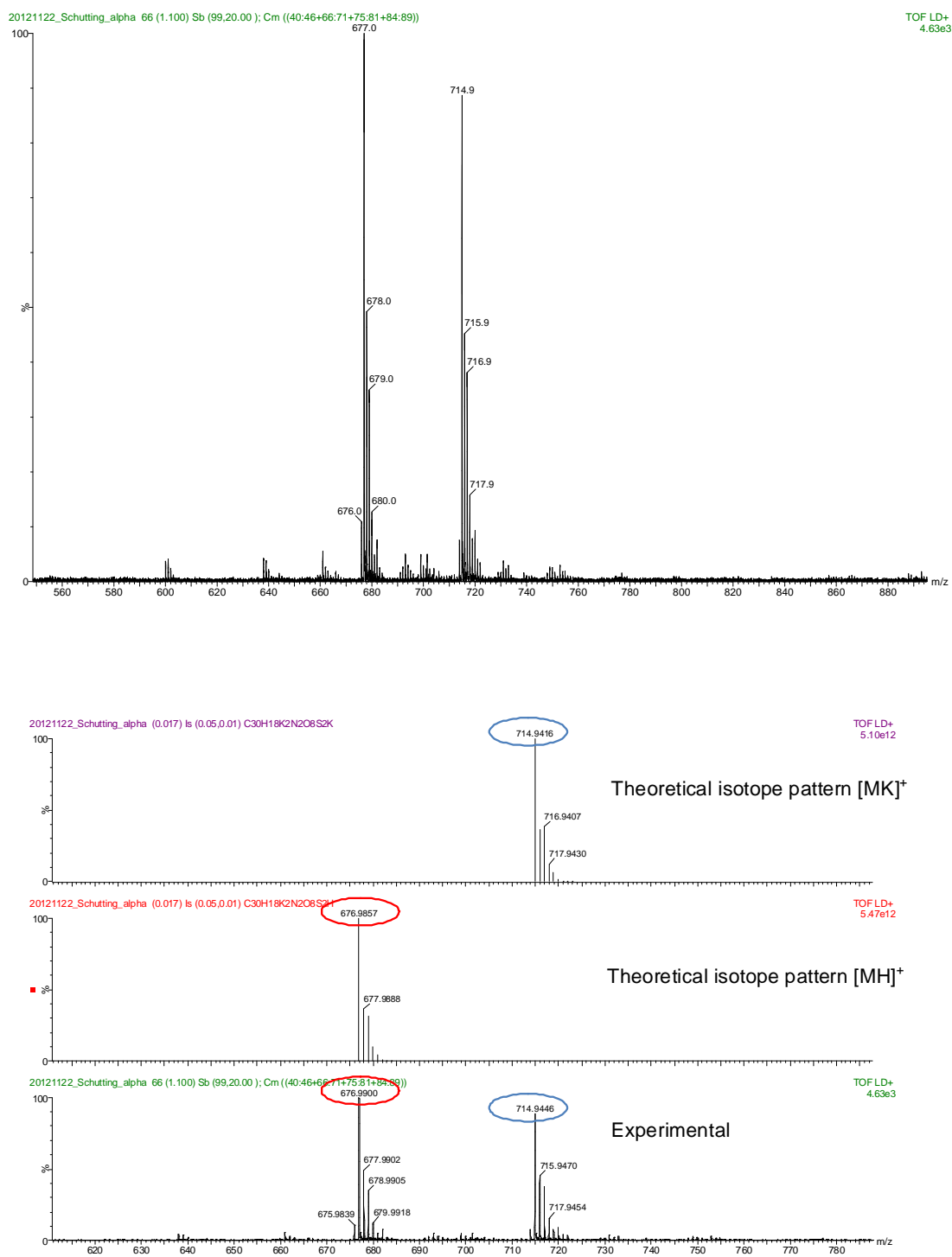
Figure S1.14. *MALDI-TOF mass spectrum of* **1**.

Figure S1.15. ^{1}H *NMR spectrum of* **2** *(300 MHz, CDCl₃).*

Figure S1.16. *MALDI-TOF mass spectrum of **2**.*

Figure S1.17. *^{1}H NMR spectrum of **3** (300 MHz, DMSO-d6).*

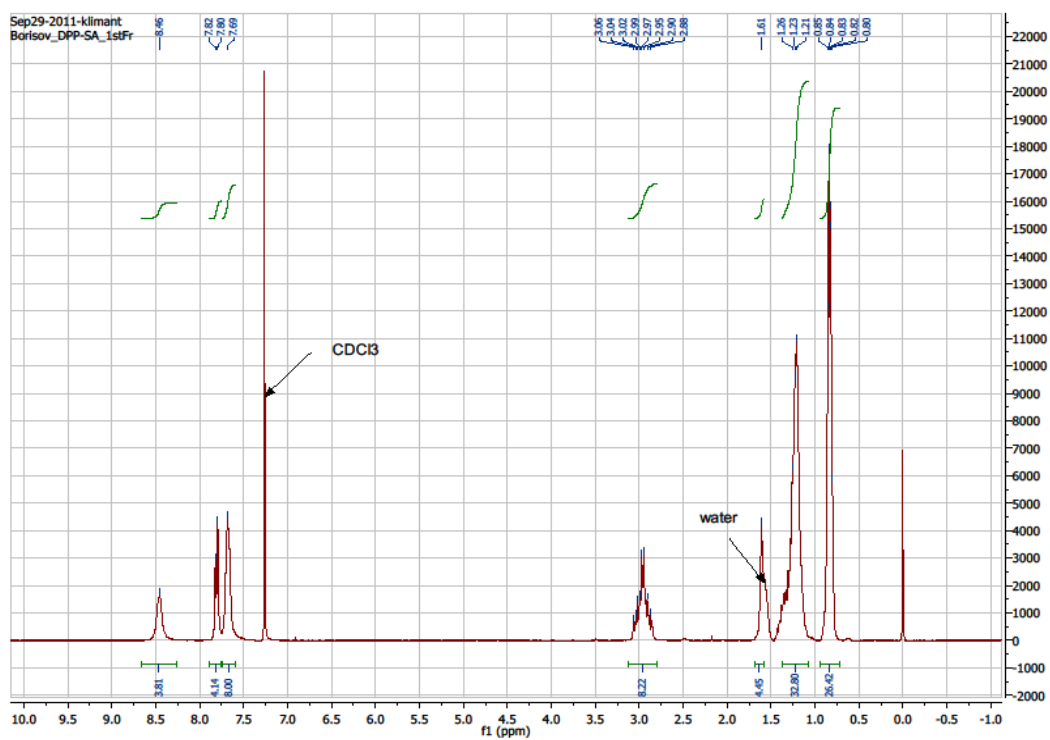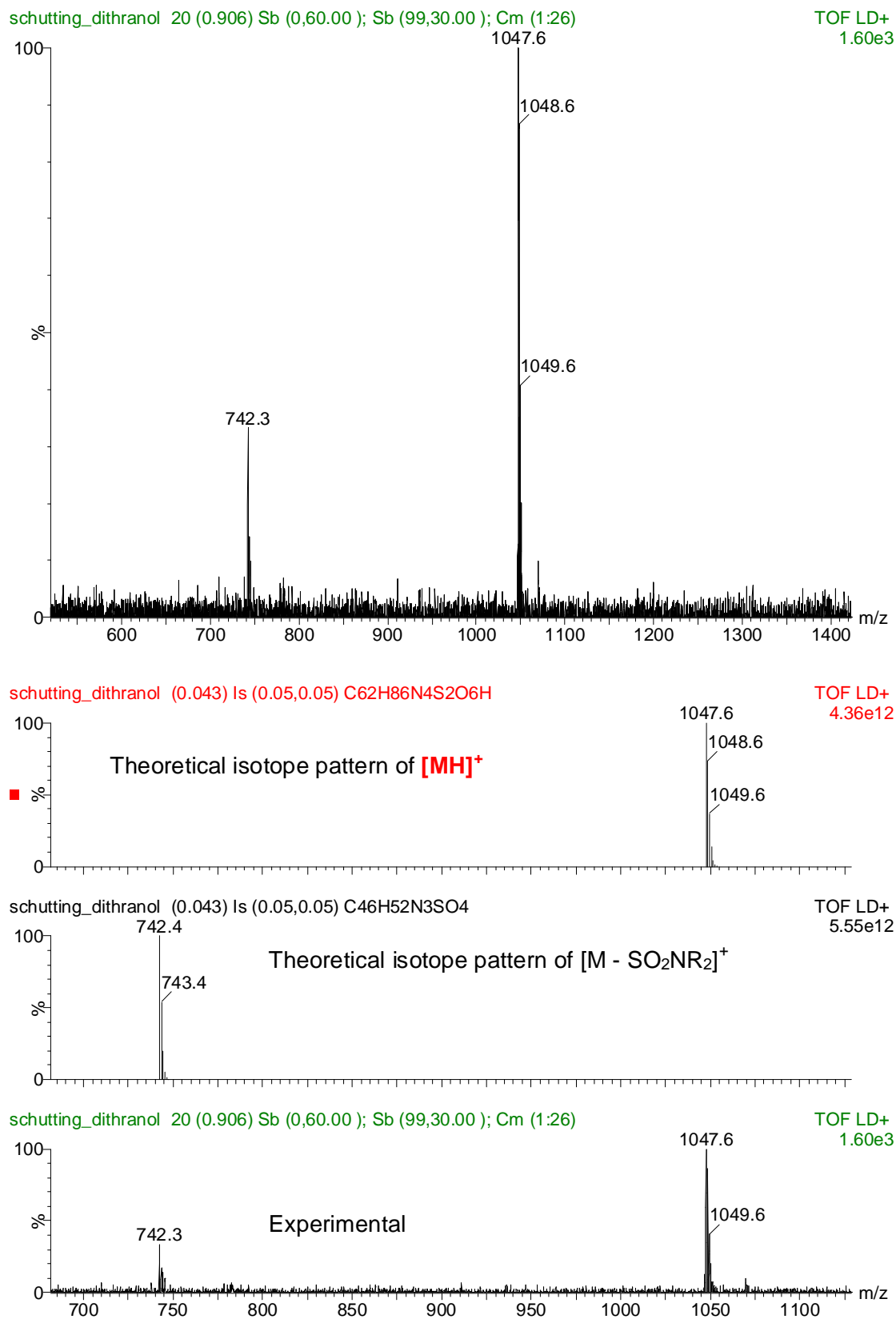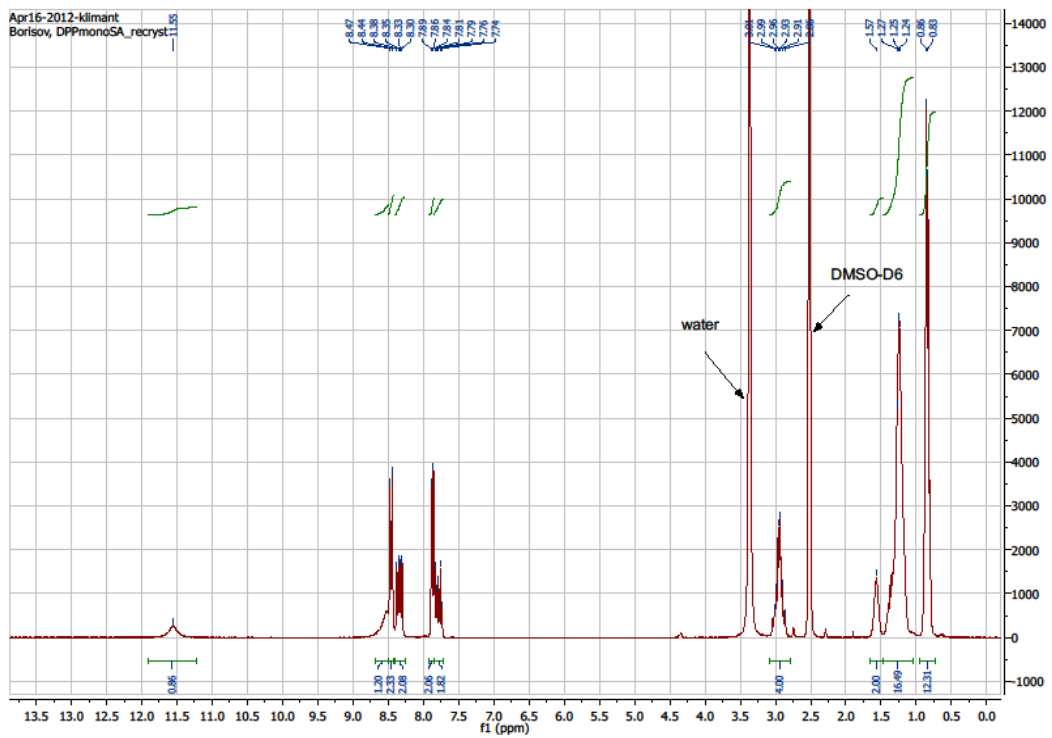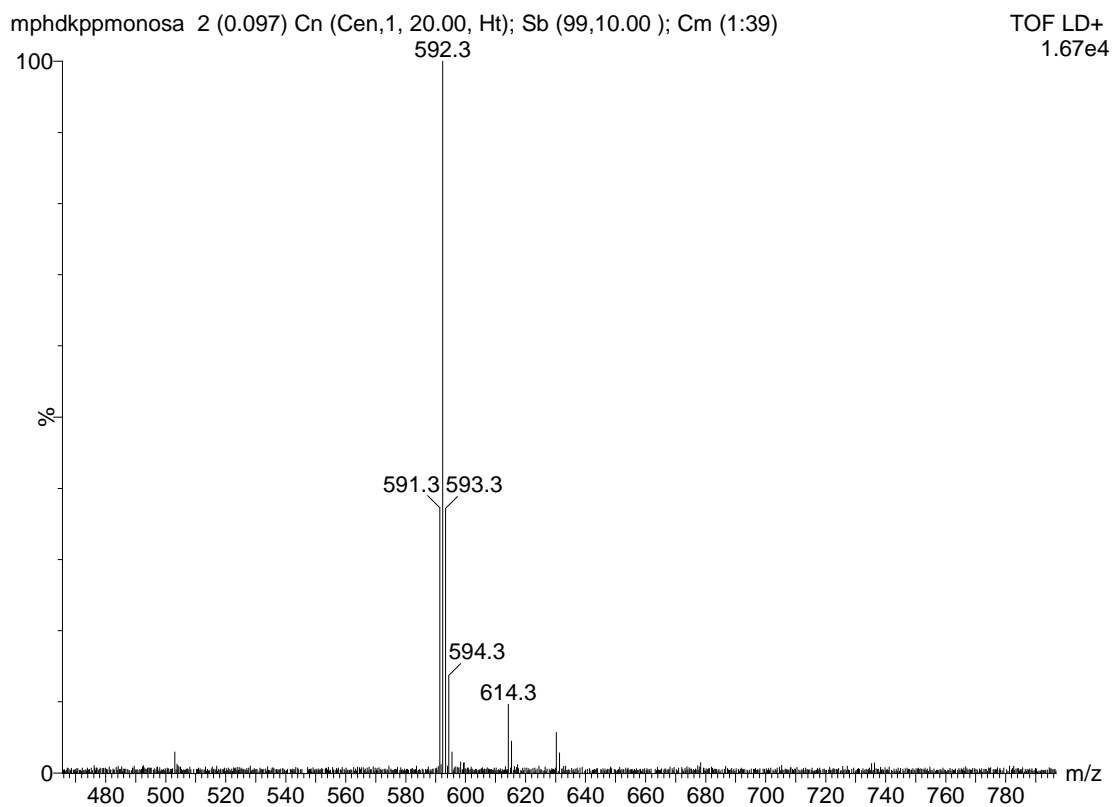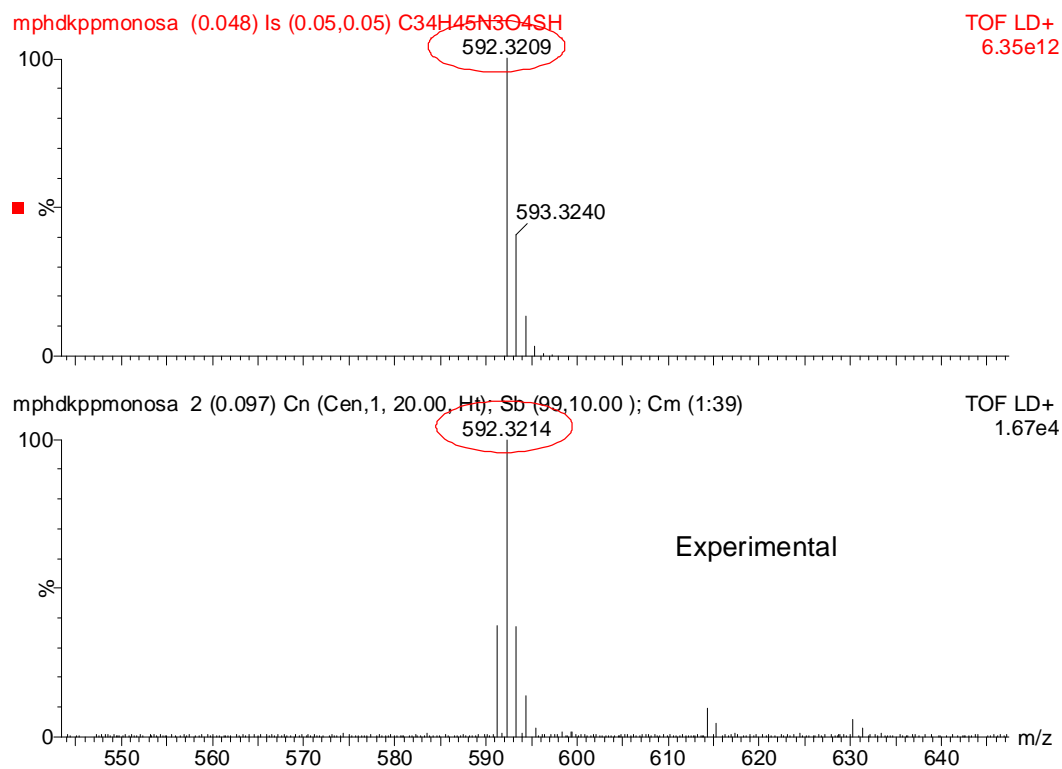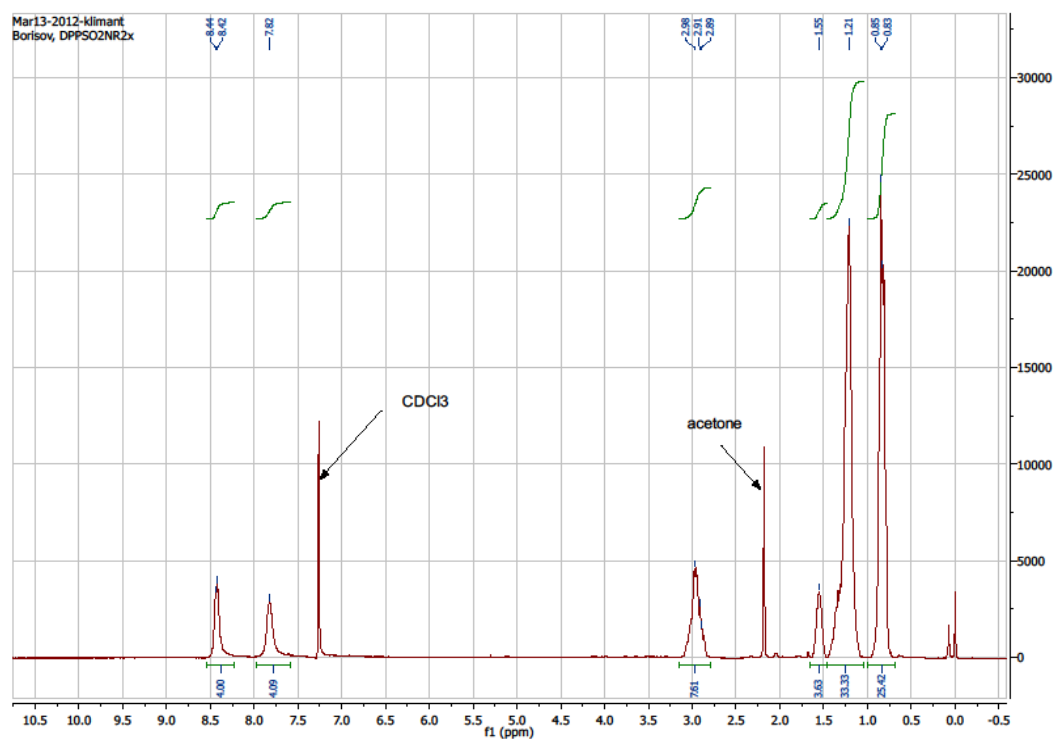**Figure S1.18.** *MALDI-TOF mass spectrum of **3**.*

Figure S1.19. *¹H NMR spectrum of **4** (300 MHz, CDCl₃).*
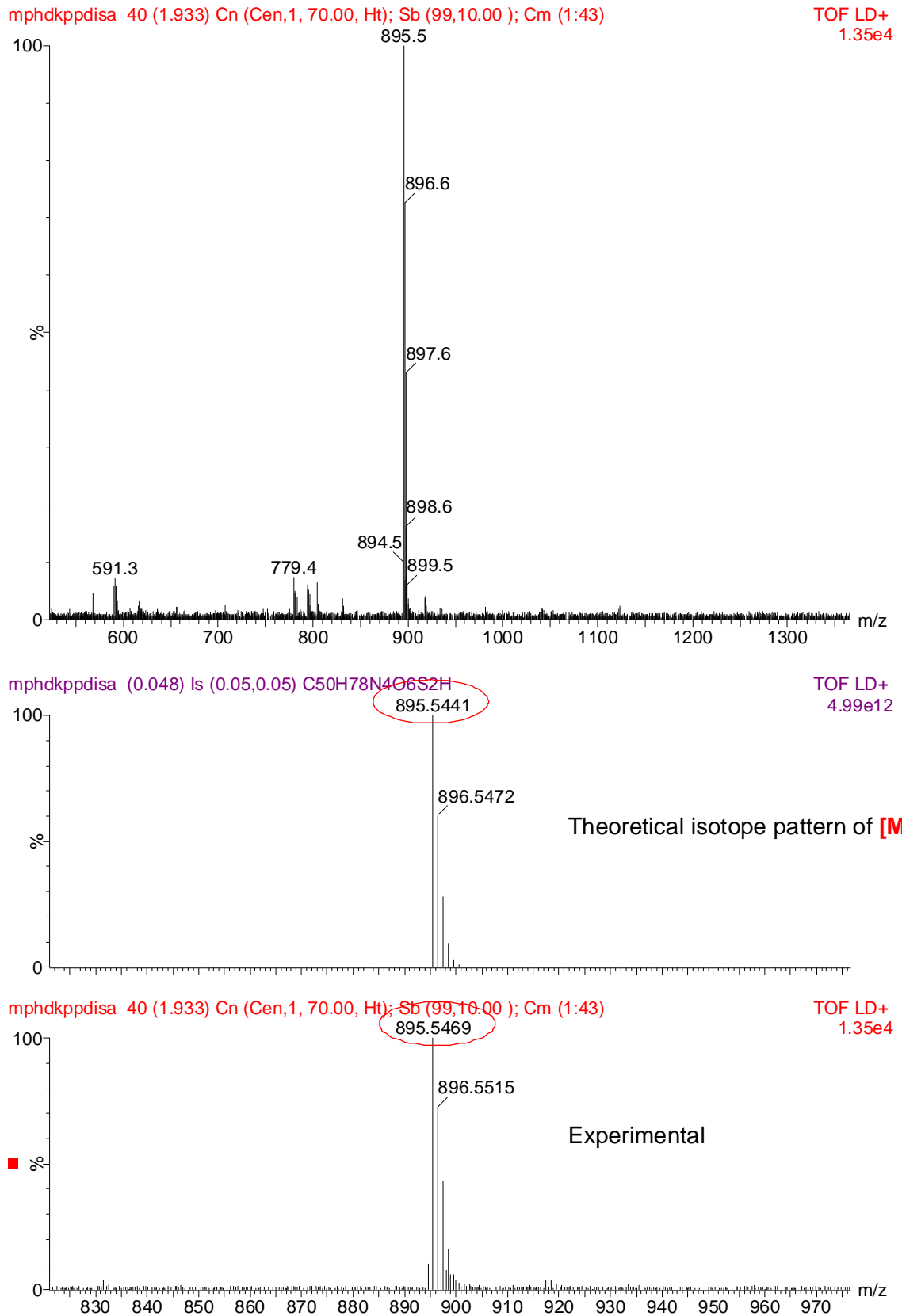
Figure S1.20. MALDI-TOF mass spectrum of 4.

Table S1.1. *Elementary analysis for the starting pigments Irgazin Ruby and Irgazin Scarlet, as well as for the fluorescence standards Lumogen Orange and Lumogen Red. The analysis indicates high purity of the used dyes and pigments.*

Irgazin Ruby	%N	%C	%H
found	6,31	81,35	4,53
calculated	6,36	81,80	4,58

Irgazin Scarlet	%N	%C	%H
found	9,71	74,70	4,09
calculated	9,72	74,99	4,20

Lumogen Orange	%N	%C	%H
found	3,92	80,59	5,94
calculated	3,94	81,10	5,96

Lumogen Red	%N	%C	%H
found	2,61	79,87	5,34
calculated	2,60	80,13	5,42

Chapter 2

Scope of this chapter

In the previous chapter a new indicator class based on diketo-pyrrolo-pyrroles was presented. It was shown, that this class is a promising alternative to known state-of-the-art indicators, such as HPTS. It was also shown, that there are still demands to meet, such as high quantum yields for the deprotonated indicator forms or even higher sensitivity.

In chapter 2, an enhancement of this indicator class will be presented. The pK_a value of the new indicator was even more increased due to substitution with electron-donating groups. Thus, the presented carbon dioxide sensors featured extremely high sensitivity.

Furthermore, the spectral properties were tuned to match the color channels of a commercially available red/green/blue (RGB) camera enabling read-out via imaging. Additionally, the quantum yields for both, the protonated and the deprotonated form, are very high.

New Highly Fluorescent pH Indicator for Ratiometric RGB Imaging of pCO$_2$

Authors: Susanne Schutting, Ingo Klimant, Dirk de Beer and Sergey M. Borisov

A new diketo-pyrrolo-pyrrole (DPP) indicator dye for optical sensing of carbon dioxide is prepared via a simple 1 step synthesis from commercially available low cost "Pigment Orange 73". The pigment is modified via alkylation of one of the lactam nitrogens with a tert-butylbenzyl group. The indicator dye is highly soluble in organic solvents and in polymers and shows pH-dependent absorption (λmax 501 and 572 nm for the protonated and deprotonated form, respectively) and emission spectra (λmax 524 and 605 nm for the protonated and deprotonated form, respectively). Both the protonated and the deprotonated form show high fluorescence quantum yields (Φprot 0.86; Φdeprot 0.66). Hence, colorimetric read-out and ratiometric fluorescence intensity measurements are possible. The emission of the two forms of the indicator excellently matches the response of the green and the red channel of an RGB camera. This enables imaging of carbon dioxide distribution with simple and low cost optical set-up. The sensor based on the new DPP dye shows very high sensitivity and is particularly promising for monitoring of atmospheric levels of carbon dioxide.

Introduction

Carbon dioxide is one of the most important parameters for environmental monitoring, marine research and oceanography. The increase of carbon dioxide concentration in the oceans causes acidification, which severely affects the flora and fauna therein.[9,14,96–98,138] The analytical tools for detection of dissolved carbon dioxide are limited to only a few such as the Severinghaus electrode[77] or IR analyzers. The former suffers from electromagnetic interferences and has slow response. IR analyzers are fast,[61] but are

mostly suitable for measurements in gaseous phase[85,86] since water causes a significant interference. Several new concepts of carbon dioxide chemosensors were published in recent years;[116–118,139,140] however so called 'plastic type' sensors remain the most common ones.[51,89] These materials contain a pH-sensitive dye and a base (most commonly a quaternary ammonium base) dissolved in a polymer matrix. The pH indicator responds to the analyte by altering its optical properties, mostly the absorption or emission characteristics. In case of the fluorescent sensors referencing of the fluorescence intensity is required to enable reliable measurements. This can be achieved by adding a second analyte-insensitive dye which emission spectrum is clearly separated from that of the indicator (ratiometric read-out) or which luminescence decay time is significantly different from the lifetime of the indicator (dual lifetime referencing scheme).[141–143] In both schemes photobleaching (indicator, reference dye or both) causes a dramatic change of the emission ratio of the indicator and the reference dye. Therefore, self-referencing indicator dyes are highly desirable; however only a few such dyes have been reported.[144–147] Spectral compatibility with commercially available red/green/blue (RGB) cameras is also of great interest. The read-out with RGB cameras is a simple and low cost technique for imaging different parameters such as CO_2,[148] pH[149–152] or oxygen,[153–156] to name only a few. Recently, we presented a new class of pH-sensitive indicator dyes based on diketo-pyrrolo-pyrroles (DPPs).[152,157] DPPs are usually insoluble in organic solvents and are mainly used as pigments.[119] The soluble derivatives (mainly N-alkylated dyes)[120,158–164] are also of much practical interest and are applied e.g. in photovoltaics.[158–160] So far only a few applications of DPPs as fluorescent probes are found in the literature.[127,128,152,165] The new DPP-based pH indicators were shown to be highly promising for application in optical pH and carbon dioxide sensors.[152,157] Particularly, dual emission from the protonated and deprotonated forms enabled ratiometric read-out, but the emission from the deprotonated form was much weaker than that of the protonated form ($\Phi_{prot} \approx 1$ and $\Phi_{deprot} \approx 0.1$). Unfortunately, these dually emitting dyes were not fully compatible with the green and red channels of the digital cameras.[166] In this study, we present a new DPP-based pH indicator which overcomes these drawbacks. It will be shown that the new dye possesses high fluorescence quantum yields for both the protonated and the deprotonated form and is excellently suitable for the RGB read-out. The CO_2 sensor shows very high sensitivity and is particularly useful for monitoring atmospheric levels of the analyte.

Experimental Details

Materials

1,4-diketo-3,6-bis(4-tert-butyl-phenyl)-2,5-dihydro pyrrolo[3,4-c]pyrrole (Pigment Orange 73), 1,6,7,12-tetraphenoxy-N,N´-bis(2,6-diisopropylphenyl)-perylene-3,4:9,10-tertracarboxylic bisimide (Lumogen-Red) and N,N´-bis(2,6-diisopropylphenyl)-perylene-3,4:9,10-tertracarboxylic bisimide (Lumogen-Orange) were purchased from Kremer Pigments (Germany, www.kremer-pigmente.com). Ethyl cellulose 49 (EC49, ethoxyl content 49%), sodium sulfate (anhydrous), sodium tert-butoxide, 4-tert-butylbenzyl bromide, tetraoctylammonium hydroxide solution (TOAOH, 20% in methanol) and anhydrous dimethylformamide were obtained from Sigma-Aldrich (www.sigmaaldrich.com). All other solvents were purchased from VWR (Austria, www.vwr.com). The silicone components: vinyl terminated polydimethylsiloxane (viscosity 1000 cSt.), (25-35% methylhydrosiloxane)-dimethylsiloxane copolymer (viscosity 25-35 cSt.), 1,3,5,7-tetravinyl-1,3,5,7-tetramethylcyclotetrasiloxane and the platinum-divinyltetramethyldisiloxane complex were received from ABCR (Germany, www.abcr.de). Ultrafine hydrophobic titanium dioxide P170 was purchased from Kemira (www.kemira.com). High purity nitrogen, 5% carbon dioxide in nitrogen, 0.2% carbon dioxide in nitrogen and carbon dioxide were obtained from Air Liquide (Austria, www.airliquide.at). Poly(ethylene terephthalate) (PET) support Melinex 505 was obtained from Pütz (Germany, www.puetz-folien.com). Silica-gel was received from Roth (www.carlroth.com). Synthesis of BiPh-DiSA (3,6-bis[4´-bis(2-ethylhexyl)sulfonylamide-1,1´-biphenyl-4-yl]-2,5-dihydropyrrolo[3,4-c]pyrrole-1,4-dione) and MoPh-DiSA (3,6-bis[4-bis(2-ethylhexyl)sulfonylamide-phenyl]-2,5-dihydropyrrolo[3,4-c]pyrrole-1,4-dione) was described before.[157]

Synthesis of 2-hydro-5-tert-butylbenzyl-3,6-bis(4-tert-butyl-phenyl)-pyrrolo[3,4-c]pyrrole-1,4-dione (DPPtBu³)

Pigment Orange 73 (2 g, 4.9 mmol) and sodium tert-butoxide (0.96 g, 10 mmol) were dissolved in anhydrous dimethylformamide (80 ml). 4-tert-butylbenzyl bromide (1.1 ml, 6.0 mmol) was added dropwise. After stirring for 8 h at 60 °C the mixture was diluted with deionized water. The dye was extracted with dichloromethane and hydrochloric acid and sodium chloride were added to facilitate the phase separation. The organic

phase was collected, dried over anhydrous sodium sulfate and evaporated to dryness under reduced pressure. The crude product was purified via column chromatography on silica gel using dichloromethane/tetrahydrofuran (98:2). The product was dissolved in dichloromethane and precipitated with hexane to give an orange powder (0.23 g, 8.3% of theoretical yield of DPPtBu$_3$). DI-EI-TOF: m/z of [MH]$^+$ found 546.3259, calculated 546.3246. ^{1}H NMR (300MHz, CDCl3) δ 9.38 (s, 1H), 8.28 (d, 2H), 7.77 (d, 2H), 7.53 (d, 2H), 7.50 (d, 2H), 7.34 (d, 2H), 7.16 (d, 2H), 5.04 (s, 2H), 1.35 (s, 18H), 1.30 (s, 9H). Analysis for $C_{37}H_{42}N_2O_2$ found: C81.12, H7.59, N5.12, calculated: C81.28, H7.74, N5.12.

Preparation of the Planar Optodes

"Cocktail 1" containing X mg of the dye and 100 µl the tetraoctylammonium hydroxide solution (20% TOAOH in methanol) was purged with carbon dioxide gas. X was 3.0 mg and 0.5 mg for the absorption and emission measurements, respectively. "Cocktail 2" containing 200 mg ethyl cellulose (EC49) dissolved in 3800 mg of a toluene:ethanol mixture (6:4 w/w) was added to the "cocktail 1". The resulting solution was knife-coated on a dust-free PET or glass support. A sensing film of ~7.5 µm thickness was obtained after evaporation of the solvent. The sensing film was covered with a gas-permeable ~22 µm-thick silicone layer by knife-coating "cocktail 3" consisting of 800 mg vinyl terminated polydimethylsiloxane, 32 µl (25-35% methylhydrosiloxane)-dimethylsiloxane copolymer, 2 µl 1,3,5,7-tetravinyl-1,3,5,7-tetramethylcyclotetrasiloxane and 4 µl platinum-divinyltetramethyldisiloxane complex dissolved in 1600 mg hexane. For emission measurements a similar layer was prepared but 200 mg of titanium dioxide were dispersed in "cocktail 3". The sensors were kept in an oven (60 °C) for 10-15 min to complete polymerization of the silicone rubber.

Methods

^{1}H NMR spectra were recorded on a 300 MHz instrument (Bruker) in CDCl$_3$ with TMS as standard. Absorption spectra were recorded on a Cary 50 UV-Vis spectrophotometer (www.varianinc.com). Determination of the molar absorption coefficients was carried out as an average of 3 independent measurements. Photobleaching experiments were performed by irradiating the samples (2.5 ml) with the light of a high-power 10 W LED array (λ_{max} 458 nm, 3 LEDs, www.led-tech.de) operated at 6 W input power. A lens

(Edmund optics, www.edmundoptics.de) was used to focus the light of the LED array on the glass cuvette (photon flux: ~4000 µmol·s^{-1}·m^{-2} as determined with a Li-250A light meter from Li-COR, www.licor.com). The photodegradation profiles were obtained by monitoring the absorption spectra of the respective dye dissolved in tetrahydrofuran and represented an average from three independent experiments. The solutions were homogenized by shaking after each illumination period. Fluorescence spectra were recorded on a Hitachi F-7000 fluorescence spectrometer (www.hitachi.com) equipped with a red-sensitive photomultiplier R928 from Hamamatsu (www.hamamatsu.com). Relative fluorescence quantum yields were determined according to Demas and Crosby.[129] The solutions of Lumogen-Orange ($\Phi \approx$ 1) and Lumogen-Red ($\Phi \approx 0.96$)[130,131] in chloroform were used as standards for the protonated and the deprotonated form, respectively. Three independent measurements were performed for determination of the relative quantum yields and the average value obtained was used. In case of the sensing materials only the absolute quantum yields were determined. These measurements were performed on a Fluorolog3 fluorescence spectrometer (www.horiba.com) equipped with a NIR-sensitive photomultiplier R2658 from Hamamatsu (300-1050 nm) and an integrating sphere (Horiba).

Gas calibration mixtures were obtained using a gas mixing device from MKS (www.mksinst.com). The gas mixture was humidified to about 85% relative humidity (saturated KCl solution) prior entering the calibration chamber. Temperature was controlled by a cryostat ThermoHaake DC50. Photographic images were acquired with a Canon 5D camera equipped with a Canon 24-105L objective and two layers of a LEE plastic filter "spring yellow". The same high-power 10 W LED array (λ_{max} 458 nm, 3 LEDs, www.led-tech.de) as for the photodegradation experiments combined with a short-pass BG-12 filter served as an excitation source.

Results and Discussion

Synthesis

The DPP chromophores possess planar structure and are poorly soluble in organic solvents.[133] Low solubility prevents the dyes from application as indicators in optical sensors. We previously demonstrated that the dyes are pH-sensitive due to the

deprotonation of the lactam nitrogen.[152,157] Modification of the phenyl rings with bulky substituents rendered the pigments soluble in organic solvents and polymers and the pH sensitivity was preserved. On the other hand, alkylation of both lactam nitrogens is another simple way to greatly enhance the solubility of DPPs.[134] Evidently such modification renders the DPPs pH-insensitive. Mono-N-alkylation of the commercially available *Pigment Orange 73* (scheme 2.1) with a tert-butylbenzyl-group preserves pH sensitivity and dramatically improves the solubility of the dye in such common solvents as toluene, tetrahydrofuran (THF), dichloromethane, chloroform, etc. Thus, the dye becomes suitable for application in optical plastic carbon dioxide sensors.
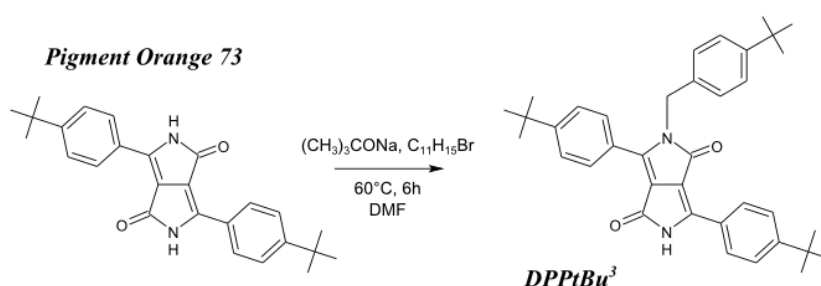
Scheme 2.1. *Synthesis of DPPtBu³ starting from Pigment Orange 73.*

Photophysical Properties

Absorption and emission spectra for DPPtBu³ dissolved in THF are shown in figure 2.1. The protonated form of the dye absorbs in the blue and emits in the green part of the electromagnetic spectrum. Absorption and emission spectra for the deprotonated form are bathochromically shifted by ~70 nm compared to the protonated form. This is about 50 nm less than in case of previously reported DPP dye MoPh-DiSA (3,6-bis[4-bis(2-ethylhexyl)sulfonylamide-phenyl]-2,5-dihydropyrrolo[3,4-c]pyrrole-1,4-dione, table 2.1).[157] The mono-alkylated dye shows spectral maxima at shorter wavelengths than not alkylated MoPh-DiSA. The molar absorption coefficients are typical for the DPP dyes (table 2.1). The fluorescence quantum yields are rather high and are comparable for both forms of DPPtBu³ (table 2.1). On the contrary, the emission of the deprotonated form of MoPh-DiSA is much weaker than the emission of the protonated form.
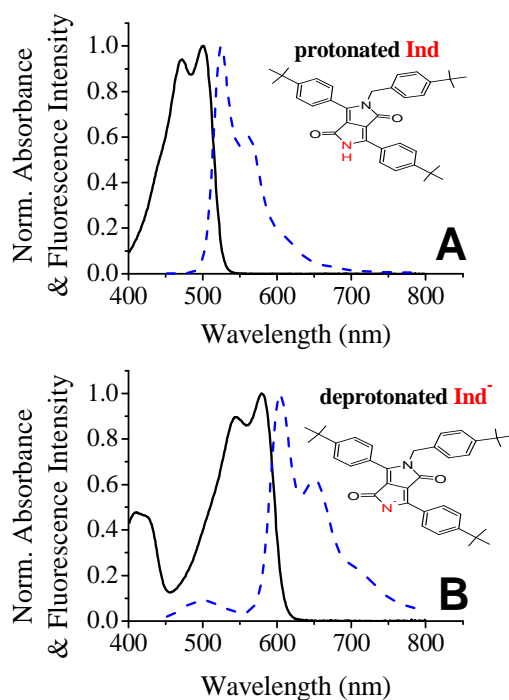
Figure 2.1. *Absorption (solid lines) and emission (λ_{exc} 430nm, dashed lines) spectra of the protonated form (**A**) and the deprotonated form (**B**) of DPPtBu^3 in THF.*

Table 2.1. *Comparison of the photophysical properties of DPPtBu^3 and the DPP dye MoPh-DiSA in tetrahydrofuran (THF) at 25 °C.*

	Protonated form			Deprotonated form		
Dye	λ_{abs} ($\varepsilon \cdot 10^{-3}$) [nm ($M^{-1}cm^{-1}$)]	λ_{em} [nm]	Φ	λ_{abs} ($\varepsilon \cdot 10^{-3}$) [nm ($M^{-1}cm^{-1}$)]	λ_{em} [nm]	Φ
DPPtBu^3	472(25.2); 501(26.8)	524	0.86	572(17.6)	605	0.66
MoPh-DiSA	491(29.8); 528(36.9)	543;583	1	655(23.0)	708	0.11

DPPtBu^3 is highly soluble in organic solvents, but is not soluble in water. Therefore, determination of the pK_a in aqueous buffers is not possible. The pK_a value in a mixture of tetrahydrofuran and aqueous buffer (1:1 v/v) was estimated to be rather high (~12.7; supporting information, figure S2.1). It should be noted that this is very rough estimation because of the high content of organic solvent and the alkali error of the pH electrode at high pH. The pK_a value for DPPtBu^3 is likely to be higher than that for the recently presented DPP dye (3,6-bis[4´(3´)-disulfo-1,1´-biphenyl-4-yl]-2,5-

dihydropyrrolo[3,4-c]pyrrole-1,4-dione dipotassium salt)[157] which showed a pK_a of ~11.8 since electron-donating tert-butyl groups of DPPtBu[3] are expected to elevate the dissociation constant.

Carbon Dioxide Sensors

DPPtBu[3] and the base tetraoctylammonium hydroxide (TOAOH) were non-covalently entrapped in an ethyl cellulose (EC49) matrix to obtain plastic type carbon dioxide sensors. The response of the sensor can be described by the following equation:

$$Ind^-TOA^+ + CO_2 + H_2O \leftrightarrow IndH + TOA^+HCO_3^-$$
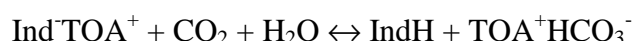
It is essential that the carbon dioxide sensors are kept humid during the measurements to enable reversible and reliable response (supporting information, figure S2.3). The sensors respond to increasing pCO_2 with a color change from pink in the absence of CO_2 to yellow in the presence of CO_2. This corresponds to the change in the absorption spectra of the sensing material (figure 2.2A). Isosbestic points (IP) at 430 nm and 522 nm are clearly visible which indicates that only two forms of the dye are present in the acid-base equilibrium. The sensor shows red fluorescence at low pCO_2 and green fluorescence at high pCO_2 (figure 2.2B). For emission measurements commercially available intense LEDs emitting at wavelengths between 430 nm and 470 nm are suitable as excitation sources. As can be seen, the emission intensity of the deprotonated form decreases, whereas the intensity of the protonated form increases with increasing pCO_2 (figure 2.2C). Importantly, virtually no fluorescence of the protonated form (λ_{max} 529 nm) is detectable in the absence of carbon dioxide, so that the relative signal changes are very high at low pCO_2. Comparison of the absorption and emission spectra (figure 2.2A and 2.2B) indicates the effect of Förster resonance energy transfer (FRET) from the protonated form of the indicator to its deprotonated form. Indeed, the emission spectrum of the former and the absorption spectrum of the latter show almost perfect overlap (figure 2.1). The dye concentration dramatically affects the emission due to FRET (supporting information, figure S2.4). For example, in case of high dye concentration (1.5% w/w) the emission spectrum is dominated by the deprotonated form at pCO_2 below 5 kPa. Hence, the dynamic range of the sensing materials relying on fluorescence intensity read-out can be tuned by adjusting the concentration of the

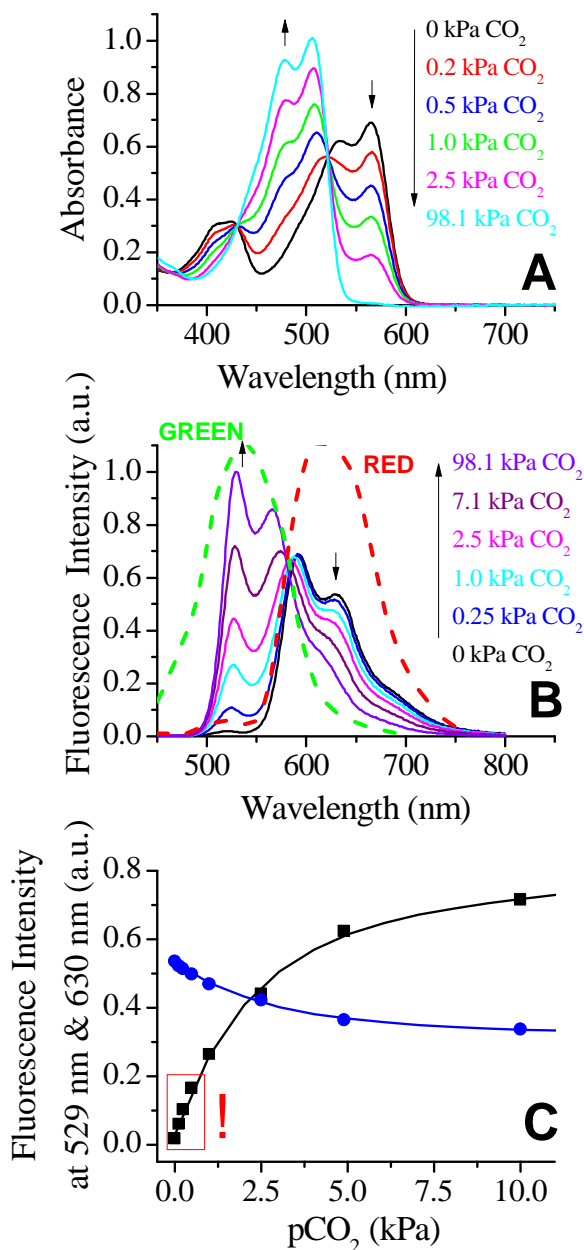indicator dye. Highly sensitive fluorescent sensors are obtained only for relatively low dye concentrations.

Figure 2.2. *Absorption (**A**) and emission (**B**) spectra (λ_{exc} 430 nm) of the CO_2 sensor based on DPPtBu[3] in ethyl cellulose 49 and TOAOH as base including the spectral sensitivity for the green and the red detection channels of the RGB camera (green and red dotted lines, B). (**C**) the fluorescence intensity changes for the protonated form (at 529 nm, black curve) and the deprotonated form (at 630 nm, blue curve) with increasing pCO_2, the fit is performed according to the exponential growth/decay model, respectively; high relative signal changes at low pCO_2 values (red box and exclamation mark) are indicated.*

Compared to the solution the spectral properties of the indicator are mostly preserved (figure 2.1 and figure 2.2). The fluorescence quantum yields are high ($\Phi \approx 1.0$ and 0.63) for the protonated form and the deprotonated form, respectively. Carbon dioxide sensors based on DPPtBu[3] are highly sensitive to pCO_2 at 25°C (red box and exclamation mark in figure 2.2C). Due to better solubility of CO_2 at lower temperatures, the sensitivity is even higher at 5°C (figure 2.3). It should be mentioned that rather strong temperature dependence is common for the *plastic type* carbon dioxide sensors,[61] but development of the materials with lower temperature cross-talk was beyond the scope of this study. Low levels of pCO_2 need to be measured in a completely decarbonated system – from gas lines, gas mixing device and humidifier to the flow-through cell – which is difficult to achieve in practice. Particularly, precise calibration at the atmospheric level of 0.04 kPa pCO_2 and lower is challenging. The exchange of PET foil to gas-impermeable glass support improved the linearity at low pCO_2, but did not solve the contamination problem entirely. This is well observable in the absorption measurements where such contamination results in larger deviation than during fluorescence measurements influenced by FRET (figure 2.3B and 2.3D, respectively). Determination of the limit of detection (LOD) was therefore not possible. Nevertheless, it can be concluded that the sensor shows excellent response at atmospheric levels (pCO_2 0.04 kPa $\approx$ 400 ppm in the gas phase $\approx$ 11.6 µmol/L in water at 298.15 K) of carbon dioxide and therefore is highly promising for e.g. oceanographic applications.
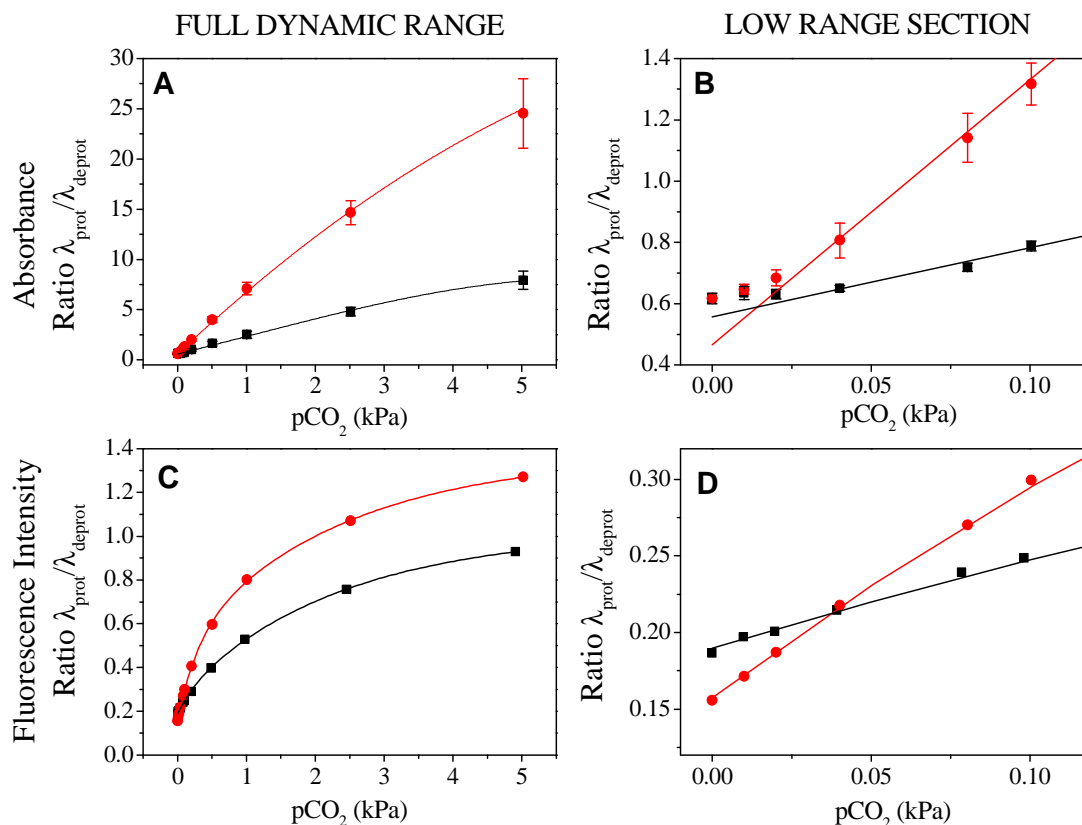
Figure 2.3. *Absorption (A, B) and emission (C, D) calibration curves of carbon dioxide sensor based on DPPtBu[3] for the full dynamic range from 0 to 4.9 kPa pCO_2 (A, C) at 5°C (red dots) and 25°C (black squares) and for the respective low range sections (B, D). A linear fit (B, D), polynomial 2 fit (A) and exponential growth fit (C) were used.*

Photostability

The sulfonamide-based DPP indicators reported previously possessed adequate photostability for practical applications. Electron-withdrawing groups often improve the photostability of the fluorescent dyes and the electron-donating groups have an opposite effect.[62] Thus, photostability of DPPtBu[3] bearing two electron-donating tert-butyl groups may be significantly lower than that for the sulfonamide-based indicators such as BiPh-DiSA.[157] However, photobleaching experiments carried out for the THF solutions of DPPtBu[3] and BiPh-DiSA and an optical CO_2 sensor based on DPPtBu[3] (using a high power blue LED array, λmax = 458 nm, for the excitation of the protonated form of the dye; photon flux: ~4000 µmol·s^{-1}·m^{-2}) revealed that the photostability of both dyes is very similar. Both dyes showed about 50%

photodegradation in solution after 27 min of continuous irradiation. Photostability of the optical sensor based on DPPtBu[3] was very similar to that of the solution of the indicator (40 min for 50% photodegradation; supporting information, figure S2.2). Thus, the new dye is suitable for practical applications. The light intensities necessary for the read-out of the sensors are typically much lower (10-100 fold) and only a pulse of short duration (20-50 ms) is required to obtain a measurement point. However, photobleaching can become more critical if very high light intensities are used such as in microscopy. In the absence of photobleaching the response of the sensor is fully reversible during prolong measurements (figure 2.4).
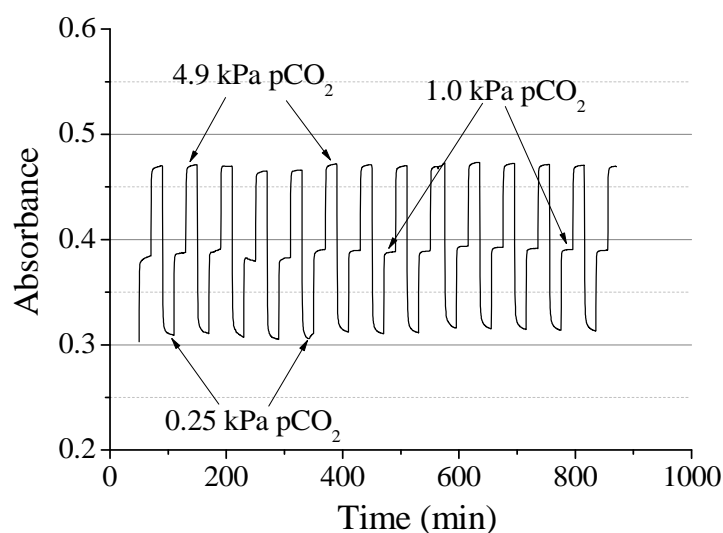

Figure 2.4. Absorption of the protonated form (λ_{max} 505 nm) at alternating pCO_2 at 25°C.

RGB Imaging

The emission of the protonated and deprotonated form of the sensing material shows excellent compatibility with the green and red channels, respectively, of a color camera (figure 2.2B). Importantly, both forms of the dye have comparable fluorescence quantum yields. Fluorescence imaging was performed using a consumer digital camera (Canon 5D). The change in the emission color can be easily distinguished with naked eye (figure 2.5). The intensity in the red channel does not change significantly ($\pm$ 10%) in the entire pCO_2 range. On the other hand the sensor shows dramatic increase of the signal in the green channel. Thus, referenced ratiometric imaging of pCO_2 with a simple set-up and using a single indicator dye becomes possible for the first time.
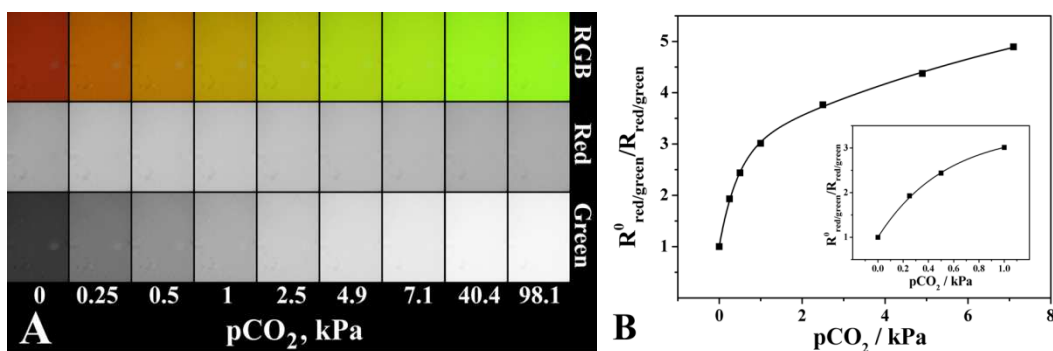
Figure 2.5. *Photographic images of the planar optode based on DPPtBu[3] under illumination with a 458-nm LED array acquired with a Canon 5D digital camera equipped with a long-pass "spring yellow" filter (Leefilters) (**A**) and the respective calibration plot for the ratio of fluorescence intensities for the red and green channel (**B**). The insert shows the curve for low pCO_2 range.*

Conclusions

A new pH-sensitive indicator dye based on a diketo-pyrrolo-pyrrole chromophore is presented. A low cost starting pigment was chemically modified in one step via N-alkylation. The resulting dye is well soluble in organic solvents and polymers and is highly promising for preparation of carbon dioxide sensors. The features include high fluorescence quantum yields for the protonated and the deprotonated form of the dye and excellent compatibility of both emissions with the green and red channels of an RGB camera. These properties enable self-referenced ratiometric imaging of pCO_2 with a single indicator. The optode shows excellent sensitivity at atmospheric levels of carbon dioxide. This makes the sensor a promising analytical tool for application in environmental monitoring, marine research and oceanography, for example for monitoring of ocean acidification.

Acknowledgments

Supporting Information

to *New Highly Fluorescent pH Indicator for Ratiometric RGB Imaging of pCO₂*
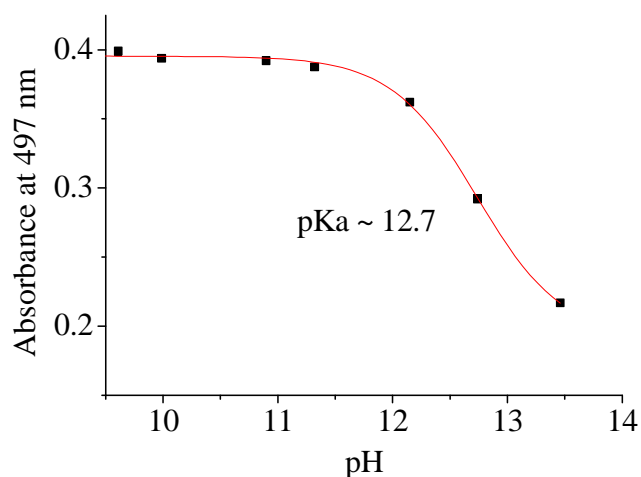

Figure S2.1. *pK$_a$ value estimation carried out in a mixture of tetrahydrofuran and buffer (1:1).*
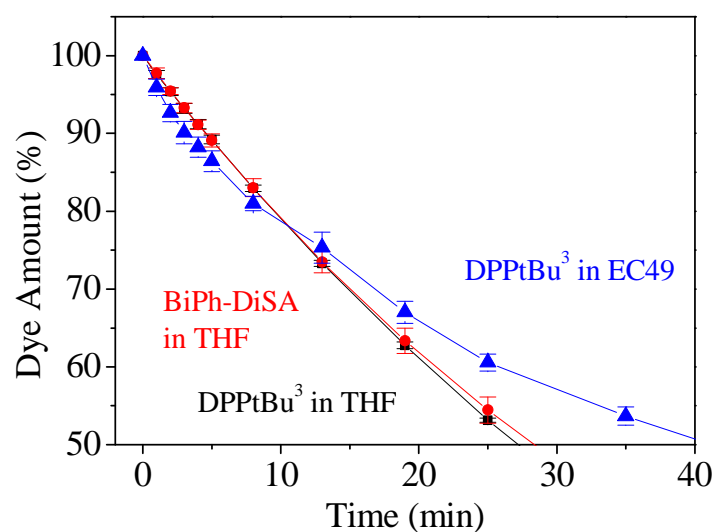

Figure S2.2. *Photodegradation profiles for DPPtBu[3] and BiPh-DiSA dissolved in air-saturated tetrahydrofuran (red dots and black squares, respectively) and for DPPtBu[3] embedded in ethyl cellulose (blue triangles) obtained from the absorption spectra of the protonated form. The data points represent an average value from 3 independent experiments.*
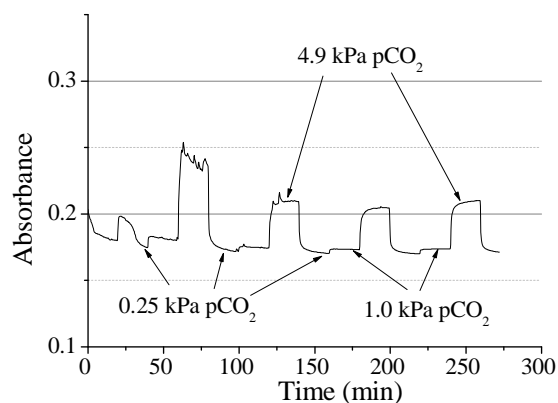
Figure S2.3. *Absorption of the protonated form (505 nm) at alternating levels of pCO$_2$ (0.25 kPa, 1.0 kPa and 5.0kPa) at 25°C under dry conditions.*
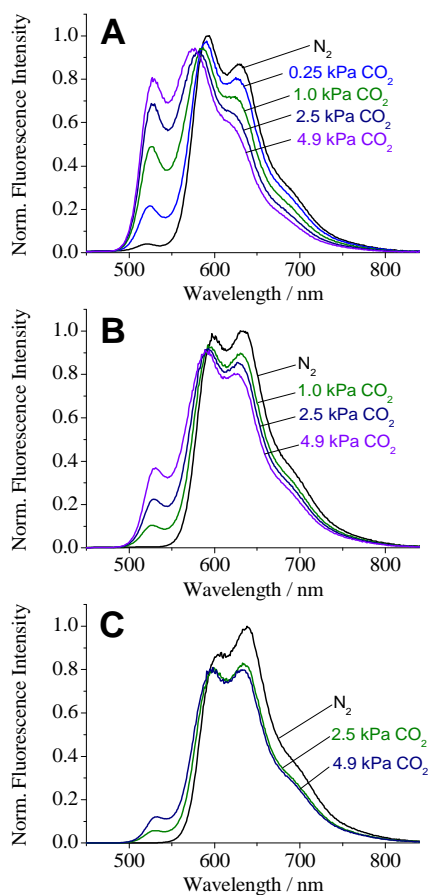

Figure S2.4. *Emission (λ_{exc} = 430 nm) spectra for 0.25% w/w (**A**), 0.75% w/w (**B**) and 1.5% w/w (**C**) of DPPtBu^3 in ethyl cellulose (EC 49) at 25 °C.*

Chapter 3

Scope of this chapter

Optical chemosensors operating in the near-infrared (NIR) region of the spectrum are under investigation because of several advantages, e.g. low light scattering, dramatically reduced autofluorescence and availability of low-cost optical components (excitation sources, photodetectors, filters). As BF_2-chelated tetraarylazadipyrromethenes – aza-BODIPYs – were found out to be promising pH-sensitive indicators in the NIR region, they were further investigated and developed for the application in optical carbon dioxide sensors.

In chapter 3 a new pH-sensitive indicator class – the di-OH-aza-BODIPY class – suitable for optical CO_2 sensors is presented. These colorimetric and self-referencing dyes feature extremely high photostability, high molar absorption coefficients and tuneable sensitivity depending on their substitution pattern. Luminescence based read-out was enabled by making use of the inner-filter effect.

Further development of this class could possibly lead to luminescent indicators, which would make luminescence based read-out easier and are therefore highly desireable.

NIR Optical Carbon Dioxide Sensors Based on Highly Photostable Dihydroxy-aza-BODIPY Dyes

Authors: Susanne Schutting, Tijana Jokic, Martin Strobl, Sergey M. Borisov, Dirk de Beer and Ingo Klimant

A new class of pH-sensitive indicator dyes for optical carbon dioxide sensors based on di-OH-aza-BODIPYs is presented. These colorimetric indicators show absorption maxima in the near infrared range (λ_{max} 670-700 nm for the neutral form, λ_{max} 725-760 nm for the mono-anionic form, λ_{max} 785-830 nm for the di-anionic form), high molar absorption coefficients up to 77000 $M^{-1}cm^{-1}$ and unmatched photostability. Depending on the electron-withdrawing or electron-donating effect of the substituents the pK_a values are tunable (8.7-10.7). Therefore, optical carbon dioxide sensors based on the presented dyes cover diverse dynamic ranges (0.007-2 kPa; 0.18-20 kPa and 0.2-100 kPa), which enables different applications varying from marine science and environmental monitoring to food packaging. The sensors are outstandingly photostable in absence and presence of carbon dioxide and can be read out via absorption or via luminescence-based ratiometric scheme using absorption-modulated inner-filter effect. Monitoring of the carbon dioxide production/consumption of a Hebe plant is demonstrated.

Introduction

Carbon dioxide is one of the most important parameters in many scientific and industrial fields, such as medicine,[61,167,168] marine science,[95,96,98,169] food packaging,[99] bio processing[92,93] or environmental and industrial monitoring.[170] Routine techniques of CO_2 quantification like infrared (IR) spectroscopy, gas chromatography (GC) or the Severinghaus electrode are well established, but suffer from different drawbacks.[49,171]

For instance IR spectroscopy is mainly used for gas samples,[85,86] because of strong interferences of water and the Severinghaus electrode is strongly affected by osmotic effects. A promising alternative are carbon dioxide chemosensors,[41,116–118,139,140,172,173] where so called *plastic type* sensors are the most common ones.[51,65,66,89,111–113,174] The core of this type of sensor is a pH-sensitive indicator dye. It is embedded in a polymer matrix together with a base (mainly a quaternary ammonium base) and responds to carbon dioxide by changing its spectral properties according to degree of protonation. Read-out of these sensors can be carried out via absorption or luminescence intensity. In case of a fluorescent indicator dye referencing of the fluorescence intensity is necessary to achieve reliable results. This can be realized by using an analyte-insensitive reference dye with different spectral properties to the indicator, either a different emission spectrum or a different luminescence decay time. Although necessary in many cases, the addition of reference materials can cause dramatic ratio changes when photobleaching of one dye (reference or indicator) or both occurs. Therefore, self-referencing indicator dyes are highly desired for ratiometric read-out. However, only a few self-referencing dyes (absorption and fluorescence intensity) where published so far.[71,144–147,157,175] Optical carbon dioxide sensors are also of great interest in biological applications.

Here, indicators with absorption/fluorescence intensity maxima in the infrared (IR) or near-infrared (NIR) region are preferred, because of several advantages, e.g. low light scattering, dramatically reduced autofluorescence and availability of low-cost excitation sources and photodetectors. Recently our group presented pH-sensitive BF_2-chelated tetraarylazadipyrromethene indicators (aza-BODIPYs).[71] This indicator class represents an interesting alternative to state-of-the-art dyes for biological applications like SNARF indicators[68] or cyanine dyes.[69,70] The aza-BODIPYs showed absorption/fluorescence intensity spectra in the near-infrared region and were highly photostable. Although pH-sensitive, these dyes could not be used for optical carbon dioxide sensors. Here, the formation of the ion pair was irreversible and the indicator could not be protonated anymore, even at 100% CO_2. In this study we present a new class of pH-sensitive indicator dyes suitable for optical carbon dioxide sensors, the di-OH-aza-BODIPYs containing two de-/protonatable hydroxyl groups. It will be shown, that the pK_a values of the di-OH-aza-BODIPYs can be tuned by using different substituents with either electron-withdrawing or electron-donating effect. Luminescence-based ratiometric read-out can be realized via absorption-modulated inner-filter effect.[102,176–178] An application

example demonstrating the carbon dioxide production/consumption of a Hebe plant will also be presented.

Experimental

Materials

Ethyl cellulose (EC49, ethoxyl content 49%), thymol-blue (A.C.S. reagent), *m*-cresol-purple (indicator grade), poly(styrene-*co*-divinylbenzene) microspheres (8 µm mean particle size; PS-microparticles), 3´-chloro-4´-hydroxyacetophenone, ammonium acetate, benzaldehyde, *N,N*-diisopropylethylamine (DIPEA), dry dichloromethane, boron trifluoride diethyl etherate, MOPS buffer salt, sodium sulfate (anhydrous) and tetraoctylammonium hydroxide solution (TOAOH, 20% in methanol) were obtained from Sigma-Aldrich (www.sigmaaldrich.com). Deuterated dimethyl sulfoxide (DMSO-d_6) was purchased from Euriso-top (www.eurisotop.com). Perfluorodecalin (98%; *cis* and *trans*), 1-butanol (99%, BuOH) and nitromethane were received from ABCR (Germany, www.abcr.de), Hyflon AD 60 from Solvay (www.solvay.com). Nitrogen, 2% oxygen in nitrogen, 5% carbon dioxide in nitrogen, 0.2% carbon dioxide in nitrogen, argon and carbon dioxide (all of 99.999% purity) were obtained from Air Liquide (Austria, www.airliquide.at). Toluene, ethanol (EtOH), tetrahydrofuran (THF), hydrochloric acid (37%), dichloromethane (DCM) and hexane were purchased from VWR (Austria, www.vwr.com). 3´-methyl-4-hydroxyacetophenone, 4´-butoxyacetophenone and 2-fluoro-4-hydroxyacetophenone were from TCI Europe (www.tcichemicals.com). Poly(ethylene terephthalate) (PET) support Melinex 505 was obtained from Pütz (Germany, www.puetz-folien.com). Potassium chloride, potassium carbonate (pro analysi), potassium hydroxide and silica gel 60 (0.063-0.200 mm) were received from Merck (www.merck.at). Sodium hydroxide, ethyl acetate, the buffer salts CHES, MES and CAPS were purchased from Roth (www.carlroth.com). De-ionized water was filtered *via* a Barnstead NANOpure ultrapure water system. 1-(4-hydroxyphenyl)-4-nitro-3-phenylbutan-1-one (compound 1b) was synthesized according to Jokic et al.[71] Silanized Egyptian Blue particles were prepared according to the literature procedure.[42]

Synthesis of 3,7-bis(4-butoxyphenyl)-5,5-difluoro-1,9-diphenyl-5*H*-4λ^4,5λ^4-dipyrrolo[1,2-*c*:2',1'-*f*][1,3,5,2]triazaborinine (di-butoxy-complex)

(E)-1-(4-butoxyphenyl)-3-phenylprop-2-en-1-one (compound a): 4'-butoxyacetophenone (1 eq, 2.00 g, 15.5 mmol) was dissolved in absolute ethanol (15 ml). Benzaldehyde (1 eq, 1580 μL, 15.5 mmol) and potassium hydroxide (3 eq, 2.61 g, 46.4 mmol in 5 ml H$_2$O) were added to the solution and the reaction was stirred at room temperature for 12 h. Then, the reaction solution/suspension was acidified with 0.1 M HCl and the resulting precipitate was collected by filtration and was washed with water three times (3 x 100 ml). The precipitate was dried on a rotary evaporator and was used for the next step without further purification (3.87 g, 89.2 %). *1-(4-butoxyphenyl)-4-nitro-3-phenylbutan-1-one (compound b):* A solution of (E)-1-(4-butoxyphenyl)-3-phenylprop-2-en-1-one (1 eq, 3.87 g, 13.8 mmol), nitromethane (20 eq, 14.8 ml, 276 mmol) and KOH (0.3 eq, 0.232 g, 4.1 mmol) in 30 ml absolute ethanol was heated under reflux for 12 h. After cooling to room temperature the solvent was removed on a rotary evaporator. The resulting oily residue was acidified with 0.1 M HCl and was partitioned with ethyl acetate and water in a separating funnel. The organic layer was separated, dried over sodium sulfate and the solvent removed under reduced pressure (4.035 g, 85.7 %). *(5Z)-5-(4-butoxyphenyl)-N-(5-(4-butoxyphenyl)-3-phenyl-2H-pyrrol-2-ylidene)-3-phenyl-1H-pyrrol-2-amine (c):* Compound **b** (1 eq, 2.5 g, 7.33 mmol) and ammonium acetate (35 eq, 19.77 g, 256 mmol) were dissolved in 50 ml 1-butanol and the reaction solution was heated under reflux for 24 h. The reaction was cooled to room temperature and the solvent removed under reduced pressure. Then, the solid was redissolved in DCM and washed with water three times (3 x 100 ml). The crude solid was purified by column chromatography on silica gel eluting with DCM/cyclohexane (1:1 v/v). The product was recrystallized from a hexane/THF mixture to give metallic blue crystals (983 mg, 45.4%). ^{1}H NMR (300 MHz, CDCl$_3$) δ 8.06 (d, *J* =7.1 Hz, 4 H), 7.88-7.83 (m, 4 H), 7.44-7.31 (m, 6 H), 7.11 (s, 2 H), 7.02 (d, *J* = 8.8 Hz, 4 H), 4.06 (t, *J* = 6.5 Hz, 4 H), 1.91-1.72 (q, *J* = 8.5 Hz, 4 H), 1.6-1.48 (m, 4 H), 1.01 (t, *J* = 7.4 Hz, 6 H). *3,7-bis(4-butoxyphenyl)-5,5-difluoro-1,9-diphenyl-5H-4λ^4,5λ^4-dipyrrolo[1,2-c:2',1'-f][1,3,5,2]triazaborinine:* Compound **c** (1 eq, 300 mg, 0.51 mmol) was dissolved in 200 ml dry DCM. *N,N*-Diisopropylethylamine (DIPEA, 10 eq, 839 μL, 5.06 mmol) and boron trifluoride diethyl etherate (15 eq, 953 μL, 7.58 mmol) were added and the reaction solution was stirred under nitrogen for 12 h. The green solution was washed

with water three times (3 x 200 ml) and dried over anhydrous sodium sulfate. The crude product was purified by column chromatography on silica-gel eluting with DCM/cyclohexane (1:1 v/v). The product was recrystallized from a hexane/THF mixture to give metallic red needles (179 mg, 55.2%). ^{1}H NMR (300 MHz, CDCl$_3$) δ 8.09 - 8.05 (m, 8 H), 7.49 - 7.38 (m, 6 H), 7.04 - 6.98 (m, 6 H), 4.07 – 4.02 (t, J = 6.4 Hz, 4 H), 1.58 – 1.45 (q, J = 14.4 Hz, 4 H), 1.62 – 1.42 (m, 4 H), 1.02 – 0.97 (t, J = 7.4 Hz, 6 H). Electron impact-direct insertion-time of flight (DI-EI-TOF): m/z of [M]$^+$ found 641.3007, calc. 641.3032.

Synthesis of 4,4'-(5,5-difluoro-1,9-diphenyl-5H-4λ^4,5λ^4-dipyrrolo[1,2-c:2',1'-f][1,3,5,2]triazaborinine-3,7-diyl)bis(2-chlorophenol) (di-Cl-di-OH-complex)

1-(3-chloro-4-hydroxyphenyl)-3-phenylpropenone (compound 1a): 3´-chloro-4´-hydroxyacetophenone (1 eq, 2 g, 11.7 mmol) and benzaldehyde (1 eq, 1.24 g, 11.7 mmol) were dissolved in 10 ml ethanol absolute. 10 ml of aqueous potassium hydroxide solution (3 eq, 1.96 g, 35.1 mmol) were added dropwise. The resulting solution was stirred for 8-12 h, during which the product precipitated as the potassium salt. The solution/suspension was poured into 10 ml hydrochloric acid (1 M) and further concentrated hydrochloric acid was added until the solution was acidic. The obtained yellow solid was washed with water and used for further synthesis without purification (2.33 g, 77%). *1-(3-chloro-4-hydroxyphenyl)-4-nitro-3-phenylbutan-1-one (compound 1b)*: A solution of compound **1a** (1 eq, 2 g, 7.7 mmol), nitromethane (20 eq, 8.35 ml, 154.7 mmol) and potassium hydroxide (1.2 eq, 0.52 g, 9.28 mmol) in 10 ml ethanol was heated at 60°C under reflux for 12 h. After cooling to room temperature, the solvent was removed in vacuo and the oily residue obtained was acidified with hydrochloric acid (4 M) and partitioned between ethyl acetate (50 ml) and de-ionized water (50 ml). The organic layer was separated, dried over anhydrous sodium sulfate and evaporated under reduced pressure. The obtained product was used for further synthesis without purification (2.4g, 97.2%). *[5-(3-chloro-4-hydroxyphenyl)-3-phenyl-1H-pyrrol-2-yl]-[5-(3-chloro-4-hydroxyphenyl)-3-phenylpyrrol-2-ylidene]amine (compound 1c)*: Compound **1b** (1 eq, 2.02 g, 8.76 mmol) and ammonium acetate (35 eq, 19.03 g, 307 mmol) in 50 ml 1-butanol were heated under reflux for 24 h. The reaction was cooled to room temperature, salt was removed by extraction with de-ionized water/DCM and the product was purified by column chromatography on silica gel eluting with 5% ethyl

acetate/DCM (after eluting impurities with hexane, 20% DCM/hexane, 1% ethyl acetate/DCM and 2% ethyl acetate/DCM) to yield **1c** as a blue-black solid. The product was recrystallized from a hexane/THF mixture to give metallic green crystals (0.097 g, 5.77%). ^{1}H NMR (300 MHz, DMSO-d_6) δ 8.09 (d, J = 7.6 Hz, 6H), 7.90 (d, J = 8.5 Hz, 2H), 7.62 (s, 2H), 7.54 – 7.32 (m, 6H), 7.19 (d, J = 8.5 Hz, 2H). EI-DI-TOF: m/z [MH]$^+$ found 549.1007, calc. 549.1011. *4,4'-(5,5-difluoro-1,9-diphenyl-5H-4λ4,5λ4-dipyrrolo[1,2-c:2',1'-f][1,3,5,2]triazaborinine-3,7-diyl)bis(2-chlorophenol)* *(di-Cl-di-OH-complex)*: Compound **1c** (0.017 g, 0.07 mmol) was dissolved in 50 ml of dry DCM, treated with DIPEA (10 eq, 0.053 ml, 0.32 mmol) and boron trifluoride diethyletherate (15 eq, 0.061 ml, 0.48 mmol) and stirred under argon for 24 h. Purification was carried out *via* column chromatography on silica gel eluting with 2% ethanol/DCM (after eluting impurities with DCM). Recrystallization from hexane/THF gave the final product di-Cl-di-OH-complex as a metallic red solid (0.008 g, 44%). ^{1}H NMR (300 MHz, DMSO-d_6) δ 8.29 (s, 2H), 8.16 (d, J = 7.0 Hz, 4H), 8.03 (d, J = 8.7 Hz, 2H), 7.65 (s, 2H), 7.60 – 7.41 (m, 6H), 7.13 (d, J = 8.7 Hz, 2H). EI-DI-TOF: m/z [MH]$^+$ found 597.0968, calc. 597.0999.

Synthesis of 4,4'-(5,5-difluoro-1,9-diphenyl-5*H*-4λ^4,5λ^4-dipyrrolo[1,2-*c*:2',1'-*f*][1,3,5,2]triazaborinine-3,7-diyl)bis(3-fluorophenol) (di-F-di-OH-complex)

The synthesis was performed analogously to that of di-Cl-di-OH-complex, but starting from 2´-fluoro-4´-hydroxyacetophenone (728 mg). Step 1 and 2 yielded 1.033 g (90.2%) and 1.28 g (99.4%) of the crude product, respectively. After synthesis step 3, the crude product was purified by column chromatography on silica gel eluting with 4% THF/DCM to yield [5-(2-fluoro-4-hydroxyphenyl)-3-phenyl-1*H*-pyrrol-2-yl]-[5-(2-fluoro-4-hydroxyphenyl)-3-phenylpyrrol-2-ylidene]amine **2c** as a blue-black solid. The product was recrystallized from a hexane/THF mixture to give metallic green crystals (0.23 g, 20.9%). ^{1}H NMR (300 MHz, DMSO-d_6) δ 8.04-8.06 (d, J = 7.0 Hz, 6H), 7.35-7.47 (m, 8H), 6.78-6.86 (m, 4H). DI-EI-TOF: m/z of [M]$^+$ found 517.1626, calc. 517.1602. *4,4'-(5,5-difluoro-1,9-diphenyl-5H-4λ4,5λ4-dipyrrolo[1,2-c:2',1'-f][1,3,5,2]triazaborinine-3,7-diyl)bis(3-fluorophenol)* *(di-F-di-OH-complex)* was synthesized using the same procedure. Purification was carried out *via* column chromatography on silica gel eluting with 4% THF/DCM. Recrystallization from hexane/THF gave the final product di-F-di-OH-complex as a metallic red solid (0.044 g,

19.6%). ^{1}H NMR (300 MHz, DMSO-d_6) δ 8.12 (d, J = 7.0 Hz, 4H), 7.82 (t, J = 8.7 Hz, 2H), 7.56-7.48 (q, J = 9.4, 7.9 Hz, 6H), 7.31 (d, J = 3.4 Hz, 2H), 6.77 (d, J = 10.7 Hz, 4H). DI-EI-TOF: m/z of [M]$^+$ found 565.1615, calc. 565.1591.

Synthesis of 4,4'-(5,5-difluoro-1,9-diphenyl-5H-4λ^4,5λ^4-dipyrrolo[1,2-c:2',1'-f][1,3,5,2]triazaborinine-3,7-diyl)diphenol (di-OH-complex)

Compound **3a** 1-(4-hydroxyphenyl)-3-phenylpropenone was commercially available. Further synthesis steps were performed analogously to the synthesis steps of the di-Cl-di-OH-complex. Synthesis of compound **3b** gave 2.06 g (80%) of the crude product, starting from 2.02 g of 4'-hydroxychalcone. The crude **3c** was purified by column chromatography on silica gel eluting with 4% THF/DCM to yield [5-(4-hydroxyphenyl)-3-phenyl-1H-pyrrol-2-yl]-[5-(4-hydroxyphenyl)-3-phenylpyrrol-2-ylidene]amine as a blue-black solid. The product was recrystallized from a hexane/THF mixture to give metallic green crystals (0.41 g, 23.5%). ^{1}H NMR (300 MHz, DMSO-d_6), δ 8.09 (d, J = 7.3 Hz, 4H), 7.93 (d, J = 8.6 Hz, 4H), 7.53 (s, 2H), 7.42 (m, 6H), 7.01 (d, J = 8.6 Hz, 4H). EI-DI-TOF: m/z [MH]$^+$ found 481.1773, calc. 481.179. Purification of 4,4'-(5,5-difluoro-1,9-diphenyl-5H-4λ^4,5λ^4-dipyrrolo[1,2-c:2',1'-f][1,3,5,2]triazaborinine-3,7-diyl)diphenol was carried out *via* column chromatography on silica gel eluting with DCM/ethyl acetate (4:1). Recrystallization from hexane/THF gave the final product di-OH-complex as a metallic red solid (0.26 g, 57.8%). ^{1}H NMR (300 MHz, DMSO-d_6) δ 8.13 (dd, J = 18.6, 8.0 Hz, 8H), 7.65 – 7.39 (m, 8H), 6.95 (d, J = 8.8 Hz, 4H). EI-DI-TOF: m/z [MH]$^+$ found 529.1771, calc. 529.1779.

Synthesis of the 4,4'-(5,5-difluoro-1,9-diphenyl-5H-4λ^4,5λ^4-dipyrrolo[1,2-c:2',1'-f][1,3,5,2]triazaborinine-3,7-diyl)bis(2-methylphenol) (di-CH$_3$-di-OH-complex)

The synthesis was carried out analogously to that of di-Cl-di-OH-complex, starting from 3´-methyl-4´-hydroxyacetophenone (1.88 g). Step 1 and 2 yielded 2.77 g (93%) and 1.84 g (53%) of the crude product, respectively. After synthesis step 3, the crude product was purified by column chromatography on silica gel eluting with 5% ethyl acetate/DCM (after eluting impurities with hexane/DCM 1:1, DCM) to yield [5-(3-methyl-4-hydroxyphenyl)-3-phenyl-1H-pyrrol-2-yl]-[5-(3-methyl-4-hydroxyphenyl)-3-phenylpyrrol-2-ylidene]amine **4c** as a blue-black solid. The product was recrystallized from a hexane/THF mixture to give metallic green crystals (0.091 g, 5.8%). ^{1}H NMR

(300 MHz, DMSO-d_6) δ 8.10 (d, J = 7.3 Hz, 4H), 7.91 – 7.75 (m, 4H), 7.57 – 7.33 (m, 8H), 7.00 (d, J = 8.4 Hz, 2H), 2.29 (s, 6H). EI-DI-TOF: m/z [MH]$^+$ found 509.2086, calc. 509.2103. Purification of 4,4'-(5,5-difluoro-1,9-diphenyl-5H-4λ^4,5λ^4-dipyrrolo[1,2-c:2',1'-f][1,3,5,2]triazaborinine-3,7-diyl)bis(2-methylphenol) was carried out *via* column chromatography on silica gel eluting with 5% ethyl acetate/DCM (after eluting impurities with DCM, 1% ethyl acetate/DCM and 2% ethyl acetate/DCM). Recrystallization from hexane/THF gave the final product di-CH$_3$-di-OH-complex as a metallic red solid (0.04 g, 40%). ^{1}H NMR (300 MHz, DMSO-d_6) δ 8.16 (d, J = 7.2 Hz, 4H), 8.08 – 7.90 (m, 4H), 7.52 (m, 8H), 6.95 (d, J = 8.5 Hz, 2H), 2.22 (s, 6H). EI-DI-TOF: m/z [MH]$^+$ found 557.2082, calc. 557.2092.

Staining of PS-Microparticles

0.50 g PS-particles were dispersed in a solution of 5 mg (1% w/w in respect to the PS-particles) di-butoxy-complex in 10 ml tetrahydrofuran (THF) and stirred for 1.5 h. Then 8 ml of de-ionized water were added dropwise. After 10 min of stirring the dispersion was transferred rapidly into a beaker with 50 ml of de-ionized water. The dispersion was again stirred for 10 min. Then the particles were filtered through a cellulose filter and rewashed with 20 ml ethanol. Afterwards the particles were transferred into a milling cup and were overlaid with a mixture of ethanol/de-ionized water (1:1) to diminish friction and to enhance heat dissipation during grinding in the planet mill. The particles were washed with ethanol and dried in the oven at 70°C.

Sensor Preparation

Absorption: a "cocktail" containing 100 mg ethyl cellulose and 1 mg dye (1% w/w in respect to the polymer) dissolved in a toluene: ethanol mixture (6:4 v/v, 1.9 g) was purged with carbon dioxide. Afterwards 100 µl tetraoctylammonium hydroxide solution (20% w/w TOAOH in MeOH) were added. The "cocktail" was knife-coated on a dust-free PET support. A sensing film of ~7 µm thickness was obtained after evaporation of the solvent. For luminescence-based measurements a second layer was added to the absorption-based sensing foils. To prepare the "cocktail" for the second layer, 0.180 g Hyflon AD 60 were dissolved in 2.820 g perfluorodecalin, which was washed prior to use with 1 mol l^{-1} potassium carbonate solution. Then 0.360 g Egyptian Blue powder (200% w/w with respect to the polymer) and 0.054 g stained PS-particles (30% w/w in

respect to the polymer) were dispersed homogeneously in the Hyflon solution. The thickness of this layer after evaporation of the solvent was estimated to be ~4.5 µm.

Methods

^{1}H NMR spectra were recorded on a 300 MHz instrument (Bruker) in DMSO-d_6 with TMS as standard. Absorption spectra were recorded on a Cary 50 UV-Vis spectrophotometer (Varian). The determination of the molar absorption coefficients was carried out as an average of three independent measurements. Fluorescence spectra were recorded on a Fluorolog3 fluorescence spectrometer (Horiba) equipped with a NIR-sensitive photomultiplier R2658 from Hamamatsu (300-1050 nm). Photobleaching experiments were performed by irradiating the sensor foils in a glass cuvette with the light of a high-power 10 W LED array (λ_{max} 458 nm, 3 LEDs, www.LED-TECH.de) operated at 6 W input power. A lens (Edmund Optics) was used to focus the light of the LED array on the glass cuvette (photon flux: ~3900 µmol s^{-1} m^{-2} as determined with a Li-250A light meter from Li-COR). The photodegradation profiles were obtained by monitoring the absorption spectra of a sensor foil based on the respective dye. The cuvette was flushed with either carbon dioxide gas for the mono-anionic form, or with nitrogen for the di-anionic form and sealed. Thymol-blue and *m*-cresol-purple were used for comparison. In case of the anionic form of thymol-blue, *m*-cresol-purple, the di-OH-complex and the di-CH$_3$-di-OH-complex (di-anionic forms) sodium hydroxide was placed at the bottom of the cuvette to capture carbon dioxide traces. Gas calibration mixtures were obtained using a gas mixing device from MKS (www.mksinst.com). The gas mixture was humidified to about 85% relative humidity, using silica gel soaked with a saturated potassium chloride solution, prior to entering the calibration chamber. Temperature was controlled by a cryostat ThermoHaake DC50. Dyed particles were filtered through cellulose filters type 113A from Roth (www.carlroth.com). Particle milling was carried out using an 80 ml milling cup, zirconia spheres (Ø 5 mm) and a Pulverisette 6 planet mill from Fritsch (www.fritsch.de). For the determination of the pK$_a$ values titration curves in aqueous buffer/ethanol mixtures (1:1) were measured and the average value of the point of inflection obtained was used. For the production/consumption measurements of carbon dioxide two Firesting-Mini devices and an oxygen trace sensor from PyroScience (www.pyro-science.com) were used. Illumination of the sample was performed with 3 commercially available halogen bulb
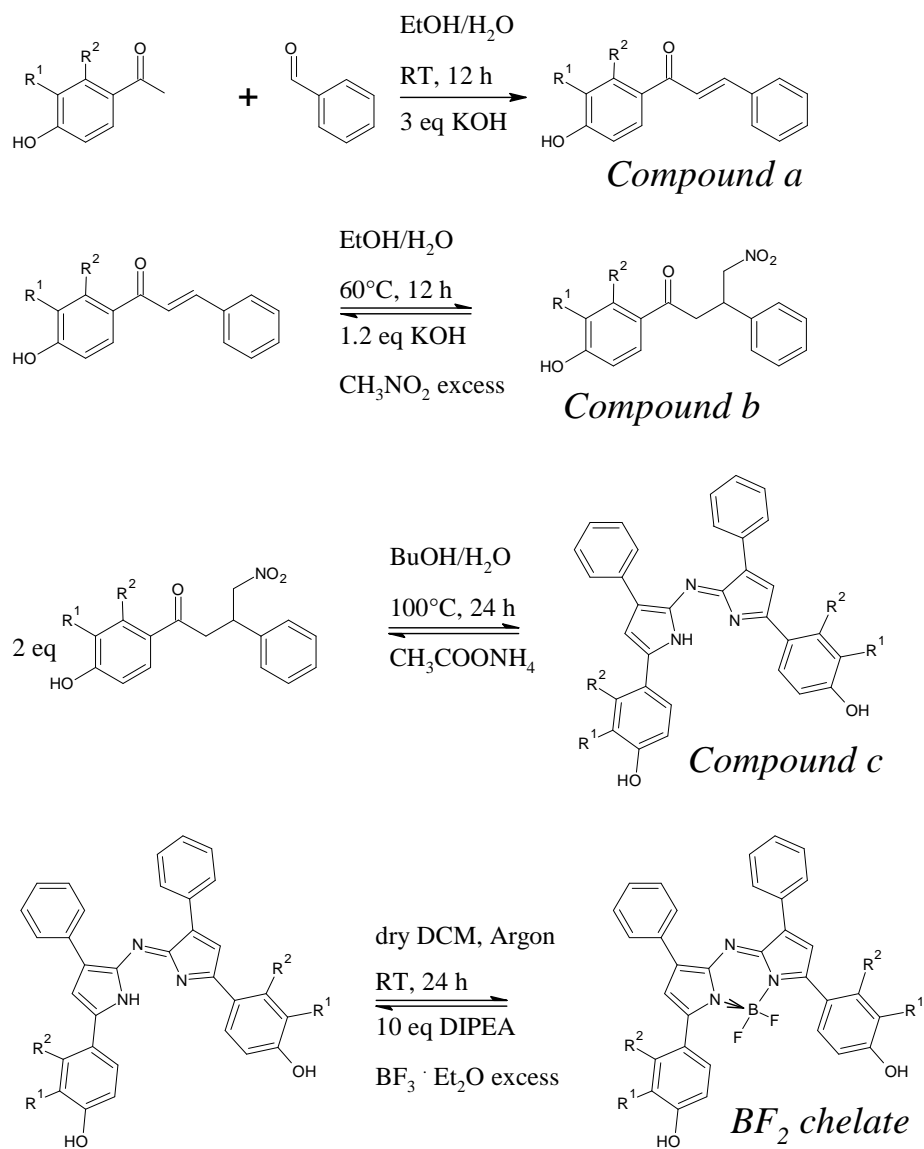
lamps with an averaged photon flux of ~217 µmol s^{-1} m^{-2} per lamp. The plant was positioned in a glass desiccator, which was flushed with a gas mixture of 2% oxygen in nitrogen.

Results and Discussion

Synthesis

As reported by Jokic et al.[71] there are two ways for the preparation of azadipyrromethenes to obtain either asymmetrical[179] or symmetrical[180] chromophores. The previously published asymmetrical dyes bearing one hydroxyl group were proved to be promising pH indicators.[71] Unfortunately, they were found to be unsuitable for optical carbon dioxide sensors. The ion pair built between the hydroxyl group and the tetraoctylammonium base was comparatively strong. Even after exposure of the sensors to pure carbon dioxide, the amount of CO_2 was not enough to achieve re-protonation of the indicators and only after exposure to strong acid vapors (e.g. hydrochloric acid) the indicators were irreversibly re-protonatable.

Dissociation of both hydroxyl groups in symmetrical azadipyrromethenes was expected to be more difficult compared to the mono-hydroxy derivatives since two ion pairs with bulky cations would be built upon deprotonation. Therefore, this new class of pH indicators potentially suitable for CO_2 sensing was investigated. The starting point of our synthesis were diaryl-α,β-unsaturated ketones (chalcones) either commercially available or readily made by an aldol condensation of the corresponding aldehyde and acetophenone (Scheme 3.1). The Michael addition of nitromethane to the chalcones, with KOH as base, yields the 1,3-diaryl-4-nitrobutan-1-ones in essentially quantitative yields. Their condensation with ammonium acetate in refluxing butanol gave the azadipyrromethenes. Finally, the azadipyrromethenes were converted to the corresponding BF_2 chelates via reaction with BF_2-etherate using diisopropylethylamine as a base at room temperature for 24 h, giving yields ranging from 20-70%.

Reaction scheme showing:

EtOH/H$_2$O
RT, 12 h
3 eq KOH
→ *Compound a*

EtOH/H$_2$O
60°C, 12 h
1.2 eq KOH
CH$_3$NO$_2$ excess
→ *Compound b*

2 eq
BuOH/H$_2$O
100°C, 24 h
CH$_3$COONH$_4$
→ *Compound c*

dry DCM, Argon
RT, 24 h
10 eq DIPEA
BF$_3$ · Et$_2$O excess
→ *BF$_2$ chelate*

di-OH-complex: R^1 = R^2 = H

di-F-di-OH-complex: R^1 = H, R^2 = F

di-Cl-di-OH-complex: R^1 = Cl, R^2 = H

di-CH$_3$-di-OH-complex: R^1 = CH$_3$, R^2 = H

Scheme 3.1. *4-step-synthesis of the di-OH-aza-BODIPY chelates.*

Photophysical Properties

Dissolved in an ethanol/aqueous buffer mixture (1:1) all di-OH-aza-BODIPY dyes showed absorption spectra corresponding to the two protonation steps of the hydroxyl groups (figure 3.1). The neutral forms showed maxima at 670-700 nm and the mono-

anionic forms at 725-760 nm. The di-anionic forms were again bathochromically shifted for approximately 60 nm (λ_{max} 785-830 nm). Generally, the di-CH$_3$-di-OH-complex bearing electron-donating methyl groups showed absorption maxima shifted to higher wavelengths compared to the non-substituted di-OH-complex (table 3.1). In contrast, complexes bearing electron-withdrawing groups displayed absorption maxima at shorter wavelengths.
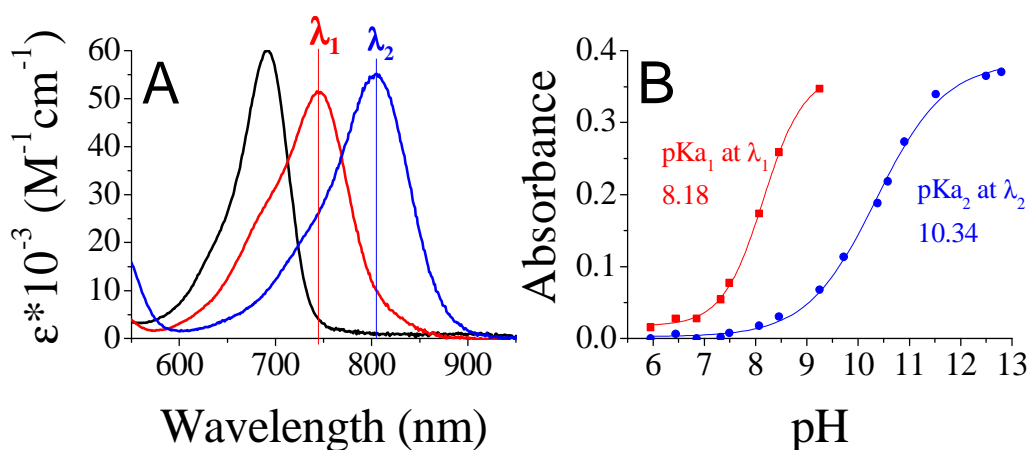

Figure 3.1. *(A) Absorption spectra for the neutral (black line, pH 6.4), the mono-anionic (red line, pH 9.3) and the di-anionic (blue line, pH 12.8) forms of the di-OH-complex dissolved in ethanol/aqueous buffer mixture (1:1) at 25°C and (**B**) the titration curves for pK$_{a1}$ determined at 745 nm (red) and pK$_{a2}$ at 805 nm (blue), respectively.*

An overview for the spectroscopic properties of the presented dyes is given in table 1. Molar absorption coefficients are rather high: 55000-77000 M^{-1}cm^{-1}. pK$_a$ determination was carried out in a mixture of ethanol/aqueous buffer solution (1:1). For all di-OH-aza-BODIPY dyes two protonation steps can be observed (table 3.1). Here, the complex with electron-donating methyl groups in *ortho*-position to the hydroxyl groups showed the highest pK$_a$ values, followed by the non-substituted di-OH-complex. Electron-withdrawing chlorine atoms located in proximity of the hydroxyl groups (*ortho*-position) have the strongest impact on the pK$_a$ values, whereas the electron-withdrawing effect of fluorine atoms in the *meta*-position is significantly lower.

Table 3.1. *Absorption maxima, molar absorption coefficients (ε) and pK_a values of the di-OH-aza-BODIPY-complexes dissolved in ethanol/aqueous buffer mixture (1:1), as well as the absorption maxima for optical CO_2 sensors (EC49) based on the respective aza-BODIPY-complexes.*

Chelate	**neutral form**		**mono-anionic form**			**di-anionic form**	
	λ_{max} ($\varepsilon*10^{-3}$)	pK_{a1}	λ_{max} ($\varepsilon*10^{-3}$)	λ_{max}	pK_{a2}	λ_{max} ($\varepsilon*10^{-3}$)	λ_{max}
	EtOH/ aq. buffer 1:1	EtOH/ aq. buffer 1:1	EtOH/ aq. buffer 1:1	EC49	EtOH/ aq. buffer 1:1	EtOH/ aq. buffer 1:1	EC49
	[nm ($M^{-1}cm^{-1}$)]		[nm ($M^{-1}cm^{-1}$)]	[nm]		[nm ($M^{-1}cm^{-1}$)]	[nm]
di-CH$_3$-di-OH	701 (76.8 ± 1.9)	8.40	762 (65.5 ± 0.4)	775	10.68	827 (70.7 ± 0.6)	908
di-OH	692 (59.9 ± 2.0)	8.18	745 (51.3 ± 1.2)	772	10.34	805 (55.2 ± 1.5)	876
di-F-di-OH	669 (51.1 ± 2.0)	7.32	725 (46.7 ± 2.4)	760	9.35	784 (52.8 ± 0.8)	860
di-Cl-di-OH	688 (61.4 ± 2.5)	6.52	752 (52.6 ± 2.2)	781	8.72	808 (57.9 ± 0.7)	890

Carbon Dioxide Sensors

The pH-sensitive di-OH-aza-BODIPY dyes were embedded in an ethyl cellulose matrix (EC49) along with tetraoctylammonium hydroxide as base to obtain optical carbon dioxide sensors. Clearly, the sensors showed well observable spectral changes in the near infrared (NIR) range according to the protonation of the di-anionic form giving the mono-anionic form (figure 3.2). The neutral forms of the di-OH-complexes showed slight fluorescence in solution, and the sensors based on the indicators did not show detectable fluorescence, neither for the mono-anionic nor for the di-anionic form. Compared to the measurements in solution the CO_2 sensors based on the di-OH-aza-BODIPY dyes showed significantly bathochromically shifted absorption spectra with maxima at 760-780 nm for their mono-anionic forms and maxima at 860-910 nm for their di-anionic forms. Generally, a similar trend for the absorption maxima of the CO_2 sensors based on the respective complexes was observed (table 3.1). Here, the shift between the mono-anionic and the di-anionic form was enlarged to over 100 nm. This fact is advantageous for optical sensors, because peak separation becomes easier.
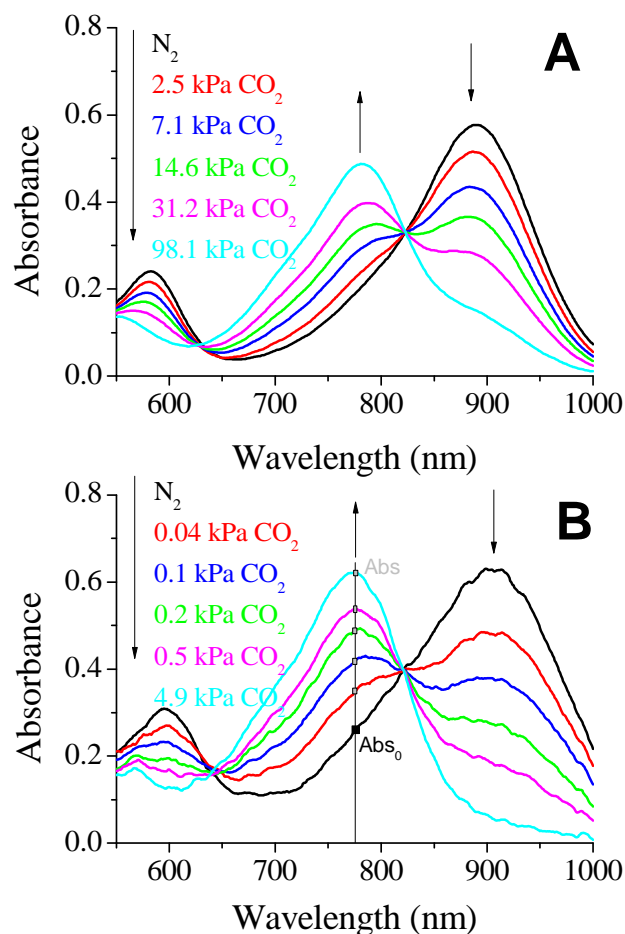
Figure 3.2. Absorption spectra of optical carbon dioxide sensors based on (A) the di-Cl-di-OH-complex and (B) the di-CH$_3$-di-OH-complex in EC49 (base: TOAOH) at 25°C at various pCO$_2$ values.

Despite that all di-OH-aza-BODIPY dyes showed two protonation steps in aqueous solution, only one protonation step was observed in optical sensors based on these indicators. In fact, in absence of carbon dioxide both hydroxyl groups build ion pairs with the quaternary ammonium base and the spectra for the di-anionic forms are observable. The mono-anionic form is built in presence of carbon dioxide and is stable even at 100% CO$_2$. Spectra for the neutral forms are not observable anymore (figure 3.2). Therefore, the pK$_{a2}$ values measured in solution are most relevant for optical carbon dioxide sensors based on the di-OH-aza-BODIPY dyes. Indeed, these values correlate very well with the sensitivities of the optical CO$_2$ sensors (table 3.1, figure 3.3). The sensitivity increases in the following order: di-Cl-di-OH < di-F-di-OH < di-OH < di-CH$_3$-di-OH. Notably, for the most sensitive sensor based on di-CH$_3$-di-OH

about 25% of the overall signal change is observed already at atmospheric pCO_2 which is, to the best of our knowledge, one of the highest sensitivities reported so far. Di-F-di-OH and di-Cl-di-OH complexes bearing electron-withdrawing groups displayed diminished pK_{a2} values of 9.35 and 8.72, respectively, and enabled measurements up to 100% CO_2. These great differences in sensitivity lead to a broad range of applications, varying from food packaging and capnography for di-F-di-OH and di-Cl-di-OH complexes to environmental monitoring for di-OH and di-CH$_3$-di-OH complexes.

Figure 3.3 shows the increasing absorption of the mono-anionic form in relation to the absorption at 0 kPa (Abs-Abs$_0$) carbon dioxide (see figure 3.2 B). The higher the sensitivity of the sensor, the steeper the respective calibration curves in figure 3.3 and the lower the amount of carbon dioxide necessary to fully protonate the sensor. Sensors based on the di-Cl-di-OH-complex and the di-F-di-OH-complex showed limits of detection (LOD) of 0.19 kPa and 0.18 kPa, respectively. However, determining the LOD value for very sensitive sensors can be very challenging. For measurements of low levels of carbon dioxide the measuring system (gas mixer, gas lines, flow cell, etc.) has to be completely decarbonized, which is very difficult to achieve in reality. Especially for atmospheric levels of pCO_2 (0.04 kPa $\approx$ 400 µatm in the gas phase $\approx$ 11.6 µmol l^{-1} in water at 298.15 K) and below, traces of environmental carbon dioxide disturbed the measurements for sensors based on the di-CH$_3$-di-OH-complex and the di-OH-complex. Hence, the determined LODs for these two complexes (0.011 kPa for di-OH and 0.007 kPa for di-CH$_3$-di-OH) were only rough estimations.
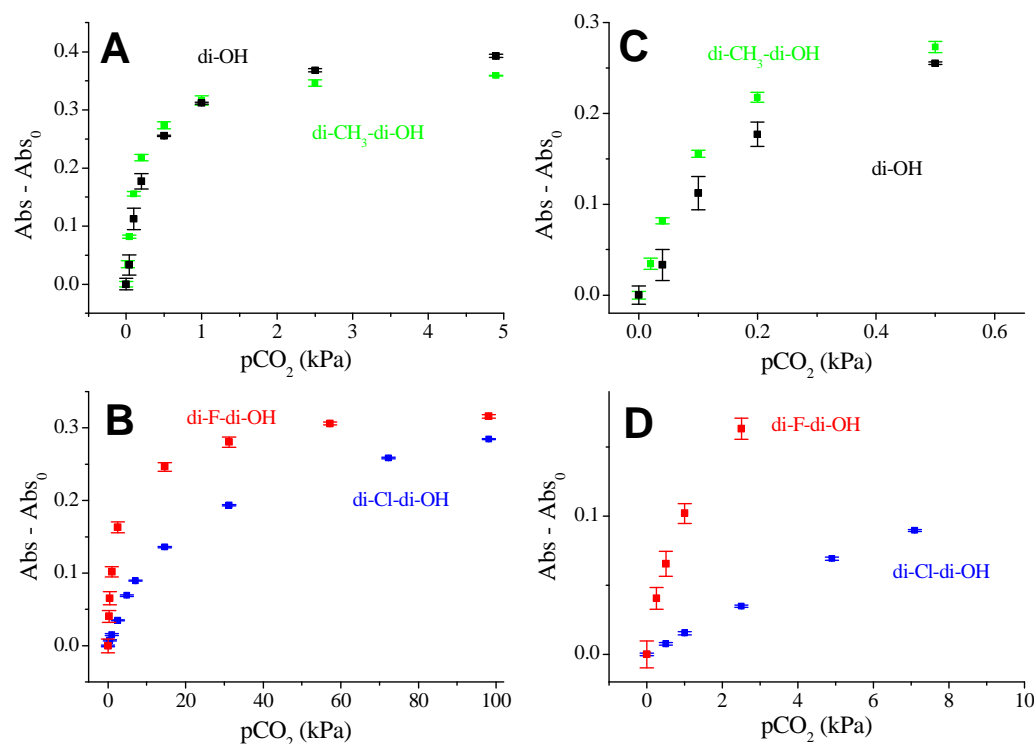
Figure 3.3. (A) *Calibration curves (absorption – absorption at 0 kPa of the mono-anionic form) for the carbon dioxide sensors based on di-OH-complex (black) and di-CH₃-di-OH-complex (green) and* ***(B)*** *di-Cl-di-OH-complex (blue) and di-F-di-OH-complex (red) 25°C under humid conditions with the respective "zoom-in" sections (****C and D****).*

Photodegradation profiles of the carbon dioxide sensors were obtained from the absorption spectra after illuminating the sensor foils with a high-power LED array (λ_{max} 458 nm). For comparison, state-of-the-art indicator dyes such as *m*-cresol-purple, thymol-blue and HPTS were used (supporting information, figure S3.1). The photostability of both the mono-anionic and the di-anionic form were investigated. Therefore, the cuvette was filled either with pure carbon dioxide (mono-anionic form) or with pure nitrogen (di-anionic form). Clearly, all of the di-OH-aza-BODIPY dyes showed outstanding photostability, much better than the reference indicators embedded in the same ethyl cellulose matrix. After 1.5 h of illumination the presented dyes showed hardly any photobleaching effects for both the mono-anionic and di-anionic form, whereas *m*-cresol-purple (neutral form), thymol-blue (neutral form) and HPTS (only anionic form) were degraded to less than 80%. The anionic forms of *m*-cresol-

purple and thymol-blue were even less photostable than there neutral forms (supporting information, figure S3.1).

Luminescence-based Ratiometric Read-out using IFE (Inner-Filter Effect) based Sensors

Read-out of the planar optodes and fiber-optic sensors based on colorimetric systems is significantly more challenging than that of the luminescent systems. The inner-filter effect (IFE) was made use of in order to enable read-out via luminescence. Additionally to the first layer containing the absorption-based indicator dye along with TOAOH in ethyl cellulose, a second layer containing the secondary emitters was used.[176] It included the pH-insensitive di-butoxy-complex entrapped in PS-particles as fluorophore and Egyptian blue (EB) as phosphor, both embedded in Hyflon AD 60. The absorption spectra of the di-OH-complex and the emission spectra of the secondary emitters are shown in figure 3.4 A. Here, the broad emission band of the phosphor (EB) overlaps with the absorption spectrum of the di-anionic form of the indicator and the emission band of the fluorophore (di-butoxy-aza-BODIPY-complex) overlaps with the absorption spectrum of the mono-anionic form of the indicator. The isosbestic point of the di-OH-indicator is located at 610 nm and represents an ideal wavelength for exciting the secondary emitters matching the maxima of the red LEDs available (605, 617 nm). The fluorescence spectra of the sensor based on the combination of EB, di-butoxy-complex and the non-substituted di-OH indicator are shown in figure 3.4 B. Emission peaks in the absence (λ_{max} 913 nm) and presence (λ_{max} 738 nm) of carbon dioxide were well observable. Hence, luminescence-based ratiometric read-out becomes possible. This can be realized either by using two emission filters isolating the respective components or by measuring the luminescence phase shift. In fact, the phase shift for luminescent Egyptian Blue is 55.8° at 2000 Hz and the phase shift of the fluorophore is 0 at this modulation frequency.
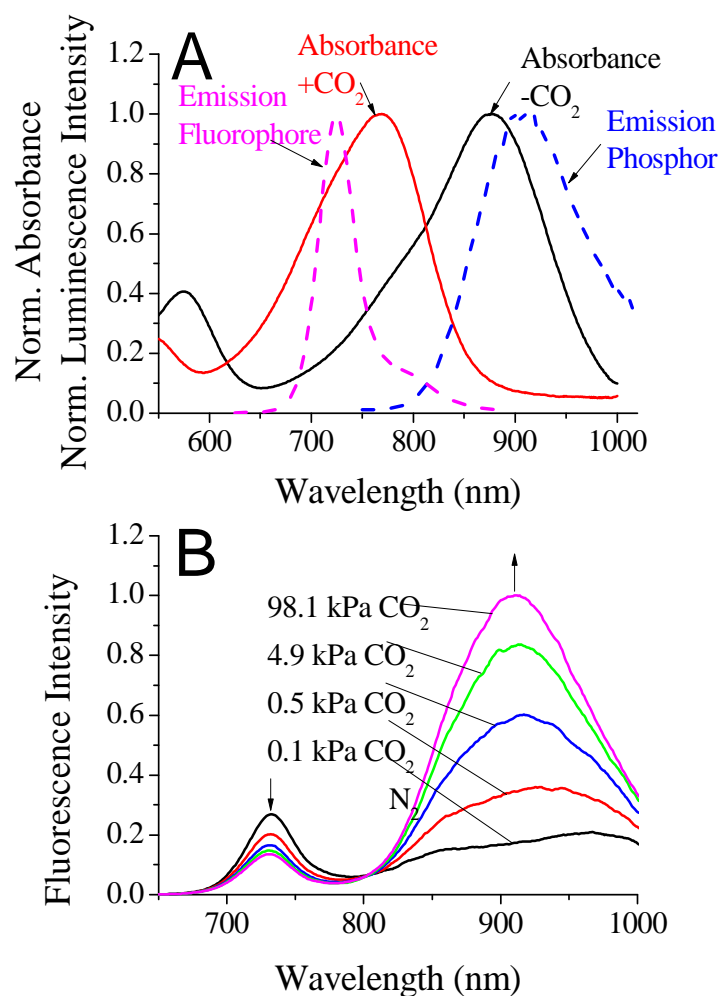
Figure 3.4. *(A) Emission spectra (λ_{exc} 610 nm) for Egyptian Blue (EB; blue dashed line; "Emission Phosphor") and the di-butoxy-complex (dissolved in tetrahydrofuran; magenta dashed line; "Emission Fluorophore"); absorption spectra of the sensor based on the di-OH-complex in absence (black line) and in presence (red line) of carbon dioxide at 25°C. (B) Emission spectra (λ_{exc} 610 nm) for a carbon dioxide sensor based on di-OH complex and inner-filter effect read-out at 25°C and humidified conditions.*

Carbon Dioxide Production/Consumption of a Hebe Plant

The applicability of the presented carbon dioxide sensors is demonstrated by showing the respiration of a Hebe plant. The Hebe plant in soil, a carbon dioxide sensor based on the di-CH_3-di-OH-complex and an oxygen trace sensor were placed in a desiccator. The desiccator was purged for 15 min with a gas mixture of 2% oxygen in nitrogen (in order to achieve better dynamics when measuring with an optical oxygen sensor compared to air saturation) and then closed tightly. During the measurement the setup was alternately kept in darkness and illuminated for 30 min using three halogen lamps. According to

this illumination sequences the production/consumption of carbon dioxide was observed (figure 3.5). In darkness an increase of carbon dioxide occurred due to respiration, whereas during illumination the concentration of CO_2 decreased. Over the whole measurement more CO_2 was produced than consumed which may be due to stress-induced respiration of the Hebe plant. Correspondent to the applied light sequences also the oxygen concentration was affected. Note that over the whole experiment the oxygen concentration was increasing which can be explained by slow diffusion of oxygen into the desiccator. Surprisingly, oxygen concentration did not increase significantly during the light phase, but it increased abruptly immediately after the light was switched off, reaching a plateau after about 30 min (figure 3.5). This effect may be attributed to the storage of generated oxygen in the plant and its release in the beginning of the dark phase. After this time the equilibrium between oxygen consumption during respiration and oxygen diffusion from outside is reached. As can be seen, the same phenomenon is observed if the light and dark cycles are extended to 60 min each (see hour 2 to 4 in figure 3.5). The above plant behavior is beyond the scope of the paper and calls for more detailed investigation.
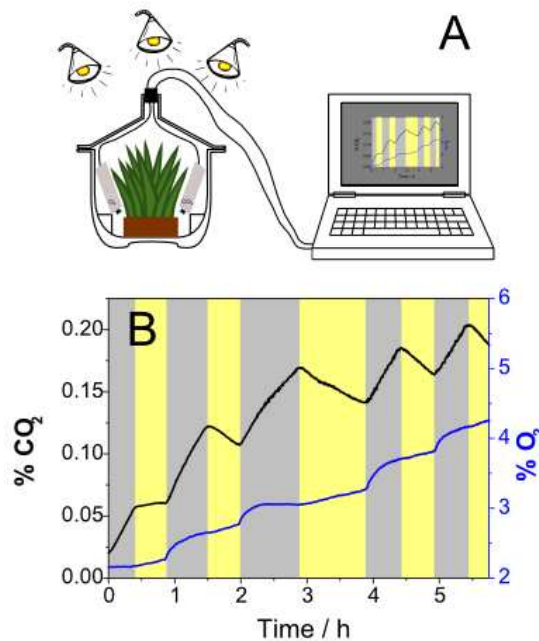
Figure 3.5. *(**A**) Experimental set-up and (**B**) carbon dioxide and oxygen dynamics in a desiccator containing a Hebe plant during illumination (yellow zones) and in darkness (grey zones).*

Conclusion

A new class of colorimetric pH-sensitive indicators for carbon dioxide sensors is presented. The di-OH-aza-BODIPY dyes show characteristic CO_2-dependent absorption spectra in the near-infrared region. In addition to the remarkable photostability of the indicators and the high molar absorption coefficients, the dynamic ranges of the sensors can be tuned via electron-donating and electron-withdrawing substituents. This enables a broad range of applications from environmental monitoring to food packaging or capnography. The sensors based on di-CH_3-di-OH-aza-BODIPY belong to the most sensitive ever reported and resolve well below atmospheric CO_2 levels. Absorption-modulated inner-filter effect was used to enable referenced luminescence-based ratiometric read-out. As an example the production/consumption of carbon dioxide of a Hebe plant was demonstrated.

Acknowledgment

Supporting Information

to *NIR Optical Carbon Dioxide Sensors Based on Highly Photostable Dihydroxy-aza-BODIPY Dyes*
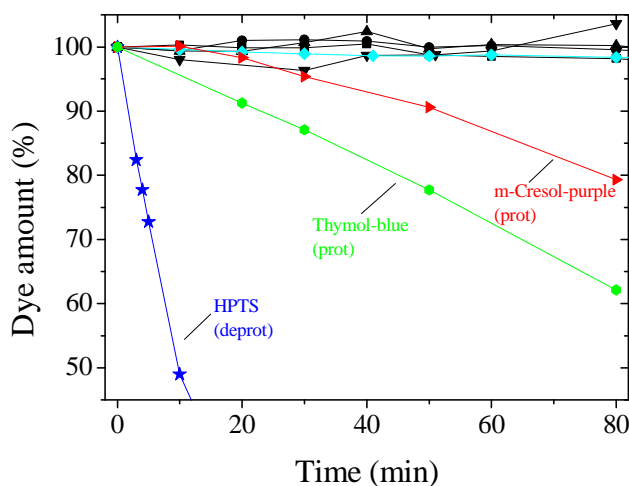
Figure S3.1. *Photodegradation profiles for carbon dioxide sensors (EC49; base: TOAOH; T=25°C) based on the di-OH-aza-BODIPY dyes (black), m-cresol-purple (red triangles), thymol-blue (green dots) obtained from the absorption spectra of the respective neutral form and the absorption spectra of the deprotonated forms of the di-Cl-di-OH-complex (cyan) and HPTS(TOA)₃ (blue stars).*
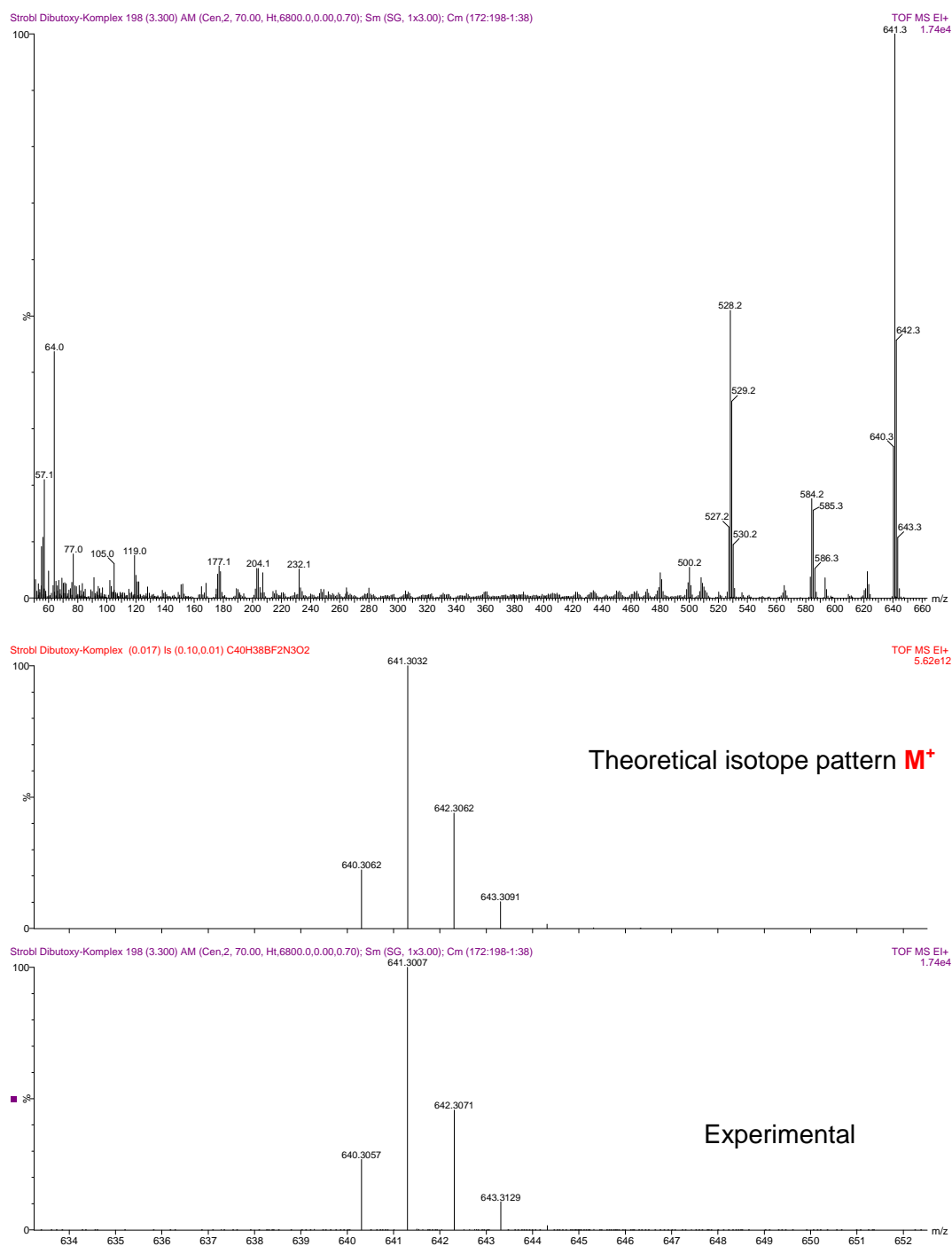
Figure S3.2. *EI-DI Mass spectrum of 3,7-bis(4-butoxyphenyl)-5,5-difluoro-1,9-diphenyl-5H-4λ⁴,5λ⁴-dipyrrolo[1,2-c:2',1'-f][1,3,5,2]triazaborinine (di-butoxy-complex).*
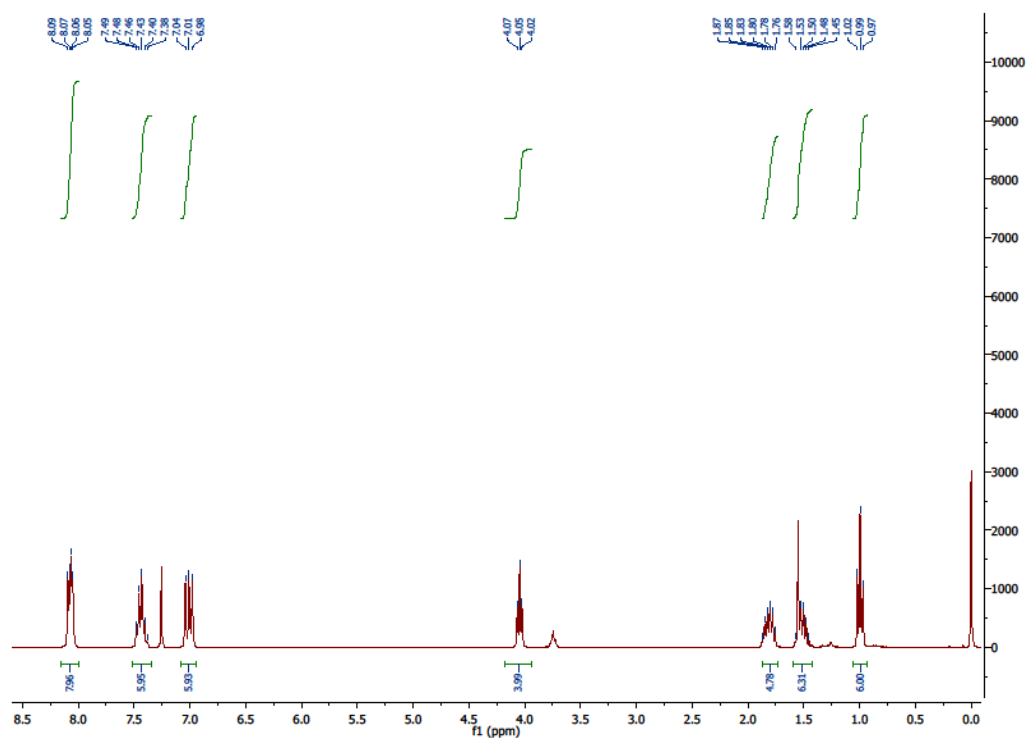
Figure S3.3. *^{1}H NMR of 3,7-bis(4-butoxyphenyl)-5,5-difluoro-1,9-diphenyl-5H-4λ^4,5λ^4-dipyrrolo[1,2-c:2',1'-f][1,3,5,2]triazaborinine (di-butoxy-complex).*
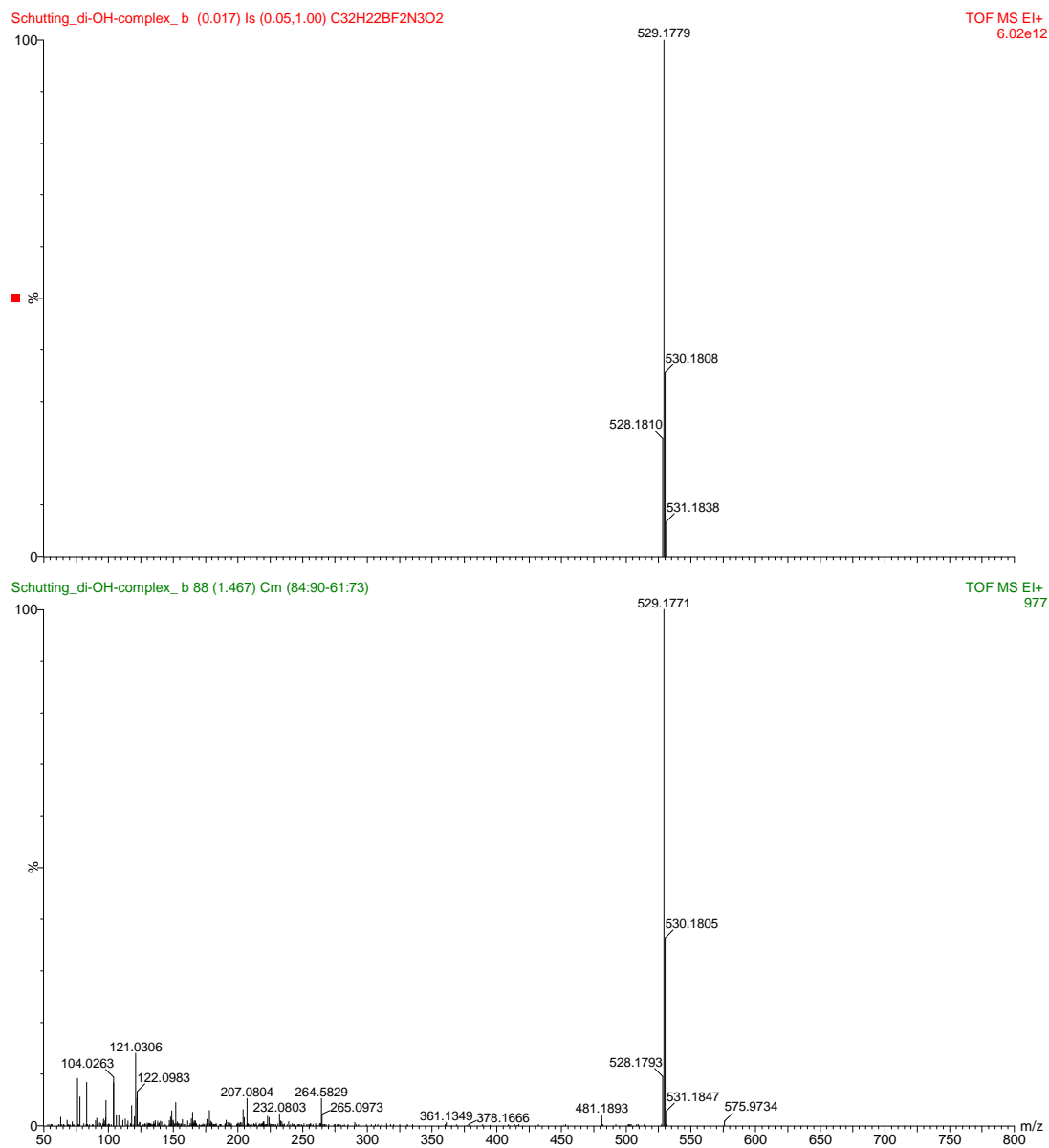
Figure S3.4. *EI-DI Mass spectrum of 4,4'-(5,5-difluoro-1,9-diphenyl-5H-4λ⁴,5λ⁴-dipyrrolo[1,2-c:2',1'-ƒ][1,3,5,2]triazaborinine-3,7-diyl)diphenol (di-OH-complex).*
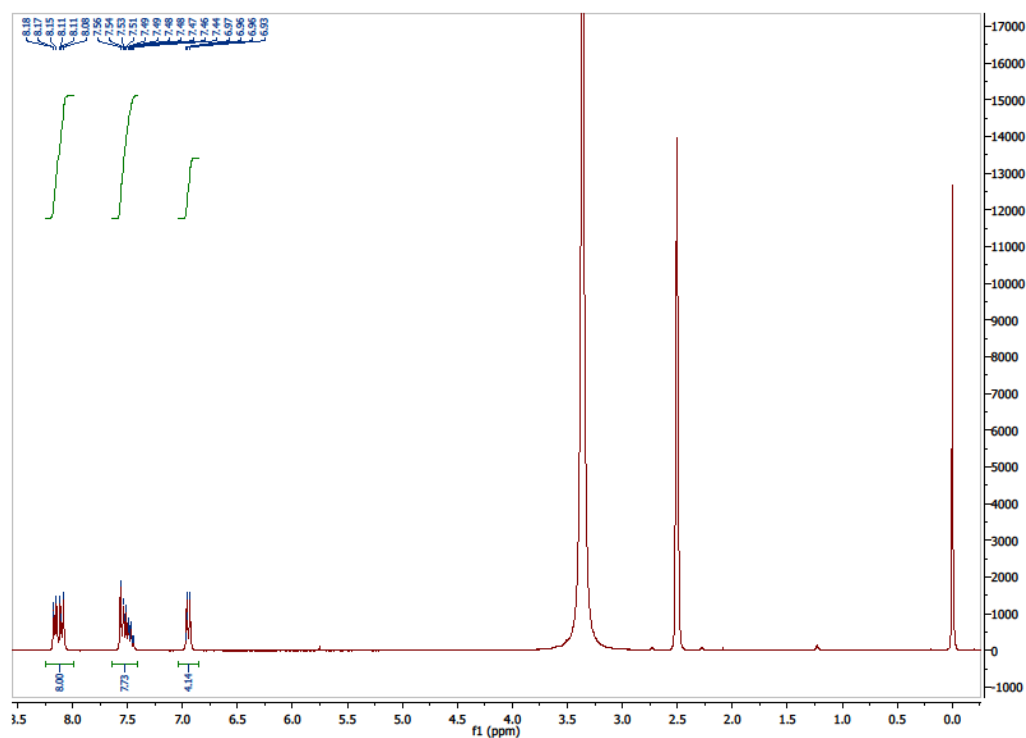
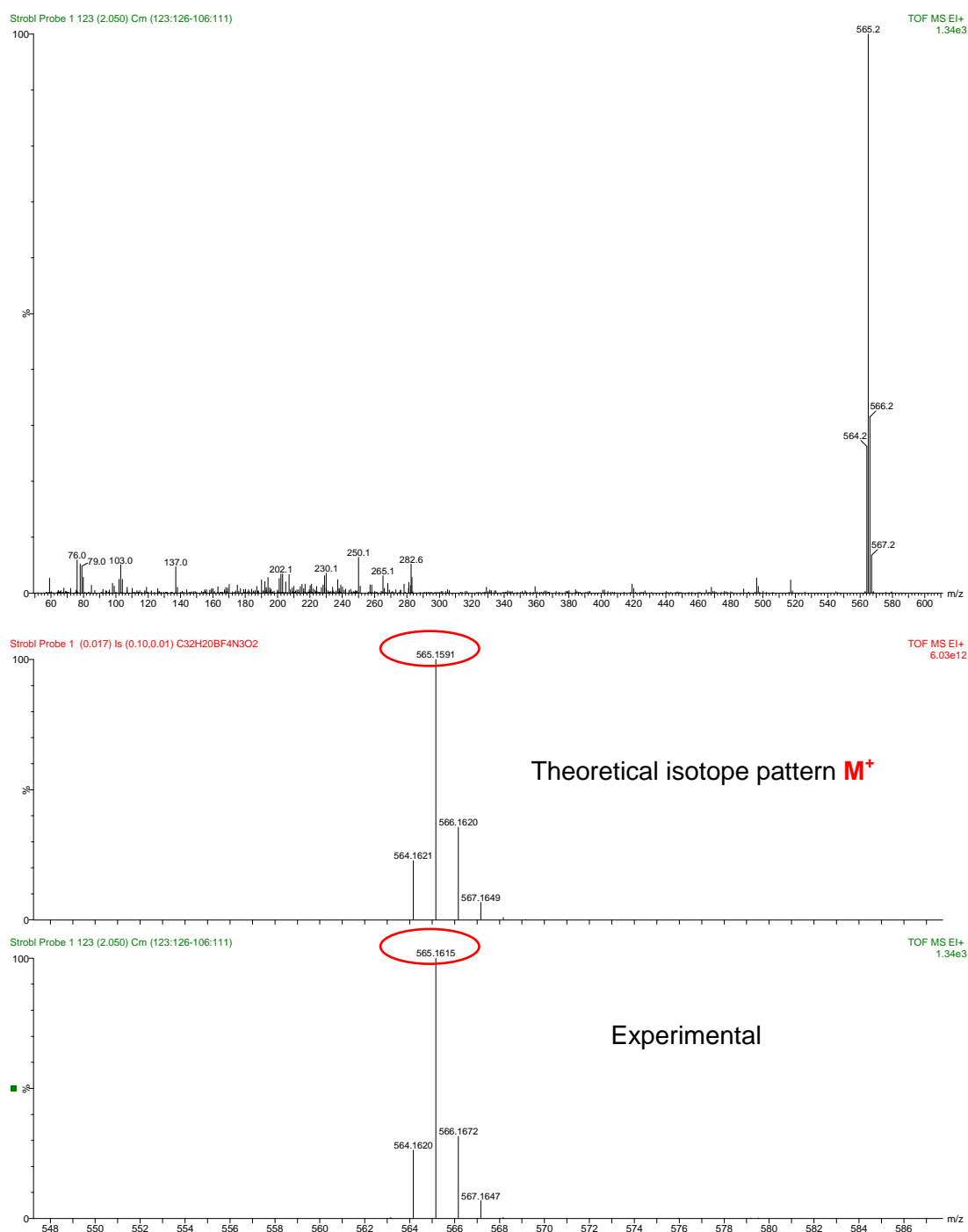**Figure S3.5.** ^1H NMR of 4,4'-(5,5-difluoro-1,9-diphenyl-5H-4λ^4,5λ^4-dipyrrolo[1,2-c:2',1'-f][1,3,5,2]triazaborinine-3,7-diyl)diphenol (di-OH-complex).

Figure S3.6. *DI-EI Mass spectrum of 4,4'-(5,5-difluoro-1,9-diphenyl-5H-4λ⁴,5λ⁴-dipyrrolo[1,2-c:2',1'-f][1,3,5,2]triazaborinine-3,7-diyl)bis(3-fluorophenol)   (di-F-di-OH-complex).*
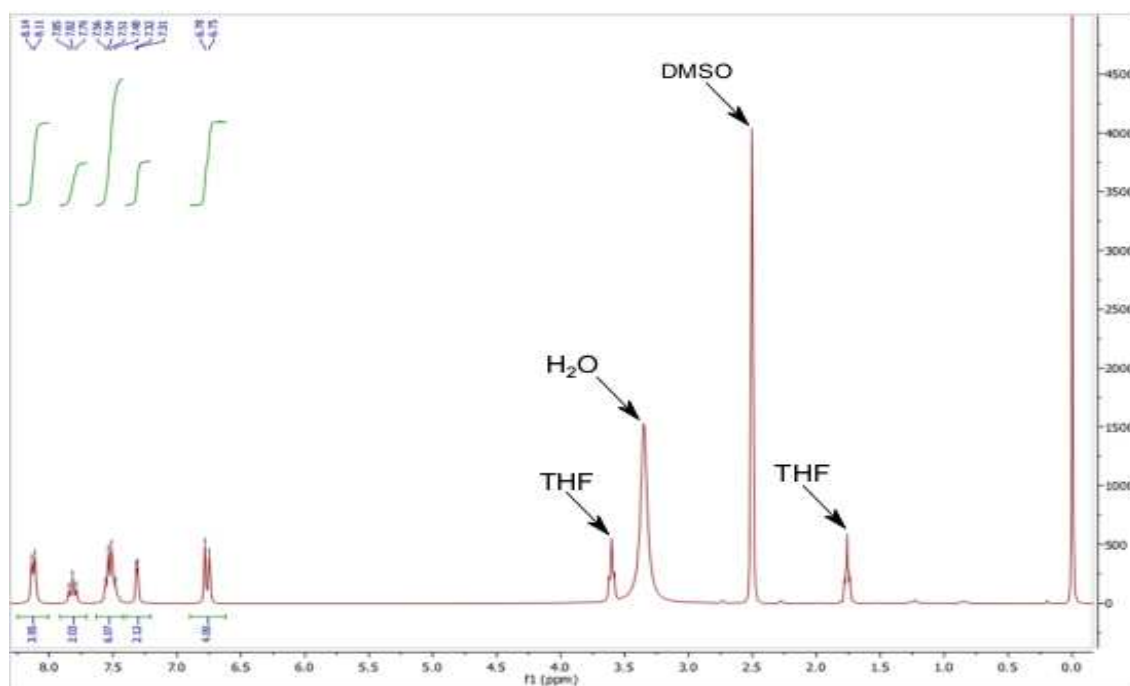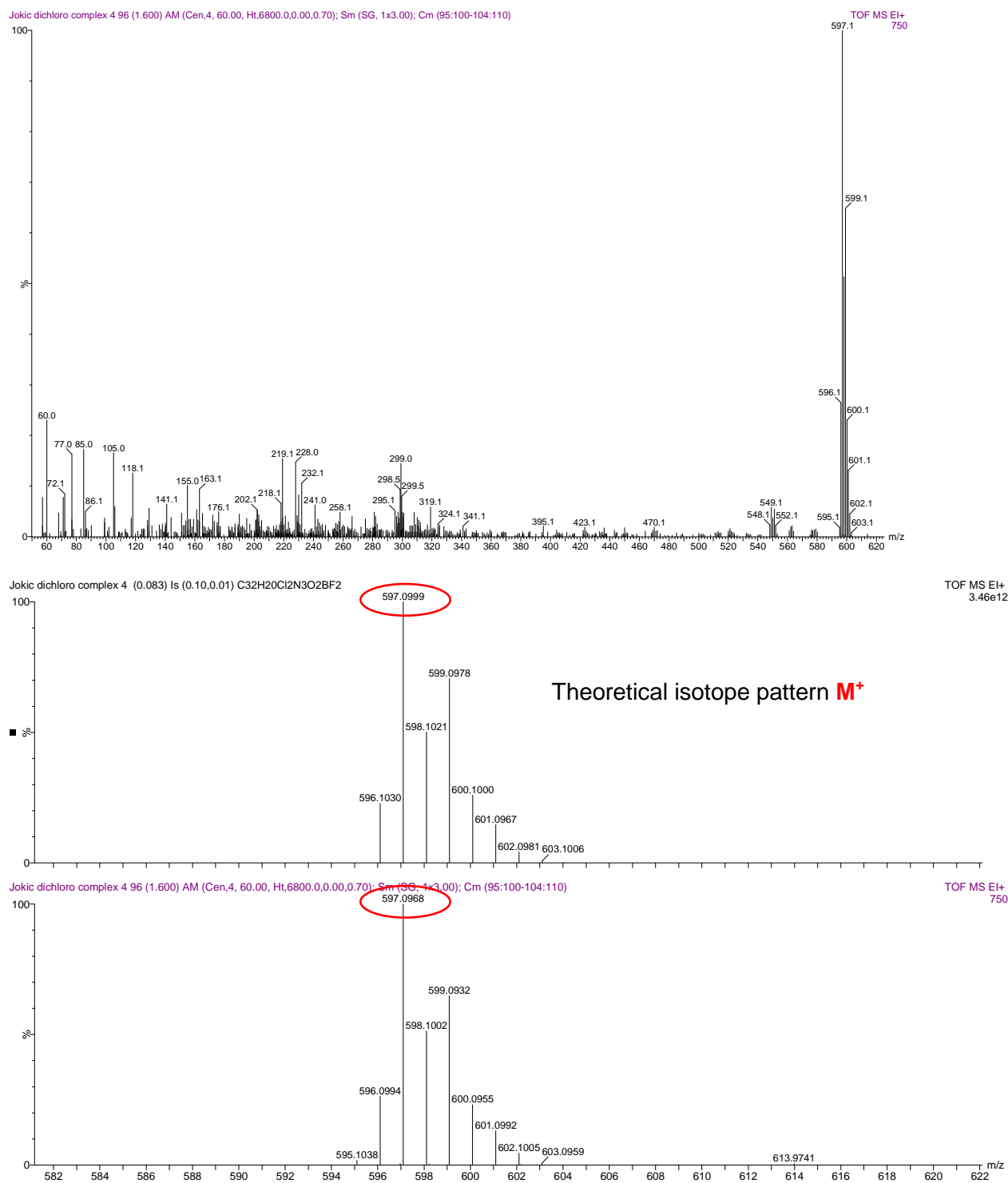
Figure S3.7. *^1H NMR of 4,4'-(5,5-difluoro-1,9-diphenyl-5H-4λ^4,5λ^4-dipyrrolo[1,2-c:2',1'-f][1,3,5,2]triazaborinine-3,7-diyl)bis(3-fluorophenol) (di-F-di-OH-complex).*

Figure S3.8. *EI-DI Mass spectrum of 4,4'-(5,5-difluoro-1,9-diphenyl-5H-4λ^4,5λ^4-dipyrrolo[1,2-c:2',1'-f][1,3,5,2]triazaborinine-3,7-diyl)bis(2-chlorophenol) (di-Cl-di-OH-complex).*
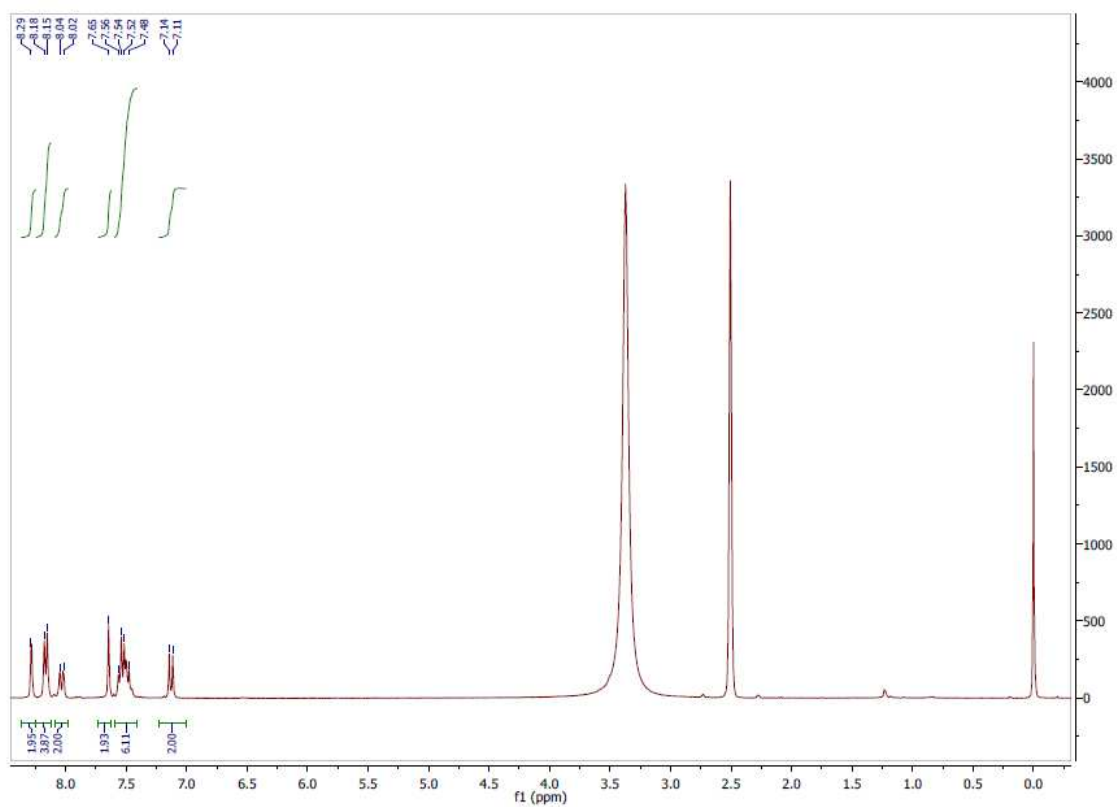
Figure S3.9. ^1H NMR of 4,4'-(5,5-difluoro-1,9-diphenyl-5H-4λ^4,5λ^4-dipyrrolo[1,2-c:2',1'-f][1,3,5,2]triazaborinine-3,7-diyl)bis(2-chlorophenol) (di-Cl-di-OH-complex).
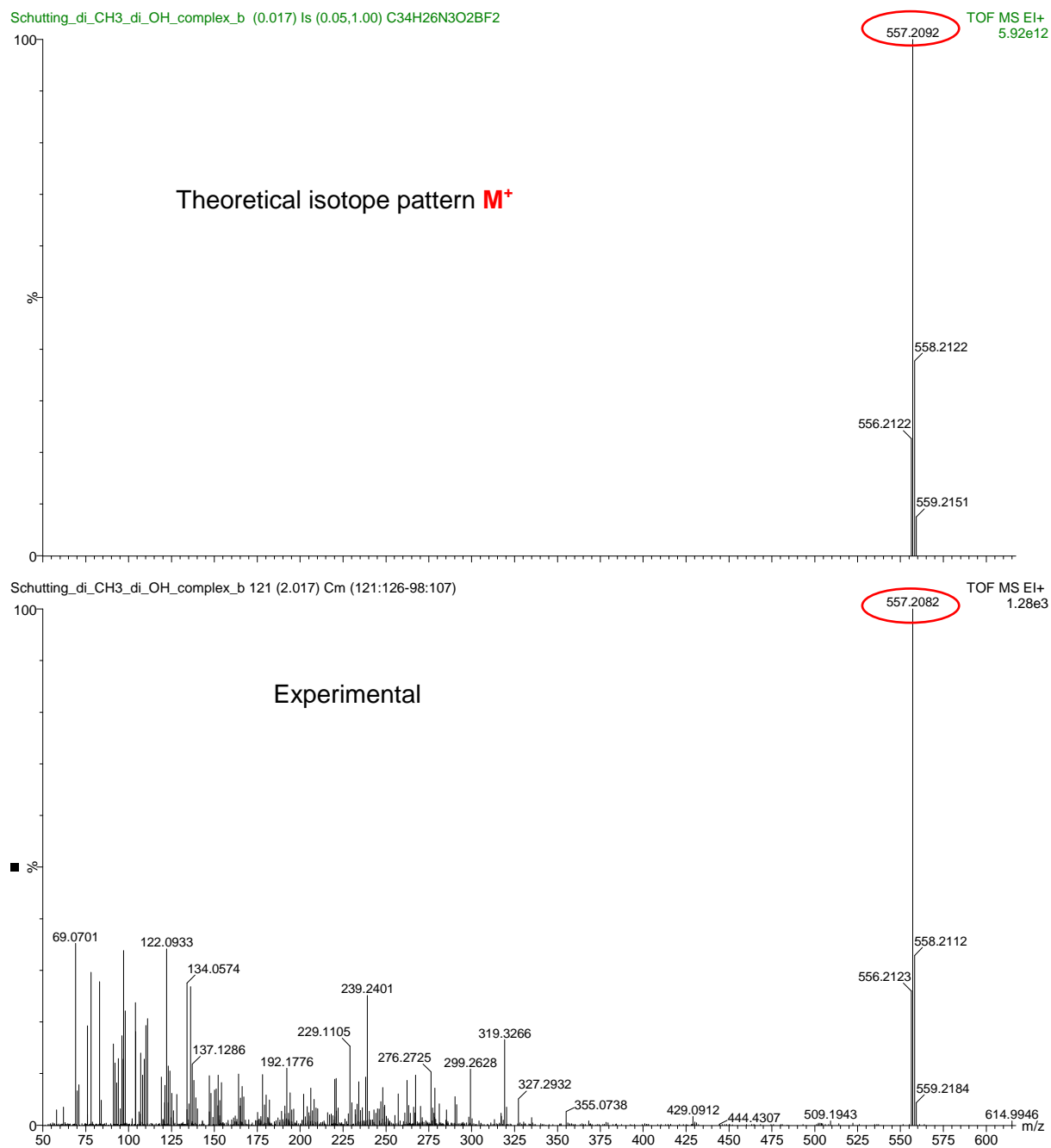
Figure S3.10. EI-DI Mass spectrum of 4,4'-(5,5-difluoro-1,9-diphenyl-5H-4λ⁴,5λ⁴-dipyrrolo[1,2-c:2',1'-f][1,3,5,2]triazaborinine-3,7-diyl)bis(2-methylphenol) (di-CH₃-di-OH-complex).

Figure S3.11. *¹H NMR of 4,4'-(5,5-difluoro-1,9-diphenyl-5H-4λ⁴,5λ⁴-dipyrrolo[1,2-c:2',1'-f][1,3,5,2]triazaborinine-3,7-diyl)bis(2-methylphenol) (di-CH₃-di-OH-complex).*
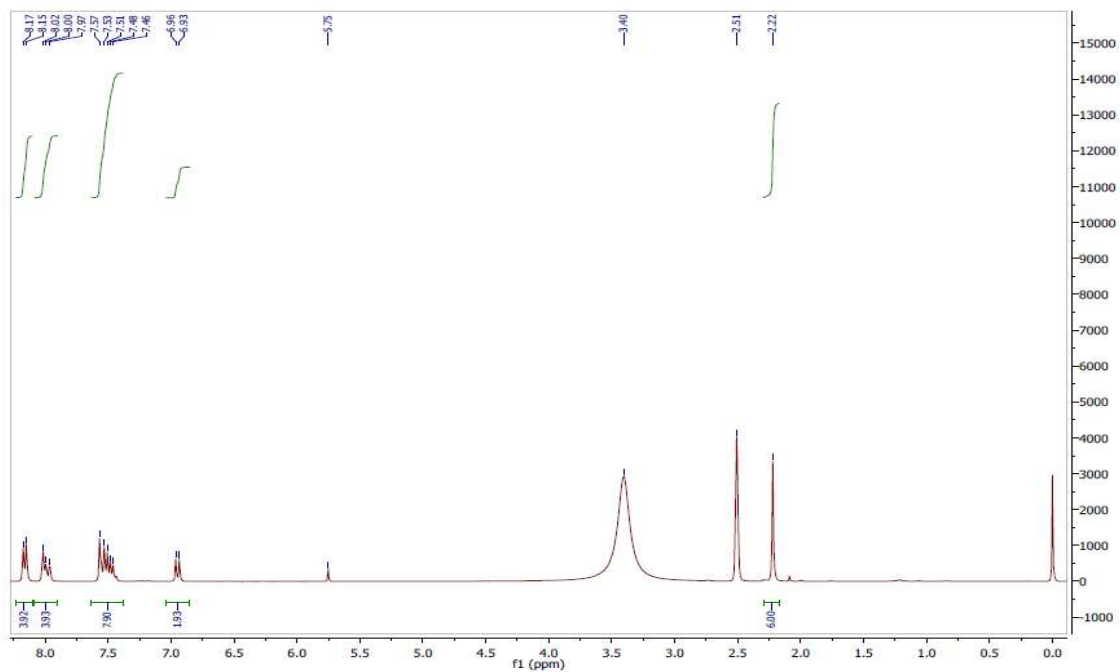
135

Chapter 4

Scope of this chapter

In chapter 4 a possible application of optical carbon dioxide sensors in marine environments is presented. The device was constructed to especially meet the demands of field experiments in marine science, where time, staff, and equipment are limited. It should give as much simultaneous information as possible concerning spatial and temporal distribution of the analyte concentration. Thus, one hundred optical fiber sensors for carbon dioxide with one collective excitation source and imaging read-out were attached to the housing containing the RGB camera and the electronics. Characterization of the device was first carried out under lab conditions.

Afterwards, the prototype was tested under real conditions off Panarea Island (Sicily, Italy). Panarea Island is located in the southern Tyrrhenian Sea north of Sicily and is known to be in a volcanically active area, as for example in 2002 a huge underwater outbreak of carbon dioxide occurred and still carbon dioxide is outgasing there from the seafloor. It is not yet definitely known if the CO_2 reaches the seawater either continuously and point-by-point via bubbles, or discontinuously via tidally affected pore-water dynamics. To answer this question, the multi-branched sensor device was applied off Panarea Island (Sicily, Italy).

Multi-Branched Optical Carbon Dioxide Sensors for Marine Applications

The distribution of CO_2 in natural waters can vary significantly within small areas due to physical, chemical and biological processes. To achieve more information about these systems, simultaneous detection of CO_2 concentration at many different positions is highly desired. In this contribution a multi-branched optical carbon dioxide sensor system is presented. The ends of 100 optical fibers are coated with optical carbon dioxide sensing foils, which – after excitation – emit light in either the red or the green part of the spectrum according to the ambient pCO_2. These ends are freely moveable, whereas the opposite ends are reunited in a polished fiber head building a 10 x 10 matrix of fiber spots. This fiber head is positioned in front of a commercially available red/green/blue (RGB) camera, which enables read-out via imaging. Images are then divided in their color channels, which contain the analytical information. Here, the intensity in the red and green channel is used (ratio red/green). The system was tested off Panarea Island (Sicily, Italy), which is located in the Tyrrhenian Sea in a volcanically active area, where carbon dioxide is outgasing from the seafloor. A significant effect of tides, but no correlation with photosynthesis was observed via the measured CO_2 dynamics.

Introduction

It is known that increasing carbon dioxide concentrations in the atmosphere cause elevated CO_2 levels in the oceans. Marine scientists are investigating this phenomenon - also known as ocean acidification - and its strong effects on the marine ecosystem.[9,181–186] Therefore, an appropriate detection method is necessary. Especially for field experiments where time, equipment and staff are limited, it is important that the method is easily adaptable to the respective conditions of the experiment and that it gives as much simultaneous information as possible concerning spatial and temporal distribution of the analyte concentration.

Optical chemosensors[116–118,139,140] are ascending and promising detection tools for analytes such as pH,[143,150,152,187–189] oxygen[155,190–193] or carbon dioxide.[61,92,111,132,167,171,194] The most common ones for carbon dioxide are so called *plastic type* sensors[51,65,66,89,112,113] with a pH-sensitive indicator dye as core-component of the sensing film. The indicator shows changing spectral properties – absorption and/or luminescence properties – due to its degree of protonation. If an experiment requires a certain mobility of the sensor, to measure in small volumes, to be non-invasiv or to overcome a certain distance, the application of fiber optodes[195–198] becomes preferable. Here, optical fibers, either made of glass or polymer, guide the excitation light to the sensing element (foil or coated tip) and the emitted light back. If simultaneous detection at more than one measurement point is required, those optical fibers can also be used in so called multi-fiber arrays.[190,199,200]

In 2012 Fischer and Koop-Jakobsen published the *multiple fiber optode (MuFO)*, a novel system for simultaneous analysis of multiple fiber optic oxygen sensors.[201] The device was based on simultaneous lifetime imaging of optical sensing foils, which were based on the principle of oxygen quenching of a fluorescent indicator dye enabling measurements at 100 positions at the same time. As the used principle was not applicable for carbon dioxide, the read-out method had to be adapted for optical CO_2 sensors, which are based on a pH-sensitive indicator dye. Here, an enhancement of the previous device, enabling simultaneous interrogation of one hundred optical carbon dioxide fiber optodes based on imaging read-out, is presented.

Experimental

Materials

Ethyl cellulose (EC49, ethoxyl content 49%), thymol-blue (A.C.S. reagent), *m*-cresol-purple (indicator grade) and tetraoctylammonium hydroxide solution (TOAOH, 20% in methanol) were obtained from Sigma-Aldrich (www.sigmaaldrich.com). Nitrogen, 5% carbon dioxide in nitrogen, 0.2% carbon dioxide in nitrogen, argon and carbon dioxide (all of 99.9990% purity) were obtained from Air Liquide (Austria, www.airliquide.at). Toluene, ethanol (EtOH), sodium chloride, sodium bicarbonate and hexane were purchased from VWR (Austria, www.vwr.com). Poly(ethylene terephthalate) (PET)

support Melinex 505 was obtained from Pütz (Germany, www.puetz-folien.com). The buffer salts di-sodium phosphate ($\geq$ 99%, p.a.) and monopotassium phosphate (p.a.) were purchased from ROTH (www.carlroth.com) and MERCK (www.merck.at), respectively. The silicone components vinyl terminated polydimethylsiloxane (viscosity 1000 cSt.), (25-35% methylhydrosiloxane)-dimethylsiloxane copolymer (viscosity 25-35 cSt.), 1,3,5,7-tetravinyl-1,3,5,7-tetramethylcyclotetrasiloxanen and the platinum-divinyltetramethyldisiloxane complex were received from ABCR (Germany, www.abcr.de). The pigments brick-red and lemon-yellow were purchased from Kremer Pigments (Germany, www.kremer-pigmente.com). Black silicone-rubber ELASTOSIL N189 was obtained from Wacker (www.wacker.com). De-ionized water was filtered via a Barnstead NANOpure ultrapure water system. The optical plastic fibers LUMINOUS (type C-1000; Ø 2.2 mm) from Asahi Chemical Japan were ordered via Sojitz Europe plc. (www.sojitz.de). The material for the metal sleeves, a stainless steel pipe (inner Ø2.2 mm; type 1.4571), was purchased from SW-Stahl (www.sw-stahl.de). The RGB camera (type EOS 1000D, internal infrared filter removed) and the objective (type EF-S 60 mm) were from Canon (www.canon.at). A SDHC card (32 GB) from Sandisk (www.sandisk.de) was used for image-storage during the measurements. LEDs (type LUXEON Rebel LXML PB01 0030, blue 470 nm, 75l m; incl. LED star board) were purchased from LUMITRONIX LED-Technik GmbH (www.leds.de) and the respective LED driver from PCB components (www.pcb-components.de). Optical filter DT-Blue and the NIR blocking filter Calflex X were obtained from Qioptiq (www.qioptiq-shop.com). A 500 nm long pass filter from Schott (www.schott.com) and a LEE plastic filter (medium yellow; www.leefilters.com) were used in front of the camera. The material for the housing and the fiber head ERTACETAL (POM C, Polyoxymethylen) was purchased from ARTHUR KRÜGER GmbH (www.arthur-krueger.de). The cutting pliers Rennsteig 600 001 3 was obtained from (www.rennsteig.com/de). Electronics: USB/ LAN converter (4x) was received from Sharkoon (www.sharkoon.com) and the LAN switch (FS105 5 Port 10/100MBit) from Netgear (www.netgear.at). Accumulator packs 4x 16Ah 3.2C cells (Headway 40160SE) were obtained from Lipopower (www.lipopower.de).

Sensing Chemistry

The sensing foils consist of three layers, which were knife-coated on a PET support (figure 4.1):

The first layer contained the pH-sensitive indicator dye and tetraoctylammonium hydroxide (TOAOH) as base, embedded in an ethyl cellulose matrix (EC49) with an ethoxyl content of 49%. Here, 1.5 mg of the indicator dye (thymol-blue or *m*-cresol-purple; 1.5%w/w with respect to the polymer) and 100 mg EC49 were first dissolved in 1900 mg of a mixture of toluene/ethanol (6:4), then 100 µl TOAOH solution (20% in methanol) were added. After knife-coating and evaporation of the solvents a film thickness of ~13 µm was achieved.

The second layer contained the pigments *brick-red* and *lemon-yellow* dispersed in a four-component-silicone layer: 50 mg of *brick-red* and *lemon-yellow*, respectively, dispersed in a silicone solution consisting of 800 mg vinyl terminated polydimethylsiloxane, 32 µl (25-35% methylhydrosiloxane)-dimethylsiloxane copolymer, 2 µl 1,3,5,7-tetravinyl-1,3,5,7-tetramethylcyclotetrasiloxane and 4 µl platinum-divinyltetramethyldisiloxane complex dissolved in 1600 mg hexane. After knife-coating and evaporation of the organic solvent a film thickness of ~40 µm was achieved.

A commercially available black silicone-rubber was used as third layer (film thickness ~30 µm) for protection against ambient light and mechanical damages.
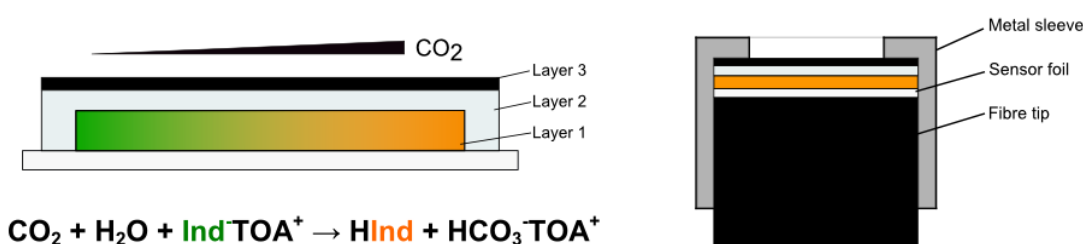

$$CO_2 + H_2O + Ind^-TOA^+ \rightarrow HInd + HCO_3^-TOA^+$$

Figure 4.1. Left: Sensing foil with dye layer 1, silicone layer with "brick-red" and "lemon-yellow" (layer 2), protective black silicone-rubber layer 3 and protonation/deprotonation principle of the pH-sensitive indicator in the dye layer (below). Right: Sensing foils stamped out and fixed on the optical fibers by using custom-made metal sleeves.

Methods

Characterization of the sensing chemistry: Absorption spectra were recorded on a Cary 50 UV-vis spectrophotometer (www.varianinc.com). Photobleaching experiments were performed by irradiating the sensor foils in a glass cuvette with light of a high-power 10 W LED array (λ_{max} 458 nm, 3 LEDs, LED-TECH.de) operated at 6 W input power. A lens (Edmund Optics) was used to focus the light of the LED array on the glass cuvette (photon flux: ~3900 µmol s^{-1} m^{-2} as determined with a Li-250A light meter from Li-COR). The photodegradation profiles were obtained by monitoring the absorption spectra of a sensor foil based on the respective dye. The cuvette was flushed with either carbon dioxide gas for the protonated form, or with nitrogen for the deprotonated form and sealed with Parafilm. Fluorescence intensity measurements of the sensing foils were recorded on a Hitachi F-7000 Fluorescence spectrometer (www.hitachi.com) equipped with a red-sensitive photomultiplier R928 from Hamamatsu (www.hamamatsu.com). Gas calibration mixtures were obtained using a gas mixing device from MKS (www.mksinst.com). The gas mixture was humidified to about 85% relative humidity (saturated KCl solution) prior entering the calibration chamber. Temperature was controlled by a cryostat ThermoHaake DC50. The phosphate buffer solution (~700 mM) was composed of 13.60 g di-sodium phosphate, 0.72 g monopotassium phosphate and 35.06 g sodium chloride dissolved in 1000 ml of de-ionized water and showed a pH value of 7.7-7.8. Calibration measurements were carried out by flushing the phosphate buffer solution first with pure nitrogen gas until a plateau was reached. Afterwards a solution of 1.59 g sodium bicarbonate dissolved in 50 ml of de-ionized water was added stepwise to give increasing levels of carbon dioxide concentration.

The multi-branched optical carbon dioxide sensing device was built similar to the MuFO device from Fischer and Koop-Jakobson,[201] except for the read-out via RGB camera and the sensing chemistry: The electronic system, the RGB camera (EOS 1000D, internal infrared filter removed) and the excitation sources (3 LEDS, 470 nm) were positioned in a cylindrical housing made of POM. The camera was equipped with a macro objective (type EF-S 60 mm), a Calflex X filter, a LEE plastic filter (medium-yellow) and a 500 nm long pass filter in front of the objective to avoid excitation light and wavelengths >500 nm. The 3 LEDs (470 nm) for excitation were positioned on a metal ring in equal distance/angle to each other around the objective of the RGB camera and filtered through a optical DT-Blue filter. They were focused on the 10 x 10 matrix

of the fiber head (photon flux: 22.7 µmol s^{-1} m^{-2}; determined with a Li-250A light meter from Li-COR, www.licor.com). A custom-made trigger source was used to trigger and synchronize camera and LED excitation. One end of every waveguiding fiber (cut to 5.5 m length) was stripped (~4 cm) and positioned in the fiber head in the pre-drilled 10 x 10 matrix (within an area of 15 x 15 mm). Fixation was performed by gluing. The fiber head and the integrated fibers were polished all together using commercially available polishing materials. The moveable ends of the fibers were cut with cutting pliers for polymer optical fibers to ensure a plain cut surface. The sensing foils were stamped out and fixed on the optical fibers by using custom-made metal sleeves (length 2 cm; inner Ø2.2 mm; stainless steel type 1.4571). Analysis of the color channels of the images were carried out using a home-made matlab script (see supporting information).

Results and Discussion

Principle

The device consists of three main parts (figure 4.2): (1) the housing, containing the electronic assembly, the collective excitation source and the RGB camera; (2) the waveguiding fibers and the fiber head; (3) the sensing foils on the freely moveable end of every fiber (figure 4.1).

As mentioned before, the system is based on the principle of a pH-sensitive indicator dye, which is protonated/ deprotonated in presence/ absence of carbon dioxide according to the following principle:

$$CO_2 + H_2O + Ind^-TOA^+ \leftrightarrow IndH + TOA^+HCO_3^-$$
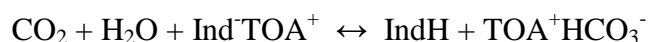
The indicator dye (Ind$^-$; IndH) is embedded in a polymer matrix together with a base (TOA$^+$). This sensing foil is fixed on the freely moveable end of each of the optical fibers. The fibers guide the excitation light from 3 LEDs to the sensing foils and the emitted light back to the fiber head, which is positioned in front of the housing. The RGB camera takes images of the fiber head. These images are then divided in their color channels, which contain the analytical information. For this device the blue channel was used for excitation and the ratio of the red and the green channel was used

for analysis of the pCO$_2$ level. The analysis of the images was carried out using a home-made matlab script (see supporting information).
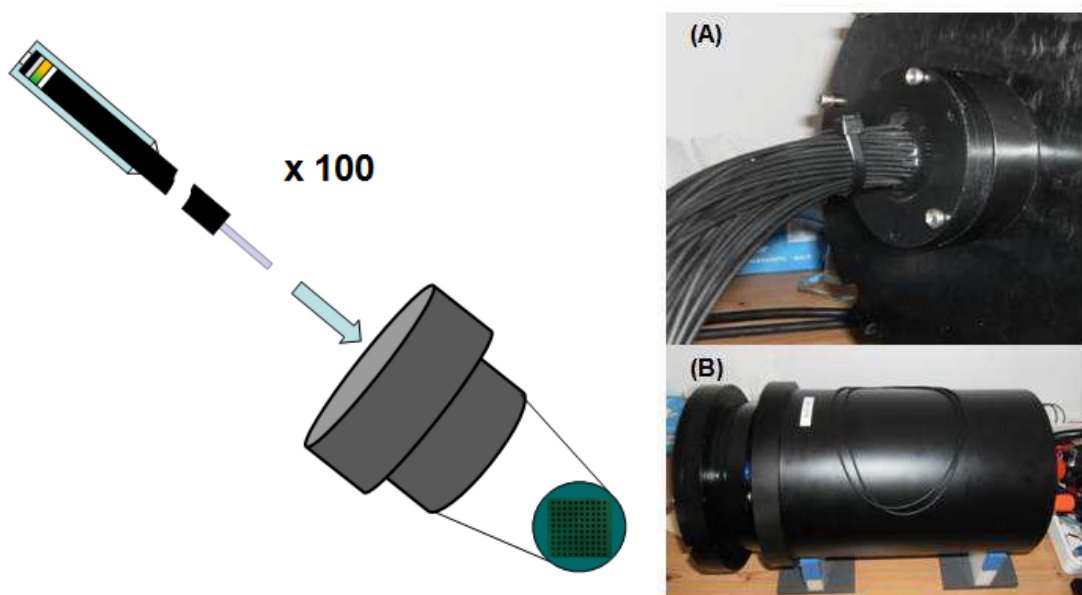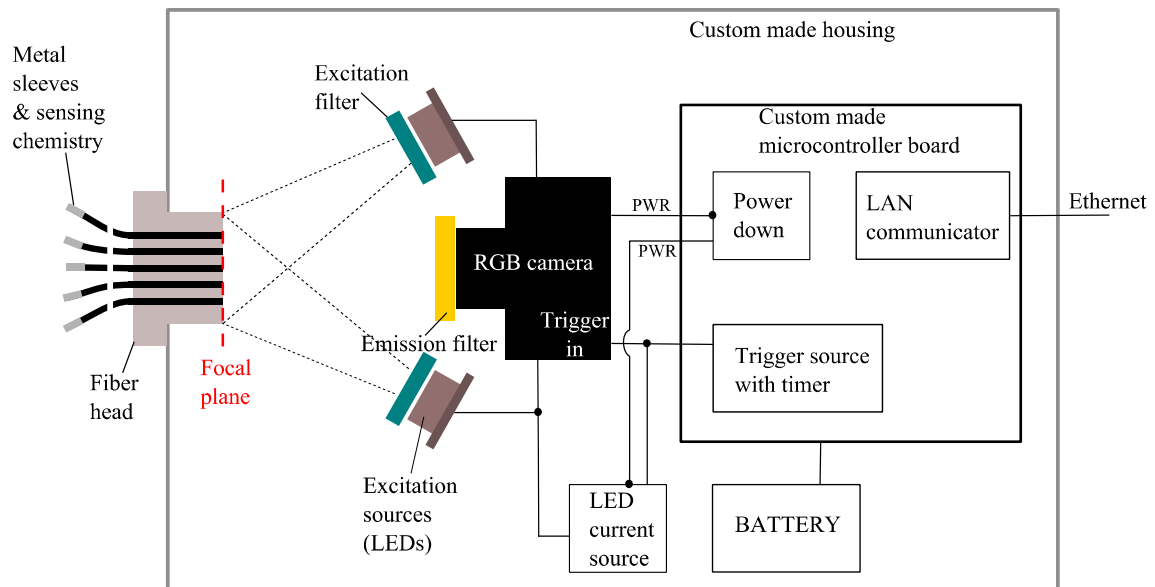

Figure 4.2. Above: *Principle of the multi-branched optical carbon dioxide sensing device and electronical system.* ***Below:*** *Scheme of the 10 x 10 matrix; (**A**) fixation of the fiber head to the (**B**) housing with camera and excitation LEDs inside.*

Sensing Chemistry

The self-referencing colorimetric triphenylmethane dyes thymol-blue and *m*-cresol-purple were used as pH-sensitive indicators. Those indicators are well known and often

used for optical carbon dioxide sensors.[57,58] Both dyes show similar absorption maxima, but generally, sensors based on thymol-blue display higher sensitivity than sensors based on *m*-cresol-purple, due to the slightly higher pK_a value of thymol-blue (table IV). Hence, sensors based on both indicators were investigated to demonstrate the adaptability of the system to applications with different requirements concerning pCO_2 ranges.

To realize a fluorescence based ratiometric read-out within the red and green color channel of the RGB camera[166] the pigments *brick-red* and *lemon-yellow* were used as secondary emitters in the silicone layer to enable an inner-filter effect based system. The emission of *lemon-yellow* overlaps only slightly with the absorption of the protonated form of the indicator, but the emission of the pigment *brick-red* matches the absorption of the deprotonated form of the indicator and furthermore, causes a big change of the final emission spectra of the sensor. This overall signal of the sensing foils matched the corresponding color channels of the camera, were only small changes in the green channel were observed, but rather high changes occured in the red color channel (figure 4.3).
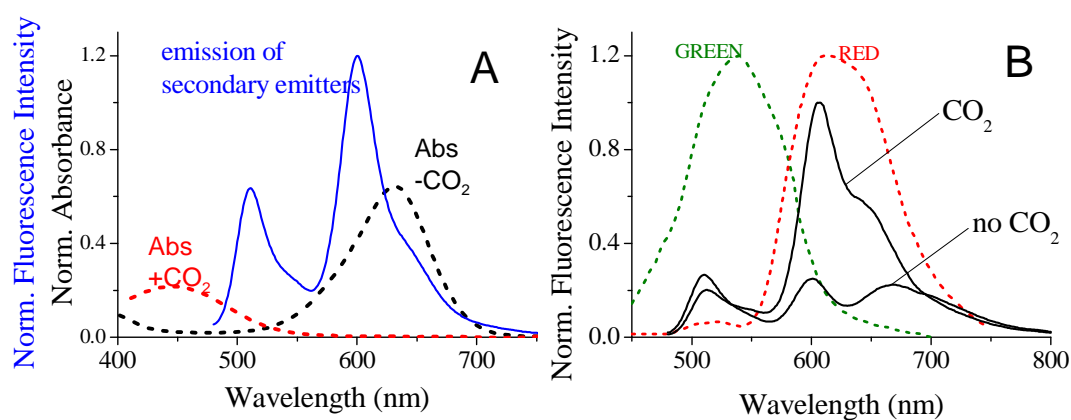

Figure 4.3. *(A) Overlap of the emission spectra of the mixture of the secondary emitters (1:1; brick-red and lemon-yellow) and the absorption spectra of the protonated and deprotonated form of thymol-blue (embedded in EC49 with TOAOH as base). (**B**) Emission spectra of the sensing foil based on thymol-blue in absence ("no CO₂") and presence ("CO₂") of carbon dioxide at 25°C (λ_{exc} 470 nm) under humid conditions and red (red dashed line) and green (green dashed line) color channels of a commercially available RGB camera.*

Photobleaching experiments were carried out for sensing foils based on thymol-blue and *m*-cresol-purple. A high power blue LED array (λ_{max} = 458 nm) was used for the

excitation of the neutral forms of the indicators. 8-Hydroxy-pyrene-1,3,6-trisulfonate (HPTS), which is the most common state-of-the-art indicator[50,57,64,65,67] for plastic carbon dioxide sensors, was used for comparison. Since only the deprotonated form of HPTS is absorbing at 458 nm, only the photodegradation profiles of this form are used for comparison. For thymol-blue and *m*-cresol-purple both, the protonated and the deprotonated form are absorbing light at 458 nm. Photodegradation profils are displayed in figure 4.4. Generally the protonated form of the indicator is more photostable than the deprotonated form, but *m*-cresol-purple showed slightly better photostability than thymol-blue – protonated as well as deprotonated. The photostability of both thymol-blue and *m*-cresol-purple (protonated and deprotonated form, each) was higher than the deprotonated form of HPTS.
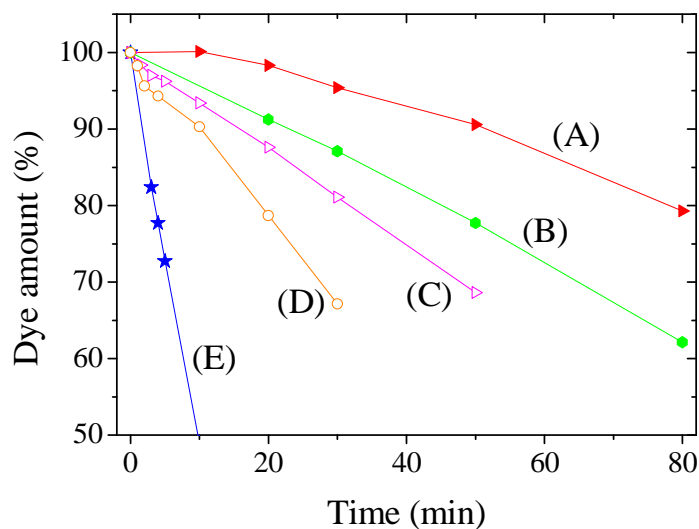

Figure 4.4. *Photodegradation profiles for carbon dioxide sensors (EC49; base: TOAOH; T = 25°C) based on **(A)** m-cresol-purple (protonated form, red filled triangles), **(B)** thymol-blue (protonated form, green dots), **(C)** m-cresol-purple (deprotonated form, magenta triangles), **(D)** thymol-blue (deprotonated form, orange circles) and **(E)** HPTS (deprotonated form, blue stars) obtained from the absorption spectra of the respective form of the respective dye under humid conditions.*

Calibration and Temperature Dependence

The calibration was carried out in a phosphate buffer solution (S = 35; ~700 mM), which was first decarbonated (flushing with nitrogen gas) until the sensors reached a plateau. Afterwards, a sodium hydrogen carbonate solution (0.36 mol/l) was added stepwise to reach CO_2 concentrations from ~150 to 46520 µatm (~3 to 370 µmol/l).

Sensing foils based on thymol-blue showed slightly higher sensitivity than sensors based on *m*-cresol-purple (figure 4.5).

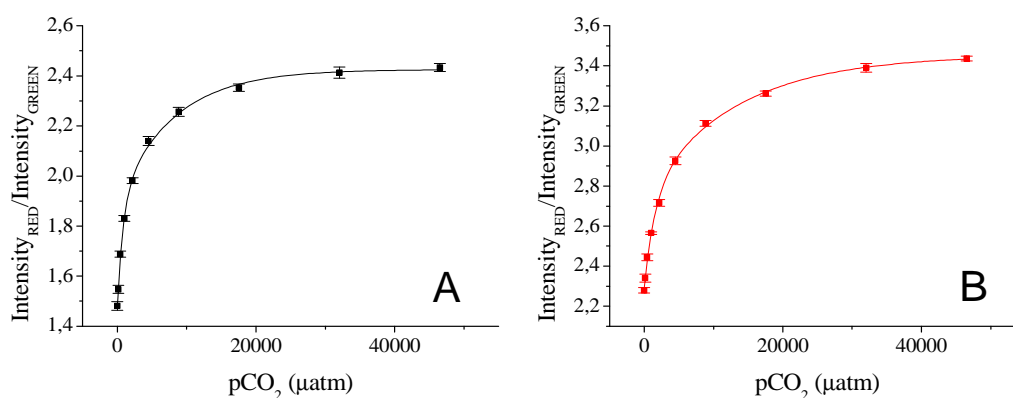***Figure 4.5.*** *Calibration curves for sensing foils based on thymol-blue (**A**) and m-cresol-purple (**B**) at 25°C in a phosphate buffer solution (S = 35; ~700 mM); read-out via imaging using a commercially available RGB camera.*

It is well known, that all optical carbon dioxide sensors show temperature dependent sensitivity, which is increasing with decreasing temperature and vice versa. Using other matrix materials instead of ethyl cellulose may diminish this temperature cross-talk, as the reason for the dependence is a better solubility of carbon dioxide at lower temperatures. Nevertheless, for the calibration of sensing foils based on thymol-blue (and *m*-cresol-purple) in ethyl cellulose the temperature was kept constantly at 25°C during lab experiments. In case of different temperatures expected for the following field experiment the temperatures were adjusted accordingly for every deployment.

The metal sleeves were additionally sealed with black silicone rubber to prevent entering of seawater into the sensing foils from the backend of the sleeves. This technique was tested prior with a sensing chemistry based on the di-OH-aza-BODIPY dyes presented in chapter 3. The optodes were calibrated before and after storage in H_3PO_4 (0.1 mmol/l) for 14 h. Calibration curves showed similar behavior before and after the storage, respectively. Thus, no invasion of the aqueos medium occurred (supporting information, figure S4.1).

LOD and Response Time

The determination of the limit of detection (LOD) was also carried out using a phosphate buffer solution, which was flushed with pure nitrogen gas. Sensors based on thymol-blue and on *m*-cresol-purple showed LOD values of 51 µatm and 126 µatm, respectively.

For the determination of the response time the fiber ends coated with sensing foil were immerged alternately in phosphate buffer solution in two graduated cylinders. One was treated with pure nitrogen gas and the other one with pure carbon dioxide gas. The t_{90} time (time needed for 90% of the signal to occur) for sensing foils based on both thymol-blue and *m*-cresol-purple was about 19 seconds. Obviously, the response time is affected by the thickness of the sensing layers. Therefore, one could reduce the t_{90} time by using thinner sensing layers, but has to deal with decreased signal intensity dynamics caused by a thinner dye layer.

Improvement of the system could be realized using fluorescent pH-sensitive indicator dyes, which match also the color channels of the RGB camera, e.g. the recently presented diketo-pyrrolo-pyrrole dyes (chapter 1 and 2 of this thesis).[157,175] This could also reduce the response/ recovery times because of the reduced number of layers, as only one dye layer and a protective layer would be necessary. Additionally, it would decrease the sensor thickness.

Carbon Dioxide Dynamics at Panarea Island (Sicily, Italy)

In 2013 the multi-branched optical carbon dioxide sensor device was taken to Panarea Island (Sicily, Italy) for a scientific cruise to measure pCO_2 under real conditions. Panarea Island is located in the north of Sicily in the Tyrrhenian Sea and is known to be located in a volcanically active area. Carbon dioxide is outgasing there from the seafloor. It is not yet definitely known if the CO_2 reaches the seawater either continuously and point-by-point via bubbles, or discontinuously via tidally affected pore-water dynamics. The multi-branched sensor device was applied off Panarea Island to answer this question.

The sensors were combined in 5 bundles of 20 sensors each, distributed along a pole (length 2 m), that was placed flat out on the seafloor near seeps, crossing seagrass patches and active seepage (figure 4.6).

Figure 4.6. *MuFO device at the sea ground with fiber bundles positioned over sea grass and sand. (image © HYDRA)*

The system was deployed 6 times at three different sampling sites, once during the night and once during the day, respectively. The first sampling site *Grey Minus* featured grey colored sediment and no obvious outgasing (bubbling) from the seafloor. Hence, it was chosen as *reference site*. The second site *Grey Plus* also showed grey colored sediment, but slight bubbling, whereas the third site *Red Plus* showed red colored sediment and moderate to strong bubbling (figure 4.7).

At the *reference site* both measurements, day time and night time, displayed rather typical pCO_2 levels of 350 to 400 µatm, which correlates well with the atmospheric carbon dioxide level.

At the *Grey Plus* site the pCO_2 resembled the level of *Grey Minus* during the day time measurement, but showed small fluctuations. During the night excursions up to 700 µatm were observed.

At the *Red Plus* site the pCO_2 level was similar to *Grey Minus* and *Grey Plus* during the day time measurement. During the night time measurement, all sensors showed strong simultaneous excursions, especially during the first 4 hours of the measurement. The excursions were much faster than the tidal dynamics and had an amplitude up to 3000 µatm. Afterwards a sudden decrease to levels ~400 µatm was observable (figure 4.7).
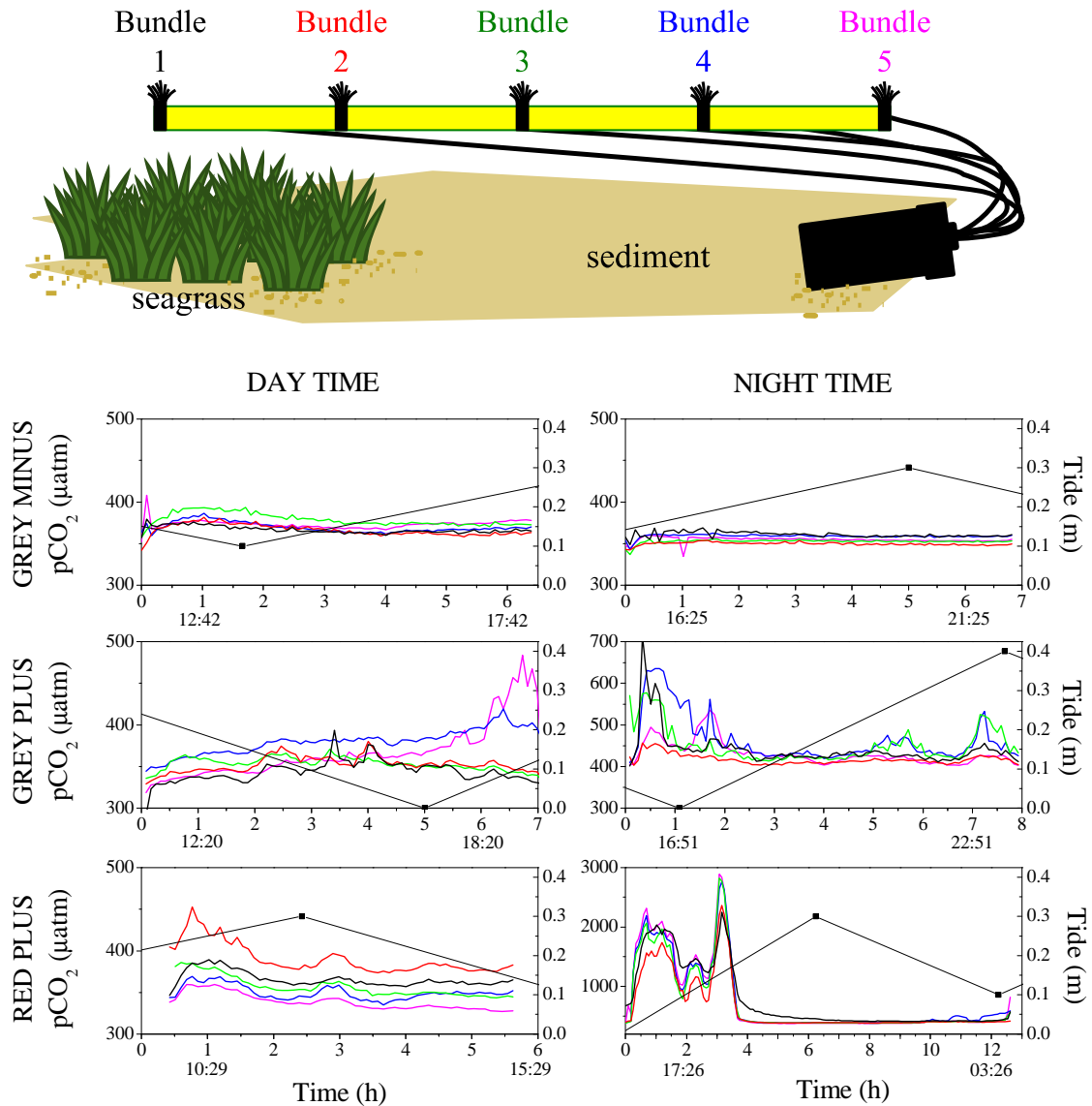
Figure 4.7. Above: *Scheme of the fiber bundle positioning along the pole: bundle 1 and 2 over seagrass; bundle 3, 4 and 5 over sediment.* ***Below:*** *Carbon dioxide dynamics during 6 deployments of the multi-branched sensor: 3 sampling sites "Grey Minus" (1.line), "Grey Plus" (2.line) and "Red Plus" (3.line), measured during day time (left column) and during night time (right column), respectively. Displayed are 5 signals per graph representing the mean value of one sensor bundle: bundle 1 (black) and bundle 2 (red) were positioned over seagrass; bundle 3 (green), bundle 4 (blue) and bundle 5 (magenta) were positioned over sediment.*

Despite the heterogeneous habitats (seagrass patches and seeps) we found no evidence of horizontal heterogeneity. The dynamics were the same in all channels. The CO_2 levels did vary significantly with tide at all three sampling sites. This confirmed the observations with loggers from a previous cruise in 2012, where low tides correlated with elevated carbon dioxide levels, lowered pH values and decreased redox potential. Furthermore, we found no effect of photosynthesis on the CO_2 signals. Bundle 1 and 2 showed similar pCO_2 values than bundle 3, 4 and 5, respectively.

The simultaneous behavior of all sensors and the correlation with tides indicated, that the elevated pCO_2 values are the result of tidally affected pore-water dynamics. A detailed comparison of all data loggers during this field experiment, giving information about temperature, pressure, etc, will be discussed in a final publication debating this issue.

Conclusion and Outlook

A multi-branched optical carbon dioxide sensor was presented. The device features 100 freely positionable optical CO_2 sensors, which are excited and read out collectively on the opposite end of the waveguiding optical fibers. This enables measurements with a high spatial resolution. The dynamic range of the sensors can be adjusted to different dynamic ranges from "normal" atmospheric level up to very high pCO_2 values, e.g. at CO_2 seeps. Read-out was carried out via imaging with a commercially available RGB camera. As an example the marine carbon dioxide dynamics at Panarea Island (Sicily, Italy) were demonstrated. From the obtained data we can conclude that the CO_2 levels around seeps are controlled by tides, but are not influenced by even strong photosynthesis. As additionally all sensors showed simultaneous dynamics, it is concluded, that the carbon dioxide level is affected by tidally driven pore-water dynamics, which is enriched with CO_2, rather than by bubbling. More detailed comparison of data giving information about temperature, pressure, redox potential, etc. from the same field experiment will be provided in a final publication combining all information to corroborate this ecological question.

Acknowledgment

Supporting Information

to *Multi-branched optical carbon dioxide sensors for marine applications*
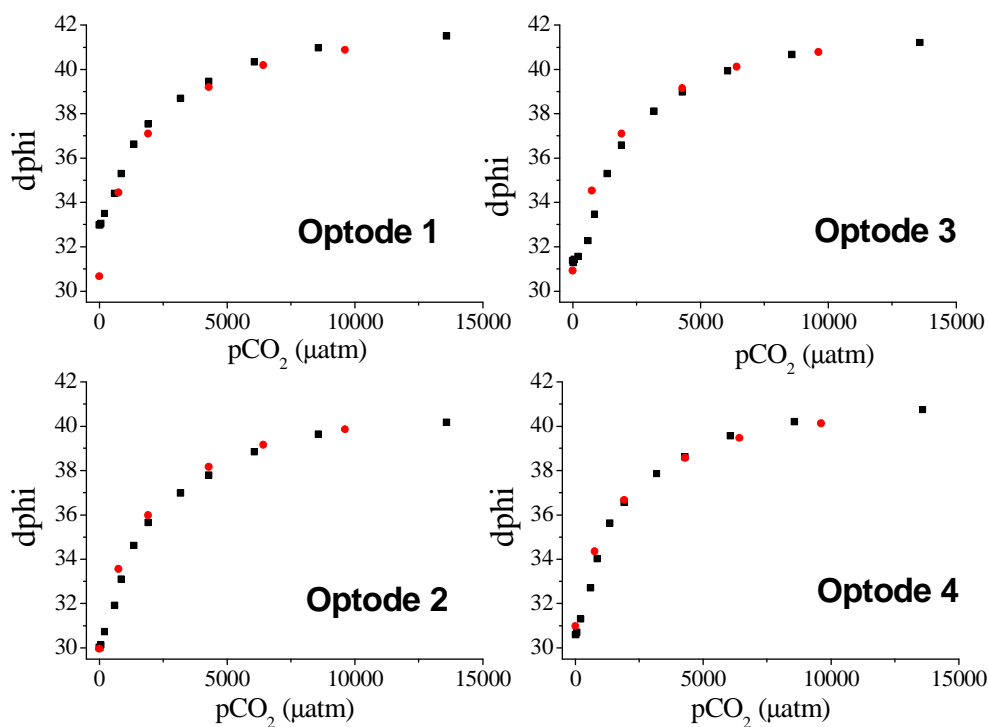

Figure S4.1. *Calibration curves of four sealed optodes before (black squares) and after (red dots) storage in H_3PO_4 (0.1 mmol/l) for 14 hours.*

Matlab script for analysis of the color channels of the images (written by Günter Mistlberger):

```matlab
%% Script for processing MuFO data
% USAGE: navigate to the folder containing the data and run the script
%
% Version 0.1 (2014-01-16) (c) G. Mistlberger & S. Schutting
% Working for evaluation.
% Version 0.2 (2015-02-16) (c) G. Mistlberger & S. Schutting
% Minor improvements and code clean-up

% house keeping
clear
close all

% defining variables
darkimage_filename = 'DARKIMAGE.CR2'; % file name of the darkimage
roisize = 50; % size of the region of interest
scaling_factor = 4; % scaling factor
```

```matlab
GM = GM_load_standard_settings; % loading standard settings
GM_colormap = jet(256); % defining a colormap for later

% save evaluation figures true or false
% save_figures = true;
save_figures = false;

% Find all raw image files with the pattern IMG*.CR2) in the current directory
files = dir('IMG*.CR2');
if isempty(files) % if no files were found throw an error and exit
    error('No ''IMG*.CR2'' image files found in this directory! Will quit here.')
end

% calculate number of files
no_files = numel(files);

% extract file names
fnames = cell(no_files,1); % preallocating space for the filenames
date_time = fnames; % preallocating space for date_time
for fc = 1:no_files
    fnames{fc,1} = files(fc).name;
    date_time{fc,1} = files(fc).date;
end

% check if there is a special dark image to be subtracted from all images
if isempty( dir( darkimage_filename ) )
    fprintf('Dark image %s not found. Assuming alternating dark and bright images.',darkimage_filename)
    is_calibration = 0;
else
    darkimage = imread(darkimage_filename);
    fprintf('Dark image %s found. Running in calibration mode.',darkimage_filename)
    is_calibration = 2;
end

%%

% open one image for roi selection
hf1 = figure;

if is_calibration
    temp_image = imread(fnames{round(no_files/2)}); % choose some image in the middle
else % otherwise use the 10th image
    temp_image = imread(fnames{10});
end

% show the temporary image
imshow(temp_image);

% select the rectangle around
hpoly = impoly;
t_pos = wait(hpoly);

% hide the polygone after transmission of positions
set(hpoly,'Visible','Off')

% get x and y positions of the 4 points
xt = t_pos(:,1);
yt = t_pos(:,2);

% define the number of spots in x and y direction and the spot size
% (diameter)
answer = inputdlg({'Spots in X-direction?','Spots in Y-direction?','Spot diameter (px)'},'Define Spot
numbers in X and Y direction',1,{'10','5',num2str(roisize)});
nx = str2double(answer{1});
ny = str2double(answer{2});
roisize = str2double(answer{3});
```

155

```matlab
% calculate the number of spots
no_spots = nx*ny;

% interpolating x and y positions of the spot centers in the first and
% last column
x_firstcolumn = linspace(xt(1),xt(4),ny);
x_lastcolumn = linspace(xt(2),xt(3),ny);
y_firstcolumn = linspace(yt(1),yt(4),ny);
y_lastcolumn = linspace(yt(2),yt(3),ny);

% pre-allocating space for xv, yv
xv = zeros(ny,nx);
yv = xv;

% calculating the centers of all selected spots
for yc = 1:ny;
    xv(yc,:) = linspace(x_firstcolumn(yc),x_lastcolumn(yc),nx);
    yv(yc,:) = linspace(y_firstcolumn(yc),y_lastcolumn(yc),nx);
end

% allocate space for BW_mask image and hcirc
BW_mask_image_temp = zeros(size(temp_image(:,:,1)));
hcirc = cell(numel(xv),1);
BW_mask = cell(numel(xv),1);

% for each spot, generate a circular BW mask
for spotcounter = 1:numel(xv) % for each spot

    % plot circles to show where data is taken
    viscircles([xv(spotcounter) yv(spotcounter)], roisize/2,'EdgeColor','w','LineWidth',1);
    hold on

    % label the spots

text(xv(spotcounter),yv(spotcounter),sprintf('%d',spotcounter),'FontSize',roisize/scaling_factor,'Color','w','HorizontalAlignment','center');

    % generate an ellipse for the current spot to get vertices
    hcirc{spotcounter} = imellipse(gca,[xv(spotcounter)-roisize/2 yv(spotcounter)-roisize/2 roisize roisize]);
    api=iptgetapi(hcirc{spotcounter});
    vert=api.getVertices();
    set(hcirc{spotcounter},'Visible','Off')

    % generate Black/White mask using the vertices
    BW_mask{spotcounter} =
poly2mask(vert(:,1),vert(:,2),size(temp_image(:,:,1),1),size(temp_image(:,:,1),2));
    BW_mask_image_temp = BW_mask_image_temp + BW_mask{spotcounter};
end

% wait one second
pause(1);

set(gcf,'inverthardcopy','off')
saveas(hf1,'spot_numbering.pdf')
close(hf1);

%% Mathematical calculations

% progress calculation (for long calculations)
progress = ones(size(BW_mask_image_temp));

% full screen figure
h_temp_figure = figure('units','normalized','outerposition',[0 0 1 1]);

% wait shortly
pause(0.01);
```

156

```matlab
if is_calibration

    % initializing the time vector
    time_vector = zeros(no_files,1);

    % preallocating space
    Ratio = zeros(no_files,no_spots);
    hp = zeros(size(Ratio,2),1);

    for fc = 1:no_files % for each file

        % calculating the progress of the calculation
        progress(:,1:ceil(fc/no_files*size(progress,2))) = 0;

        % generate the time vector by calculating the difference to the
        % starting point (in seconds)
        time_vector(fc,1) = (datenum(date_time{fc})-datenum(date_time{1}))*24*3600;

        % get current image and dark image
        curr_image = imread(fnames{fc});
        curr_dark_image = darkimage;

        % subtracting the dark image
        im_corr = curr_image - darkimage;

        % calculating R/G ratio
        im_ratio = double(im_corr(:,:,1))./double(im_corr(:,:,2));

        % replace INF and NaN values by zero
        im_ratio(isinf(im_ratio)) = 0;
        im_ratio(isnan(im_ratio)) = 0;

        % ratio image for plotting (replace zero by NaN)
        im_ratio_plot = im_ratio.*BW_mask_image_temp;
        im_ratio_plot(im_ratio_plot == 0) = NaN;

        % calculation of average ratios in all spots
        for spot_count = 1:no_spots
            curr_average_ratio =
sum(sum(im_ratio.*double(BW_mask{spot_count}))) ./double(sum(sum(BW_mask{spot_count})));

            % print result for information
            fprintf('R(av) in Spot#%d (file#: %d): %0.4f ¥n',spot_count,fc,curr_average_ratio)

            % save result in 'Ratio' array
            Ratio(fc,spot_count) = curr_average_ratio;
        end

        % make figure 'h_temp_figure' the current figure
        figure(h_temp_figure);

        % generate 3x3 subplot and show current image in the first subplot
        subplot(3,3,1), imshow(curr_image)

        hold on

        % draw spot circles in the image
        for spotcounter=1:numel(xv)
            viscircles([xv(spotcounter) yv(spotcounter)], roisize/2,'EdgeColor','w','LineWidth',1);
        end
        hold off

        % title
        title(sprintf('Current image (%s)',fnames{fc}),'Interpreter','none');

        % show dark image in subplot 2
```

```matlab
        subplot(3,3,2), imshow(darkimage), title(sprintf('Dark image
(%s)',darkimage_filename),'Interpreter','none');

        % show image - dark image in subplot 3
        subplot(3,3,3), imshow(im_corr), title('Image - Dark Image');

        % show dark image corrected red channel in subplot 4
        subplot(3,3,4), imshow(im_corr(:,:,1)), title('Red Channel');

        % show dark image corrected green channel in subplot 5
        subplot(3,3,5), imshow(im_corr(:,:,2)), title('Green Channel');

        % show ratio image in subplot 6
        subplot(3,3,6), imshow(im_ratio_plot)
        colormap(jet), title('R/G image');

        % plot calibration in subplot 7
        subplot(3,3,7)
        hp = zeros(size(Ratio,2),1);
        for pc = 1:size(Ratio,2)

            % get current colorbar index
            cidx = ceil(pc/size(Ratio,2)*size(GM_colormap,1));

            % plot
            hp(pc) = plot( ...
                1:size(Ratio,1),Ratio(:,pc),'-', ...
                'Marker','o', ...
                'Color',GM_colormap(cidx,:));
            hold on
        end
        hold off
        xlim([0 size(Ratio,1)+1])
        title('Ratio vs. Time in each spot');
        xlabel('Frame');
        ylabel('R/G Ratio');

        % plot the progress of the evaluation
        subplot(3,3,9), imshow(progress), title('Progress');

        % export current figure if the option was chosen in the preamble
        if save_figures
            fig_name = sprintf('Fig_%s.jpg',strrep(fnames{fc},'.CR2',''));
            set(gcf,'inverthardcopy','off')
            saveas(h_temp_figure,fig_name)
        else
            drawnow
        end
    end

else % if measurement, NOT calibration

    % check if the file number is even
    if mod(no_files,2) ~= 0
        error('Odd number of image files (%d) detected. Check your files.',no_files)
    end

    % initializing the time vector
    time_vector = zeros(no_files/2,1);

    % preallocating space
    Ratio((fc+1)/2, spot_count) = zeros(no_files/2,no_spots);
    hp = zeros(size(Ratio,2),1);

    for fc = 1:2:no_files

        % calculating the progress of the calculation
```

158

```matlab
        progress(:,1:ceil(fc/no_files*size(progress,2))) = 0;

        % time vector for export
        time_vector((fc+1)/2,1) = (datenum(date_time{fc})-datenum(date_time{1}))*24*3600;

        % subtracting the dark image
        curr_image = imread(fnames{fc+1});
        curr_dark_image = imread(fnames{fc});

        im_corr = curr_image - curr_dark_image;

        % calculating R/G ratio
        im_ratio = double(im_corr(:,:,1))./double(im_corr(:,:,2));
        im_ratio(isinf(im_ratio)) = 0;
        im_ratio(isnan(im_ratio)) = 0;

        % ratio image for plotting (replace zero by NaN)
        im_ratio_plot = im_ratio.*BW_mask_image_temp;
        im_ratio_plot(im_ratio_plot == 0) = NaN;

        for spot_count = 1:no_spots
            curr_average_ratio =
sum(sum(im_ratio.*double(BW_mask{spot_count}))))./double(sum(sum(BW_mask{spot_count})));
            fprintf('R(av) in Spot#%d (file#: %d): %0.4f ¥n',spot_count,fc,curr_average_ratio)
            Ratio((fc+1)/2,spot_count) = curr_average_ratio;
        end

        % debugging information
        figure(h_temp_figure);

        subplot(3,3,1), imshow(curr_image)
        hold on
        for spotcounter=1:numel(xv)
            viscircles([xv(spotcounter) yv(spotcounter)], roisize/2,'EdgeColor','w','LineWidth',1);
        end
        hold off
        title(sprintf('Current image (%s)',fnames{fc+1}),'Interpreter','none');
        subplot(3,3,2), imshow(curr_dark_image), title(sprintf('Current dark image
(%s)',fnames{fc}),'Interpreter','none');
        subplot(3,3,3), imshow(im_corr), title('Image - Dark Image');
        subplot(3,3,4), imshow(im_corr(:,:,1)), title('Red Channel');
        subplot(3,3,5), imshow(im_corr(:,:,2)), title('Green Channel');
        subplot(3,3,6), imshow(im_ratio_plot), set(gca, 'CLim', [min(min(Ratio)), max(max(Ratio))]),
colormap(jet), title('R/G image');
        subplot(3,3,7)
        for pc = 1:size(Ratio,2)
            cidx = ceil(pc/size(Ratio,2)*size(GM_colormap,1));
            hp(pc) = plot(1:size(Ratio,1),Ratio(:,pc),'-','Marker','o','Color',GM_colormap(cidx,:));
            hold on
        end
        hold off
        xlim([0 size(Ratio,1)+1])
        title('Ratio vs. Time in each spot');
        xlabel('Frame');
        ylabel('R/G Ratio');

        subplot(3,3,9), imshow(progress), title('Progress');

        % export current figure if the option was chosen in the preamble
        if save_figures
            fig_name = sprintf('Fig_%s.jpg',strrep(fnames{fc+1},'.CR2',''));
            set(gcf,'inverthardcopy','off')
            saveas(h_temp_figure,fig_name)
        end
    end

end
```

```matlab
%% Genarate array containing the time vector with the respective ratios

Ratio_final = [time_vector Ratio];

%% Data and Figure export

% preallocating data of legend array
legend_array = cell(no_spots,1);

hf_plot = figure('units','normalized','outerposition',[0 0 1 1]);

% plot ratio trends vs image number in each spot
for pc = 1:no_spots
    cidx = ceil(pc/size(Ratio,2)*size(GM_colormap,1));
    hp(pc) = plot(1:size(Ratio,1),Ratio(:,pc),'-','Marker','o','Color',GM_colormap(cidx,:));
    hold on
    grid on
    legend_array{pc} = sprintf('spot %d',pc);
end
hold off
title(sprintf('Ratio plot'));
legend(legend_array,'Location','EO')
saveas(gcf,sprintf('%s_Ratio_plot.pdf',datestr(datenum(date),29)))

% export data
ratio_data_filename = sprintf('%s_ratio_data.csv',datestr(datenum(date),29));
csvwrite(ratio_data_filename,Ratio_final);
```

Conclusion and Outlook

A new pH-sensitive indicator class based on diketo-pyrrolo-pyrroles (DPPs) was introduced (chapter 1 and 2). The new indicators were convenient to synthesize from low-cost starting materials and feature high solubility in organic solvents and polymers, good photostability, high quantum yields and tunable sensitivity (pK$_a$ values) due to their substitution pattern. Even very high sensitivity was achieved by introducing electron-donating groups. The indicators show self-referencing (dual-emitting) absorption and fluorescence spectra in the visible range after excitation in the blue range of the spectrum. They are usable for imaging applications after tuning their spectral properties to meet the color channels of commercially available RGB cameras (chapter 2). The presented indicator class represents a promising alternative to state-of-the-art indicators, e.g. HPTS.

Here, different starting materials and substituents would lead to a broader range of possible indicator dyes. Thus, photostability and quantum yields of the deprotonated forms could maybe improved. The DPP indicator of chapter 2 may be combined with the multi-branched optical carbon dioxide sensor (chapter 4). The dual-emitting properties of this dye fit perfectly to the color channels of the RGB camera and would lead to less layers of the sensing foils (no inner-filter effect system needed) and therefore to thinner layers and faster response times.

Furthermore, a second class of pH-sensitive indicators based on di-OH-aza-BODIPYs was introduced (chapter 3). Using these indicators in optical carbon dioxide sensors enables measurements in the near infrared (NIR) region, where background signals are diminished, light scattering is low and low-cost excitation sources can be used. The dyes feature very high and tunable pK$_a$ values (high/tunable sensitivity), excellent photostability and absorption maxima in the NIR region. Luminescence based read-out can be realized by making use of the inner-filter effect.

This class could also be expanded by using more different substituents. This could lead to optimized spectral properties for low-cost materials, e.g. excitations sources (LEDs), detectors or filters. Achieving fluorescent indicator dyes in the NIR region would enable luminescence based read-out without needing an inner-filter effect based multi-layer

system. This would combine the advantages of the NIR region with luminescence based read-out techniques.

In the end, a multi-branched optical carbon dioxide sensor was presented, possessing not one, but 100 freely positionable optical fibers with one collective excitation source and imaging read-out via the color channels of an RGB camera (chapter 4). This enables measurements with a very high spatial resolution. The applicability was demonstrated by measuring the subsea CO_2 dynamics off Panarea Island (Sicily, Italy).

Of course, this device is only a prototype and there are several improvement possibilities: A housing made of titanium would be more stable against pressure. Hence, the device would be applicable for deep sea measurements. As titanium is rather expensive, the size of the device should be diminished. Thus, the spatial demands within the housing (excitation, electronic system, camera, etc.) have to be minimized and optimized. Data download should be enabled via cable connection to save time and to avoid the refocusing of the camera. Up to now, the camera was fixed with only one screw and was displaced sideways when the device was hit by greater impacts. Therefore, the camera fixation should be extended to an (at least) two-point fixation. As already mentioned, the combination with self-referencing and fluorescent indicator dyes would lead to less layers of the sensing foils and therefore, to thinner and faster sensors.

Both of the presented indicator classes and the multi-branched optical carbon dioxide sensor are promising alternatives to their respective state-of-the-art materials/devices. Nevertheless, one should spend respect to the fact that there are still difficulties to overcome when it comes to practical applications:

Poisoning. The pH-sensitive indicator dyes used in this thesis show changing spectral properties according to their degree of protonation. It does not matter if the protons are released because of the reaction mechanism with carbon dioxide or by the reaction of e.g. weak volatile acids entering the matrix. These volatile acids can enter the protection layer and the matrix because they are not charged. Afterwards, they dissociate and protonate the indicator. As the remaining species are charged they can not leave the sensor again. Hence, the indicator dye stays protonated. This so called poisoning causes an increasing signal as consequence of an increasing degree of protonation of the

indicator. In marine science H_2S represents the most widespread example of a weak volatile acid causing this problem. Protection layers for this issue are highly desired.

Adhesion of layers. As mentioned in the introduction the sensing chemistry should stick to the support and should withstand chemical, thermal and mechanical stress. In the majority of cases the sensing chemistry consists not only of one, but two or more layers. The requirements for adhesion are even more difficult to meet with increasing number of layers, especially when they display different properties concerning water uptake or their temperature dependent expansion coefficients. For example, if a multi layer system is exposed to altering or extreme temperatures, the single layers expand different and thus, lose their adhesion. This makes the development of protection layers even more complicated, but not negligible.

Stability. Sensors should feature chemical, thermal and mechanical stability. During practical applications conditions can be harsh, long-lasting and show extreme fluctuations.

Response time. Sensors should response fast and reversible. In marine science for example divers are performing transect measurements, where the sensor is moved over a certain path over the seafloor. If the sensors show too long response times these kind of measurements are not feasible.

Cross-talks. Optical chemical sensors can measure various parameters, but this means on the other hand that these parameters can influence the sensor. One should know the possible influences of temperature, viscosity or electrochemical properties of the sensor system and should plan experiments with respect to those influences.

Biofouling. If sensors are applied in marine environments, microorganisms tend to build biofilms on the devices. Microelectrodes are less affected. When such a biofilm is built on the sensor-sample interface, e.g. a membrane or an optode, it can falsify the measurement results, e.g. oxygen consumption of the biofilm in front of an oxygen sensor. Biofilms can lead to an increase of the response time, to possible cross-talks to substances produced by the films or to poisoning of the sensor. Most widely discussed strategies to prevent the building of biofouling are copper meshes covering the part to be protected or silver ions. A solution for this problem is highly desired.

Protection layers. The protection layers should meet several demands. They should act as ion barrier to prevent cross-talks to the samples pH or other ionic species. Ambient light should be excluded from the measurement. For example during sediment measurements light scattering caused by the sediment can occur. This can change the signal ratio and thus, the measurement results. Ideally, protection layers should stop species like H_2S (see above). They should be as thin as possible (response times!), but stable against mechanical stress – ideally, even more as the layers below. They should withstand scratching or impacts as e.g. in case of measurements in the sediment. Additionally, they should feature good adhesion to the layer below and/or to the support, similar expansion coefficients and similar water uptake. If the protection layer is prepared with organic solvents, one has to pay attention that those are not dissolving the upper part of the covered layer. Additionally, the indicator dye – if not covalently coupled - should not be forced to migrate into the protection layer.

Protection layers are a significant part of optical sensing systems. Hence, one should not underestimate the importance of this part of the sensor and should investigate great care into the development.

References

(1)   Falkowski, P.; Scholes, R. J.; Boyle, E.; Canadell, J.; Canfield, D.; Elser, J.; Gruber, N.;
        Hibbard, K.; Hogberg, P.; Linder, S.; Mackenzie, F. T.; Moore, B.; Pedersen, T.; Rosenthal,
        Y.; Seitzinger, S.; Smetacek, V.; Steffen, W. *Science* **2000**, *290* (5490), 291–296.

(2)   Post, W.; Peng, T.; Emanuel, W.; King, A.; Dale, V.; Deangelis, D. *Am. Sci.* **1990**, *78* (4),
        310–326.

(3)   Baar, H. J. W. de; Stoll, M. H. C. In *Climate and Energy: The Feasibility of Controlling CO2
        Emissions*; Okken, P. A., Swart, R. J., Zwerver, S., Eds.; Springer Netherlands, 1989; pp
        143–177.

(4)   Change, I. P. on C. *Climate Change 2007 - The Physical Science Basis: Working Group I
        Contribution to the Fourth Assessment Report of the IPCC*; Cambridge University Press,
        2007.

(5)   Hall-Spencer, J. M.; Rodolfo-Metalpa, R.; Martin, S.; Ransome, E.; Fine, M.; Turner, S.
        M.; Rowley, S. J.; Tedesco, D.; Buia, M.-C. *Nature* **2008**, *454* (7200), 96–99.

(6)   Schlesinger, W. H.; Andrews, J. A. *Biogeochemistry* **2000**, *48* (1), 7–20.

(7)   Field, C. B.; Raupach, M. R.; MacKenzie, S. H. *The Global Carbon Cycle: Integrating
        Humans, Climate, and the Natural World*, New.; Island Pr: Washington, 2004.

(8)   Fischer, null; Wahlen, null; Smith, null; Mastroianni, null; Deck, null. *Science* **1999**,
        283 (5408), 1712–1714.

(9)   Fabry, V. J.; Seibel, B. A.; Feely, R. A.; Orr, J. C. *Ices J. Mar. Sci.* **2008**, *65* (3), 414–432.

(10)   Cramer, W.; Bondeau, A.; Schaphoff, S.; Lucht, W.; Smith, B.; Sitch, S. *Philos. Trans. R.
        Soc. Lond. Ser. B-Biol. Sci.* **2004**, *359* (1443), 331–343.

(11)   Dickinson, R. E.; Cicerone, R. J. *Nature* **1986**, *319* (6049), 109–115.

(12)   Juntueng, S.; Towprayoon, S.; Chiarakorn, S. *Resour. Conserv. Recycl.* **2014**, *87*, 46–56.

(13)   Sabine, C. L.; Feely, R. A.; Gruber, N.; Key, R. M.; Lee, K.; Bullister, J. L.; Wanninkhof, R.;
        Wong, C. S.; Wallace, D. W. R.; Tilbrook, B.; Millero, F. J.; Peng, T. H.; Kozyr, A.; Ono, T.;
        Rios, A. F. *Science* **2004**, *305* (5682), 367–371.

(14)   Riebesell, U.; Fabry, V. J.; Hansson, L.; Gattuso, J.-P. *Guide to best practices for ocean
        acidification research and data reporting*; Luxembourg: Publications Office of the
        European Union, 2011.

(15)   Zeebe, R. E.; Wolf-Gladrow, D. *CO2 in Seawater: Equilibrium, Kinetics, Isotopes:
        Equilibrium, Kinetics, Isotopes*; Elsevier, 2001.

(16)   Dickson, A. G.; Sabine, C. L.; Christian, J. R. *Guide to Best Practices for Ocean CO2
        measurements*; PICES Special Publication 3, 2007.

(17)   Salmon, K. H.; Anand, P.; Sexton, P. F.; Conte, M. *Biogeosciences* **2015**, *12* (1), 223–235.

(18)   Schiebel, R. *Glob. Biogeochem. Cycles* **2002**, *16* (4), 1065.

(19)   Kara, A. B.; Rochford, P. A.; Hurlburt, H. E. *J. Geophys. Res. Oceans* **2000**, *105* (C7), 16803–16821.

(20)   Sugimura, Y.; Suzuki, Y. *Mar. Chem.* **1988**, *24* (2), 105–131.

(21)   Cripps, I. L.; Munday, P. L.; McCormick, M. I. *Plos One* **2011**, *6* (7), e22736.

(22)   Caldeira, K.; Wickett, M. E. *J. Geophys. Res. Oceans* **2005**, *110* (C9), C09S04.

(23)   Cox, P. M.; Betts, R. A.; Jones, C. D.; Spall, S. A.; Totterdell, I. J. *Nature* **2000**, *408* (6809), 184–187.

(24)   Rayner, P. J.; Stavert, A.; Scholze, M.; Ahlström, A.; Allison, C. E.; Law, R. M. *Biogeosciences* **2015**, *12* (3), 835–844.

(25)   Pettit, E. C.; Lee, K. M.; Brann, J. P.; Nystuen, J. A.; Wilson, P. S.; O'Neel, S. *Geophys. Res. Lett.* **2015**, *42* (7), 2309–2316.

(26)   Jeppesen, E.; Brucet, S.; Naselli-Flores, L.; Papastergiadou, E.; Stefanidis, K.; Noges, T.; Noges, P.; Attayde, J. L.; Zohary, T.; Coppens, J.; Bucak, T.; Menezes, R. F.; Sousa Freitas, F. R.; Kernan, M.; Sondergaard, M.; Beklioglu, M. *Hydrobiologia* **2015**, *750* (1), 201–227.

(27)   Moss, B.; Kosten, S.; Meerhoff, M.; Battarbee, R. W.; Jeppesen, E.; Mazzeo, N.; Havens, K.; Lacerot, G.; Liu, Z.; De Meester, L.; Paerl, H.; Scheffer, M. *Inland Waters* **2011**, *1* (2), 101–105.

(28)   De Silva, C. S.; Weatherhead, E. K.; Knox, J. W.; Rodriguez-Diaz, J. A. *Agric. Water Manag.* **2007**, *93* (1-2), 19–29.

(29)   Widdicombe, S.; Spicer, J. I. *J. Exp. Mar. Biol. Ecol.* **2008**, *366* (1–2), 187–197.

(30)   Lapennas, G. N. *Respir. Physiol.* **1983**, *54* (2), 161–172.

(31)   Dixson, D. L.; Munday, P. L.; Jones, G. P. *Ecol. Lett.* **2010**, *13* (1), 68–75.

(32)   Jutfelt, F.; Hedgaerde, M. *Front. Zool.* **2013**, *10*, 81.

(33)   Wyatt, N. J.; Kitidis, V.; Woodward, E. M. S.; Rees, A. P.; Widdicombe, S.; Lohan, M. *J. Plankton Res.* **2010**, *32* (5), 631–641.

(34)   Hassenrueck, C.; Hofmann, L. C.; Bischof, K.; Ramette, A. *Environ. Microbiol. Rep.* **2015**, *7* (3), 516–525.

(35)   Ow, Y. X.; Collier, C. J.; Uthicke, S. *Mar. Biol.* **2015**, *162* (5), 1005–1017.

(36)   Valeur, P. D. B. *Molecular Fluorescence: Principles and Applications*; 2001.

(37)   Wolfbeis, O. S. *Anal. Chem.* **2006**, *78* (12), 3859–3874.

(38)   McDonagh, C.; Burke, C. S.; MacCraith, B. D. *Chem. Rev.* **2008**, *108* (2), 400–422.

(39)   Wolfbeis, O. S. *J. Mater. Chem.* **2005**, *15* (27-28), 2657–2669.

(40)   Mistlberger, G.; Crespo, G. A.; Bakker, E. *Annu. Rev. Anal. Chem. Vol 7* **2014**, *7*, 483–512.

(41)   Xie, X.; Pawlak, M.; Tercier-Waeber, M.-L.; Bakker, E. *Anal. Chem.* **2012**, *84* (7), 3163–3169.

(42)   Borisov, S. M.; Wuerth, C.; Resch-Genger, U.; Klimant, I. *Anal. Chem.* **2013**, *85* (19), 9371–9377.

(43)   Fukano, H.; Hashimoto, T.; Taue, S. *Jpn. J. Appl. Phys.* **2014**, *53* (4), 04EG05.

(44)   Takeo, T.; Hattori, H. *Jpn. J. Appl. Phys. Part 1-Regul. Pap. Short Notes Rev. Pap.* **1982**, *21* (10), 1509–1512.

(45)   Pattnaik, P. *Appl. Biochem. Biotechnol.* **2005**, *126* (2), 79–92.

(46)   Ciprian, D.; Hlubina, P. *Opt. Sens. Detect. Ii* **2012**, *8439*, 843927.

(47)   Singh, S.; Gupta, B. D. *Meas. Sci. Technol.* **2010**, *21* (11), 115202.

(48)   Healey, P. *J. Light. Technol.* **1985**, *3* (4), 876–886.

(49)   Mills, A.; Hodgen, S. *Adv. Concepts Fluoresc. Spectrosc. Pt Small Mol. Sens.* **2005**, *9*, 119–161.

(50)   Mills, A.; Chang, Q. *Analyst* **1993**, *118* (7), 839–843.

(51)   Mills, A.; Chang, Q.; Mcmurray, N. *Anal. Chem.* **1992**, *64* (13), 1383–1389.

(52)   Aigner, D.; Freunberger, S. A.; Wilkening, M.; Saf, R.; Borisov, S. M.; Klimant, I. *Anal. Chem.* **2014**, *86* (18), 9293–9300.

(53)   Aigner, D.; Borisov, S. M.; Orriach Fernandez, F. J.; Fernandez Sanchez, J. F.; Saf, R.; Klimant, I. *Talanta* **2012**, *99*, 194–201.

(54)   Gareis, T.; Huber, C.; Wolfbeis, O. S.; Daub, J. *Chem. Commun.* **1997**, No. 18, 1717–1718.

(55)   de Silva, A. P.; Gunaratne, H. Q. N.; Gunnlaugsson, T.; Huxley, A. J. M.; McCoy, C. P.; Rademacher, J. T.; Rice, T. E. *Chem. Rev.* **1997**, *97* (5), 1515–1566.

(56)   Zaggout, F. R.; El-Nahhal, I. M.; Qaraman, A. E.-F. A.; Dahoudi, N. Al. *Mater. Lett.* **2006**, *60* (29-30), 3463–3467.

(57)   Mills, A.; Chang, Q. *Anal. Chim. Acta* **1994**, *285* (1-2), 113–123.

(58)   Chierici, M.; Fransson, A.; Anderson, L. G. *Mar. Chem.* **1999**, *65* (3-4), 281–290.

(59)   Peterson, J. I.; Goldstein, S. R.; Fitzgerald, R. V.; Buckhold, D. K. *Anal. Chem.* **1980**, *52* (6), 864–869.

(60)   Zaggout, F. R. *Mater. Lett.* **2006**, *60* (8), 1026–1030.

(61)   Mills, A.; Lepre, A.; Wild, L. *Sens. Actuators B-Chem.* **1997**, *39* (1-3), 419–425.

(62)   Weidgans, B. M.; Krause, C.; Klimant, I.; Wolfbeis, O. S. *Analyst* **2004**, *129* (7), 645–650.

(63)   Vasylevska, A. S.; Karasyov, A. A.; Borisov, S. M.; Krause, C. *Anal. Bioanal. Chem.* **2007**, *387* (6), 2131–2141.

(64)   Choi, M. F. *J. Photochem. Photobiol. -Chem.* **1997**, *104* (1-3), 207–212.

(65)   Bultzingslowen, C. von; McEvoy, A. K.; McDonagh, C.; MacCraith, B. D.; Klimant, I.; Krause, C.; Wolfbeis, O. S. *Analyst* **2002**, *127* (11), 1478–1483.

(66)   Oter, O.; Ertekin, K.; Derinkuyu, S. *Talanta* **2008**, *76* (3), 557–563.

(67)   Kermis, H. R.; Kostov, Y.; Harms, P.; Rao, G. *Biotechnol. Prog.* **2002**, *18* (5), 1047–1053.

(68)   Borisov, S. M.; Gatterer, K.; Klimant, I. *Analyst* **2010**, *135* (7), 1711–1717.

(69)   Briggs, M. S.; Burns, D. D.; Cooper, M. E.; Gregory, S. J. *Chem. Commun.* **2000**, No. 23, 2323–2324.

(70)   Cooper, M. E.; Gregory, S.; Adie, E.; Kalinka, S. *J. Fluoresc.* **2002**, *12* (3-4), 425–429.

(71)   Jokic, T.; Borisov, S. M.; Saf, R.; Nielsen, D. A.; Kühl, M.; Klimant, I. *Anal. Chem.* **2012**, *84* (15), 6723–6730.

(72)   Cajlakovic, M.; Suppan, M.; Pressler, H.; Ribitsch, V.; Bellouard, F.; Rault, S. *2011 Fifth Int. Conf. Sens. Technol. ICST 2011* **2011**, 411–416.

(73)   Antala, D. K.; Varshney, A. K.; Davara, P. R.; Sangani, V. P. *Packag. Technol. Sci.* **2015**, *28* (6), 557–564.

(74)   Rai, D. R.; Oberoi, H. S.; Baboo, B. *J. Food Sci. Technol.-Mysore* **2002**, *39* (3), 199–207.

(75)   Del Valle Rodriguez Castilla, M.; Jordano, R. *Alimentaria* **1997**, *35* (285), 79–99.

(76)   Stow, R. W.; Baer, R. F.; Randall, B. F. *Arch. Phys. Med. Rehabil.* **1957**, *38* (10), 646–650.

(77)   Severinghaus, J. W.; Bradley, A. F. *J. Appl. Physiol.* **1958**, *13* (3), 515–520.

(78)   Nunn, J. F. *Proc. R. Soc. Med.* **1960**, *53* (3), 180–182.

(79)   Suzuki, H.; Arakawa, H.; Sasaki, S.; Karube, I. *Anal. Chem.* **1999**, *71* (9), 1737–1743.

(80)   Hesse, M.; Meier, H.; Zeeh, B. *Spektroskopische Methoden in der organischen Chemie*, 7., überarb. A.; Thieme, Stuttgart, 2005.

(81)   Wang, X.-D.; Wolfbeis, O. S. *Anal. Chem.* **2013**, *85* (2), 487–508.

(82)   E Farish, S. *J. Anesth. Clin. Res.* **2013**, *04* (03).

(83)   Park, C. S.; Kwak, J. G.; Lee, C.; Lee, C.-H.; Lee, S. K.; Kim, Y. L. *Perfus.-Uk* **2011**, *26* (6), 524–528.

(84)   Zhi-hua, T.; Yang, Z.; Li-wen, Z.; Guo-dong, J.; Li-hua, C.; Xin-xiao, Y. *Spectrosc. Spectr. Anal.* **2015**, *35* (4), 997–1000.

(85)   Clegg, M.; Sullivan, C.; Eastin, J. *Plant Physiol.* **1978**, *62* (6), 924–926.

(86)   Arieli, R.; Ertracht, O.; Daskalovic, Y. *J. Appl. Physiol.* **1999**, *86* (2), 647–650.

(87)   Degrandpre, M.; Hammar, T.; Smith, S.; Sayles, F. *Limnol. Oceanogr.* **1995**, *40* (5), 969–975.

(88)   Lefevre, N.; Ciabrini, J.; Michard, G.; Brient, B.; Duchaffaut, M.; Merlivat, L. *Mar. Chem.* **1993**, *42* (3-4), 189–198.

(89)   Mills, A.; Monaf, L. *Analyst* **1996**, *121* (4), 535–540.

(90)   Ekeberg, D.; Ogner, G.; Fongen, M.; Joner, E. J.; Wickstrøm, T. *J. Environ. Monit.* **2004**, *6* (7), 621–623.

(91)   Fietzek, P.; Fiedler, B.; Steinhoff, T.; Koertzinger, A. *J. Atmospheric Ocean. Technol.* **2014**, *31* (1), 181–196.

(92)   Weigl, B.; Holobar, A.; Trettnak, W.; Klimant, I.; Kraus, H.; Oleary, P.; Wolfbeis, O. *J. Biotechnol.* **1994**, *32* (2), 127–138.

(93)   Beuermann, T.; Egly, D.; Geoerg, D.; Klug, K. I.; Storhas, W.; Methner, F.-J. *J. Biosci. Bioeng.* **2012**, *113* (3), 399–405.

(94)   Murray, I. P.; Modell, J. H. *Anesthesiology* **1983**, *59* (4), 344–346.

(95)   Rost, B.; Zondervan, I.; WolfGladrow, D. *Mar. Ecol. Prog. Ser.* **2008**, *373*, 227–237.

(96)   Fabricius, K. E.; Langdon, C.; Uthicke, S.; Humphrey, C.; Noonan, S.; ath, G. De'; Okazaki, R.; Muehllehner, N.; Glas, M. S.; Lough, J. M. *Nat. Clim. Change* **2011**, *1* (3), 165–169.

(97)   Orr, J. C.; Fabry, V. J.; Aumont, O.; Bopp, L.; Doney, S. C.; Feely, R. A.; Gnanadesikan, A.; Gruber, N.; Ishida, A.; Joos, F.; Key, R. M.; Lindsay, K.; Maier-Reimer, E.; Matear, R.; Monfray, P.; Mouchet, A.; Najjar, R. G.; Plattner, G.-K.; Rodgers, K. B.; Sabine, C. L.; Sarmiento, J. L.; Schlitzer, R.; Slater, R. D.; Totterdell, I. J.; Weirig, M.-F.; Yamanaka, Y.; Yool, A. *Nature* **2005**, *437* (7059), 681–686.

(98)   Doney, S. C.; Fabry, V. J.; Feely, R. A.; Kleypas, J. A. In *Annual Review of Marine Science*; Annual Reviews: Palo Alto, 2009; Vol. 1, pp 169–192.

(99)   Puligundla, P.; Jung, J.; Ko, S. *Food Control* **2012**, *25* (1), 328–333.

(100)   Oter, O.; Ertekin, K.; Topkaya, D.; Alp, S. *Sens. Actuators B-Chem.* **2006**, *117* (1), 295–301.

(101)   Nakamura, N.; Amao, Y. *Sens. Actuators B-Chem.* **2003**, *92* (1-2), 98–101.

(102)   Perez de Vargas-Sansalvador, I. M.; Carvajal, M. A.; Roldan-Munoz, O. M.; Banqueri, J.; Fernandez-Ramos, M. D.; Capitan-Vallvey, L. F. *Anal. Chim. Acta* **2009**, *655* (1-2), 66–74.

(103)   Perez de Vargas-Sansalvador, I. M.; Martinez-Olmos, A.; Palma, A. J.; Dolores Fernandez-Ramos, M.; Fermin Capitan-Vallvey, L. *Microchim. Acta* **2011**, *172* (3-4), 455–464.

(104)   Ali, R.; Saleh, S. M.; Meier, R. J.; Azab, H. A.; Abdelgawad, I. I.; Wolfbeis, O. S. *Sens. Actuators B Chem.* **2010**, *150* (1), 126–131.

(105)   Neurauter, G.; Klimant, I.; Wolfbeis, O. S. *Anal. Chim. Acta* **1999**, *382* (1-2), 67–75.

(106)   Bultzingslowen, C. von; McEvoy, A. K.; McDonagh, C.; MacCraith, B. D. *Anal. Chim. Acta* **2003**, *480* (2), 275–283.

(107)   Marazuela, M. D.; Moreno-Bondi, M. C.; Orellana, G. *Appl. Spectrosc.* **1998**, *52* (10), 1314–1320.

(108)   Schulman, S.; Chen, S.; Bai, F.; Leiner, M.; Weis, L.; Wolfbeis, O. *Anal. Chim. Acta* **1995**, *304* (2), 165–170.

(109)   Wolfbeis, O.; Weis, L.; Leiner, M.; Ziegler, W. *Anal. Chem.* **1988**, *60* (19), 2028–2030.

(110)   Spry, D. B.; Goun, A.; Fayer, M. D. *J. Phys. Chem. A* **2007**, *111* (2), 230–237.

(111)   Wolfbeis, O. S.; Kovács, B.; Goswami, K.; Klainer, S. M. *Microchim. Acta* **1998**, *129* (3), 181–188.

(112)   Borisov, S. M.; Krause, C.; Arain, S.; Wolfbeis, O. S. *Adv. Mater.* **2006**, *18* (12), 1511–1516.

(113)   Dansby-Sparks, R. N.; Jin, J.; Mechery, S. J.; Sampathkumaran, U.; Owen, T. W.; Yu, B. D.; Goswami, K.; Hong, K.; Grant, J.; Xue, Z.-L. *Anal. Chem.* **2010**, *82* (2), 593–600.

(114)   Zhujun, Z.; Seitz, W. R. *Anal. Chim. Acta* **1984**, *160* (0), 305–309.

(115)   Haugland, R. P. *The Molecular Probes Handbook - A guide to Fluorescent Probes and Labeling Technologies*, Tenth Edition.; Invitrogen Corp.: USA, 2005.

(116)   Pandey, S.; Baker, S. N.; Pandey, S.; Baker, G. A. *Chem. Commun.* **2012**, *48* (56), 7043–7045.

(117)   Liu, Y.; Tang, Y.; Barashkov, N. N.; Irgibaeva, I. S.; Lam, J. W. Y.; Hu, R.; Birimzhanova, D.; Yu, Y.; Tang, B. Z. *J. Am. Chem. Soc.* **2010**, *132* (40), 13951–13953.

(118)   Ali, R.; Lang, T.; Saleh, S. M.; Meier, R. J.; Wolfbeis, O. S. *Anal. Chem.* **2011**, *83* (8), 2846–2851.

(119)   Zollinger, H. *Color Chemistry: Syntheses, Properties, and Applications of Organic Dyes and Pigments*; John Wiley & Sons, 2003.

(120)   Luňák Jr., S.; Vala, M.; Vyňuchal, J.; Ouzzane, I.; Horáková, P.; Možíšková, P.; Eliáš, Z.; Weiter, M. *Dyes Pigments* **2011**, *91* (3), 269–278.

(121)   Wang, B.; He, N.; Li, B.; Jiang, S.; Qu, Y.; Qu, S.; Hua, J. *Aust. J. Chem.* **2012**, *65* (4), 387–394.

(122)   Zhu, Y.; Rabindranath, A. R.; Beyerlein, T.; Tieke, B. *Macromolecules* **2007**, *40* (19), 6981–6989.

(123)   Cao, D. R.; Liu, Q. L.; Zeng, W. J.; Han, S. H.; Peng, J. B.; Liu, S. P. *J. Polym. Sci. Part - Polym. Chem.* **2006**, *44* (8), 2395–2405.

(124)   Rabindranath, A. R.; Zhu, Y.; Heim, I.; Tieke, B. *Macromolecules* **2006**, *39* (24), 8250–8256.

(125)   Zhu, Y.; Heim, I.; Tieke, B. *Macromol. Chem. Phys.* **2006**, *207* (23), 2206–2214.

(126)   Zhang, X.; Richter, L. J.; DeLongchamp, D. M.; Kline, R. J.; Hammond, M. R.; McCulloch, I.; Heeney, M.; Ashraf, R. S.; Smith, J. N.; Anthopoulos, T. D.; Schroeder, B.; Geerts, Y. H.; Fischer, D. A.; Toney, M. F. *J. Am. Chem. Soc.* **2011**, *133* (38), 15073–15084.

(127)   Qu, Y.; Hua, J.; Tian, H. *Org. Lett.* **2010**, *12* (15), 3320–3323.

(128)   Jeong, Y.-H.; Lee, C.-H.; Jang, W.-D. *Chem.- Asian J.* **2012**, *7* (7), 1562–1566.

(129)   Demas, J.; Crosby, G. *J. Phys. Chem.* **1971**, *75* (8), 991 – &.

(130)   Seybold, G.; Wagenblast, G. *Dyes Pigments* **1989**, *11* (4), 303–317.

(131)   Ford, W. *J. Photochem.* **1987**, *37* (1), 189–204.

(132)   Borisov, S. M.; Seifner, R.; Klimant, I. *Anal. Bioanal. Chem.* **2011**, *400* (8), 2463–2474.

(133)   Vala, M.; Vynuchal, J.; Toman, P.; Weiter, M.; Lunak, S. *Dyes Pigments* **2010**, *84* (2), 176–182.

(134)   Vala, M.; Weiter, M.; Vynuchal, J.; Toman, P.; Lunak, S. *J. Fluoresc.* **2008**, *18* (6), 1181–1186.

(135)   Hansch, C.; Leo, A.; Taft, R. W. *Chem. Rev.* **1991**, *91* (2), 165–195.

(136)   Lunak, S.; Vynuchal, J.; Vala, M.; Havel, L.; Hrdina, R. *Dyes Pigments* **2009**, *82* (2), 102–108.

(137)   Apostolidis, A. Combinatorial Approach for Development of Optical Gas Sensors - Concept and Application of High-Throughput Experimentation, Universität Regensburg:

Regensburg, 2004.

(138) Rost, B.; Zondervan, I.; Wolf-Gladrow, D. *Mar. Ecol. Prog. Ser.* **2008**, *373*, 227–237.

(139) García-Fresnadillo, D.; Marazuela, M. D.; Moreno-Bondi, M. C.; Orellana, G. *Langmuir*
       1999, *15* (19), 6451–6459.

(140) Hong, W.; Chen, Y.; Feng, X.; Yan, Y.; Hu, X.; Zhao, B.; Zhang, F.; Zhang, D.; Xu, Z.; Lai, Y.
       Chem. Commun. **2013**, *49* (74), 8229–8231.

(141) Mayr, T.; Klimant, I.; Wolfbeis, O. S.; Werner, T. *Anal. Chim. Acta* **2002**, *462* (1), 1–10.

(142) Huber, C.; Klimant, I.; Krause, C.; Wolfbeis, O. S. *Anal. Chem.* **2001**, *73* (9), 2097–2103.

(143) Liebsch, G.; Klimant, I.; Krause, C.; Wolfbeis, O. S. *Anal. Chem.* **2001**, *73* (17), 4354–
       4363.

(144) Xu, Z.; Rollins, A.; Alcala, R.; Marchant, R. E. *J. Biomed. Mater. Res.* **1998**, *39* (1), 9–15.

(145) Hunter, R. C.; Beveridge, T. J. *Appl. Environ. Microbiol.* **2005**, *71* (5), 2501–2510.

(146) Spitzer, K. W.; Skolnick, R. L.; Peercy, B. E.; Keener, J. P.; Vaughan-Jones, R. D. *J. Physiol.*
       2002, *541* (1), 159–167.

(147) Ramshesh, V. K.; Lemasters, J. J. In *Mitochondrial Bioenergetics: Methods and Protocols*;
       Palmeira, C. M., Moreno, A. J., Eds.; 2012; Vol. 810, pp 243–248.

(148) Liebsch, G.; Klimant, I.; Frank, B.; Holst, G.; Wolfbeis, O. S. *Appl. Spectrosc.* **2000**, *54* (4),
       548–559.

(149) Wang, X.; Meier, R. J.; Wolfbeis, O. S. *Angew. Chem. Int. Ed.* **2013**, *52* (1), 406–409.

(150) Schreml, S.; Meier, R. J.; Wolfbeis, O. S.; Landthaler, M.; Szeimies, R.-M.; Babilas, P.
       Proc. Natl. Acad. Sci. U. S. A. **2011**, *108* (6), 2432–2437.

(151) Peng, H.; Stolwijk, J. A.; Sun, L.-N.; Wegener, J.; Wolfbeis, O. S. *Angew. Chem.-Int. Ed.*
       2010, *49* (25), 4246–4249.

(152) Aigner, D.; Ungerboeck, B.; Mayr, T.; Saf, R.; Klimant, I.; Borisov, S. M. *J. Mater. Chem. C*
       2013, *1* (36), 5685–5693.

(153) Wang, X.; Meier, R. J.; Link, M.; Wolfbeis, O. S. *Angew. Chem. Int. Ed.* **2010**, *49* (29),
       4907–4909.

(154) Kondrashina, A.; Dmitriev, R.; Borisov, S. M.; Klimant, I.; O´Brien, I.; Nolan, Y. M.;
       Zhdanov, A.; Papkovsky, D. *Adv. Funtional Mater. 22*, 4931–4939.

(155) Larsen, M.; Borisov, S. M.; Grunwald, B.; Klimant, I.; Glud, R. N. *Limnol. Oceanogr.-
       Methods* **2011**, *9*, 348–360.

(156) Staal, M.; Borisov, S. M.; Rickelt, L. F.; Klimant, I.; Kuhl, M. *J. Microbiol. Methods* **2011**, *85* (1), 67–74.

(157) Schutting, S.; Borisov, S. M.; Klimant, I. *Anal. Chem.* **2013**, *85* (6), 3271–3279.

(158) Wong, W. W. H.; Subbiah, J.; Puniredd, S. R.; Purushothaman, B.; Pisula, W.; Kirby, N.; Müllen, K.; Jones, D. J.; Holmes, A. B. *J. Mater. Chem.* **2012**, *22* (39), 21131–21137.

(159) Qu, S.; Wu, W.; Hua, J.; Kong, C.; Long, Y.; Tian, H. *J. Phys. Chem. C* **2010**, *114* (2), 1343–1349.

(160) Qu, S.; Tian, H. *Chem. Commun.* **2012**, *48* (25), 3039–3051.

(161) Langhals, H.; Potrawa, T.; Nöth, H.; Linti, G. *Angew. Chem. Int. Ed. Engl.* **1989**, *28* (4), 478–480.

(162) Langhals, H.; Grundei, T.; Potrawa, T.; Polborn, K. *Liebigs Ann.* **1996**, *1996* (5), 679–682.

(163) Lorenz, I.-P.; Limmert, M.; Mayer, P.; Piotrowski, H.; Langhals, H.; Poppe, M.; Polborn, K. *Chem. – Eur. J.* **2002**, *8* (17), 4047–4055.

(164) Langhals, H.; Limmert, M.; Lorenz, I.-P.; Mayer, P.; Piotrowski, H.; Polborn, K. *Eur. J. Inorg. Chem.* **2000**, *2000* (11), 2345–2349.

(165) Yamagata, T.; Kuwabara, J.; Kanbara, T. *Tetrahedron Lett.* **2010**, *51* (12), 1596–1599.

(166) Lebourgeois, V.; Bégué, A.; Labbé, S.; Mallavan, B.; Prévot, L.; Roux, B. *Sensors* **2008**, *8* (11), 7300–7322.

(167) Zhao, D.; Miller, D.; Xian, X.; Tsow, F.; Forzani, E. S. *Sens. Actuators B Chem.* **2014**, *195*, 171–176.

(168) Trivedi, S.; Mehta, H.; Kashyap, R. *Indian J. Crit. Care Med.* **2014**, *18* (6), 348.

(169) Punt, A. E.; Poljak, D.; Dalton, M. G.; Foy, R. J. *Ecol. Model.* **2014**, *285*, 39–53.

(170) Carroll, A. G.; Przeslawski, R.; Radke, L. C.; Black, J. R.; Picard, K.; Moreau, J. W.; Haese, R. R.; Nichol, S. *Cont. Shelf Res.* **2014**, *83*, 116–128.

(171) Zosel, J.; Oelßner, W.; Decker, M.; Gerlach, G.; Guth, U. *Meas. Sci. Technol.* **2011**, *22* (7), 072001.

(172) Xu, L. Q.; Zhang, B.; Sun, M.; Hong, L.; Neoh, K.-G.; Kang, E.-T.; Fu, G. D. *J. Mater. Chem. A* **2013**, *1* (4), 1207–1212.

(173) Xu, Q.; Lee, S.; Cho, Y.; Kim, M. H.; Bouffard, J.; Yoon, J. *J. Am. Chem. Soc.* **2013**, *135* (47), 17751–17754.

(174) Borchert, N. B.; Kerry, J. P.; Papkovsky, D. B. *Sens. Actuators B Chem.* **2013**, *176*, 157–165.

(175)   Schutting, S.; Klimant, I.; Beer, D. de; Borisov, S. M. *Methods Appl. Fluoresc.* **2014**, *2* (2), 024001.

(176)   Borisov, S. M.; Klimant, I. *Anal. Chim. Acta* **2013**, *787*, 219–225.

(177)   Nakamura, N.; Amao, Y. *Anal. Bioanal. Chem.* **2003**, *376* (5), 642–646.

(178)   Amao, Y.; Nakamura, N. *Sens. Actuators B Chem.* **2004**, *100* (3), 347–351.

(179)   Hall, M. J.; McDonnell, S. O.; Killoran, J.; O'Shea, D. F. *J. Org. Chem.* **2005**, *70* (14), 5571–5578.

(180)   Gorman, A.; Killoran, J.; O'Shea, C.; Kenna, T.; Gallagher, W. M.; O'Shea, D. F. *J. Am. Chem. Soc.* **2004**, *126* (34), 10619–10631.

(181)   Oliver, A. E.; Newbold, L. K.; Whiteley, A. S.; van der Gast, C. J. *Environ. Microbiol. Rep.* **2014**, *6* (6), 574–582.

(182)   Pedersen, S. A.; Vage, V. T.; Olsen, A. J.; Hammer, K. M.; Altin, D. *J. Toxicol. Environ. Health-Part -Curr. Issues* **2014**, *77* (9-11), 535–549.

(183)   Hutchins, D. A.; Fu, F.-X.; Webb, E. A.; Walworth, N.; Tagliabue, A. *Nat. Geosci.* **2013**, *6* (9), 790–795.

(184)   Iguchi, A.; Kumagai, N. H.; Nakamura, T.; Suzuki, A.; Sakai, K.; Nojiri, Y. *Mar. Pollut. Bull.* **2014**, *89* (1-2), 348–355.

(185)   Heuer, R. M.; Grosell, M. *Am. J. Physiol.-Regul. Integr. Comp. Physiol.* **2014**, *307* (9), R1061–R1084.

(186)   Green, L.; Jutfelt, F. *Biol. Lett.* **2014**, *10* (9), 20140538.

(187)   Wencel, D.; Abel, T.; McDonagh, C. *Anal. Chem.* **2014**, *86* (1), 15–29.

(188)   Aigner, D.; Borisov, S. M.; Klimant, I. *Anal. Bioanal. Chem.* **2011**, *400* (8), 2475–2485.

(189)   Zhujun, Z.; Seitz, W. *Anal. Chim. Acta* **1984**, *160* (JUN), 47–55.

(190)   Hecht, H.; Kolling, A. *Sens. Actuators B-Chem.* **2001**, *81* (1), 76–82.

(191)   Stich, M. I. J.; Borisov, S. M.; Henne, U.; Schaeferling, M. *Sens. Actuators B-Chem.* **2009**, *139* (1), 204–207.

(192)   Stahl, H.; Warnken, K. W.; Sochaczewski, L.; Glud, R. N.; Davison, W.; Zhang, H. *Limnol. Oceanogr. Methods* **2012**, *10*, 389–401.

(193)   Lippitsch, M.; Pusterhofer, J.; Leiner, M.; Wolfbeis, O. *Anal. Chim. Acta* **1988**, *205* (1-2), 1–6.

(194)   Muller, B.; Hauser, P. C. *Analyst* **1996**, *121* (3), 339–343.

(195) Preininger, C.; Klimant, I.; Wolfbeis, O. S. *Anal. Chem.* **1994**, *66* (11), 1841–1846.

(196) Klimant, I.; Meyer, V.; Kuhl, M. *Limnol. Oceanogr.* **1995**, *40* (6), 1159–1165.

(197) Warner, M. *Anal. Chem.* **1986**, *58* (7), A766 – &.

(198) Jordan, D. M.; Walt, D. R.; Milanovich, F. P. *Anal. Chem.* **1987**, *59* (3), 437–439.

(199) Holst, G.; Glud, R. N.; Kühl, M.; Klimant, I. *Sens. Actuators B Chem.* **1997**, *38* (1–3), 122–129.

(200) Yi, Z.; Zhong, Z.; Reardon, K. F.; Wang, W.; Katragadda, M.; Lear, K. L. *Proc. SPIE - Int. Soc. Opt. Eng.* **2010**, *7559*, 75590T (6 pp.).

(201) Fischer, J. P.; Koop-Jakobsen, K. *Sens. Actuators B Chem.* **2012**, *168*, 354–359.

Appendix A

List of Figures

List of Schemes

List of Tables

Appendix B – Curriculum Vitae

Susanne Schutting

Born on December 14, 1986 (Leoben, Austria)
Marital Status: unmarried
Nationality: Austria

Current Address: Dr.-Theodor-Körnerstraße 23/6
                     8600 Bruck an der Mur
                     Austria

Permanent Address: Mürzstraße 1
                     8641 St. Marein im Mürztal
                     Austria

Practical Experience:

- *Aug. 2014 to present* TU Graz – Graz University of Technology (Institute of Analytical Chemistry and Food Chemistry; university assistant/PhD student)

- *Aug. 2011 to Jul. 2014* TU Graz (Institute of Analytical Chemistry and Food Chemistry; project assistant/ PhD student)

- *Oct. 2010 to Jul. 2011* RCPE- Research Centre Pharmaceutical Engineering (and Institute for Process and Particle Engineering; project member)

- *Jul. 2010 to Sep. 2010* RCPE (trainee)

- *May 2010 to Jun. 2010* TU Graz (Institute of Analytical Chemistry; undergraduate project assistant)

- *Oct. 2009 to Jan. 2010* TU Graz (Institute of Analytical Chemistry; student assistant)

- *Jun. 2008 to Jan. 2010* Company "4a medicom"

- *Oct. 2007 to Apr. 2010* Catering Service "Ivents"

- *Feb. 2005 to Jul. 2006* Catering Service "S-Events"

Educational Background:

- *Aug. 2011 to present* PhD studies at TU Graz ("Optical carbon dioxide sensors for marine applications"); oral examination expected in Sep./Oct. 2015

- *Oct. 2010 to Jun. 2011* Master thesis at TU Graz ("Development of zinc electrodes for rechargeable zinc-air-batteries")

- *2009 to 2011* TU Graz, Master studies Technical Chemistry

- *2006 to 2009* TU Graz, Bachelor studies Chemistry (focus: Technical Chemistry)

- *Year 2001/02 to 2005/06* HTL-Kapfenberg – College of Materials Engineering in Kapfenberg (focus: Polymer and Environmental Engineering)

Special Skills:

- Driving licence (A, B)
- Languages: German (native), English (fluent), Italian (basic)
- Advanced computer skills in: MS Word, MS Power Point, MS Excel, Origin, Inkscape
- Competence Training for Student Assistants: Group Management, Communication, Teamwork and Motivation

Articles:

2015 *NIR Optical Carbon Dioxide Sensors based on Highly Photostable Dihydroxy-aza-BODIPY Dyes;* <u>S. Schutting</u>, T. Jokic, M. Strobl, S. M. Borisov, D. de Beer, I. Klimant; *J. Mater. Chem. C*, **2015**, 3, 5474-5483

2014 *New Highly Fluorescent pH Indicator for Ratiometric RGB Imaging of pCO$_2$;* <u>S.Schutting</u>, I. Klimant, D. de Beer, S. M. Borisov; *Methods Appl. Fluoresc.*, **2014**, 2, 1-8

2013 *Diketo-Pyrrolo-Pyrrole Dyes as New Colorimetric and Fluorescent pH Indicators for Optical Carbon Dioxide Sensors;* <u>S. Schutting</u>, S. M. Borisov, I. Klimant; *Anal. Chem.*, **2013**, 85, 3271-3279

Poster Presentations:

2015 *Neuartige optische pCO$_2$-Sensoren basierend auf BF$_2$-Chelatverbindungen von Dihydroxy-aza-Dipyrromethenen;* <u>E. Fritzsche</u>, S. Schutting, T. Jokic, M. Strobl, S. M. Borisov, I.Klimant; at the ANAKON conference; Graz (Austria), 23/03/2015*

New High Performance Optical pCO$_2$ Sensors based on BF$_2$-CHelates of Dihydroxy-aza-Dipyrromethene; <u>E. Fritzsche</u>, S. Schutting, T. Jokic, M. Strobl, S. M. Borisov, I.Klimant; at the Aquatic Science Meeting; Granada (Spain), 23/02/2015*

2014 *A Multiple Fibre Optic Device for Monitoring Carbon Dioxide in Marine Environments;* <u>S. Schutting</u>, J. P. Fischer, S. M. Borisov, D. de Beer, I. Klimant; at the 3rd annual project meeting (ECO2 project); Salina Island (Italy), 02/06/2014

2013 *Highly Fluorescent Diketo-Pyrrolo-Pyrrole Dyes for Optical pH and CO_2 Sensors;* <u>S. Schutting</u>, D. Aigner, S. M. Borisov, I. Klimant; at the Methods and Applications of Fluorescence conference; Genova (Italy), 08/09/2013

2012 *Diketo-Pyrrolo-Pyrrole Dyes as New pH Indicators for Optical CO_2 Sensors in Marine Research;* <u>S. Schutting</u>, S. M. Borisov, I. Klimant; at the Europt(r)ode XI conference; Barcelona (Spain), 01/04/2012

2011 *Novel Materials for Electrically Rechargeable Zinc-Air-Batteries;* <u>S. Weinberger</u>, G. Rabenstein, V. Hacker, K. Fröhlich, F. B. Wede, D. Movrin, S. Schutting, W. Taucher-Mautner, F. Duff; at the 4th International Summer School on Advanced Studies of Polymer Electrolyte Fuel Cells; Yokohama (Japan), 05/09/2011

       New Electrode Materials for the Rechargeable Zinc-Air-Battery; <u>S. Weinberger</u>, G. Rabenstein, V. Hacker, K. Fröhlich, F. Duff, F. B. Wede, S. Schutting, W. Taucher-Mautner, D. Movrin, P. Janewit; at the 62nd annual meeting of the International Society of Electrochemistry; Niigata (Japan), 11/09/2011

Oral Presentations:

2014 *Novel BF_2-Chelated Tetraarylazadipyrromethene Dyes for Optical Sensing of pH and Carbon Dioxide;* <u>S. M. Borisov</u>, T. Jokic, M. Strobl, S. Schutting, I. Klimant; at the 8th International Conference on Porphyrins and Phthalocyanines (ICPP-8); Istanbul (Turkey), 24/06/2014

       Optical Carbon Dioxide Sensors based on Novel Indicator Dyes with Outstanding Photophysical Properties; <u>S. Schutting</u>, T. Jokic, M. Strobl, S. M. Borisov, D. de Beer, I. Klimant; at the Europt(r)ode XII conference; Athens (Greece), 13/04/2014

2011 *Development of Zinc-Electrodes for Rechargeable Zinc-Air-Batteries;* <u>S. Schutting</u>, W. Taucher-Mautner, K. Fröhlich, S. Weinberger, V. Hacker; at the 14th Austrian Chemistry Days; Linz (Austria), 26/09/2011

       Optimized Carrier Particles for Dry Powder Inhalers by the Use of Spray Drying; <u>E. Littringer</u>, A. Mescher, H. Schröttner, S. Schutting, P. Walzel, N. A. Urbanetz; at the 5th International Congress on Pharmaceutical Engineering; Graz (Austria), 29/09/2011